Topics in Current Chemistry 357

LeGrande M. Slaughter *Editor*

Homogeneous Gold Catalysis

Springer

357
Topics in Current Chemistry

Aims and Scope

The series Topics in Current Chemistry presents critical reviews of the present and future trends in modern chemical research. The scope of coverage includes all areas of chemical science including the interfaces with related disciplines such as biology, medicine and materials science.

The goal of each thematic volume is to give the non-specialist reader, whether at the university or in industry, a comprehensive overview of an area where new insights are emerging that are of interest to larger scientific audience.

Thus each review within the volume critically surveys one aspect of that topic and places it within the context of the volume as a whole. The most significant developments of the last 5 to 10 years should be presented. A description of the laboratory procedures involved is often useful to the reader. The coverage should not be exhaustive in data, but should rather be conceptual, concentrating on the methodological thinking that will allow the non-specialist reader to understand the information presented.

Discussion of possible future research directions in the area is welcome.

Review articles for the individual volumes are invited by the volume editors.

Readership: research chemists at universities or in industry, graduate students.

More information about this series at
http://www.springer.com/series/128

LeGrande M. Slaughter
Editor

Homogeneous Gold Catalysis

With contributions by

A. Aponick · O.N. Faza · M.R. Gagné · G.B. Hammond · A.C. Jones · C.S. López · D. Malhotra · V. Michelet · P.H.S. Paioti · S. Shin · D. Weber · B. Xu

Springer

Editor
LeGrande M. Slaughter
Department of Chemistry
University of North Texas
Denton, Texas
USA

ISSN 0340-1022 ISSN 1436-5049 (electronic)
Topics in Current Chemistry
ISBN 978-3-319-13721-6 ISBN 978-3-319-13722-3 (eBook)
DOI 10.1007/978-3-319-13722-3

Library of Congress Control Number: 2015936667

Springer Cham Heidelberg New York Dordrecht London

Printed on acid-free paper

Springer International Publishing AG Switzerland is part of Springer Science+Business Media (www.springer.com)

Preface

The rise of homogeneous gold catalysis is the story of a long-neglected metal boldly defying expectations. Along with a general reputation for inertness, gold possesses two common oxidation states which have historically been overlooked as too uninteresting (Au^{I}) or too unstable (Au^{III}) to warrant serious study by most organometallic chemists. Despite significant activity in the area of *heterogeneous* gold catalysts from the 1970s onward, and a trickle of seminal reports of homogeneous gold catalysis by Ito, Hayashi, and Utimoto in the 1980s and 1990s, the latter area did not begin to blossom until the work of Teles and Hashmi in 1998–2000 unveiled the potential of the field. It is now well recognized that gold (in particular Au^{I}) is a potent, "soft" carbophilic Lewis acid, with an ability to activate carbon–carbon π-bonds toward nucleophilic attack which parallels the reactivity of other late transition metals such as platinum, palladium, and mercury. It is also clear that gold often outshines its metallic neighbors by activating π-bonds under exceptionally mild conditions and by channeling these transformations into unique modes of reactivity which are particularly suited for the synthesis of complex organic molecules.

Such is the pace of progress in this field that the many excellent reviews available in the literature are in frequent need of updates. The purpose of this volume is to highlight some key subareas of homogeneous gold catalysis that have spurred significant advances in the field in the past 3–5 years. The topics have been chosen in recognition of two equally powerful forces that have driven the recent evolution of gold catalysis: an increasing need for synthetic methods that deliver complex organic structures, and the renaissance of fundamental organometallic gold chemistry. The authors are active researchers who have made substantial contributions to the areas reviewed in their respective chapters.

The volume begins with a chapter by Malhotra, Hammond, and Xu, which highlights the interplay of ligand effects, substrate structure and mechanism in gold catalysis, using specific examples of ligand design and reactions mediated by gold–oxonium intermediates. Shin reviews reactions in which alkynes serve as synthons for reactive gold carbene intermediates, an approach that has yielded

numerous routes to complex organic molecules without the need for problematic diazo reagents as carbene precursors. Paiote and Aponick provide an account of gold-catalyzed transformations of unsaturated alcohols, an important reaction class in which π-activation leads to formal substitution processes via loss of H_2O. A chapter by Michelet surveys the rich area of gold-catalyzed domino processes, in which gold-mediated reactions trigger multistep transformations which can generate significant molecular complexity. On the organometallic side, Jones critically reviews recent studies of the structure and reactivity of gold π-complexes which are model intermediates for gold-catalyzed processes, and Weber and Gagné summarize the current state of knowledge of the effects of aurophilic attraction on gold catalysis. A chapter by Faza and López on computational approaches to the study of homogeneous gold catalysis completes the volume. The latter is sure to be a valuable resource for chemists working in the gold catalysis arena, given the increasingly indispensable role of computational chemistry in deciphering catalytic reaction mechanisms and the difficulty of choosing the proper approach among the growing arsenal of available methods.

It is hoped that this volume will serve as a valuable and timely resource for chemists actively pursuing research in both synthetic applications of homogeneous gold catalysis and fundamental organogold chemistry, as well as for those who are simply interested in following the rich and growing literature of this field.

Denton, TX, USA LeGrande M. Slaughter
September 2014

Contents

Top Curr Chem (2015) 357: 1–24
DOI: 10.1007/128_2014_592

Published online: 24 February 2015

Ligand Design in Gold Catalysis and Chemistry of Gold–Oxonium Intermediates

Deepika Malhotra, Gerald B. Hammond, and Bo Xu

Abstract Gold catalysis is considered one of the most important breakthroughs in organic synthesis during the last decade. Many gold-catalyzed reactions suffer from high catalyst loading, which is a serious limitation on the application of gold catalysis in larger scale synthesis. Because ligands play a major role in the tuning of reactivity of transition metal catalysts, there has been an increased effort on rationally understanding ligand effects in gold catalysis and using a rational ligand design to achieve higher efficiency. In the first part of this chapter, selected examples of ligand design in gold catalysis are discussed. In the second part, the chemistry of gold–oxonium intermediate is examined. An oxonium intermediate is generated when a oxygen nucleophile (ketone, aldehyde, or ether) attacks a cationic gold-activated multiple bond. This oxonium intermediate, being a highly energetic species, has the potential to undergo further transformations such as electron transfer/rearrangement/protodeauration to form diverse products.

Keywords Benzannulations • Cationic gold catalysis • Ligand design • Oxonium intermediates

Contents

D. Malhotra, G.B. Hammond (✉), and B. Xu (✉)
Department of Chemistry, University of Louisville, Louisville, KY 40292, USA
e-mail: gb.hammond@louisville.edu; bo.xu@louisville.edu

1 Ligand Design in Cationic Gold Catalysis

1.1 Introduction

There has been an exponential increase in the number of studies on homogeneous gold catalysis during the past decade [1–12]. Cationic gold species are regarded as the most powerful catalysts for the electrophilic activation of alkynes toward a variety of nucleophiles [2, 4–10, 13, 14]. The reason for this success can be attributed to the lower LUMO and poor back-donation of the cationic gold species [15–18]. On the other hand, the low turnover numbers observed in gold-catalyzed reactions have limited the applicability of gold catalysts in fields such as medicinal chemistry and material synthesis. Gold being a precious metal, it is difficult to recycle after each reaction; the common practice is to use 5% loading, which makes its use often impractical in larger scale synthesis. In contrast, in many palladium-catalyzed coupling reactions, such as the Suzuki reaction, the catalyst loading has been reduced to ppm levels [19].

Ligands play a major role in the tuning of reactivity of transition metal catalysts [20–22]. Initially, because of the complexity of gold-catalyzed reactions, a rational understanding of ligand effects lagged behind the development of a large number of gold-catalyzed transformations, and the development of new catalysts and reactions mostly relied upon trial and error [5]. However, in the last few years, more effort was made to achieve a rational understanding of ligand effects in gold catalysis and the use of a rational ligand design to achieve higher efficiency (TON). There has also been progress in the design of chiral ligands for enantioselective gold catalysis, but, because of page limitations, the development of chiral ligands is not covered in this chapter [23].

1.2 Ligand Effects in Gold Catalysis

1.2.1 Ligand Effects in Each Stage of the Gold Catalytic Cycle

Hammond and Xu conducted a relatively comprehensive investigation of ligand effects in gold catalysis in 2012 [24]. It is generally accepted that most gold-catalyzed reactions go through three major stages (Scheme 1). In stage 1, a nucleophile attacks an $[L–Au]^+$-activated alkyne (or alkene) to form a *trans*-alkenyl gold complex intermediate **B** (or an alkyl gold complex in the case of alkenes). In stage 2, the resulting vinyl complex **B** reacts with an electrophile (E^+), usually a proton, to yield the final product via protodeauration, which also regenerates the cationic gold species (Scheme 1). Additionally, in almost all gold-catalyzed reactions, decay or deactivation of the gold catalyst takes place (stage 3) [25]. In some gold-catalyzed reactions, the formation of off-cycle gold species such as bis-Au-vinyl species **D** was observed [26]. As in the decay of cationic gold catalysts, off-cycle gold species also reduce the turnover of product formation.

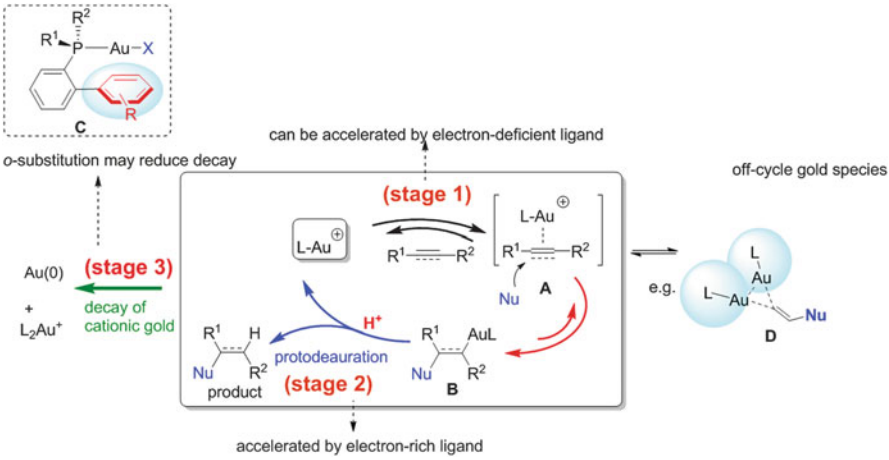

Scheme 1 Typical gold catalytic cycle

Hammond and Xu [24] found that electron-poor ligands (e.g., (p-$CF_3C_6H_4)_3P$) accelerated the electrophilic activation of an alkyne/alkene and corresponding nucleophilic attack (stage 1). This effect may be because electron-poor ligands generate a more electron-poor gold center, which in turn pulls electron density from the alkyne/alkene to make it more electrophilic. In stage 2 (protodeauration), the ligand effect is completely different: electron-rich ligands accelerate this step because protodeauration involves the protonation of **B** and regeneration of cationic gold, and therefore an electron-rich ligand capable of supplying electronic density to the gold metal center turns the vinyl gold complex **B** more reactive towards an electrophile (H^+). In stage 3 (decay of gold catalyst), *ortho*-substitution in the phosphine ligand greatly enhances the stability of the cationic gold (see the *o*-biphenyl motif in **C**, Scheme 1). Most likely, steric effects of *ortho*-substitution are responsible for the higher stability of gold(I) complexes. The unique geometry of the *ortho*-substituted phenyl ring may play an important role – an *ortho*-substituted phenyl ring or other groups very close to the gold center may protect it from decay [25]. According to a crystal structure obtained by Echavarren [27], the average distance between an *ortho* phenyl ring and the gold center is short (around 2–3 Å; see **C** in Scheme 1).

1.2.2 Categorization of Gold-Catalyzed Reactions

Based on the ligand effects shown in Scheme 1, two scenarios are possible in gold-catalyzed reactions [24].

In type I gold-catalyzed reactions, the nucleophilic addition to alkyne/allene/alkene (stage 1) is the turnover limiting stage; therefore, electron-poor ligands ought to speed-up type I reactions. Type I usually happens when the nucleophile

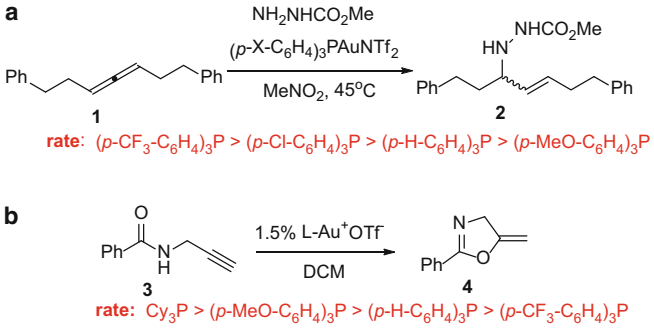

Scheme 2 Typical type I and type II gold-catalyzed reactions

is relatively weak (electron-poor amines and amides) or the substrate is a less reactive allene or alkene. A typical example – hydroamination of allenes – is shown in Scheme 2a [28]. Indeed, electron-poor ligands give faster reaction rates (Scheme 2a).

In type II gold-catalyzed reactions, the regeneration of cationic gold catalyst (e.g., protodeauration) (stage 2) is the turnover-limiting stage. Electron-rich ligands ought to facilitate this type of reaction. Type II reactions usually happen when the nucleophile is relatively strong and the substrate is a relatively reactive alkyne. A typical example – cyclization of propargyl amide – is shown in Scheme 2b [24]. Indeed, electron-rich ligands give faster reaction rates.

In theory, we should design/select electron-poor ligands for type I reactions and design/select electron-rich ligands for type II reactions. In addition, because for many reactions the decay of cationic gold is significant, we also should add special steric handles to the ligands to minimize the catalyst decay. An ideal steric handle should be able to embed or surround the cationic gold center, which may slow down catalyst decay [25]. *Ortho*-substituted phenyls in phosphine ligands are good candidates (Scheme 1). A ligand-embedded gold catalyst may also discourage the formation of off-cycle gold species such as the bis-Au-vinyl species (**D** in Scheme 1) [26].

1.3 Selected Examples of Ligand Design in Gold Catalysis

1.3.1 Electron-Poor Ligands

For type I reactions, stage 1 (the nucleophilic addition to alkyne/allene/alkene) is the turnover-limiting stage of the catalytic cycle. According to the discussion above, electron-poor ligands are helpful.

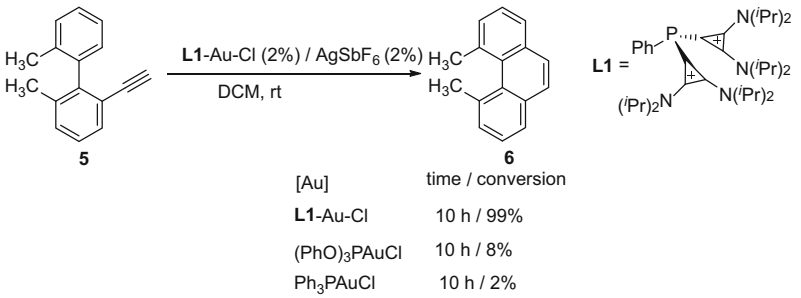

Scheme 3 Electron-poor polycationic ligand and its application (conversion values are estimated from graph in the original report)

Electron-Poor Polycationic Ligands

Most ligands are anionic or neutral; cationic ones are rare. In theory, polycationic substituents make the ligand more electron-poor, ideal for type I gold-catalyzed reactions. Alcarazo and coworkers [29, 30] developed a dicationic phosphine with no spacer between the phosphorus atom and the two positively charged groups (Scheme 3). These polycationic ligands are more electron-poor than phosphites and are comparable to highly electron-poor ligands such as PF_3 or $P(CF_3)_3$, which are toxic or pyrophoric compounds and therefore rarely used in synthesis. Polycationic ligand **L1** has been used to synthesize very sterically-hindered and naturally occurring 4,5-disubstituted phenanthrenes, providing much faster conversion than electron-poor ligands such as $(PhO)_3P$ (Scheme 3).

1.3.2 Electron-Rich Ligands

The turnover limiting stage in the majority of gold-catalyzed reactions may be stage 2 [24, 31]. According to Scheme 1 and the categorization of gold-catalyzed reactions, for type II reactions (where stage 2, protodeauration, is the turnover-limiting stage), electron-rich ligands with special steric handles such as *ortho*-substituted phenyls are preferred.

Electron-Rich Carbene-Based Ligands

Carbene-based ligands (e.g., N-heterocyclic carbene) have been used extensively in gold catalysis because of their unique electronic and steric features [32]. Hashmi and coworkers [33] prepared acyclic carbene (NAC) (**L2** and **L3**) mononuclear homogeneous gold catalysts. Very high turnover numbers have been achieved in the intramolecular addition of diol to alkyne **9** using only 0.000001 mol% of this catalyst (Scheme 4). The acyclic carbene (NAC) ligands **L2** or **L3** are highly electron-rich, and the steric hindrance of R^1, R^2, and the bulky silsesquioxane

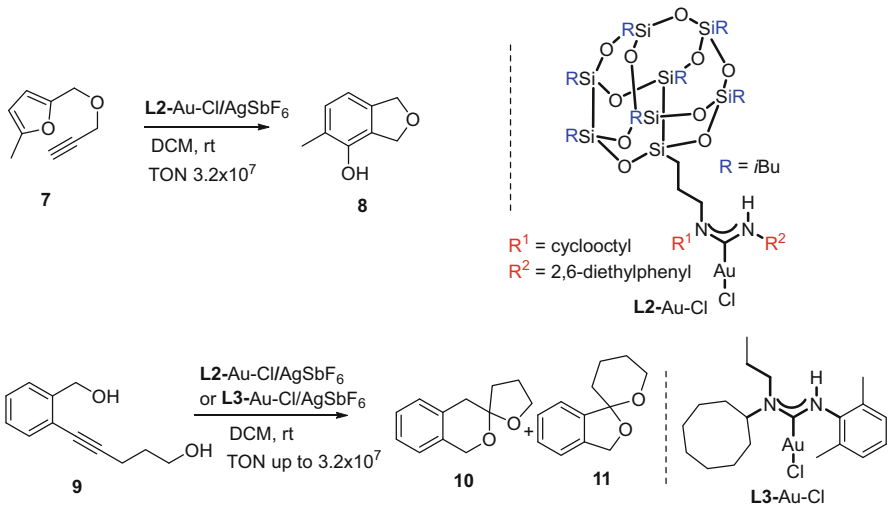

Scheme 4 Electron-rich NAC ligand-based gold catalysts

groups may have a stabilizing effect for the cationic gold catalyst and may discourage the formation of off-cycle gold species such as the bis-Au-vinyl species.

Bertrand and coworkers have also developed electron-rich cyclic carbene-based ligands in gold catalysis [34–36]. For example, hydroamination of alkynes and allenes with parent hydrazine are difficult processes, but a gold catalyst based on electron-rich and sterically-hindered cyclic carbene ligand (**L4**) can efficiently catalyzed this process (Scheme 5).

Electron-Rich BisPhePhos XD Phosphine Ligand

The Hammond and Xu group has developed a broadly applicable, readily prepared cationic gold pre-catalyst BisPhePhos XD gold(I) chloride which is efficient at low loading level and mild reaction temperature. The BisPhePhos XD (**L5**) ligand includes two electron-rich *ortho*-biphenyl motifs and one electron-rich cyclohexyl group. The crystallographic structure of **L5**-AuCl (Fig. 1)[1] demonstrated that the two *ortho*-biphenyl motifs were able to surround or embed the gold center. Because off-cycle gold species bis-Au-vinyl species **D** [26] (Scheme 1) is common in many gold-catalyzed reactions, two sterically-demanding biaryls on the phosphine ligand surrounding the gold center may discourage the formation of **D**.

A comparison between **L5** and other benchmark ligands is shown in Table 1. The IPr = 1,3-bis(2,6-diisopropylphenyl)imidazol-2-ylidene) based gold catalyst was

[1] Cambridge Crystallographic Data Centre (CCDC) depository # 973355.

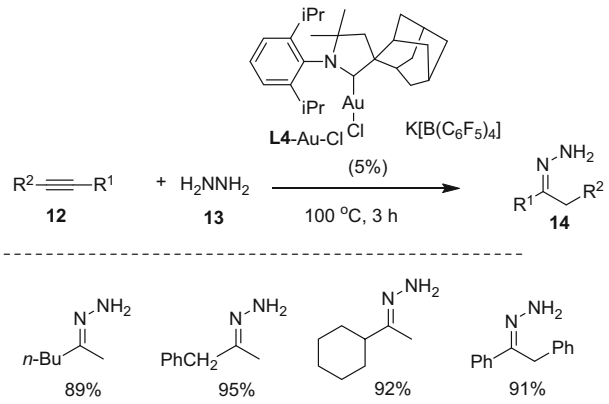

Scheme 5 Intramolecular addition of parent hydrazine to alkynes

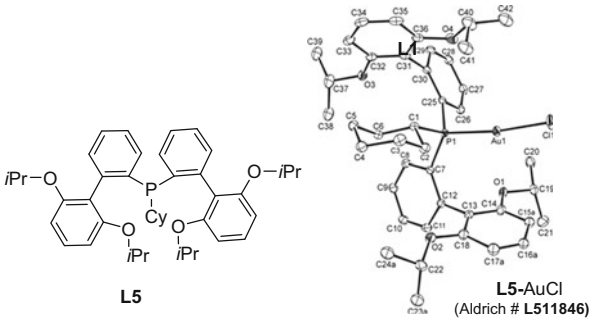

Fig. 1 Highly efficient and broadly applicable BisPhePhos XD gold(I) chloride

selected as a yardstick because of its proven efficiency towards gold-catalyzed reactions. **L5** was the most reactive ligand (Table 1). The **L5** based gold catalyst yields high turnover numbers (very low catalyst loading), in the ppm range, under mild conditions, such as room temperature or slightly elevated temperatures ($\leq$50°C) in many common gold-catalyzed reactions (Scheme 6). Examples include intra- and intermolecular X–H (X=C, N, O) additions to alkynes, cycloisomerizations of enyne, and others (Scheme 6). Potentially, **L5** could be used in larger scale synthesis (because of its ppm level loading) and in the synthesis of complex molecular targets (because of mild reaction conditions, room temperature to 50°C).

Electron-Rich P,N-Ligand

Stradiotto and coworkers reported a stereo- and regioselective gold-catalyzed hydroamination of internal alkynes with dialkylamines using an electron-rich P, N-ligand (**L6**). Substrates with a diverse range of functional groups on both the

Table 1 Relative rates of hydroamination for various ligands

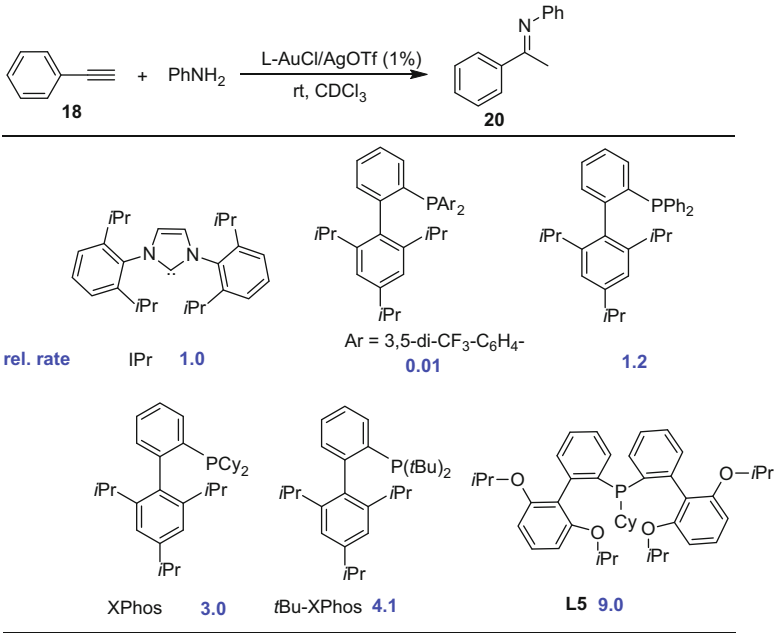

amine (ether, sulfide, N-Boc amine, fluoro, nitrile, nitro, alcohol, N-heterocycles, amide, ester, and carboxylic acid) and alkyne (ether, N-heterocycles, *N*-phthalimide amines, and silyl ethers) are well tolerated (Scheme 7). The high efficiency of **L6** may come from a combination of its high electron density (two electron-rich 1-adamantyl groups and one *ortho*-dialkylamino group) and the high steric hindrance.

Electron-Rich Carba-Closo-Dodecaborateanionic Ligand

Lavallo and coworkers developed a hyperhalogenated carba-closo-dodecaborate anionic ligand (Scheme 8) [37]. This single-component zwitterionic gold catalyst is formed by the coordination of a phosphine ligand bearing an inert and non-coordinating carborane anionic substituent ($CB_{11}Cl_{11}^-$). The highest turnover number observed for hydroamination with this catalyst exceeded 95,000. One unique feature of this ligand is its anionic substituent ($CB_{11}Cl_{11}^-$). Compared to commonly used aryl or alkyl groups, the $CB_{11}Cl_{11}^-$ anion may supply more electron density to the phosphine center, so this ligand is more electron-rich than most commonly used ligands. The $CB_{11}Cl_{11}^-$ anion is also highly steric. The high efficiency of this ligand may come from a combination of its high electron density and the high steric hindrance of $CB_{11}Cl_{11}^-$.

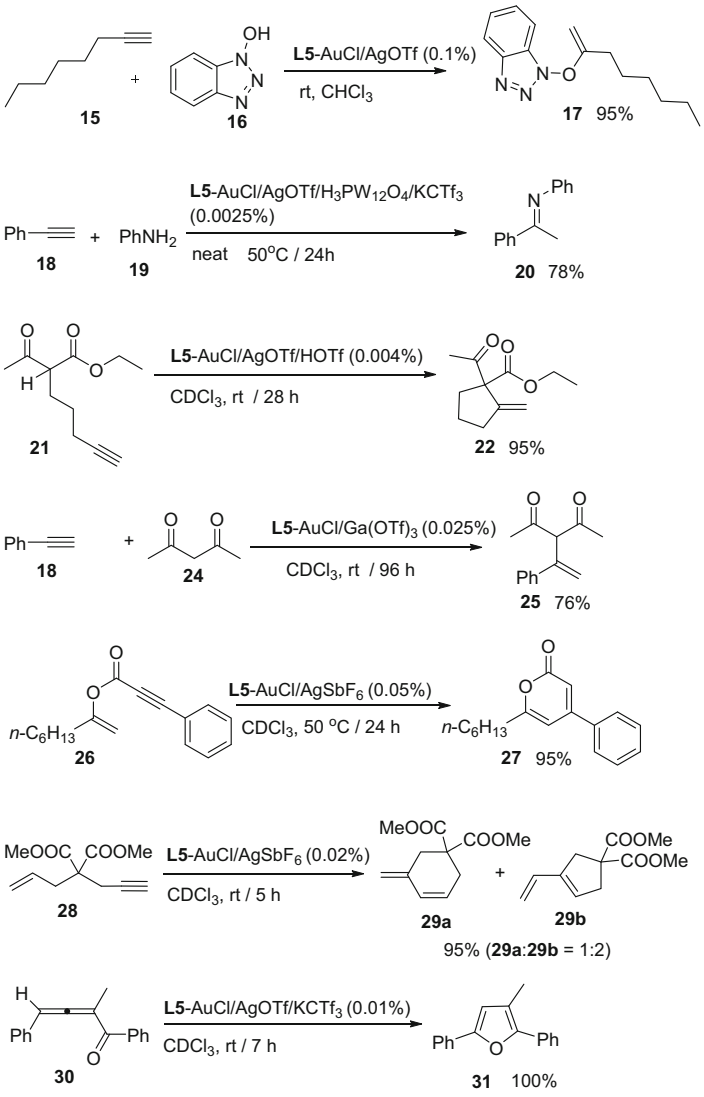

Scheme 6 Use of electron-rich BisPhePhos XD ligand in various gold-catalyzed reactions

Electron-Rich Multi-Functional Biarylphosphine Ligand

Zhang and coworkers [38] developed a novel ligand based on the (1,10-biphenyl)-2-ylphosphine framework which may dramatically lower the catalyst loading. In their design, an amide group at the 3′-position of the ligand framework directs and promotes nucleophilic attack at the ligand gold complex-activated alkyne. The **L7** gold(I) complex is highly efficient in catalyzing acid addition to alkynes, with a

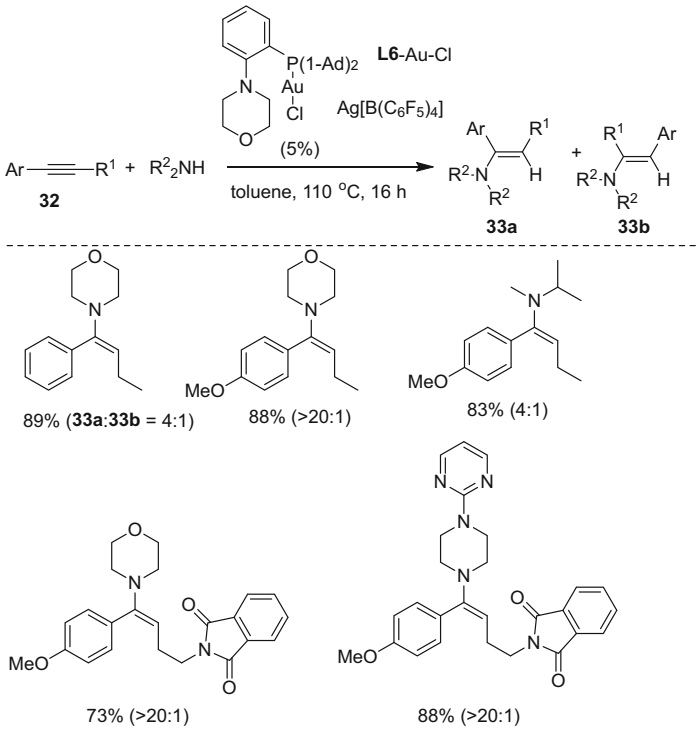

Scheme 7 Gold-catalyzed hydroamination of internal alkynes with dialkylamines

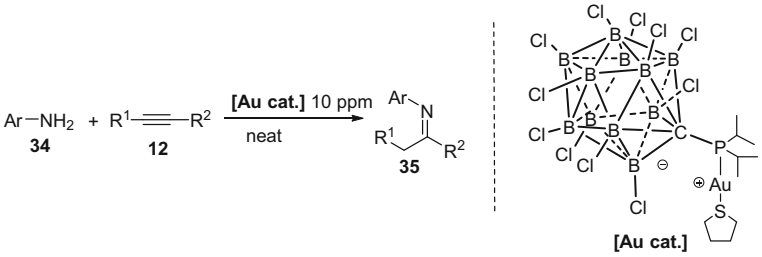

Scheme 8 Intermolecular hydroamination of alkynes with primary amines using gold catalyst having halogenated carba-closo-dodecaborate anions as ligand substituents

turnover number of up to 99,000. Density functional theory calculations support the role of the amide moiety in directing the attack of carboxylic acid via hydrogen bonding (Scheme 9).

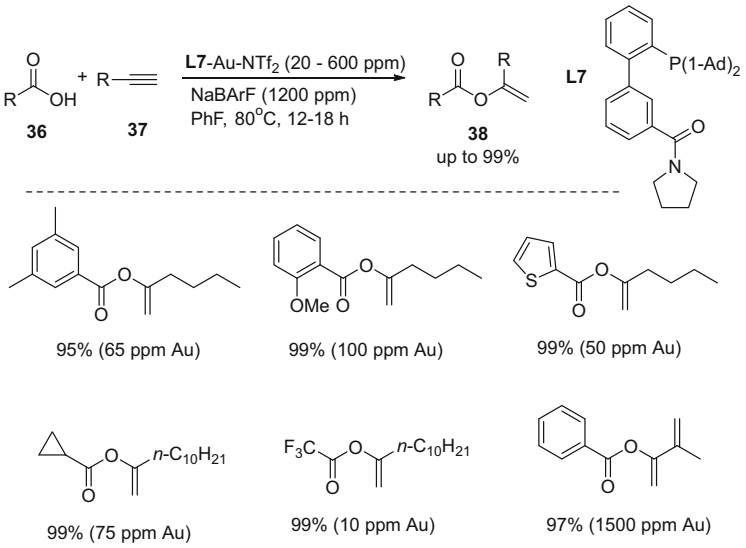

Scheme 9 Electron-rich multi-functional biarylphosphine ligand

2 Chemistry of Gold–Oxonium Intermediates

2.1 Introduction

From a mechanistic point of view, when a carbonyl oxygen nucleophile (ketone, aldehyde) attacks a cationic gold-activated multiple bond, an oxonium intermediate **E** is generated. This oxonium intermediate **E**, being a highly energetic species, has the potential to undergo further transformations such as electron transfer/rearrangement/protodeauration to form diverse products (Scheme 10, top). Similarly, when an oxygen nucleophile such as ether/epoxide attacks a cationic gold-activated multiple bond, an oxonium intermediate **F** is generated, which may also undergo further transformations to furnish synthetically useful products (Scheme 10, bottom). Because large numbers of gold-catalyzed reactions involve oxonium intermediates, only typical examples are reviewed in this chapter.

2.2 Chemistry of Gold–Oxonium Intermediates Derived from Carbonyl Compounds

First, we discuss selected reactions involving gold–oxonium intermediate **E** (Scheme 10, top). An early example of a gold-catalyzed reaction which involves gold–oxonium **E** is the intramolecular cycloisomerization of propargyl ketone **39** (Hashmi and coworkers, in 2000) (Scheme 11) [39]. The coordination of gold(III)

Scheme 10 Oxonium intermediates in gold catalysis

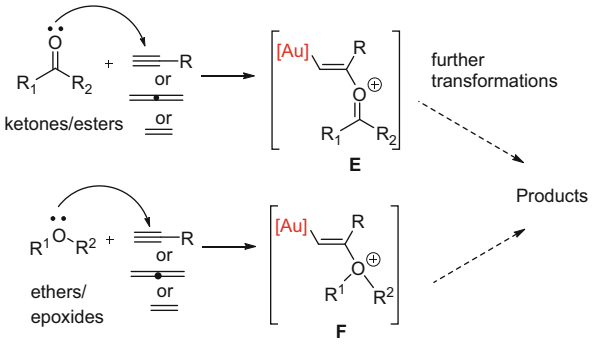

Scheme 11 Cyclo isomerization of propargyl ketone **39**

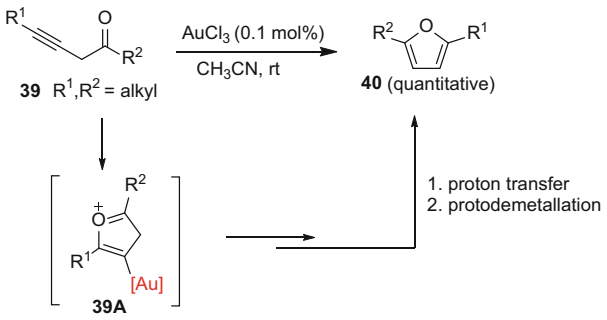

catalyst activates the alkyne moiety, which is then followed by nucleophilic attack of the carbonyl oxygen to form gold–oxonium intermediate **39A**, which, in turn, undergoes proton transfer/protodemetalation to afford a furan substrate.

The gold-catalyzed synthesis of substituted cyclic enones **41** from tethered alkynyl ketones **16** was reported by Yamamoto and coworkers in 2007 (Scheme 12) [40]. The gold-activated alkyne is attacked by the carbonyl oxygen to form an oxonium intermediate **41A**, which subsequently undergoes electron transfer and ring opening to furnish cyclic enones **42** in good yield. Later, Yamamoto and coworkers developed another gold-catalyzed cascade reaction towards the synthesis of polycyclic enones **43** [41].

In 2010, Hammond and coworkers developed an intramolecular gold-catalyzed oxygen transfer reaction of 2-alkynyl-1,5-diketones **44** to furnish cyclopentenyl ketones **45** in high yield at room temperature (Scheme 13) [1, 3]. Their mechanistic investigations, based on both quantum chemical calculations and ^{18}O isotopic experiments, revealed that the five-membered oxonium intermediate **44A** is the preferred intermediate, which then undergoes a novel [4+2] cycloaddition followed by rearrangement to afford cyclopentenyl ketones **45**.

A tandem heterocyclization/Nazarov reaction which furnished fused furan carbocycles **46** was reported in 2011 by Manoharan and coworkers (Table 2) [42]. In this transformation, the oxonium intermediate **46A** could be trapped by

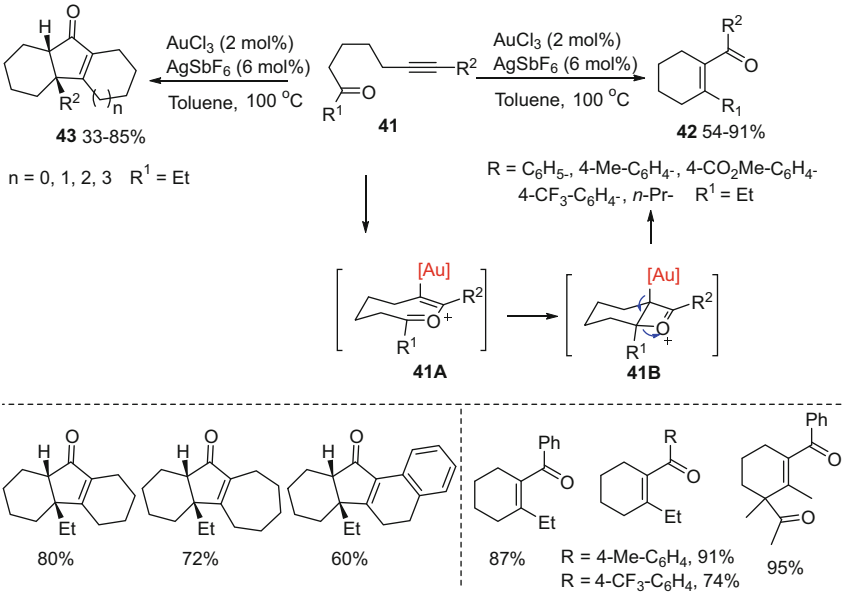

Scheme 12 Gold-catalyzed synthesis of substituted cyclic enones

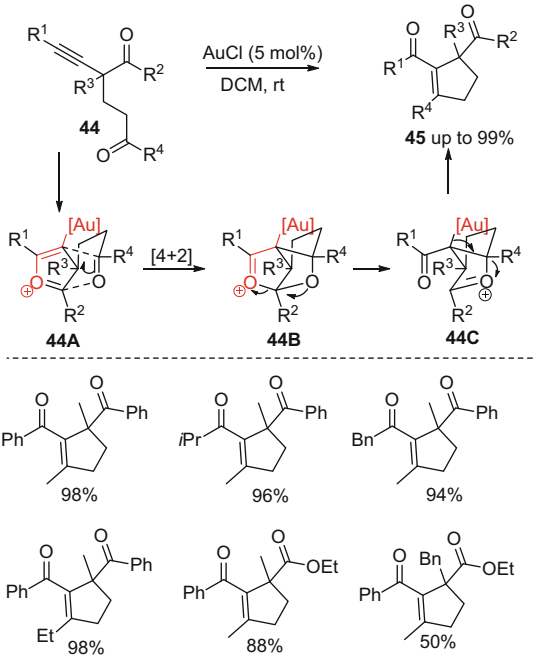

Scheme 13 Intramolecular oxygen transfer reactions of **44**

Table 2 Tandem heterocyclization/Nazarov reaction of **46**

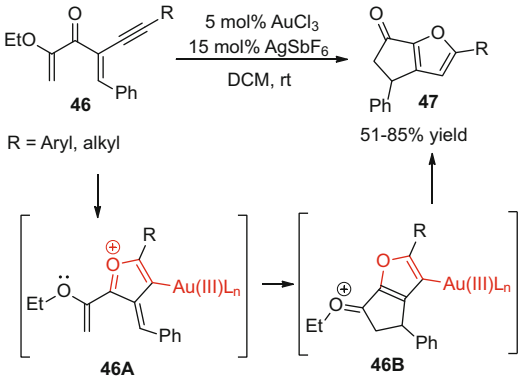

Entry	R	Time	**47** (%)
1	Phenyl	3 h	67
2	*p*-Methoxyphenyl	5 min	75
3	*p*-Nitrophenyl	36 h	54
4	*p*-Fluorophenyl	18 h	60
5	α-Naphthyl	24 h	52
6	1-Cyclohexenyl	6 h	51
7	*n*-Butyl	12 h	85

2 equiv. of methanol. The intermediate **46A** undergoes a Nazarov cyclization to form intermediate **46B**, which eventually forms the final fused furans **47**. Moran and coworkers [43] also discovered a strategy for the synthesis of substituted furans by the cycloisomerization of β-alkynyl β-ketoesters **48** (Scheme 14). In this cycloisomerization, the intramolecular attack of the carbonyl oxygen to the activated alkyne gives the oxonium intermediate **48A**, which then undergoes protodeauration and isomerization to yield substituted furans **49**.

A gold-catalyzed three-component coupling reaction was developed by Dong and coworkers for the synthesis of substituted furans **51** (Scheme 15) [44]. First, phenyl glyoxal **50**, amine, and alkyne undergo a Mannich–Grignard-type reaction to give propargyl amine **50-Int**. Then a nucleophilic attack of the carbonyl oxygen in **50-Int** to an alkyne generates an oxonium intermediate **50A**, which then undergoes deprotonation/demetalation to afford furan derivatives **51**.

Gold-catalyzed benzannulations have been well studied by Yamamoto and coworkers [45, 46]. 2-Alkynyl benzaldehydes **52** react with cyclization partners such as alkynes or aldehydes to furnish naphthalene derivatives **53** or **54** (Scheme 16). First, the intramolecular nucleophilic attack of carbonyl oxygen to alkyne generates oxonium intermediate **52A**. When an alkyne is used as cyclization

Scheme 14 Cyclo isomerization of **48**

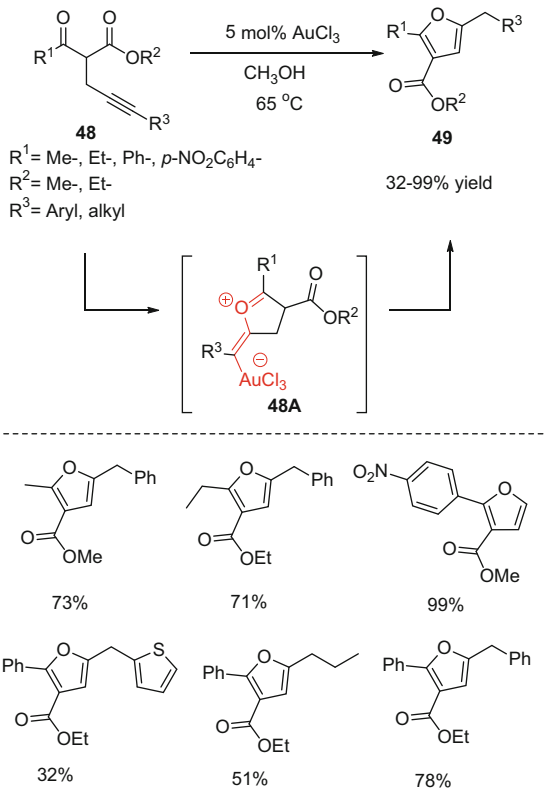

partner, **52A** undergoes [4+2] cycloaddition with the alkyne to generate intermediate **52B**, which subsequently rearranges to afford naphthalenes **53**. When an aldehyde is used as cyclization partner, intermediate **52A** undergoes inverse electron demand Diels–Alder reaction with an aldehyde to generate intermediate **52C**, which further rearranges to furnish naphthalene derivatives **54**.

Similarly, Hammond and coworkers reported a gold-catalyzed annulation of 2-alkynyl benzaldehyde **52** with vinyl ether to furnish substituted isochromene **55** and dihydronaphthalene **55′** (Scheme 17). The mechanism also involves the generation of common oxonium intermediate **52A**, which then undergoes Diels–Alder cyclization with vinyl ether to generate isochromene **55** and dihydronaphthalene **55′** via intermediate **52D** and **52E**, respectively.

Hammond and coworkers reported a gold-catalyzed intramolecular annulation of 2-(ynol)aryl aldehydes or ketones **56**, which gave access to benzochromanes **58** or benzobicyclo[4.3.1]acetals **57** [47]. In a plausible mechanism, the oxonium intermediate **56A** undergoes a series of rearrangements, followed by intramolecular aldol reaction and dehydration to yield benzochromanes **58**. However, intermediate **56A** can also undergo cyclization followed by protodeauration to yield **57** (Scheme 18).

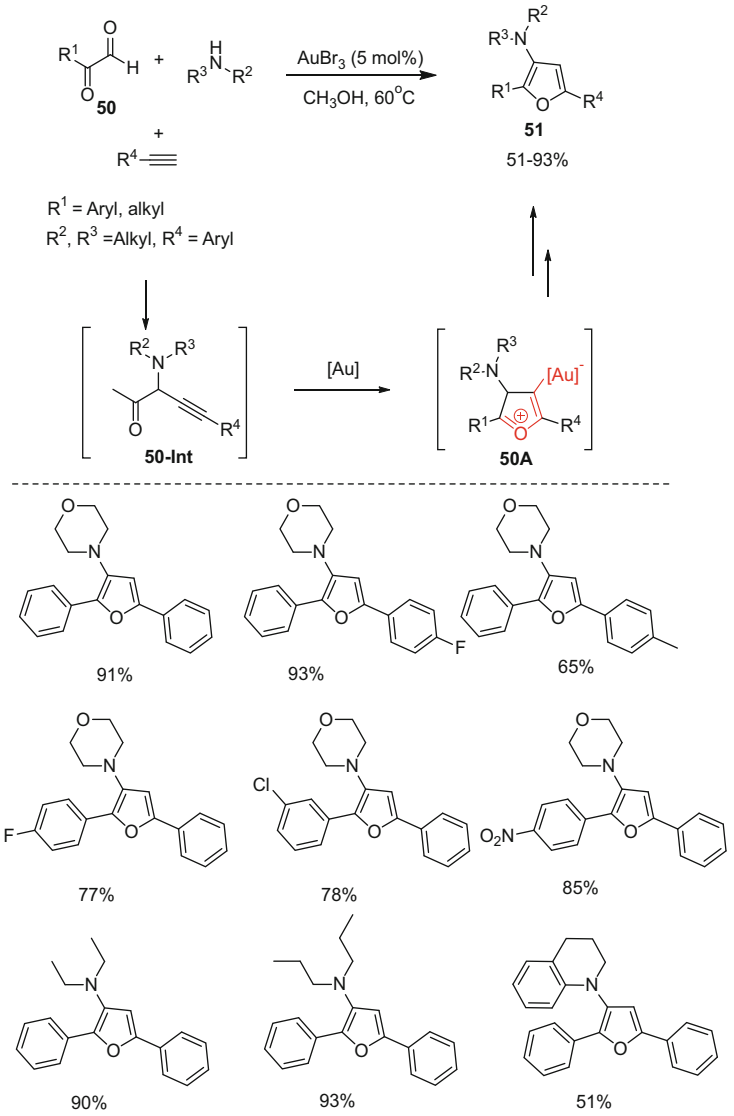

Scheme 15 Gold-catalyzed three component formation of furans **51**

2.3 Chemistry of a Gold–Oxonium Intermediate Derived from Ethers/Epoxides

A gold-catalyzed isomerization of alkynyloxiranes **59** to furans **60** (Scheme 19) was reported by Hashmi and coworkers in 2004 [48]. In the proposed mechanism, the gold catalyst activates the triple bond, followed by nucleophilic attack of the

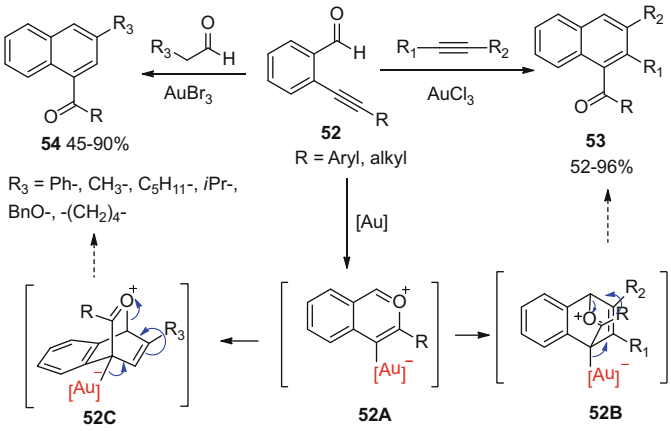

Scheme 16 Benzannulation of *o*-alkynylbenzaldehydes

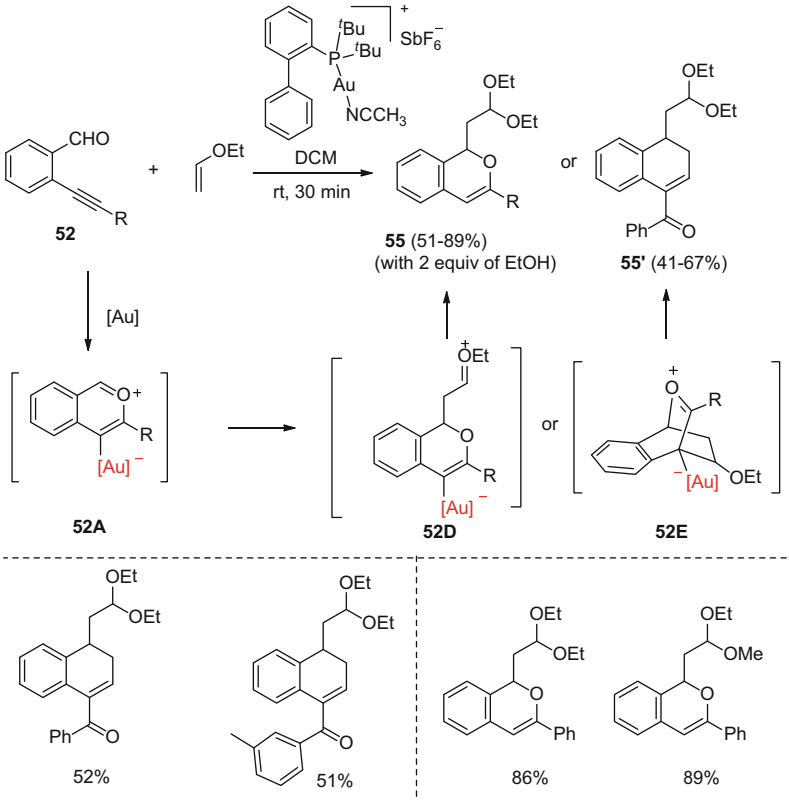

Scheme 17 Gold-catalyzed benzannulations of alkynylaldehydes **52**

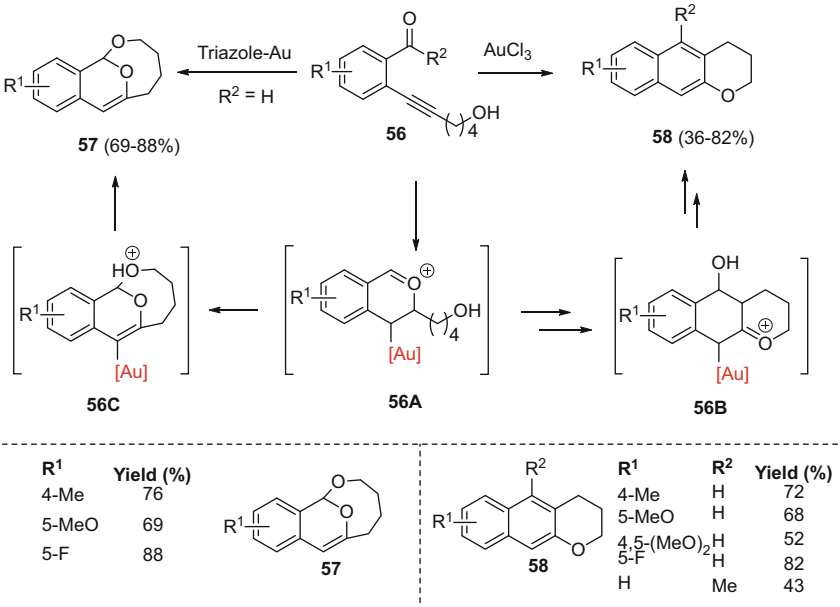

Scheme 18 Gold-catalyzed intramolecular annulations of **56**

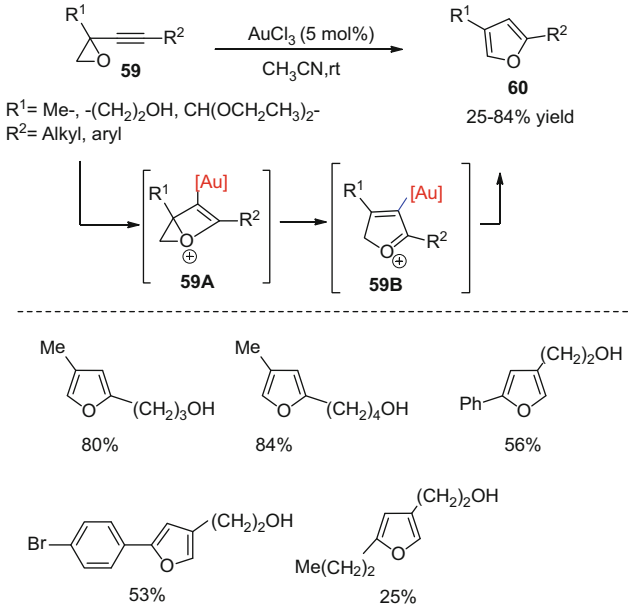

Scheme 19 Isomerization of alkynyloxiranes **59**

epoxide oxygen at the distal position of the activated alkyne to generate a five-membered oxonium intermediate **59A**, which then undergoes deprotonation/protodemetalation to yield substituted furans **60**.

Hashmi and coworkers [49] later reported another chemoselective one-pot synthesis of benzofurans **62** from alkynyl-7-oxabicyclo[4.1.0]heptan-2-one **61** (Scheme 20). The addition of the carbonyl oxygen nucleophile to the gold-activated triple bond generates the cyclic oxonium intermediate **61A**, which subsequently undergoes 1,2-hydride shift followed by sequential rearrangements to give **61B**; elimination of methanol and water yields substituted benzofurans **62**.

Liang and coworkers [50] reported an efficient cycloisomerization of alkynyloxiranes **63** to afford 2,5-disubstituted furans **64** (Scheme 21). The addition of epoxide oxygen to gold-activated alkyne generates oxonium intermediate **63A**; this intermediate then undergoes protonation to give 2,3-dihydrofuran, followed by reductive elimination to yield 2,5-disubstituted furans **64**. Later, Liang and coworkers [51] reported a tandem cyclization/Friedel–Crafts reaction to furnish furans **66** in good yield (Scheme 22). Similarly, the proposed mechanism for this reaction involves the nucleophilic attack of the epoxide oxygen on the gold-coordinated alkyne to generate gold–oxonium intermediate **65A**. Further transformations of **65A** via protonation, reductive elimination, and intermolecular Friedel–Crafts reaction generate substituted furans **67**.

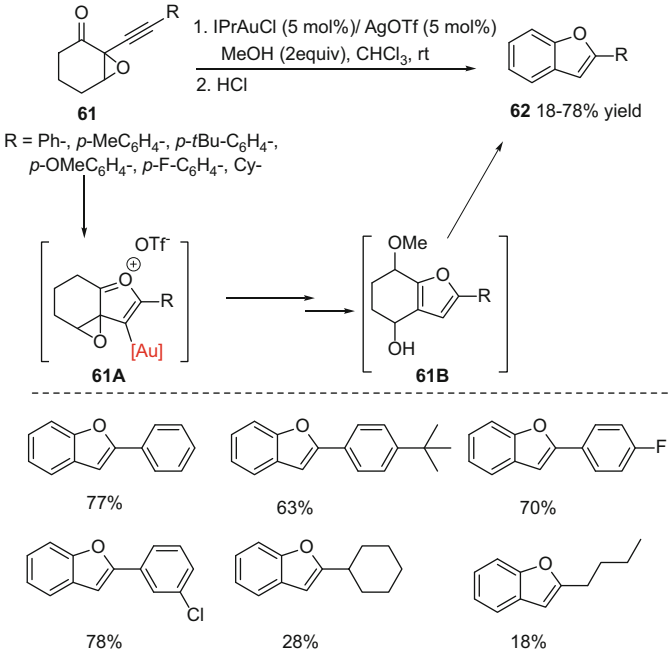

Scheme 20 Chemoselective synthesis of benzofurans **61**

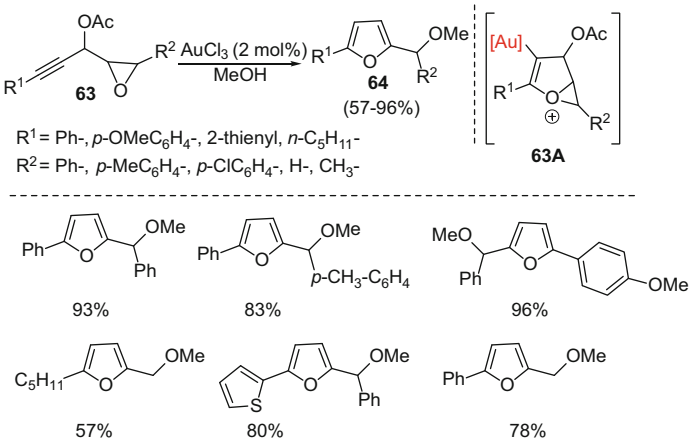

Scheme 21 Chemoselective synthesis of furan **64**

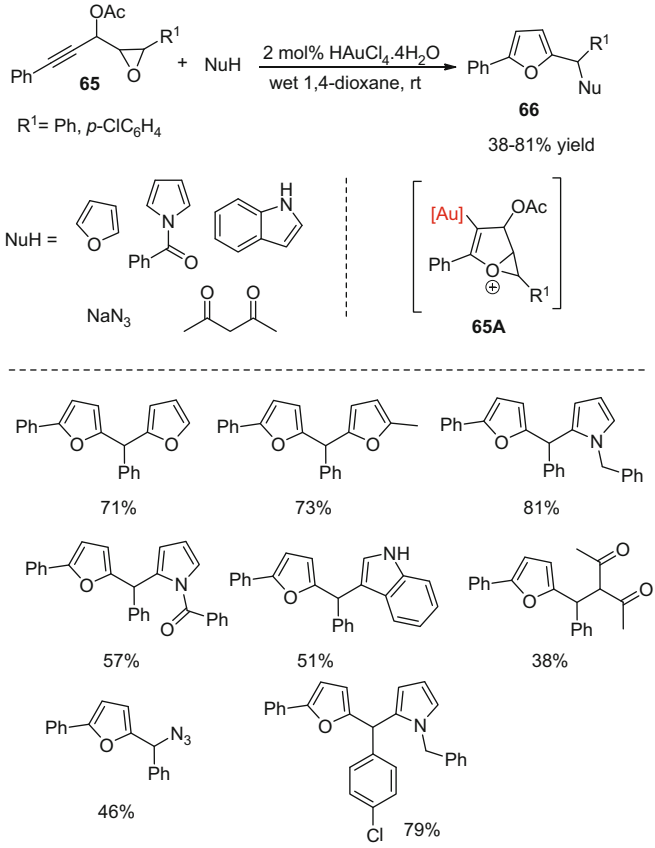

Scheme 22 Cycloisomerization and tandem cyclization/Friedel–Crafts reactions of alkynyloxiranes

Scheme 23 Gold(I)-catalyzed asymmetric carboalkoxylation of propargyl esters **67**

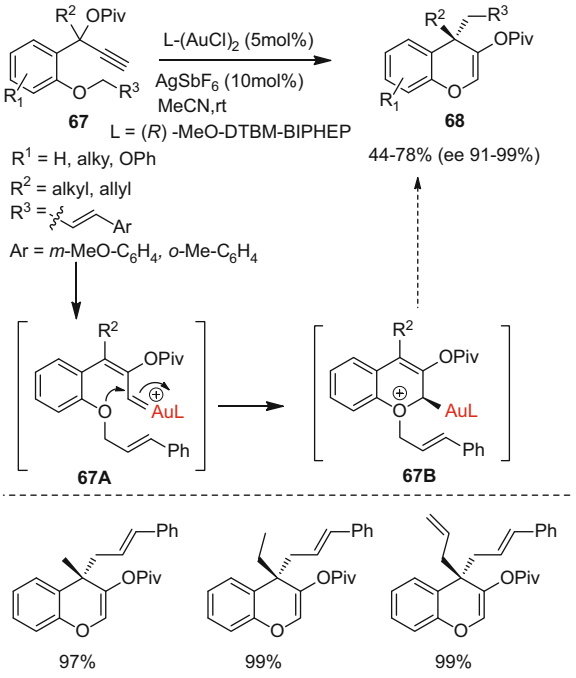

Toste and coworkers reported a gold-catalyzed enantioselective synthesis of benzopyrans **67** containing quaternary stereocenters by the carboalkoxylation reaction of propargyl ester **67** (Scheme 23) [52]. The proposed mechanism involves the formation of gold(I) carbenoid intermediate **67A** followed by nucleophilic attack of the ether oxygen to form gold–oxonium intermediate **67B**, which undergoes rearrangements to furnish benzopyrans **68**.

In 2011, Goualt and coworkers [53] developed a gold-catalyzed intramolecular reaction of allyloxyphenylpropynones **69** to afford chromones **70** (Scheme 24). The gold-activated alkyne moiety is attacked by the ether oxygen to generate the six-membered oxonium ion intermediate **69A** which then undergoes migration of R^1 via carbodemetalation to form substituted chromones **70**.

Scheme 24 Intramolecular reaction of allyloxyphenylpropynones **69**

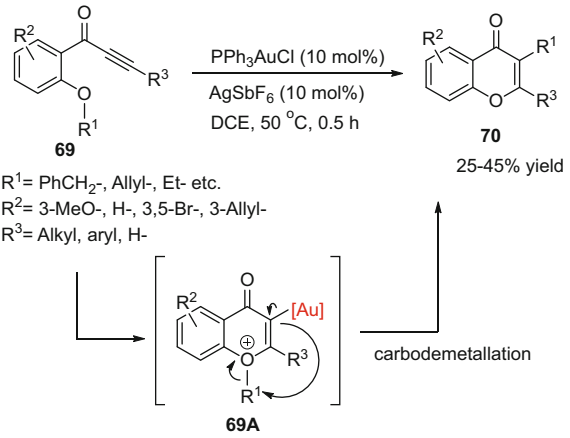

R^1	R^2	R^3	**70** (%)
Ph-CH_2-	3-MeO	*n*-Pr	45
Ph-CH_2-	H	*n*-Pr	31
Ph-CH_2-	3,5-Br	*n*-Pr	40
Ph-CH_2-	3-Allyl	*n*-Pr	38
Ph-CH_2-	H	4-MeOPh	25
Allyl	H	Ph	38
Allyl	H	H	35

Acknowledgements The authors are grateful to the National Science Foundation for financial support (grant CHE 1111316).

References

1. Liu LP, Malhotra D, Jin Z, Paton RS, Houk KN, Hammond GB (2011) Chem Eur J 17:10690
2. Garcia P, Malacria M, Aubert C, Gandon V, Fensterbank L (2010) ChemCatChem 2:493
3. Liu LP, Malhotra D, Paton RS, Houk KN, Hammond GB (2010) Angew Chem Int Ed 49:9132
4. Arcadi A (2008) Chem Rev 108:3266
5. Gorin DJ, Sherry BD, Toste FD (2008) Chem Rev 108:3351
6. Li Z, Brouwer C, He C (2008) Chem Rev 108:3239
7. Hashmi ASK (2007) Chem Rev 107:3180
8. Jimenez-Nunez E, Echavarren AM (2008) Chem Rev 108:3326
9. Hashmi ASK, Rudolph M (2008) Chem Soc Rev 37:1766
10. Widenhoefer RA (2008) Chem Eur J 14:5382
11. Rudolph M (2012) Hashmi. A. S. K. Chem. Soc, Rev
12. Brenzovich WE (2012) Angew Chem Int Ed 51:8933
13. Benitez D, Shapiro ND, Tkatchouk E, Wang Y, Goddard WA, Toste FD (2009) Nat Chem 1:482
14. Teles JH, Brode S, Chabanas M (1998) Angew Chem Int Ed 37:1415
15. Gorin DJ, Toste FD (2007) Nature 446:395
16. Lein M, Rudolph M, Hashmi SK, Schwerdtfeger P (2010) Organometallics 29:2206

17. Pernpointner M, Hashmi ASK (2009) J Chem Theory Comput 5:2717
18. Hertwig RH, Koch W, Schröder D, Schwarz H, Hrušák J, Schwerdtfeger P (1996) J Phys Chem 100:12253
19. Shen Q, Shekhar S, Stambuli JP, Hartwig JF (2005) Angew Chem Int Ed 44:1371
20. Fors BP, Watson DA, Biscoe MR, Buchwald SL (2008) J Am Chem Soc 130:13552
21. Watson DA, Su M, Teverovskiy G, Zhang Y, Garcia-Fortanet J, Kinzel T, Buchwald SL (2009) Science 325:1661
22. Cho EJ, Senecal TD, Kinzel T, Zhang Y, Watson DA, Buchwald SL (2010) Science 328:1679
23. Wang Y-M, Lackner AD, Toste FD (2014) Acc Chem Res 47:889
24. Wang W, Hammond GB, Xu B (2012) J Am Chem Soc 134:5697
25. Kumar M, Jasinski J, Hammond GB, Xu B (2014) Chem Eur J 20:3113
26. Brown TJ, Weber D, Gagné MR, Widenhoefer RA (2012) J Am Chem Soc 134:9134
27. Herrero-Gómez E, Nieto-Oberhuber C, López S, Benet-Buchholz J, Echavarren AM (2006) Angew Chem Int Ed 45:5455
28. Wang ZJ, Benitez D, Tkatchouk E, Goddard Iii WA, Toste FD (2010) J Am Chem Soc 132:13064
29. Carreras J, Gopakumar G, Gu L, Gimeno A, Linowski P, Petuškova J, Thiel W, Alcarazo M (2013) J Am Chem Soc 135:18815
30. Alcarazo M (2014) Chem Eur J 20:7868
31. Malhotra D, Mashuta MS, Hammond GB, Xu B (2014) Angew Chem Int Ed 53:4456
32. Gatineau D, Goddard J-P, Mouriès-Mansuy V, Fensterbank L (2013) Isr J Chem 53:892
33. Blanco Jaimes MC, Böhling CRN, Serrano-Becerra JM, Hashmi ASK (2013) Angew Chem Int Ed 52:7963
34. Lavallo V, Frey GD, Kousar S, Donnadieu B, Bertrand G (2007) Proc Natl Acad Sci U S A 104:13569
35. Zeng X, Kinjo R, Donnadieu B, Bertrand G (2010) Angew Chem Int Ed 49:942
36. Zeng X, Frey GD, Kinjo R, Donnadieu B, Bertrand G (2009) J Am Chem Soc 131:8690
37. Lavallo V, Wright JH, Tham FS, Quinlivan S (2013) Angew Chem Int Ed 52:3172
38. Wang Y, Wang Z, Li Y, Wu G, Cao Z, Zhang L (2014) Nat Commun 5, 3470
39. Hashmi ASK, Schwarz L, Choi J-H, Frost TM (2000) Angew Chem Int Ed 39:2285
40. Jin T, Yamamoto Y (2007) Org Lett 9:5259
41. Jin T, Yamamoto Y (2008) Org Lett 10:3137
42. Krafft ME, Vidhani DV, Cran JW, Manoharan M (2011) Chem Commun 47:6707
43. Rodríguez A, Moran WJ (2011) Tetrahedron Lett 52:2605
44. Li J, Liu L, Ding D, Sun J, Ji Y, Dong J (2013) Org Lett 15:2884
45. Asao N, Takahashi K, Lee S, Kasahara T, Yamamoto Y (2002) J Am Chem Soc 124:12650
46. Asao N, Aikawa H, Yamamoto Y (2004) J Am Chem Soc 126:7458
47. Liu L-P, Hammond GB (2010) Org Lett 12:4640
48. Hashmi ASK, Sinha P (2004) Adv Synth Catal 346:432
49. Wang T, Shi S, Vilhelmsen MH, Zhang T, Rudolph M, Rominger F, Hashmi ASK (2013) Chem Eur J 19:12512
50. Shu X-Z, Liu X-Y, Xiao H-Q, Ji K-G, Guo L-N, Qi C-Z, Liang Y-M (2007) Adv Synth Catal 349:2493
51. Ji K-G, Shu X-Z, Chen J, Zhao S-C, Zheng Z-J, Liu X-Y, Liang Y-M (2009) Org Biomol Chem 7:2501
52. Uemura M, Watson IDG, Katsukawa M, Toste FD (2009) J Am Chem Soc 131:3464
53. Renault J, Qian Z, Uriac P, Gouault N (2011) Tetrahedron Lett 52:2476

Top Curr Chem (2015) 357: 25–62
DOI: 10.1007/128_2014_589

Published online: 18 December 2014

Gold-Catalyzed Carbene Transfer Reactions

Seunghoon Shin

Abstract In homogeneous gold catalysis, generations and reactions of metal carbenes have been one of the most rapidly developing areas because of their diverse reactivity under mild conditions. This review covers recent advances in the gold-catalyzed oxygen atom transfer and carbene transfer reactions to alkynes. Atom transfer to an alkyne enables alkynes to function as metal carbene synthons. Many such reactions fulfill redox neutrality starting from safe and easily handled precursors.

Keywords Carbene transfer, Gold carbene, Gold catalysis, Oxygen atom transfer

Contents

S. Shin (✉)
Department of Chemistry and Center for New Directions in Organic Synthesis, Hanyang University, 133-791 Seoul, South Korea
e-mail: sshin@hanyang.ac.kr

Abbreviations

Ad	1-Adamantyl
cat.	Catalyst
DCE	1,2-Dichloroethane
Dipp	2,6-Diisopropylphenyl
dppm	1,1-Bis(diphenylphosphino)methane
equiv.	Equivalent
IAd	1,3-Bis(1-adamantyl)imidazole-2-ylidene
IMes	1,3-Bis(2,4,6-trimethylphenyl)imidazole-2-ylidene
IPr	1,3-Bis(2,6-diisopropylphenyl)imidazole-2-ylidene
L	Ligand
LG	Leaving group
mCPBA	*m*-Chloroperbenzoic acid
Ms	Methanesulfonyl
OAT	Oxygen atom transfer
pyr	Pyridine
rt	Room temperature
Tf	Trifluromethanesulfonyl

1 Introduction

Among the rapid developments in homogeneous gold catalysis in the past decade, those involving gold carbenes have received increasing attention from the synthetic community. This is because diverse reactivity is displayed under mild reaction conditions and these protocols do not need traditional diazo compounds as precursors to the metal carbenes [1, 2]. Although stabilized diazo compounds with electron-accepting substituents are stable under most reaction conditions, synthesis of functionalized diazo compounds often requires diazo transfer reactions which can involve potential hazards [3] and/or the use of toxic and explosive diazomethane [4]. The ability to utilize stable, readily available and easily handled precursors to gold carbenes should open up new paths to metal carbene chemistry.

This review focuses on the reactions in which oxygen (and other) atoms are transferred to alkynes to form what can be envisioned synthetically as gold carbenes (Scheme 1). Although the nature of such gold carbenes can best be described as Au (I)-coordinated carbocations, the representation of gold carbene with a double bond between Au and carbon is used in this review.

Scheme 1 General reactivity pattern

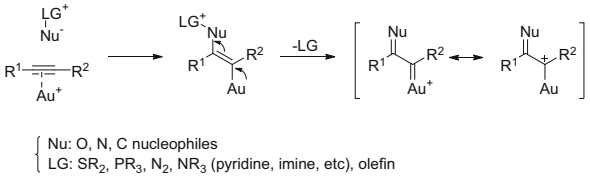

Scheme 2 Other methods of carbene generation not covered in this review

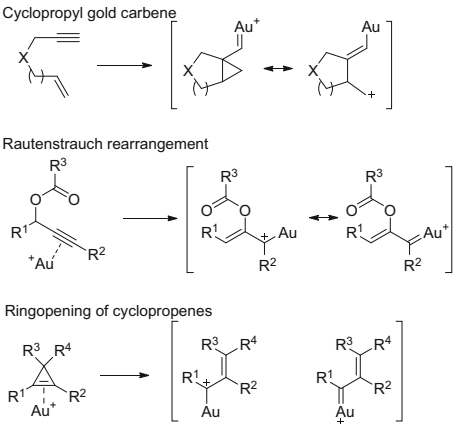

Impressive developments have been made in developing new methods of generating Au-carbenes which are covered according to the type of atom (or carbene) transfer reagents in approximately chronological order. Some of these aspects have been the topic of other recent reviews [5–8]. However, some other important methods of the generation of gold carbenes (Scheme 2) that do not fall into this category (Scheme 1) are not covered in this review [9–11].

2 General Reactivity Pattern

2.1 Nitrene Transfer by Azides and N–N Bond Reagents

A formal nitrene transfer using azides was demonstrated by Toste and coworkers in 2005 [12]. As delineated in Scheme 3, liberation of N_2 gas from the adduct **1** would lead to nitrene transfer forming α-imino Au-carbene **2**. The reactivity pattern between azides and alkynes demonstrated here was the first case of addition of a leaving group (in this case, N_2) bearing a nucleophile onto alkyne, and formed a paradigm for subsequent alkyne oxidation chemistry. Various combinations of nucleophilic atoms and leaving groups (LG) later resulted in a variety of synthetic methods for generation of Au-carbenes via alkyne oxidation. In this particular case, the Au-carbene may evolve via 1,2-H shift into pyrroles or ring expansion via a Wagner–Meerwein shift.

Scheme 3 Nitrene transfer from azide

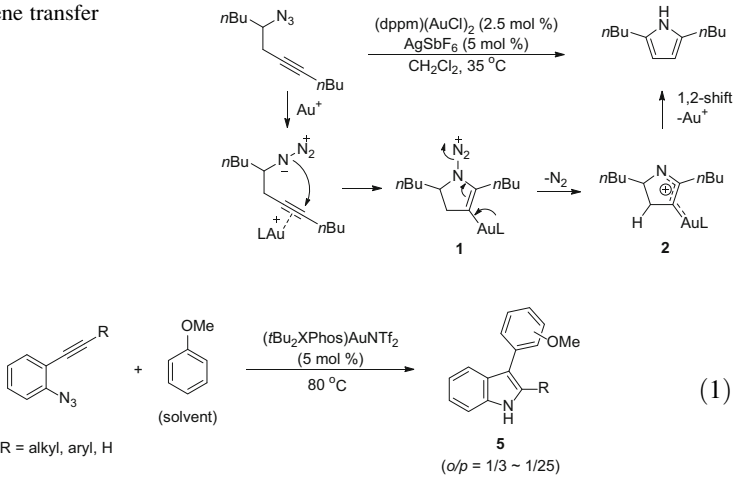

(1)

Later, in 2011, Gagosz and coworkers further developed the azide chemistry for oxindole synthesis (Scheme 4) [13]. The Au-carbene **3** could be intermolecularly trapped by an alcohol (10 equiv.), and the following Claisen rearrangement occurred under relatively mild conditions (50–60°C), providing oxindoles **4** with an α-quaternary center. In the same paper, trapping Au-carbenes with Ar–H was also reported, leading to 3-aryl indoles **5** (Eq. 1). Shortly afterwards, Zhang and coworkers reported similar reactions employing arenes, heteroarenes, and alcohols as nucleophiles [14].

Sulfilimines were shown to be viable intramolecular nitrene donors which can generate α-imino Au-carbene synthons [15]. In 2011, Zhang and coworkers introduced a new nitrene transfer reagent, namely *N*-tosyliminopyridinium ylides **6** which allowed for intermolecular nitrene transfer with activated alkynes, such as ynamides (Scheme 5) [16]. An outer-sphere attack of ylides onto Au-activated alkynes was proposed as the mechanism, similar to that for the reactions of N–O oxidants. The geometry of the imine C=N bond was determined to be (E) based on X-ray crystallographic as well as stereochemical analysis. However, unlike related *N*-oxide oxidations of alkynes ending with 1,2-H (or alkyl) shift, the geometry of the C=C bond was obtained as a mixture.

Shortly afterwards, Davies and coworkers reported a related transfer reagent, pyridine-*N*-aminides **7** (Scheme 6) [17]. In the presence of an N-acyl group which can act as an intramolecular nucleophile, the α-imino Au-carbene **8** can be transformed into oxazoles, which can be envisioned as a formal (3 + 2) cycloaddition between 1,3-N,O dipoles and alkynes. Thus, the reaction of pyridine-*N*-aminides with ynamides occurred intermolecularly in the presence of dichloro (pyridine-2-carboxylato)Au(III) complex, leading to various oxazoles. Chemoselectivity was excellent in favor of the desired oxazole formation in the presence of competing functional groups, such as alkynes and alkenes which are potentially apt for cyclization and cyclopropanation, respectively, or cyclopropyl or alkyl groups at R which can participate in a competitive ring expansion and a

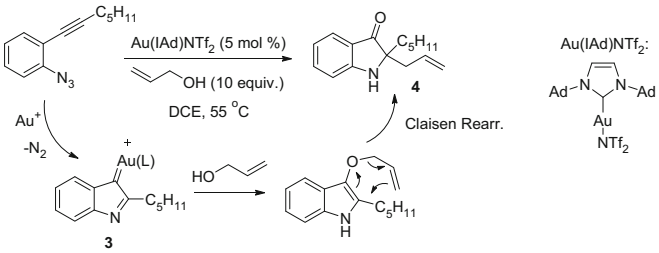

Scheme 4 Cascade nitrene transfer and Claisen rearrangement

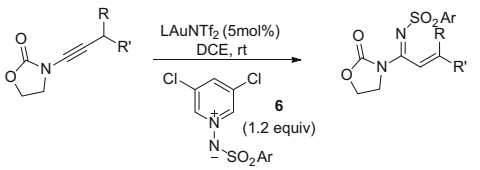

Scheme 5 *N*-Tosyliminopyridinium ylides as nitrene transfer reagents

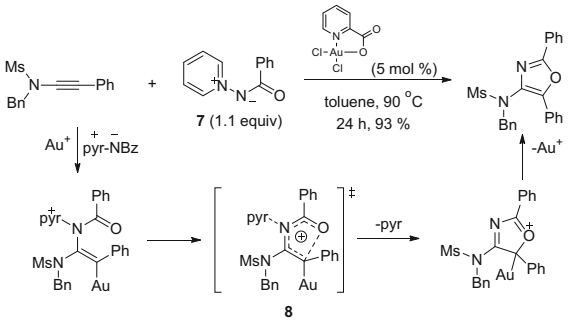

Scheme 6 Pyridine-*N*-aminides as OAT reagents

1,2-insertion, respectively. A gold-carbene route was not favored because of the mechanism based on the absence of 1,2-shift. Instead, a cationic electrocyclization of **8** in concert with N–N cleavage was suggested as a preferred mechanism.

2.2 Oxygen Atom Transfer from Sulfoxides

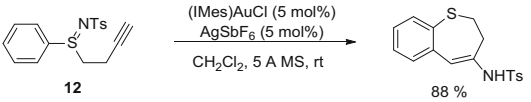

(2)

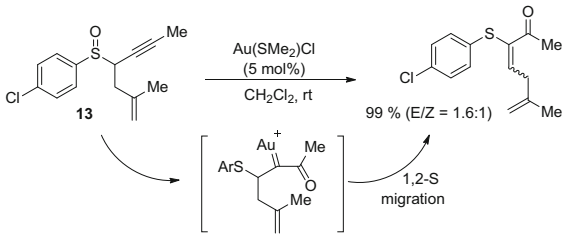

(3)

In 2007, Toste and coworkers reported a pioneering oxygen atom transfer (OAT) chemistry introducing sulfoxides (Scheme 7) [15]. Homopropargyl sulfoxide **9** underwent initial 5-exo-dig O-attack on alkynes and delivered benzothiophenones **10**. The initial addition mode (5-exo-dig vs 6-endo-dig) dictated the outcome of regioselectivity in the alkyne oxidation and the alkyne substituents had a strong influence on the products obtained (**10** or **11**). In addition to this O-transfer chemistry, sulfimine substrates **12** were shown to transfer nitrene equivalent (Eq. 2). For the propargyl sulfoxide substrates **13**, on the other hand, the posited carbene underwent a 1,2-sulfide shift as the major pathway (Eq. 3). Also notable in the last example is that a possible cycloisomerization of 1,5-enynes did not occur, indicating the chemoselectivity of this OAT protocol.

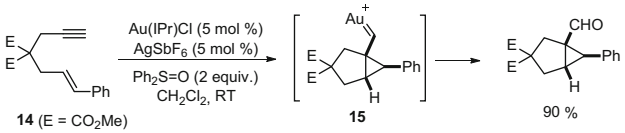

(4)

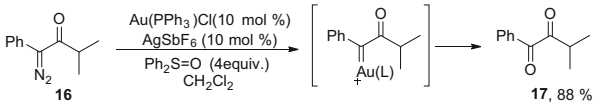

(5)

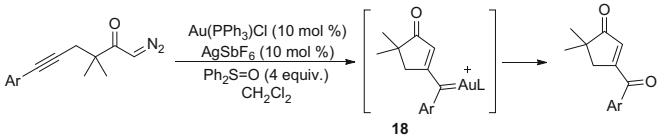

(6)

Diphenyl sulfoxide can also be an Au-carbene trap, transforming metal carbenes into the corresponding carbonyl compounds (Eqs. 4–6) [18]. The 1,6-enyne **14** transformed into carboxaldehyde derivatives in the presence of Au-catalyst and $Ph_2S{=}O$, which can best be explained by initial cycloisomerization into cyclopropyl gold carbenes **15**, followed by the oxidation with $Ph_2S{=}O$. Whether the OAT occurred first and then cyclopropanation occurred, or the initial formation of cyclopropyl carbenes followed by their oxygenation, can be inferred from the regioselectivity of the oxygen delivery, suggesting the latter scenario is in effect (Eq. 4). Further evidence of OAT to Au-carbene centers can be gleaned from the oxidation of gold carbenes generated from the α-diazoketone **16** into 1,2-diketone

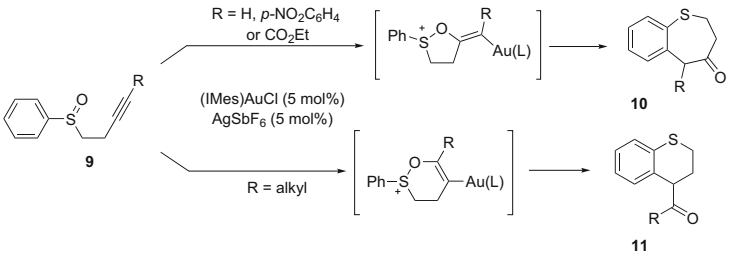

Scheme 7 Sulfoxides as OAT reagents

17 (Eq. 5). Similarly generated gold carbenes can also undergo intramolecular carbene transfer to alkynes leading to **18**, followed by oxidation (Eq. 6).

Shortly afterwards, Zhang and coworkers reported OAT from homopropargyl sulfoxides **19** leading to α,β-unsaturated enones **20** via pinacol shift (Scheme 8) [19]. The migratory aptitude among Ar, alkenyl, H and alkyl groups to the carbene center was investigated. In acyclic cases, Ar and alkenyl groups preferentially migrated over H and alkyl groups into the α-position of enones. This migratory aptitude is distinct from those observed in the Rh-catalyzed decomposition of α-diazo-β-hydroxyesters, where H migration is preferred [20].

Whether distinct Au-carbene is involved in the OAT of sulfoxides is an intriguing issue. While extending the above sulfoxide redox chemistry to an intermolecular setting, Ujaque and coworkers reported a synthetic pathway to α-aryl ketones **23** via intermolecular alkyne oxidations with sulfoxides (Scheme 9) [21]. Interestingly, the regioselectivity at the aryl ring did not follow the expected trend in the intermolecular electrophilic aromatic substitution of the purported Au-carbenes and, instead, the alkyl group ended up at the position ortho to the alkylthio group. Moreover, no cross-over products were identified [22]. Furthermore, computational study failed to identify a discreet minimum for the Au-carbene and the sulfide, and instead suggested that a concerted [3,3]-sigmatropic rearrangement of **21** into **22** was operative for the process [23].

In 2009, Davies demonstrated that gold-carbene generated from the OAT of sulfoxides can be trapped by the liberated sulfides to form sulfonium ylides **24** which were shown to undergo 2,3-sigmatropic rearrangement of the S-bound allyl unit into **25** (Scheme 10) [24]. The mechanism seems to involve a concerted sigmatropic shift of the allyl group, as can be seen in the 1,3-transposition of the substituted allyl unit. The optimized catalytic system turned out to be $PtCl_2$ (5 mol %) in DCE for terminal alkynes, and dichloro(pyridine-2-carboxylato)Au(III) for internal alkynes. Notably, in the latter case, a quaternary α-center can be formed. An interesting by-product, namely **26**, was observed in a small amount in the reaction of terminal alkynes which presumably arose from α-chlorination (from solvent DCE) of Pt-carbene species [25].

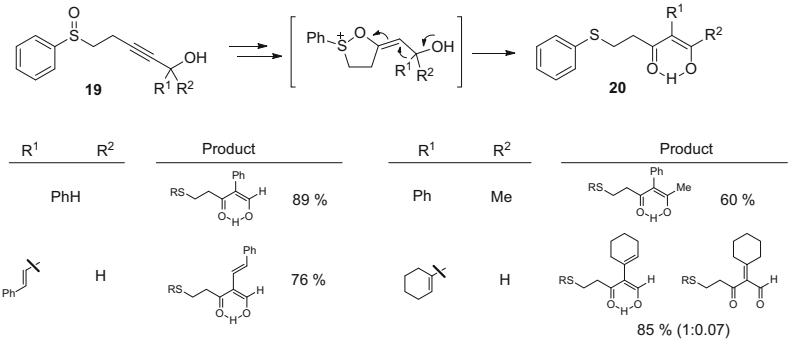

Scheme 8 Sulfoxide-mediated OAT and 1,2-alkyl shift

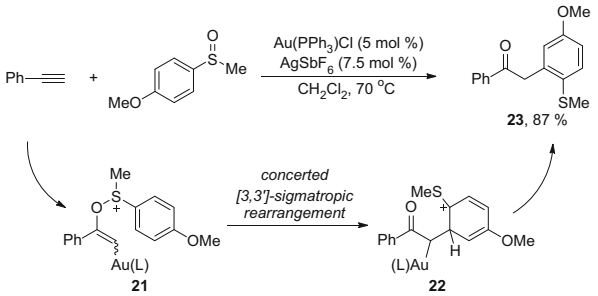

Scheme 9 Intermolecular OAT from sulfoxides via [3,3]-sigmatropic rearrangement

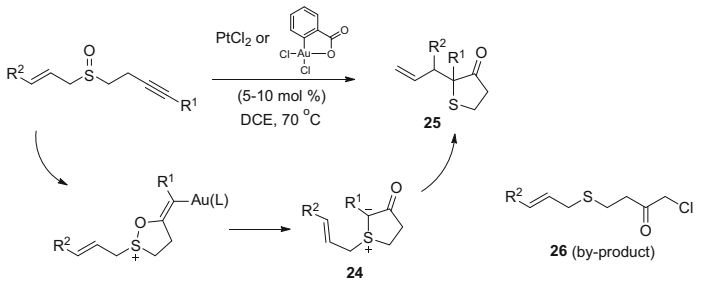

Scheme 10 Sulfoxide-mediated OAT and 2,3-Wittig rearrangement

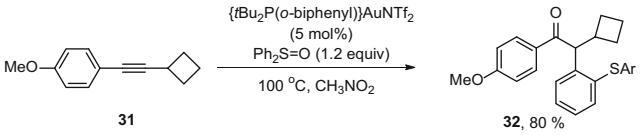

(7)

Ring expansion can be induced by the generation of a carbene center next to cyclopropyl rings [26]. Liu and coworkers examined the ability of a carbene generated from the sulfoxide redox of **27** to incur cyclopropane ring expansion to

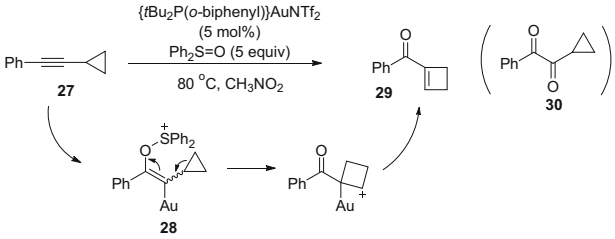

Scheme 11 Sulfoxide-mediated OAT and ring expansions of cyclopropanes

29 (Scheme 11) [22]. In the screening of appropriate OAT reagents, N–O oxidants such as amine-*N*-oxides, pyridine-*N*-oxides, and nitrones were not effective. Using 5 equiv. of $Ph_2S{=}O$, the desired acylcyclobutenes were obtained in CH_3NO_2 as solvent without competitive formation of 1,2-diketo compounds **30** [27]. Here, the ring expansion of the cyclopropane ring was faster than the competing 3,3-sigmatripic rearrangement of **28** (Scheme 8) [21]. However, the ring expansion reaction could not be extended to homologous cyclobutyl alkyne substrates **31** as these substrates followed a competitive formation of [3,3]-sigmatropic rearrangements to **32** (Eq. 7).

2.3 OAT from Epoxides

OAT from epoxides to alkynes was first reported by Hashmi and coworkers in 2008 [28]. Epoxyalkynes **33** prepared by mCPBA oxidation of the corresponding 1,5-enynes underwent a rearrangement, leading to 1-acylindenes **35** (Scheme 12). The mechanism is consistent with the formation of gold carbene **34** via attack of epoxide oxygen on the Au-activated alkynes. A small amount of by-product **36** was also observed, which results from the coordination of Au^+ on epoxide, followed by 1,2-shift. The presence of Au-carbene in this reaction was supported by the trapping of **34** with styrene or ethyl vinyl ether [29]. In the presence of $Ph_2S{=}O$ as oxidants, similar substrates **37** underwent further oxidation into 1,2-diketones **39**, which isomerize into 2-hydroxyindanones **40** with a quaternary center [30].

3 N–O Bond-Based Oxidants

3.1 Nitro Compounds

The first OAT onto alkynes in gold catalysis was reported by Asao and coworkers in 2003 (Scheme 13). They reported *o*-alkynyl nitroarenes were converted into a mixture of isatogens **41** and anthranils **42** upon treatment with $AuBr_3$ in DCE

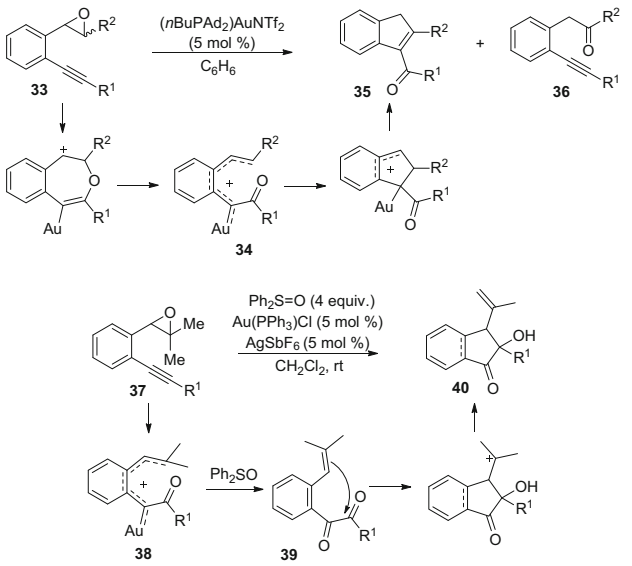

Scheme 12 OAT from epoxides

[31]. Afterwards, a similar transformation was also reported with Ir(III)-catalyst by Crabtree and coworkers [32].

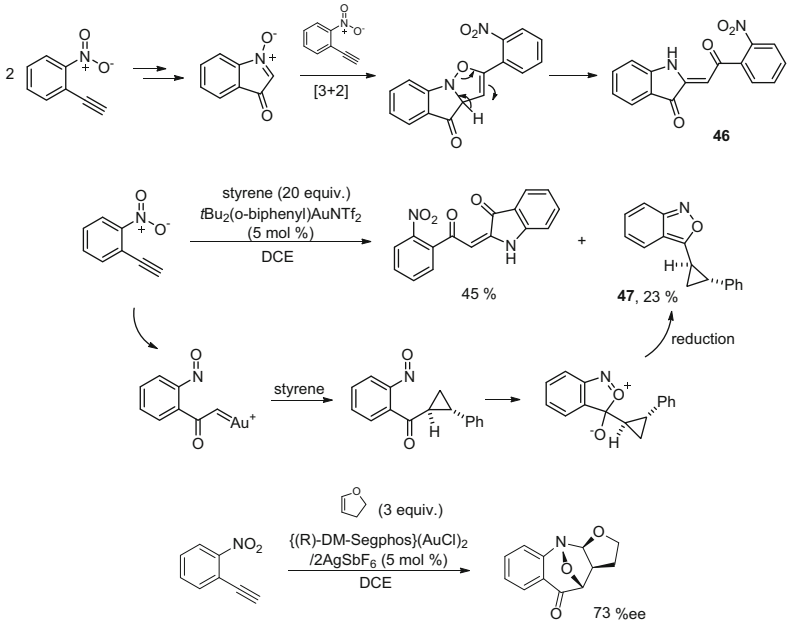

In 2011, Liu and coworkers made use of this reactivity to develop an elegant (2 + 2 + 1) formal cycloaddition involving nitroso groups, alkenes, and carbenyl carbons

Scheme 13 The first intramolecular OAT from alkynes

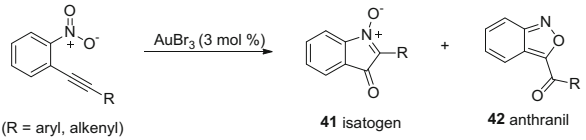

(Scheme 14) [33]. To minimize the dimerized by-product **46** resulting from [3 + 2] cycloaddition of isatogens with starting nitroalkynes (Eq. 8), slow addition of *o*-nitroethynylbenzene was required in the presence of excess dipolarophile. High regio- and diastereoselectivity was observed with a range of vinyl ethers and vinyl sulfides. The authors proposed that the mechanism of this cascade transformation involved generation of dipolar species **43**/**44** and the subsequent [3 + 2] cycloaddition with electron-rich olefin to form **45**. The high diastereoselectivity observed as well as the trapping of the gold carbene intermediate by styrene to form cyclopropyl anthranils **47** (Eq. 9) were taken as evidences for their proposal. Conspicuously, the cycloaddition could be rendered enantioselective, in the presence of (R)-DM-Segphos ligand, delivering the cycloadduct in 73% *ee* (Eq. 10).

3.2 Oximes

The ability of oximes to function as O-atom donors onto alkynes was found by Shin and coworkers in 2009 (Scheme 15) [34]. In the reaction of *o*-alkynylbenzaldoxime derivatives catalyzed by cationic of Au(I) complexes, (E)-oximes led to isoquinoline-*N*-oxides **48** [35] and (Z)-oximes formed isoindoles **50** in a mutually exclusive fashion. They proposed that the two pathways diverged at the point of the initial 6-endo-dig *N*-attack or 6-exo-dig *O*-attack. This mechanistic picture could explain the N–O cleaving steps in nitronyl alkynes by Yamamoto and coworkers [31] and laid a background for developing further N–O bond cleaving redox chemistry.

3.3 Nitrones

In 2008, Shin and coworkers reported that nitrones can function as OAT agents onto alkynes under electrophilic metal catalysis (Scheme 16) [36]. Nitrones can be easily assembled from the condensation of hydroxylamine derivatives and the corresponding aldehydes. Yet, in the presence of electrophilic metal salts, intramolecular transfer of an oxygen atom from nitrones onto alkynes occurs smoothly, leading to azomethine ylides **51**. The pendent alkenes would undergo stereospecific [3 + 2] dipolar cycloaddition with these in situ formed azomethine ylides, leading to 8-aza[3.2.1]bicyclooctanes **52**. Pt(II), Au(III), Au(I), and Ag(I) complexes were able to catalyze this process, and among them, $AuCl_3$ in CH_3NO_2 gave the best rates

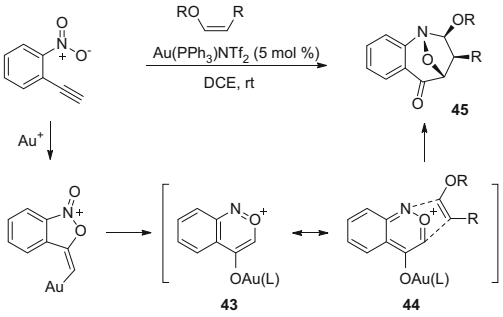

Scheme 14 Nitro group-mediated OAT and [3 + 2] cycloaddition

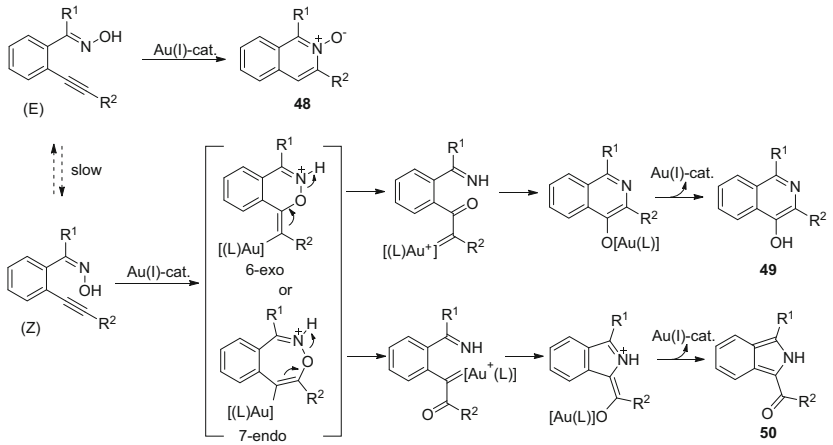

Scheme 15 OAT transfer from (Z)-oximes

and selectivity between [3 + 2] cycloaddition and isoindole products. For the mechanism of N–O bond cleavage, an alkynylnitrone substrate with alkyl tether between nitrone and alkyne groups was shown to form the desired [3 + 2] adduct, which suggested that the oxygen transfer occurs through the N–O–C=C–Au bond and not through a retro-electrocyclization mechanism. In 2011, Li and coworkers have found that the similar N–O redox reactivity of nitronyl alkyne substrates can be manifested by Ir(III), Rh(III), and Ru(II) complexes in both catalytic and stoichiometric reactions [37]. They reported the X-ray crystallographic structure of Ir(III)-bound azomethine ylides and the solid state structure had *O*-bound tautomeric form. Development of an asymmetric version of this [3 + 2] cycloaddition of azomethine ylides were examined by Shin and coworkers, resorting to the auxiliary controlled approach [38].

In 2010, Shin and coworkers further expanded the scope of nitrone redox chemistry by converting electrophilic carbenes **53** into nucleophilic enolates **54** via 1,2-pinacol shift (Scheme 17) [39]. The reaction of nitronylalkynes having tertiary alcohols at the alkynyl terminus led to cascade transformations comprising

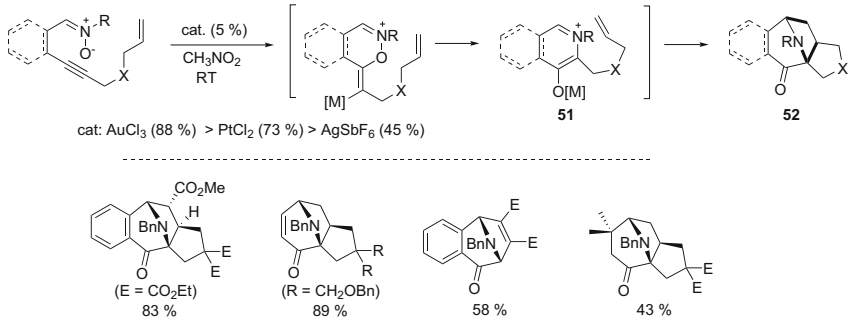

Scheme 16 Nitrone-mediated OAT and [3 + 2] dipolar cycloaddition

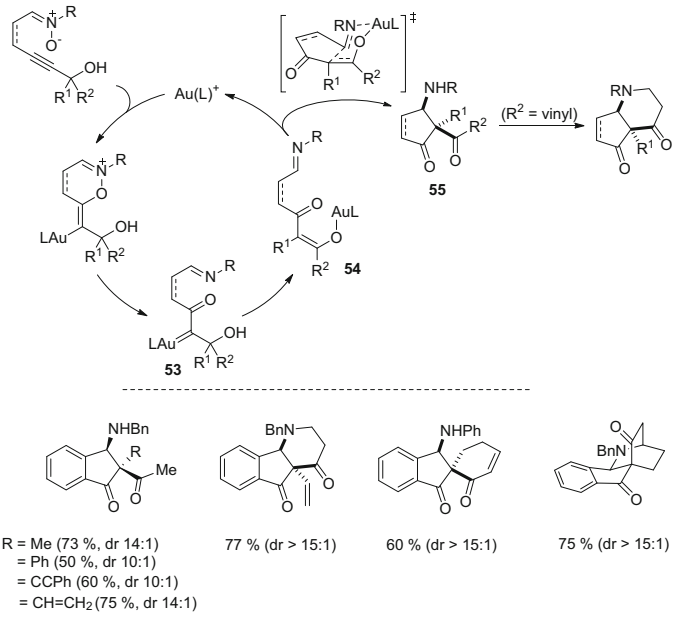

Scheme 17 Nitrone-mediated OAT, pinacol shift and Mannich (and Michael) addition sequence

OAT, pinacol, and Mannich (and Michael) addition. The migrating groups in the pinacol shift ended up at the quaternary position of the resulting 3-amino-cyclopentanones, and therefore the selectivity of various migrating groups was investigated. Among alkyl groups at R^1 and R^2, the smaller alkyl groups preferentially migrated (Me > Et > *i*Pr). π-Functional groups, such as aryl, vinyl, and alkynyl groups preferentially migrated over a methyl group. These migrating groups ended up at the quaternary position of **55** in a stereoselective fashion after Mannich addition through a cyclic transition state.

Intermolecular OAT from nitrones to alkynes was examined for the synthesis of indolin-2-ones **58** by Liu and coworkers (Scheme 18) [40]. To induce

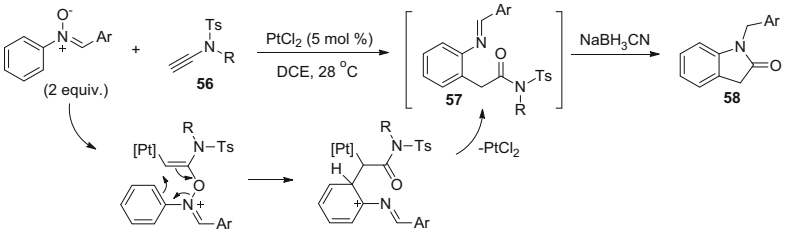

Scheme 18 Intermolecular OAT from nitrones-[3,3] sigmatropic rearrangement: oxyarylation of alkynes)

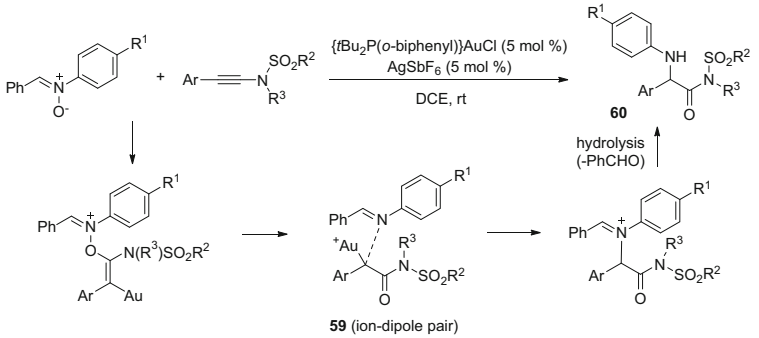

Scheme 19 Oxyamination of alkynes

intermolecular reactivity and regioselective OAT, donor-activated ynamides were selected. Notably, commonly employed cationic Au(I) complexes led to an extensive decomposition of starting materials and less acidic AuCl or $PtCl_2$ were found to be efficient catalysts. The intermediate carbonylimines **57** were isolated in good yields or they can be reduced with $NaBH_3CN$ in THF to afford indolin-2-ones **58**. Absence of cross-over indicated an intramolecular sigmatropic rearrangement mechanism.

With aryl substituted ynamides, oxyamination was followed instead of the above oxyarylation (Scheme 19) [41]. Using sterically bulky 8-methylquinoline-*N*-oxide as oxidants and tBu$_2$P(*o*-biphenyl)AuCl/$AgSbF_6$ as the catalyst, the desired oxyamination product **60** was obtained smoothly at room temperature. Use of nitrones here functioned both as aniline and oxygen donor. The authors proposed α-oxo gold carbene intermediates **59** that form a tight ion-dipole pair to explain the absence of cross-over.

With the same aryl substituted ynamides, a change of reaction partner from nitrones to nitroso arenes led instead to oxyimination instead of oxyamination (Scheme 20) [41]. This transformation is equivalent to a nitroso/alkyne metathesis and was proposed to proceed through the N-attack of nitroso compounds onto ynamides to **61**, cyclization into 4*H*-oxazet-2-ium species **62**, followed by its

fragmentation to **63**. The oxyimination products could be converted with $NaBH_4$ into synthetically useful α-amino alcohols.

*3.4 Amine-*N*-Oxides*

In 2009, Zhang and coworkers reported that 3-butynylpiperidine-*N*-oxides **65**, prepared in situ from mCPBA oxidation of the corresponding amines **64**, undergo OAT to alkynes (Scheme 21) [42]. In the presence of $(PPh_3)AuNTf_2$ (5 mol%) in dichloromethane, the substrates **65** smoothly transformed into piperidin-4-ones **66** at 0°C for 1 h via an apparent C–H activation. With substituted piperidine, pyrrolidine, and acyclic tertiary amines as substrates, high diastereoselectivity was observed, ranging from 6:1 to >20:1, depending on the substitution pattern. Interesting selectivity issues arise when the starting amines substituted with two different alkyl groups were used. Representative reactivity profile revealed that the hydride is transferred from the least hindered alkyl group and that the hydride transfer is favored in the case where the corresponding carbenium ion can be stabilized by resonance. The efficiency of the two-step piperidin-4-ones synthesis was demonstrated in the total synthesis of cermizine C from **67** (Scheme 21). The involvement of gold carbene in this transformation became even more intriguing issue because the reaction of substrates with EWG at the alkynes proceeded smoothly even in the *absence* of Au-catalyst at mild temperatures (0°C and below) [43].

Given these experimental results, the mechanism of this amine-*N*-oxide-mediated OAT was computationally studied (Scheme 22) [44]. Density functional calculation suggested that a formal 1,5-hydride shift occurred through a single concerted transition state by a hetero-retroene mechanism (from **68** to **69**), thus disfavoring the Au-carbene mechanism. Experimental evidence for disfavoring the gold carbene intermediate was based on the observation in which a related gold carbene generated from the α-diazo-precursor did not undergo this 1,5-hydride shift, but instead produced a Wolff rearrangement. The computational results also successfully accounted for the product ratio when two alkyl substituents on N are different.

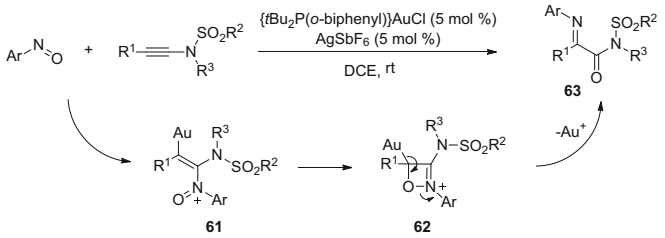

Scheme 20 Oxyimination of alkynes

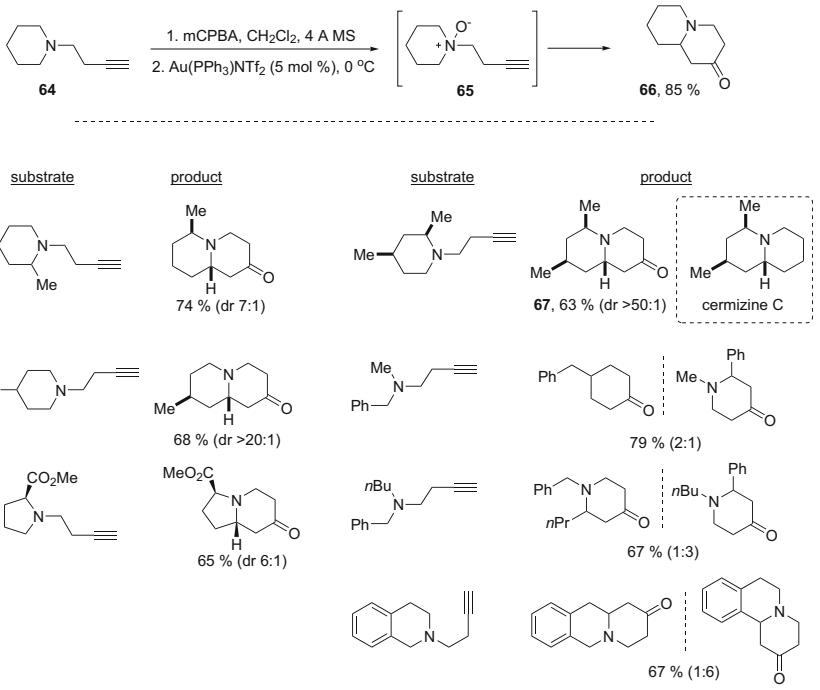

Scheme 21 Tertiary amine-*N*-oxides as OAT reagents

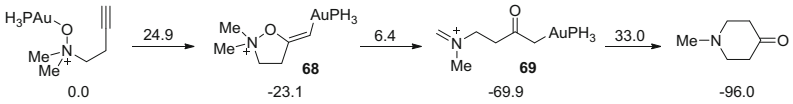

* Relative free energies and activation energies (in kcal/mol) are shown below the structure and above the reaction arrows, respectively (B3LYP-D3)

Scheme 22 DFT computational study of OAT process from 3° amine-*N*-oxides

3.5 Hydroxylamines and Nitroso Compounds

N-Hydroxylamines are appealing OAT agents because of their availability [45, 46] and their potential reactivity involving N–O cleavage. Conceptually, formal addition of N- and O-atoms in the *N*-hydroxylamines onto alkynes would provide a direct route to synthetically useful α-amino carbonyl compounds. In 2011, Shin and coworkers reported the first gold-catalyzed intramolecular reactions of *N*-hydroxyl homopropargylamines (Scheme 23) [47]. *N*-Sulfonyl hydroxylamine derivatives reacted in the presence of (IPr)AuCl and $AgBF_4$ (5 mol% each) to provided 3-pyrrolidinones **71**. Being an ambident nucleophile, the reaction of *N*-hydroxylamines with internal alkynes **72** led to initial 5-endo-dig N-addition, giving nitrones

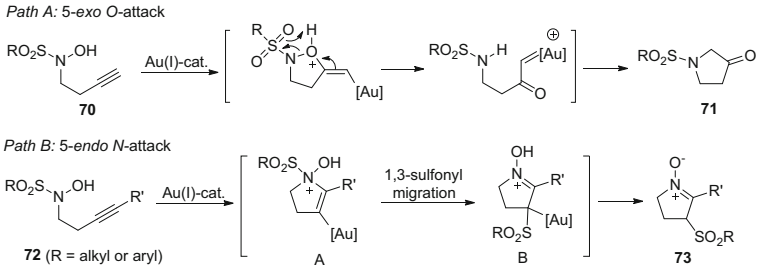

Scheme 23 *N*-Hydroxylamines as OAT reagents

73 instead. In the formation of pyrrolidinones **71**, the presence of the N-sulfonyl protecting group was essential for the N–O cleavage.

Metal-free rearrangement of *O*-vinyl-*N*-arylhydroxylamines has long been known to undergo thermal [3,3]-sigmatropic rearrangement by Coates and coworkers (Scheme 24) [48]. Utilizing efficient gold-catalyzed alkoxylation of alkynes, this [3,3]-sigmatropic rearrangement have received renewed interest in indole and pyrrole synthesis as follows.

Thermal rearrangement of *O*-vinyl-*N*-arylhydroxylamine derivatives and subsequent dehydration can lead to indoles [49]. In common with Fisher indole synthesis, a key issue in terms of selectivity lies in the preparation of *O*-vinyl-*N*-arylhydroxylamine in a regioselective manner. In 2011, Zhang and coworkers addressed this issue utilizing gold-catalyzed Markovnikov O-addition of *N*-aryl-*N*-hydroxylamines onto terminal alkynes (Scheme 25) [50]. The intermolecular addition involving addition of hydroxylamines, [3,3]-sigmatropic rearrangement, and dehydrative cyclization occurred efficiently at room temperature in the presence of $(ArO)_3PAuNTf_2$ (Ar = 2,4-di-*t*Bu-C_6H_3) complex in DCE, providing various 2-aryl and 2-alkyl indole derivatives. This protocol has advantages over conventional Fisher indole synthesis in that the reaction conditions are neutral and acid-labile-protecting groups (THP ethers) can survive. However, in some cases, disproportionation of *N*-aryl-*N*-hydroxylamines into nitrosobenzenes and anilines was noted, resulting in azoxybenzenes as by-products.

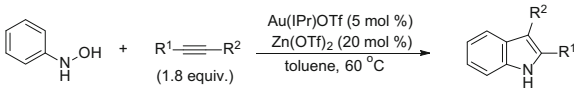

(11)

The reaction with internal alkynes required a modification of reaction conditions because of the attenuated reactivity. Zhang and coworkers found that the use of Zn (II) as a co-catalyst along with an Au(I) catalyst provided an effective solution for internal alkynes (Eq. 11) [51]. The chelation of Zn(II) ion with N-Boc-protected hydroxylamine was proposed to enhance the nucleophilicity of the O-nucleophile. The regio-selectivity in the reactions of internal alkynes ranged from 2:1 to >20:1 providing 2,3-disubstituted indoles. This regio-selectivity follows from steric and electronic effect and can be controlled by judicious choice of substituents.

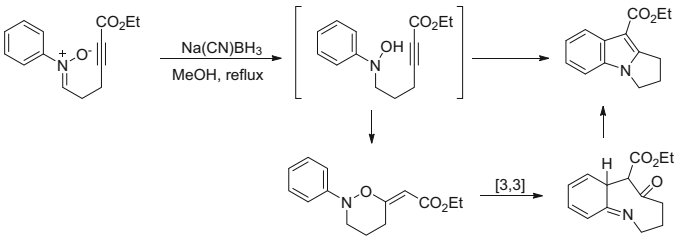

Scheme 24 Metal-free redox isomerization by Coates [48]

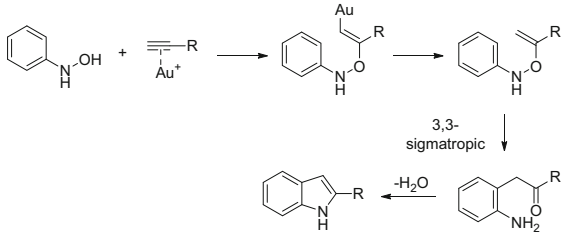

Scheme 25 Gold-catalyzed formation of *O*-vinyl hydroxylamines and [3,3]-sigmatropic rearrangement

O-Vinyl hydroxylamines can be prepared from the condensation of hydroxylamines with 1,3-dicarbonyl compounds (Scheme 26) [52]. Salt forms of hydroxylamines **74** were used as starting materials along with mild bases because salt-free forms were prone to oxidation under aerobic environments. In situ condensation and gold-catalyzed 6-exo-dig addition to alkynes led to *N*,*O*-divinyl hydroxylamines **75** which thermally underwent a known [3,3]-sigmatropic rearrangement, leading to fused pyrroles [48].

Liu and coworkers employed allenes as substrates for the indole synthesis (Scheme 27) [53]. The reaction of hydroxylamines with allenes under the gold (I) catalysis gave a complicated mixture, indicating possible instability of hydroxylamines. Addition of 2 equiv. of benzaldehyde as an additive was necessary initially to convert the hydroxylamines **76** into nitrones **77** and the resulting nitrones underwent regioselective indole formation, and the benzaldehyde was liberated by hydrolysis. The scope of allenes in this case remained terminal ones.

The intermolecular reaction of nitrosoarenes with alkynes can also lead to (*N*-hydroxy)indoles. Srivastava and coworkers reported an in situ cyclization in the presence of AuCl as a catalyst and reduction of the resulting *N*-hydroxyindoles with $NaBH_4$ (Scheme 28) [54].

In 2012, Liu and coworkers explored the gold-catalyzed generation of vinyl gold carbene intermediates from vinyl diazo compounds **78** and developed new cycloannulation pathways using nitrosoarenes as reagents (Scheme 29) [55]. Vinyl metal carbenes generated via Rh- or Cu-catalyzed decomposition of vinyl diazo compounds displays diverse cycloaddition reactivity. While other metal-catalyzed decomposition of vinyl diazo compounds led to isolation of nitrones **79** (path A), gold catalysts provided two new intermolecular

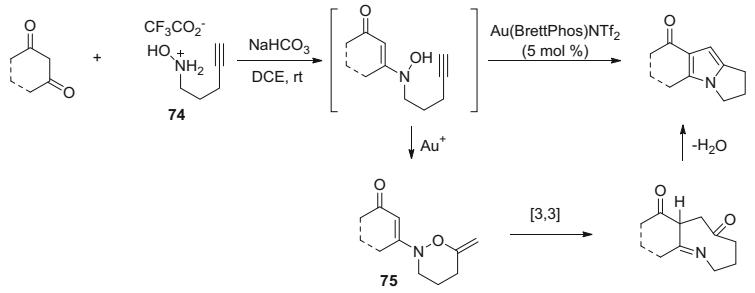

Scheme 26 Formation of *O*-vinylhydroxylamine from 1,3-dicarbonyl compounds

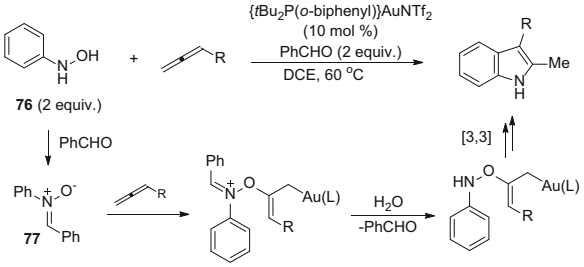

Scheme 27 Addition of hydroxylamines to allenes

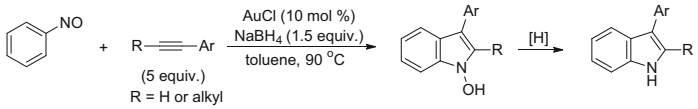

Scheme 28 Intermolecular reactions of nitrosoarenes with alkynes leading to indoles

cycloannulation products **80** and **81** [56]. From vinyl diazo precursors **78**, use of {*t*Bu$_2$P(*o*-biphenyl)}AuNTf$_2$ provided quinoline-*N*-oxides **80**, with a small amount of quinolones **81**. The mechanism involves the N-addition of nitrosoarenes at the γ-position (path B), followed by [3,3]-sigmatropic rearrangement. Liberation of Au$^+$ catalyst would provide quinolones or an oxidative aromatization would provide quinolone-*N*-oxides.

Vinyl gold carbenes **82** generated from Rautenstrauch rearrangement of propargyl carboxylates returned a different outcome, providing cycloadducts **83** (Scheme 30) [55]. With Au(IPr)NTf$_2$ as a catalyst, the mixture of propargyl pivalates and nitrosoarenes smoothly converted into 3,6-dihydro-2*H*-[1, 2]-oxazines **83**. To elucidate this intriguing reaction mechanism, vinylimine **84** was prepared and was treated under the above conditions to give the identical product, showing that the vinylimines **84** are involved as actual intermediates for the formation of **83**. The formation of the vinylimines from propargyl pivalates was rationalized by the loss of Au$^+$=O fragments which returned to Au$^+$ with the liberation of O_2.

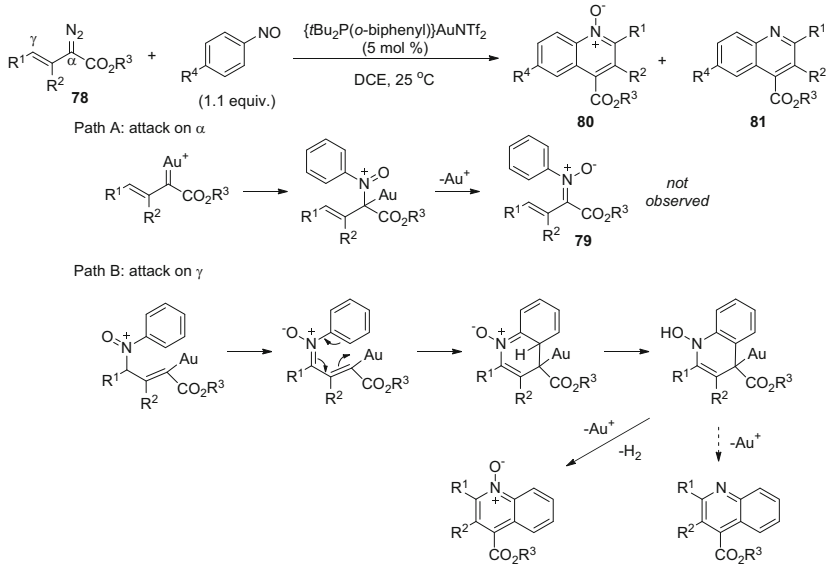

Scheme 29 Reactions of vinyl gold carbenes with nitroso compounds

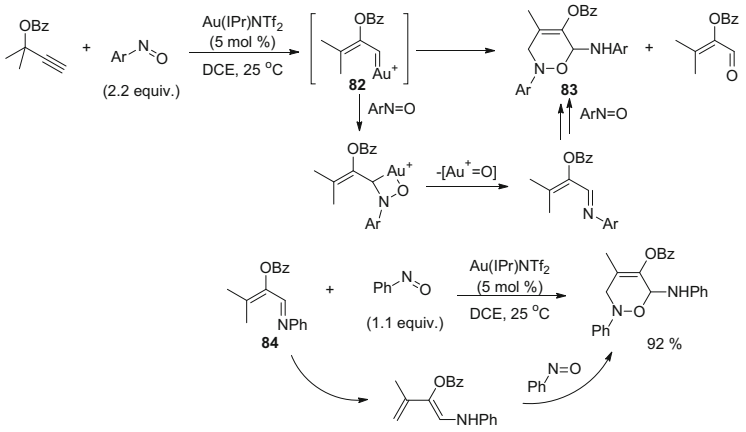

Scheme 30 Reactions of vinyl gold carbenes from propargylic esters

3.6 Pyridine-N-*Oxides*

Intermolecular OAT reaction onto alkynes was first demonstrated by Zhang and coworkers employing pyridine- *N*-oxides. Pyridine-*N*-oxide derivatives have unique features as oxygen transfer agents and this chemistry has been demonstrated in the oxyarylation of benzynes in the early literature [57]. These compounds can be readily prepared by a variety of methods, including mCPBA oxidation, metal- or

organocatalyzed oxidation by H_2O_2 or other peroxy reagents [58, 59]. In comparison, other heteroaromatic-*N*-oxides, such as those from oxazoles and imidazoles, are hydrolytically unstable and/or undergoes competitive [3 + 2] dipolar cycloaddition [60, 61]. In contrast, pyridine-*N*-oxides can often be prepared in crystalline form. Synthetically, the use of pyridine-*N*-oxides as intermolecular OAT reagents are advantageous because residual atoms from OAT reagents do not remain in the product. This results in an increased scope of applications and less efforts in the preparation of substrates. Au-carbene synthons generated thus have significantly expanded applications, now including X–H (X=O, N) insertion, cyclopropanation, cyclization, and rearrangements, covering most areas of traditional diazotransfer chemistry [1, 2]. Importantly, being able to trap the α-oxo gold carbenes by intermolecular nucleophiles requires an additional dimension of chemoselectivity. However, in recent years, increasingly elegant examples of intermolecular trapping have been reported, adding to the diversity of accessible structures.

3.6.1 Intramolecular Trapping of α-Oxo Gold Carbenes

In 2010, Zhang and coworkers reported the first intermolecular OAT of N–O bond oxidants (Scheme 31) [62]. Treating the starting homopropargyl alcohols **85** and pyridine-*N*-oxides (2 equiv.) with Au(I) catalysts in DCE provided dihydrofuran-3-ones **86** and the use of strong acid (MsOH) increased the rate and yield of the product, leading to the reaction occurring at room temperature. The reaction conditions were mildly acidic because of the buffering effect of excess pyridine-*N*-oxides, where MOM-protected alcohols and Boc-protected amines could survive. Potential side reaction, i.e., 5-exo-dig or 6-endo-dig cyclization of tethered electron-rich aromatic or heteroaromatic rings onto alkynes, did not compete, illustrating efficiency and chemoselectivity of this intermolecular OAT. However, the efficiency of the reaction dropped when extended to the bis-homopropargylic alcohols, because of a competing and very facile 5-exo-dig cyclization.

Shortly afterwards, the same group extended this intramolecular O–H insertion into propargyl alcohols delivering a facile route to oxetan-3-one **87** (Scheme 32) [63]. Optimal conditions for this transformation involve the use of Au(*o*-biphenylPCy_2)NTf_2 as catalyst, 3-methoxycarbonyl-5-bromopyridine-*N*-oxide (2 equiv.) and 1.2 equiv. of HNTf_2. The latter acid additive minimized the reaction of Au-carbene with MsOH to form α-MsO-methylketones **88** when MsOH was used. For tertiary propargyl alcohol substrates, oxetanone formation required the presence of a CO_2R group at the alkyne terminus and switching to 4-acetylpyridine-*N*-oxide (2 equiv.) and IPrAuNTf_2 (5 mol%).

Azetidin-3-ones **89** can also be synthesized from *N*-sulfonyl protected propargyl amines (Scheme 33) [64]. To alleviate the difficulty of removing the *N*-sulfonyl group, the N-Bus (*tert*-butylsulfonyl) group was installed by oxidation of the corresponding sulfoxide and, moreover, these substrates could be easily prepared in enantiopure forms via Ellman's protocol [65].

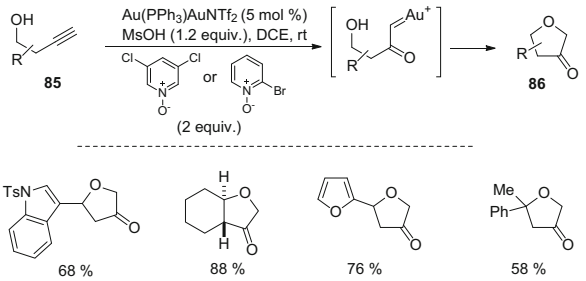

Scheme 31 OAT and formation of furan-3-ones

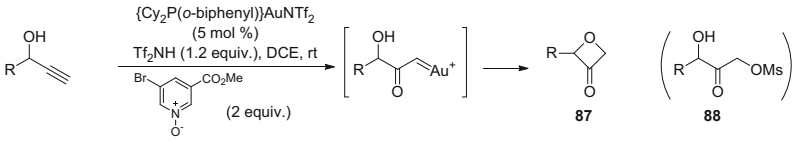

Scheme 32 OAT and formation of oxetan-3-ones

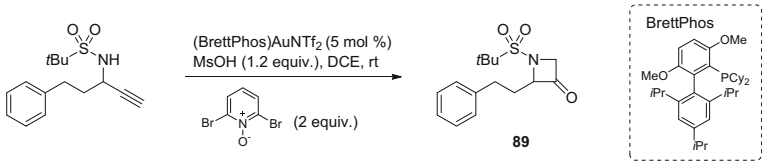

Scheme 33 OAT and formation of azetidin-3-ones

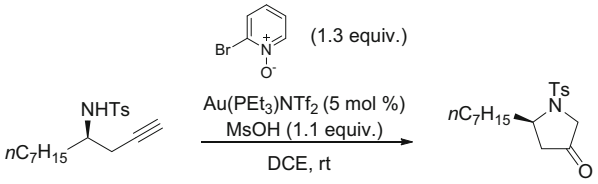

Scheme 34 OAT and formation of pyrrolidin-3-ones

A similar strategy was explored in the synthesis of pyrrolidin3-ones by Ye and coworkers (Scheme 34) [66]. Switching substrates to homopropargyl amines led to an efficient synthesis of pyrrolidin-3-ones using $Au(PEt_3)NTf_2$ as a catalyst, 2-bromopyridine-*N*-oxide as an oxidant, and MsOH as an additive. *tert*-Butyl sulfinimine chemistry allowed access to enantiopure *N*–Ts sulfonamides which, in turn, led to the optically pure pyrrolidin-3-ones.

Generally, oxidation of triple bonds has had limited synthetic applications so far compared to that of alkenes, because of the low chemoselectivity. In comparison, alkyne oxidations mediated by the OAT from pyridine-*N*-oxides to alkynes

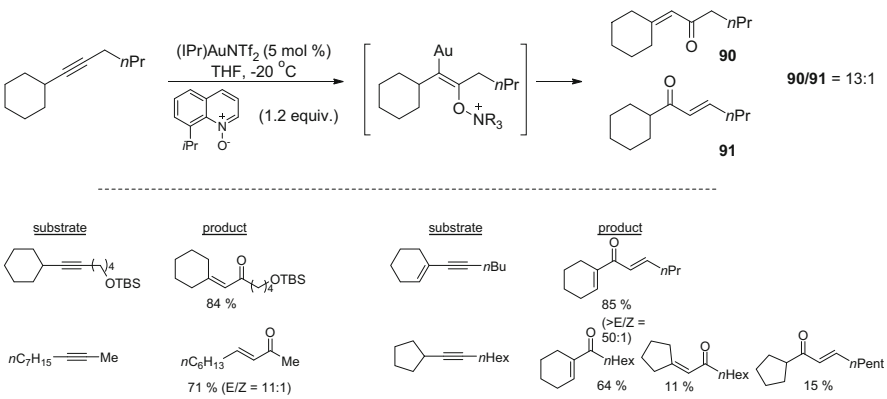

Scheme 35 OAT and 1,2-H shift

provides α-oxo gold carbenes synthons. Such an example employing internal alkynes has been demonstrated, providing α,β-unsaturated enones via 1,2-H-shift (Scheme 35) [67]. Transformation of internal alkynes into the α,β-unsaturated enones requires a regioselective OAT from pyridine-*N*-oxides. With a small bias in the alkyne substituents (i.e., primary vs secondary alkyl), gold-catalyzed OAT allowed the oxygen atom to add onto the less hindered alkyne carbon, where the selectivity increased as the steric bulk *N*-oxides increased. Also, by using hindered 8-isopropylquinoline-*N*-oxide, the addition of buffering acid was not needed. In the case when one of alkyne substituents is a cyclopentyl group, ring expansion via 1,2-shift onto carbene center is observed, leading to cyclohexenyl ketones.

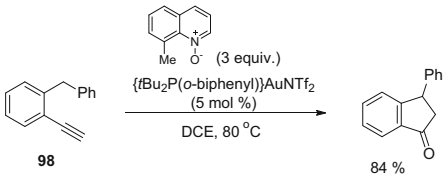

(12)

In 2011, Liu and coworkers reported formal *sp2* C–H insertion and intramolecular cyclopropanations of α-oxo gold carbenes generated from ynamides and terminal alkynes, respectively (Schemes 36 and 37) [68]. The former transformation can be explained by a sequence consisting of the ynamide-controlled regioselective OAT of **92** from 8-methylquinoline-*N*-oxide, intramolecular cyclization to form benzyl cation, and a concerted 1,2-hydride migration with the turnover of Au-catalyst to form **93**. The reaction of terminal acetylene substrates **94** required higher temperature (80°C) and 4 equiv. of 8-methylquinoline-*N*-oxide and led instead to cyclopropanation product **95**. This transformation can be explained by the initial OAT followed by intramolecular cyclopropanation to **95** or by the formation cyclopropyl gold carbenes **96**/**97** first, which are then trapped via OAT to form **95**. Initially, the authors proposed the former pathway is operative based on the analysis that the benzylic cation such as **96** would be highly prone to aromatization to afford naphthalene derivatives, and on the experimental

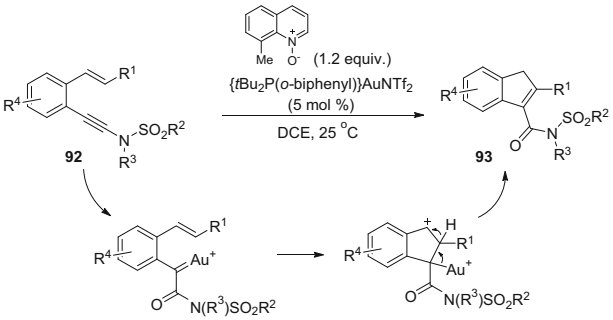

Scheme 36 OAT and synthesis of indenes

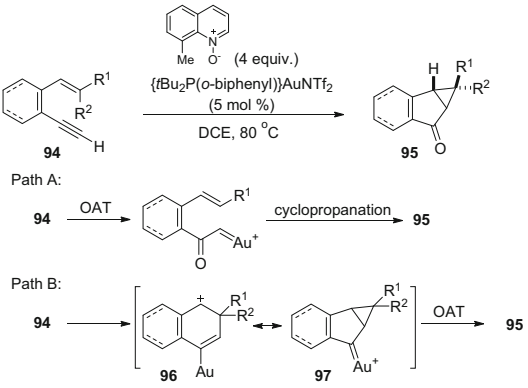

Scheme 37 OAT and intramolecular cyclopropanation

observation where an apparent benzylic C–H activation occurred in the reaction of **98** (Eq. 12). However, the apparent C–H activation product was later found to form via 1,5-H-shift, not through α-oxo gold carbenes by the same group [69].

In 2012, Liu and coworkers reported benzylic C–H functionalization/cyclization in the gold-catalyzed reaction of *o*-alkynylbenzenes (Scheme 38) [69]. As benzylic substituents (R), various groups including relatively electron-deficient aromatic and heteroaromatic groups, functionalized alkyl groups and hydrogen can be accommodated. Deuterium labeling experiments and other control experiments suggested that the α-oxo gold carbene route was not likely. Instead, a fast 1,5-hydrogen shift, following by aromatization with the N–O bond cleavage, was proposed to explain the outcome.

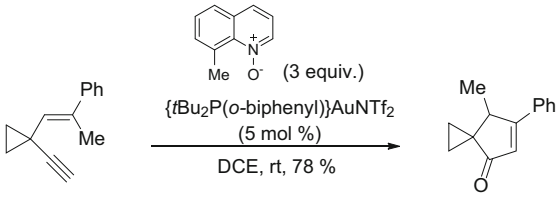

(13)

Scheme 38 Intramolecular C–H functionalization/ cyclization

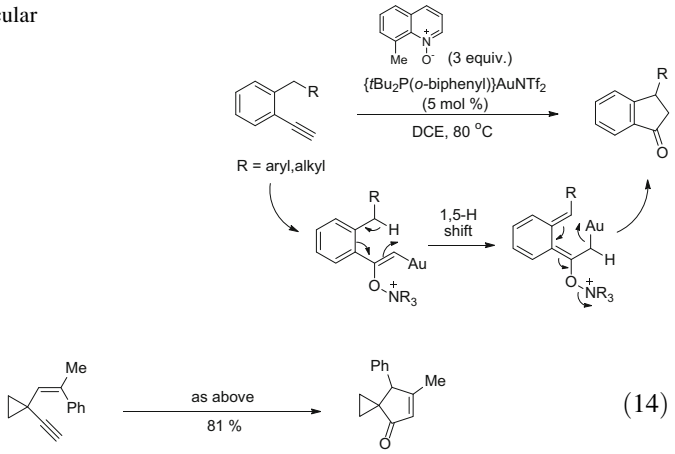

(14)

More recently, Liu and coworkers reported an interesting observation in the oxidative cyclization of 1,4-enynes for the formation of cyclopentenones (Eqs. 13 and 14) [70]. Interestingly, the carbocationic intermediate **100** (Scheme 39) underwent a stereospecific migration of an alkyl group positioned at the *cis*-position (R^1) in the substrate and a surprisingly high level of stereospecificity was demonstrated. Electron-rich ligands on gold – such as Me_3P – showed higher stereospecificity than electron-deficient phosphite ligands and, finally, *t*Bu2P(*o*-biphenyl) ligand gave almost complete stereospecificity. The dependence of migratory aptitude on the stereochemistry at the γ-carbon to the cationic center is very rare. The authors proposed that the observed stereospecificity can be explained by a *disrotatory* closure of the α-oxo gold carbene with pendent olefins to form **100**, followed by *anti*-selective migration onto the cationic center. The formation of the cationic intermediate **100** can also be rationalized by a concerted N–O cleavage with the formation of the new C–C bond from the **99**.

In 2012, Zhang and coworkers developed synthesis of chroman-3-ones **101** via intramolecular oxyarylation using pyridine-*N*-oxides (Scheme 40) [71]. In this transformation, Buchwald-type ligands with increasingly bulky biphenyl moieties turned out to be more effective and Me_4*t*BuXPhos was chosen as the optimal ligands. Competitive formation of benzopyran via 6-endo-dig cyclization slowed down in the presence of pyridine-*N*-oxides, possibly because of coordination of the gold complex onto pyridine-*N*-oxides. Among the oxidants tried, electron-deficient and sterically bulky oxidants such as **102** returned the best results. As a note, a high degree of *o*-/*p*-selectivity was observed in the case of *m*-substituted substrates.

Liu and coworkers reported intramolecular reactions of nitriles onto the electrophilic α-oxo gold carbenes (Scheme 41) [72]. Interestingly, two theoretical equivalents of pyridine-*N*-oxides were utilized, one for OAT to alkynes to form α-oxo gold carbenes and the other for oxyarylation of the strained nitrilium ion **102**. Thus, the initially formed nitrilium species undergo addition of pyridine-*N*-oxides, followed by five-membered ring closure to **103** and fragmentation with the N–O

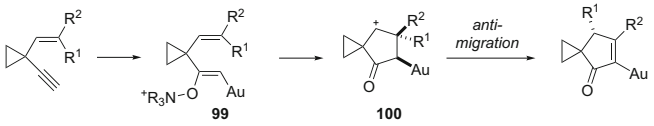

Scheme 39 Possible mechanism of selective migration of *cis*-substituent

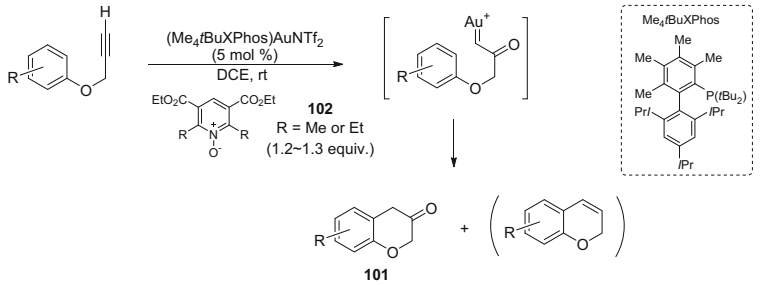

Scheme 40 Intramolecular trapping with arenes

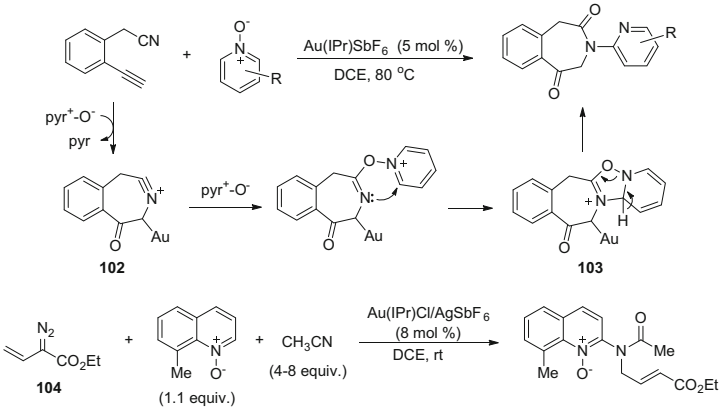

Scheme 41 Trapping of α-oxo gold carbenes with nitriles

bond cleavage. The oxyarylation of the nitrilium species can also occur intermolecularly, starting from vinyl diazoesters **104** with 1.1 equiv. of 8-methylquinonine-*N*-oxide.

In 2006, Toste and coworkers reported that *o*-ethynylbenzyl ethers undergo intramolecular carboalkoxylation to afford indenyl ethers catalyzed by gold (Scheme 42) [73]. During this process, the benzylic center underwent an overall inversion of configuration at the benzylic center via an axially chiral transition state. In 2013, Liu and coworkers employed similar substrates in the oxidative gold-catalyzed cyclization (Scheme 43) [74]. The α-oxo gold carbenes formed would be intramolecularly trapped by ether oxygen, which is followed by a new C–O bond

Scheme 42 Chirality transfer in the carboalkoxylation: *overall inversion*

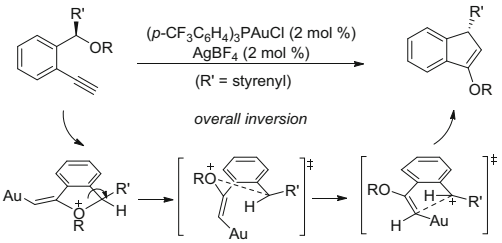

Scheme 43 Chirality transfer in the oxidative dialkoxylation: *overall retention*

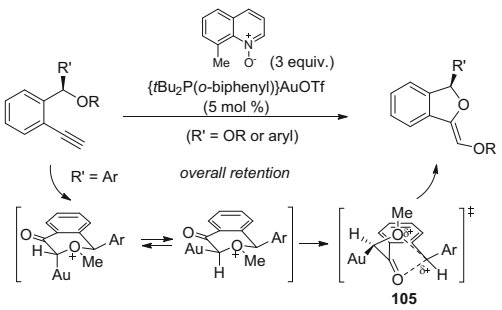

Scheme 44 Intramolecular oxidative cyclopropanation by pyridine-*N*-oxides

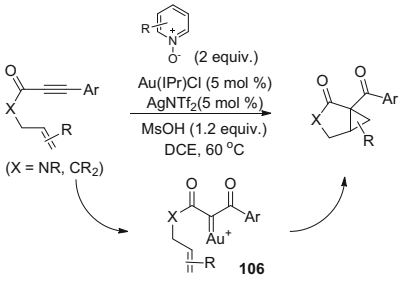

formation, leading to cyclic enol ethers or acetals (R′=OR) with (Z) geometry. A notable feature during this transformation is the complete transfer of chirality at the benzylic center, in this case, with overall retention of configuration. This process was explained by a 'front-on' substitution transition state **105** where the developing cationic charge is compensated for by the incoming ketone oxygen.

In 2011, Zhang and coworkers reported intramolecular oxidative cyclopropanation starting with 1,6-enynes derived from propiolamides (Scheme 44) [75]. In their screening of oxidants, $Ph_2S{=}O$ did not effectively provide the desired products and pyridine-*N*-oxides or quinoline-*N*-oxides were optimal oxidants, depending on substrates. The reaction could be rationalized by the initial formation of gold carbenes **106**, followed by intramolecular cyclopropanation. Subsequently, related substrates with terminal alkynes were investigated by Shin and coworkers (Scheme 45) [76]. Interestingly, in this case, 2-bromopyridine-*N*-oxide was ineffective, forming a conjugate addition adduct instead. Formation of cyclopropyl gold

Scheme 45 Intramolecular oxidative cyclopropanation by sulfoxides

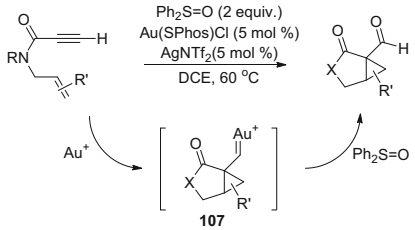

Scheme 46 Formation of enones

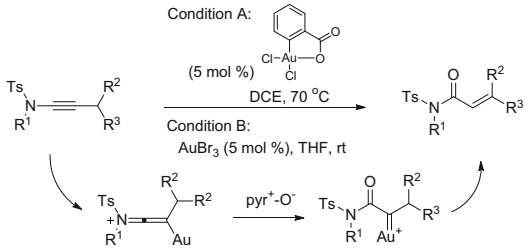

carbene **107** formed from the cyclization of 1,6-enynes, followed by trapping the carbenes with $Ph_2S{=}O$, was the most reasonable explanation.

Davis and coworkers introduced ynamides for intermolecular reaction of pyridine-*N*-oxides, providing α,β-unsaturated imides via 1,2-H shift (Scheme 46) [77]. The polarized nature of ynamide electrophiles were utilized for inducing intermolecular reactivity as well as controlling regioselectivity in the addition to alkynes. A potentially competing process is the reaction of Au-carbene with another equivalent of pyridine-*N*-oxide, producing 1,2-dicarbonyl compounds. Apparently, intramolecular 1,2-shift turned out to be faster than the over-oxidation of the α-oxo gold carbenes by pyridine-*N*-oxides. The double bond geometry ranged from 1.9:1 to 7.7:1 in favor of the E-isomer, unless the β-alkoxy group is present.

3.6.2 Intermolecular Trapping of α-Oxo Gold Carbenes

During the oxidation of alkyne by OAT from pyridine-*N*-oxides, chloride abstraction from solvents, such as DCE, are often observed as a side reaction. Xiang and coworkers have examined the generality of this reaction (Scheme 47) [78]. The viability of chloride abstraction indicates the highly electrophilic nature of the α-oxo gold carbene **108**/**109** and the mechanism was proposed to involve the formation of the cyclic chloronium intermediate **110**, which reacts with MsOH to form the experimentally observed 2-chloroethyl mesylate. Alternatively, switching solvent to chlorobenzene led to selective formation of α-mesyloxymethyl ketones [79].

Nitriles can trap the α-oxo Au-carbene generated from OAT of pyridine-*N*-oxides intermolecularly (Scheme 48) [80]. This required use of nitriles as reaction solvents and the resulting nitrilium species undergo 5-endo-dig cyclization leading

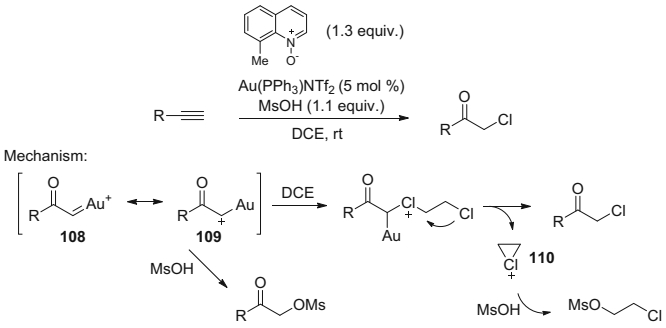

Scheme 47 Intermolecular trapping by DCE solvent

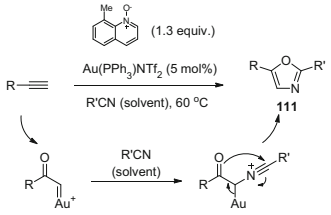

Scheme 48 Intermolecular trapping by nitrile solvents

to 2,5-disubstituted oxazoles. For example, using 8-methylquinoline-*N*-oxide as an oxidant in acetonitrile, terminal alkynes were efficiently converted into 2,5-dialkyl oxazoles **111**. It should be noted that this report constitutes the first intermolecular trapping of gold carbenes generated via gold-catalyzed OAT although the nucleophile came from solvent.

Variation of structures of ligands in terms of steric and electronic environment and/or coordinating atoms may play a vital part in the reaction outcome of transition metal catalysis. Previously, Zhang and coworkers developed 2,5-disubstituted oxazole synthesis involving trapping of α-oxo gold carbenes with a large excess of nitrile compounds as solvents [80]. In contrast, using the P,N ligand system, they were able to access 2,4-disubstituted oxazoles without using a large excess of reactants (Scheme 49) [81]. In this effort, Zhang and coworkers applied Mor-DalPhos [82] ligand having bulky adamantyl groups at the P atom and an *o*-morpholine. While typical ligands on cationic gold, such as Cy-JohnPhos, led to no desired product, a combination of Mor-DalPhos and $NaBAr^F{}_4$ as a counter-anion source provided respectable yields of the desired product. Although the mainstay of Au(I) catalysis is represented by di-coordinated Au(I) species, they proposed that trivalent P,N-coordinated Au(I) complexes would be less electron-deficient and thus allow more back-donation from Au to the cationic center, resulting in a more chemo-selective functionalization. DFT computational results were also provided, indicating a shortened Au–C bond caused by the increased backbonding and shorter Au–N distance (2.930 Å).

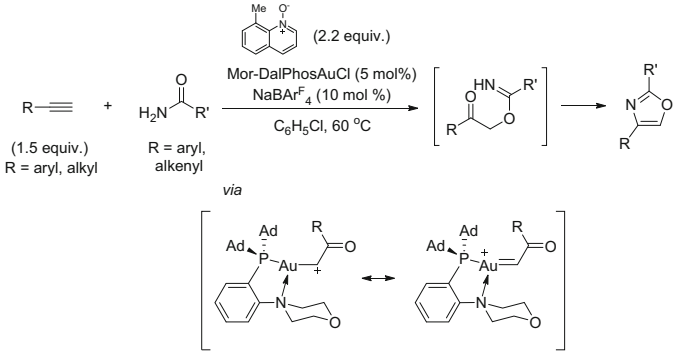

Scheme 49 P,N ligand strategy: oxazoles formation

In a subsequent study, Zhang and coworkers expanded upon their P,N-bidentate ligands-based strategy (Scheme 50) [83]. As external nucleophiles, carboxylic acids were employed, producing α-benzoxymethyl ketones. A systematic variation of N-substituents of the P,N-bidentate ligands was tried, aimed at exploring requisite steric environment around the Au-carbenic center. Among them, **112** provided a significant improvement over Mor-DalPhos. Carboxylic acid, being less nucleophilic than carboxamide above, requires more steric protection of α-oxo gold carbene intermediate from competing side pathways. With the help of X-ray crystallography, the two equatorial methyl groups in **112** were reasoned to provide a conformational lock to provide an effective shielding of the cationic gold and thus the gold carbene can be protected from decomposition by bigger nucleophiles, including oxidants, and is selectively allowed to react with smaller nucleophiles, such as carboxylic acids. The generality of Mor-DalPhos in the trapping with MsOH was also explored in the synthesis of α-mesyloxymethyl ketones [84].

Intermolecular trapping of α-oxo gold carbenes by nucleophiles adds to the complexity of chemoselectivity because of the highly electrophilic nature of such intermediate and competing intramolecular side reactions. The scope of stoichiometric nucleophiles has remained rather limited, including carboxylic acids, sulfonic acids, and carboxamides. Recently, Zhang and coworkers addressed this deficiency in the reaction of allyl sulfides with the α-oxo gold carbenes (Scheme 51) [85]. The intermolecular trapping with allyl sulfides and the thio-Wittig [2, 3] rearrangement of **112** as described by Davies in the intramolecular setting [24] led to a new C–C bond with allylic transposition, leading to **113**. In order to reduce further the amount of the allyl sulfides and the *N*-oxides, P,S-ligand was introduced. The resulting γ,δ-unsaturated ketones could be converted to conjugated dienones in subsequent transformations.

In 2014, Ye and coworkers reported indole-3-functionalization through pyridine-*N*-oxide-based alkyne oxidation (Scheme 52) [86]. They demonstrated that the use of water as solvent alleviated the above-mentioned over-oxidation of alkynes into 1,2-diketones **117** in comparison with organic solvent such as 1,2-DCE. Direct addition of indoles to the activated ynamides to form **118** could also be minimized.

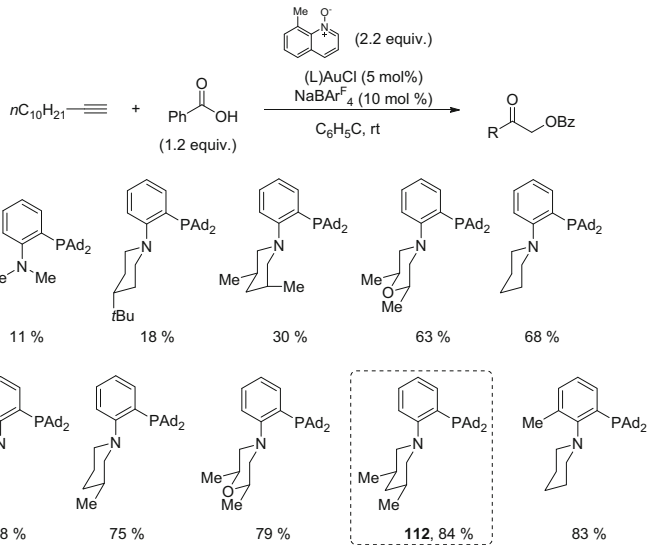

Scheme 50 Investigation of P,N bidentate ligands

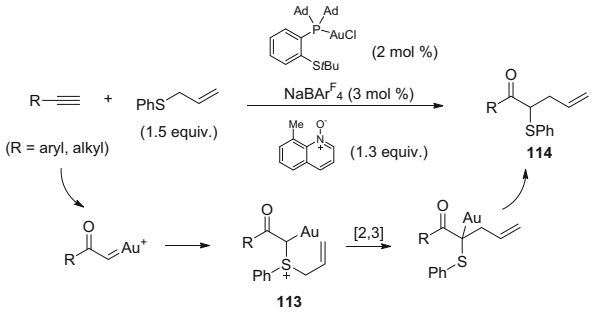

Scheme 51 Intermolecular trapping with allyl sulfides

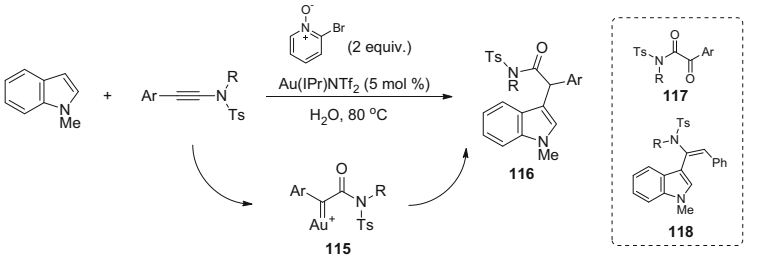

Scheme 52 Intermolecular trapping with indoles

This protocol allows efficient access to a pharmaceutical agent UK-350,926, by C–C bond formation between indoles and α-oxo gold carbenes, leading to **116**.

In using water as a medium, potentially competing side-pathways can be considered, namely an insertion of the O–H bond of water into the highly electrophilic Au-carbene **115** and a hydration of ynamides. The former O–H insertion has not been observed, unlike in the case of other transition metals, and the latter hydration could be minimized by increasing the concentration of electron-rich arenes, without complication resulting from the direct addition into ynamides to form **118**. To track down the origin of the beneficial effect of water, water-insoluble *N*-oxides have been prepared and tested. Their reaction gave a significant amount of over-oxidation by-product, just as in organic solvents. These results suggested water-soluble 2-bromo-pyridine-*N*-oxides mostly reside in the aqueous phase so that a low concentration of this oxidant is maintained in the organic phase during the reaction. This simulates a situation in which a slow addition of pyridine-*N*-oxides is adopted.

4 Other Carbene Transfer Agents

Ylides can be appropriate carbene transfer agents which can generate gold carbenoids or can be added to alkynes to generate metal carbenes. Initial studies in this category include those using diazo compounds [18, 55, 72]. More diverse ylidic species have been reported in recent years, including sulfonium and phosphonium ylides. These reagents are often stable in storage and, importantly, are safer to handle than classical diazo compounds.

4.1 Gold-Carbenes from Phosphonium Ylides

In 2008, Chen and coworkers reported observation of the first non-Fischer type gold-carbene complex of general formula (L)Au=CHR by mass spectroscopy (ESI-MS/MS) in the gas phase (Scheme 53). The precursor **119**, a gold ylide complex, was synthesized by substitution of acetoacetyl Au(I) complex with phosphorus ylide and it underwent a collision-induced dissociation (CID) by Xe atoms to generate a cationic species whose mass corresponds to **120**. Its reactivity was examined with various olefins. With *cis*-1,2-dimethoxyethene, cross metathesis reactivity to Fischer carbene **121** and β-methoxystyrene **122** dominated, while with 1,2-alkylethene, cyclopropanation to **123** prevailed, suggesting its carbene character.

4.2 Gold-Carbenes from α-Sulfonium Salts

Ingenious approaches toward new carbene precursors are continuously being developed, most notably by Chen and coworkers, from sulfonium salts (Scheme 54)

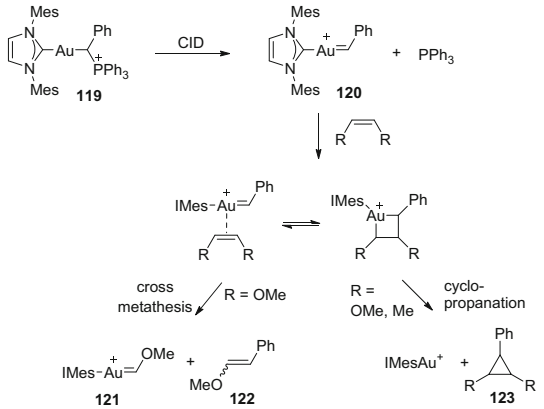

Scheme 53 Gas-phase reactivity of non-Fisher-type gold carbenes

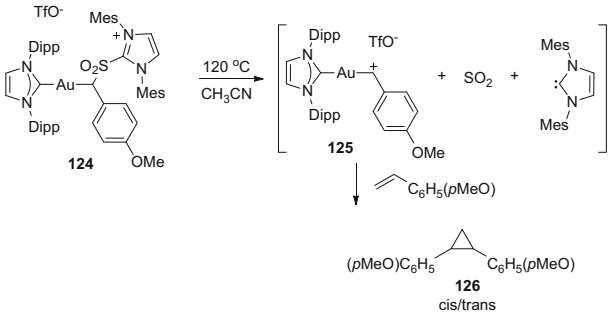

Scheme 54 Solution cyclopropanation of non-Fisher-type gold carbenes

[87]. The isolable gold complex **124** was generated by the reaction of a lithium anion of the corresponding sulfonium salt with cationic (NHC)Au^+. Upon heating, this gold alkyl complex fragmented into SO_2 gas, free NHC carbene, and gold carbene complex **125** which was identified in the gas phase. Notably, cyclopropanation of **125** with styrene derivatives has been demonstrated in a solution phase, providing the cyclopropane as a mixture of isomers.

4.3 Gold-Carbenes from Sulfonium Ylides

In 2012, Skrydstrup and coworkers reported that sulfonyl ylides can react intermolecularly with terminal alkynes, leading to formation of 2,4-disubstituted furans (Scheme 55) [88]. They envisioned the addition of sulfonium ylides **127** onto the alkynes followed by liberation of the alkyl aryl sulfide, forming a vinyl Au-carbene intermediate **128**. This, in turn, can be intramolecularly trapped by

Scheme 55 Synthesis of furans

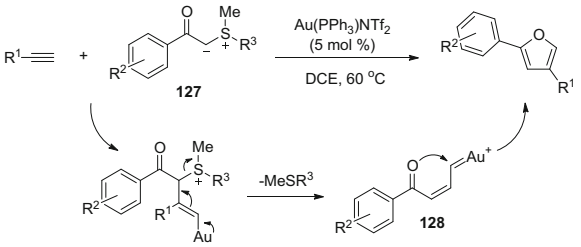

Scheme 56 Synthesis of fused furans

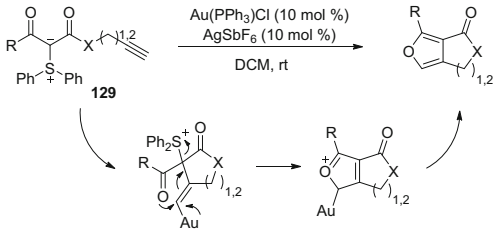

the ketone, delivering furans. The accessibility of stable zwitter-ionic sulfonium ylides that can be isolated by column chromatography was key to the successful implementation of this strategy. The scope of the alkynes is limited to aliphatic terminal alkynes. They supported a mechanism involving vinyl Au-carbene **128**, because alternative concerted nucleophilic 5-endo-dig addition of carbonyl onto the vinyl gold should be disfavored according to Baldwin's rule.

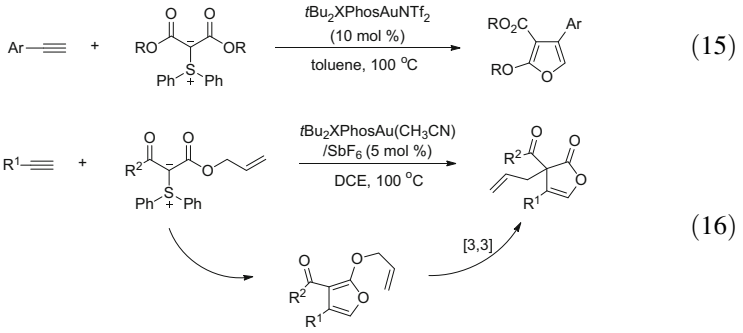

Shortly after this report, Maulide and coworkers reported a related strategy involving diphenyl sulfonium ylides **129** [89] which were, in turn, prepared by a ylide transfer protocol developed by themselves (Scheme 56) [90]. The reaction between sulfonium ylides and alkynes occurred intramolecularly, and trapping the formal Au-carbene by keto- or ester-carbonyl led to fused furans. The coupling of diphenylsulfonium ylides with alkynes can also occur intermolecularly with aryl alkynes, delivering 2,3,4-trisubstituted furans (Eq. 15). For allyl β-ketoesters, the

intermediate furan underwent a [3,3] sigmatropic rearrangement at 100°C, leading to δ-lactones with a quaternary α-center (Eq. 16). According to their DFT study, the Au-carbene could not be located as an intermediate. However, the cleavage of the S–C bond was suggested to be the rate-determining step.

Afterwards, Maulide and coworkers found that the same substrate in the absence of alkyne components underwent intramolecular cyclopropanation in highly diastereoselective fashion (Scheme 57) [91]. It is conceivable that this process is occurring through initial carbene transfer to gold, followed by intramolecular cyclopropanation. However, control experiments and DFT computation indicated that the anionic carbon of the sulfonium ylides attacks the Au-activated alkene **130** first, and the following substitution of Ph_2S in **131** closes the cyclopropane rings. In accord with this, β-ketoesters underwent slower reactions than malonate-derived substrates (R^1=O-alkyl) because of their more stabilized and lower carbon nucleophilicity. It should be noted that the present reaction by gold catalysis outperformed diazo-mediated Rh(I)-catalyzed cyclopropanation, where C–H activation products are accompanied as by-products [92].

Sulfonium ylides can also be transferred to allenes to form vinyl cyclopropanes (VCPs) [93]. As in the reaction with alkenes, the reaction with allenylamides occurs with the initial addition of sulfonium ylidic carbon at the γ-carbon of allene **132**, followed by intramolecular substitution of the sulfonium moiety (Scheme 58).

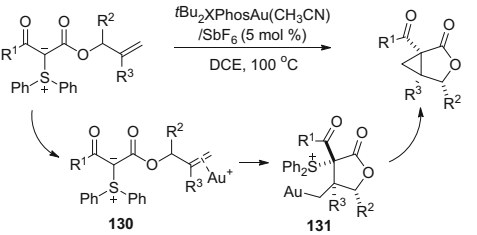

Scheme 57 Intramolecular cyclopropanation

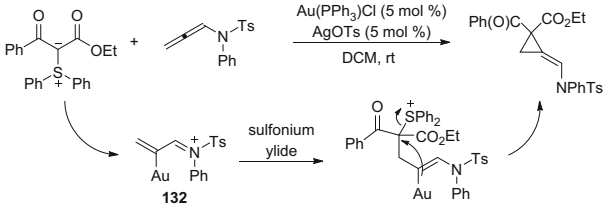

Scheme 58 Synthesis of vinylcyclopropanes

5 Conclusion

The ability of gold metal to stabilize an α-carbocation has spurred interest in the methods of generation and reactions of gold carbenes. In this field, one of the most prominent approaches has been the reactions of leaving group-bearing nucleophiles with alkynes which have been discussed in this review. Novel catalytic methodologies have been developed at a rapid pace, employing various combinations of nucleophilic atoms and leaving groups, which resulted in a large repertoire of useful reactions. The prospects are that new carbene precursors or OAT transfer reagents should continue to be developed in the future.

Acknowledgments This work was supported by a National Research Foundation of Korea (NRF) grant funded by the Korean Government (2014-011165, 2012-015662 and 2012M3A7B4049653).

References

1. Davies HML, Beckwith REJ (2003) Chem Rev 103:2861
2. Davies HML, Deton JR (2009) Chem Soc Rev 38:3061
3. Fischer N, Goddard-Borger ED, Greiner R, Klapotke TM, Skelton BW, Stierstorfer J (2012) J Org Chem 77:1760
4. Proctor LD, Warr AJ (2002) Org Process Res Dev 6:884
5. Li X (2011) Angew Chem Int Ed 50:7226
6. Nevado C, de Haro T (2012) Synthetic potential behind gold-catalyzed redox processes. In: Pignataro B (ed) New strategies in chemical synthesis and catalysis. Wiley, Weinheim
7. Yeom H-S, Shin S (2014) Acc Chem Res 47:966
8. Zhang L (2014) Acc Chem Res 47:877
9. Marion N, Nolan SP (2007) Angew Chem Int Ed 46:2750
10. Mauleon P, Toste FD (2012) Gold-catalyzed reactions of propargyl esters, proparyl alcohols, and related compounds. In: Hashmi ASK, Toste FD (eds) Modern gold catalyzed synthesis. Wiley, Weinheim
11. Miege F, Meyer C, Cossy J (2011) Beilstein J Org Chem 7:717
12. Gorin DJ, Davis NR, Toste FD (2005) J Am Chem Soc 127:11260
13. Wetzel A, Gagosz F (2011) Angew Chem Int Ed 50:7354
14. Lu B, Luo Y, Liu L, Ye L, Wang Y, Zhang L (2011) Angew Chem Int Ed 50:8358
15. Shapiro ND, Toste FD (2007) J Am Chem Soc 129:4160
16. Li C, Zhang L (2011) Org Lett 13:1738
17. Davies PW, Cremonesi A, Dumitrescu L (2011) Angew Chem Int Ed 50:8931
18. Witham CA, Mauleon P, Shapiro ND, Sherry BD, Toste FD (2007) J Am Chem Soc 129:5838
19. Li G, Zhang L (2007) Angew Chem Int Ed 46:5156
20. Xiao FP, Liu Y, Wang JB (2007) Tetrahedron Lett 48:1147
21. Cuenca AB, Montserrat S, Hossain KM, Mancha G, Lledós A, Medio-Simón M, Ujaque G, Asensio G (2009) Org Lett 11:4906
22. Li C-W, Pati K, Lin G-Y, Sohel SMA, Hung H-H, Liu R-S (2010) Angew Chem Int Ed 49:9891
23. Lu B, Li Y, Wang Y, Aue DH, Luo Y, Zhang L (2013) J Am Chem Soc 135:8512
24. Davies PW, Albrecht SJC (2009) Angew Chem Int Ed 48:8372
25. Pirrung MC, Zhang J, Lackey K, Sternbach DS, Brown F (1995) J Org Chem 60:2112
26. Xu H, Zhang W, Shu D, Werness JB, Tang W (2008) Angew Chem Int Ed 47:8933

27. Xu C-F, Xu M, Jia Y-X, Li C-Y (2011) Org Lett 13:1556
28. Hashmi ASK, Bührle M, Salathé R, Bats JW (2008) Adv Synth Catal 350:2059
29. Lin G-Y, Li C-W, Hung S-H, Liu R-S (2008) Org Lett 10:5059
30. Chaudhuri R, Liu R-S (2011) Adv Synth Catal 353:2589
31. Asao N, Sato K, Yamamoto Y (2003) Tetrahedron Lett 44:5675
32. Li X, Vogel T, Incarvito CD, Crabtree RH (2005) Organometallics 24:62
33. Jadav AM, Bhunia S, Liao H-Y, Liu R-S (2011) J Am Chem Soc 133:1769
34. Yeom H-S, Lee Y, Lee J-E, Shin S (2009) Org Biomol Chem 7:4744
35. Yeom H-S, Shin S (2008) Synlett 924
36. Yeom H-S, Lee JE, Shin S (2008) Angew Chem Int Ed 47:7040
37. Song G, Chen D, Su Y, Han K, Pan C-L, Jia A, Li X (2011) Angew Chem Int Ed 50:7791
38. Jeong J, Yeom H-S, Kwon O, Shin S (2011) Chem Asian J 6:1977
39. Yeom H-S, Lee Y, Jeong J, So E, Hwang S, Lee J-E, Shim S, Shin S (2010) Angew Chem Int Ed 49:1611
40. Bhunia S, Chang C-J, Liu R-S (2012) Org Lett 14:5522
41. Mukherjee A, Dateer RB, Chaudhuri R, Bhunia S, Karad SN, Liu R-S (2011) J Am Chem Soc 133:15372
42. Cui L, Peng Y, Zhang L (2009) J Am Chem Soc 131:8394
43. Cui L, Zhang G, Peng Y, Zhang L (2009) Org Lett 11:1225
44. Noey EL, Luo Y, Zhang L, Houk KN (2012) J Am Chem Soc 134:1078
45. Porzelle A, Woodrow MD, Tomkinson NCO (2009) Synlett 797
46. Jones KL, Porzelle A, Hall A, Woodrow MD, Tomkinson NCO (2008) Org Lett 10:797
47. Yeom H-S, So E, Shin S (2011) Chem Eur J 17:1764
48. Coates RM, Hutchins CW (1979) J Org Chem 44:4742
49. Joule JA (2000) Sci Synth 10:380
50. Wang Y, Ye L, Zhang L (2011) Chem Commun 47:7815
51. Wang Y, Liu L, Zhang L (2013) Chem Sci 4:739
52. Zheng Z, Tu H, Zhang L (2014) Chem Eur J 20:2445
53. Kawade RK, Huang P-H, Kara SN, Liu R-S (2014) Org Biomol Chem 12:737
54. Murru S, Gallo AA, Srivastava RS (2011) ACS Catal 1:29
55. Pagar VV, Jadav AM, Liu R-S (2011) J Am Chem Soc 133:20728
56. Xu Z-J, Zhu D, Zeng X, Wang F, Tan B, Hou Y, Ly Y, Zhong G (2010) Chem Commun 46:2504
57. Abramovitch RA, Shinkai I (1974) For early use of pyridine-N-oxides. J Am Chem Soc 96:5265
58. Caron S, Do NM, Sieser JE (2000) Tetrahedron Lett 41:2299
59. Veerakumar P, Balakumar S, Velayudham M, Lu K-L, Rajagopal S (2012) Catal Sci Tech 2:1140
60. Takahashi S, Kano H (1963) Tetrahedron Lett 25:1687
61. Lee TD, Keana JFW (1976) J Org Chem 41:3237
62. Ye L, Zhang G, Zhang L (2010) J Am Chem Soc 132:3258
63. Ye L, He W, Zhang L (2010) J Am Chem Soc 132:8550
64. Ye L, He W, Zhang L (2011) Angew Chem Int Ed 50:3236
65. Robak MT, Herbage MA, Ellman JA (2010) Chem Rev 110:3600
66. Shu C, Li L, Yu Y-F, Jiang S, Ye L-W (2014) Chem Commun 50:2522
67. Lu B, Li C, Zhang L (2010) J Am Chem Soc 132:14070
68. Vasu D, Hung H-H, Bhunia S, Gawade SA, Das A, Liu R-S (2011) Angew Chem Int Ed 50:6911
69. Bhunia S, Ghorpade S, Huple DB, Liu R-S (2012) Angew Chem Int Ed 51:2939
70. Ghorpade S, Su M-D, Liu R-S (2013) Angew Chem Int Ed 52:4229
71. Wang Y, Ki K, Lan S, Zhang L (2012) Angew Chem Int Ed 51:1915
72. Karad NS, Liu R-S (2014) Angew Chem Int Ed 53:5444
73. Dubé P, Toste FD (2006) J Am Chem Soc 128:12062

74. Pawar SK, Wang C-D, Bhunia S, Jadhav AM, Liu R-S (2013) Angew Chem Int Ed 54:7559
75. Qian D, Zhang J (2011) Chem Commun 47:11152
76. Yeom H-S, Shin S (2013) Org Biomol Chem 11:1189
77. Davies PW, Cremonesi A, Martin N (2011) Chem Commun 47:379
78. He W, Xie L, Xu Y, Xiang J, Zhang L (2012) Org Biomol Chem 10:3168
79. Xie L, Liang Z, Yan D, He W, Xiang J (2013) Synthesis 24:1809
80. He W, Li C, Zhang L (2011) J Am Chem Soc 133:8482
81. Luo Y, Ji K, Li Y, Zhang L (2012) J Am Chem Soc 134:17412
82. Hesp KD, Stradiotto M (2010) J Am Chem Soc 132:18026
83. Ji K, Zhao Y, Zhang L (2013) Angew Chem Int Ed 52:6508
84. Wu G, Zheng R, Nelson J, Zhang L (2014) Adv Synth Catal 356:1229
85. Li J, Ji K, Zheng R, Nelson J, Zhang L (2014) Chem Commun 50:4130
86. Li L, Shu C, Zhou B, Yu Y-F, Xiao X-Y, Ye L-W (2014) Chem Sci 5:4057
87. Ringger DH, Chen P (2013) Angew Chem Int Ed 52:4686
88. Kramer S, Skrydstrup T (2012) Angew Chem Int Ed 51:4681
89. Huang X, Peng B, Luparia M, Gomes LFR, Veiros LF, Maulide N (2012) Angew Chem Int Ed 51:8886
90. Huang X, Goddard R, Maudide N (2010) Angew Chem Int Ed 49:8979
91. Huang X, Klimczyk S, Veiros LF, Maulide N (2013) Chem Sci 4:1105
92. Bonnaud B, Funes P, Jubault N, Vacher B (2005) Eur J Org Chem 3360
93. Sabbatani J, Huang X, Veiros LF, Maulide N (2014) Chem Eur J 20:10636

Top Curr Chem (2015) 357: 63–94
DOI: 10.1007/128_2014_590

Published online: 18 December 2014

Gold-Catalyzed Transformation of Unsaturated Alcohols

Paulo H.S. Paioti and Aaron Aponick

Abstract The use of gold-complexes to activate carbon–carbon π-bonds has become a well-known and highly reliable mode of reactivity for applications in organic synthesis. This review covers the use of gold-catalysts for activation of unsaturated alcohols to effect substitution with concomitant loss of water and is mostly focused on reactions where the π-acidity appears to overcome the inherent Lewis acidity of the complexes for alcohol activation. Select examples from the literature which demonstrate advances made between 2011 and 2014 are presented.

Keywords Allylic alcohols · Benzyl alcohols · Gold-catalysis · Heterocycles · Natural products · Propargyl alcohols · S_N2'

Contents

P.H.S. Paioti and A. Aponick (✉)
Department of Chemistry, Center for Heterocyclic Compounds, University of Florida, P.O. Box 117200, Gainesville, FL 32607
e-mail: aponick@chem.ufl.edu

1 Introduction

Homogeneous gold-catalyzed reactions of alkynes, allenes, and alkenes have dominated the landscape of the chemical literature on this topic because of the extreme ease of bond formation in a wide variety of settings in combination with a broad functional group tolerance. Numerous reviews have appeared to document the progress of the field since approximately 1998 [1–10], when some of the most influential seminal contributions began to appear [11, 12]. It is clear that both catalyst development and system design have had tremendous impact on the area, but one of the most important reactions continues to be the gold-catalyzed addition of heteroatom nucleophiles to π-bonds [13–15]. Interestingly, in addition to nucleophilic addition reactions, substitution reactions can also be effected with judicious substrate choice. While substitution reactions employing the gold-catalyst to act as a Lewis acid for cation formation are known, the more traditional π-acidity of the catalyst can also be harnessed in alternative mechanistic schemes. We reviewed this area in 2011 [16] and other reviews have also covered this now broad topic [17, 18]. Herein we describe advances in the field which have appeared since 2011 and focus on select examples where the catalyst effects substitution reactions by activating the π-bond, generally resulting in two-step processes.

1.1 Reaction Discovery

Gold-catalyzed reactions of heteroatom nucleophiles to alkynes, allenes, and alkenes are well known and effective conditions for these reactions have long been established [19, 20]. Interestingly, reactions of alkynes and allenes typically proceed under very mild conditions, while the gold-catalyzed addition to olefins requires much more forcing conditions [21]. It is now well accepted that this is because of a difficult protodeauration of Au–σ-complexes containing the Au–C_{sp3} bond [22]. Essentially, the catalyst cannot turn over very easily, often necessitating alternative pathways [23].

In 2006 we began to screen conditions in an attempt to develop a one-pot hydroalkoxylation/Claisen rearrangement whereby the addition of an allylic alcohol to an alkyne to form an allyl vinyl ether would immediately be followed by a gold-catalyzed Claisen rearrangement. Unfortunately, this reaction proved to be very difficult because of competing side-reactions of the substrates. Although we and others were eventually successful at developing a protocol for this reaction [24, 25], a very interesting competing reaction was responsible for this difficulty. During these attempted reactions, two molecules of allylic alcohol seemed to condense to form diallyl ether, albeit in a very inefficient process. In 2008, after optimization, the Aponick group published what was, to the best of our knowledge, the first Au-catalyzed formal S_N2' reaction of

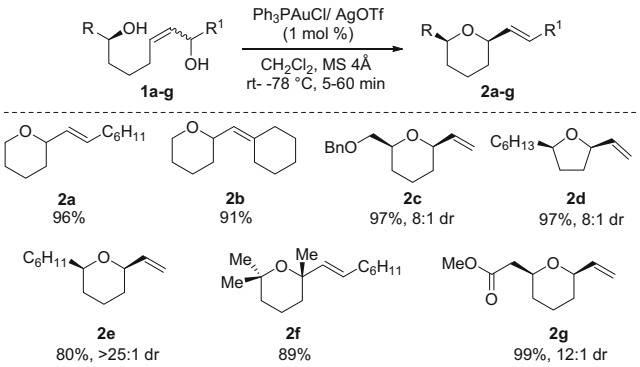

Scheme 1 First report of gold-catalyzed addition to allylic alcohols

allylic alcohols **1a–g** (Scheme 1) [26]. In contrast to previous reports for the Au-catalyzed addition of heteroatom nucleophiles to alkenes, the reactions proceeded under the very mild conditions most often observed for addition to alkynes and allenes. Although there are many other catalysts based upon different metals [27, 28], the gold-catalyzed variant has two distinct advantages: (1) the catalyst loading is usually very low and the conditions are very mild and (2) it appears that gold-catalyzed reactions proceed by a non-cationic mechanism, enabling the development of highly stereoselective processes. Interestingly, this report was preceded by gold-catalyzed substitution reactions of aryl-substituted propargyl alcohols, but mechanistically these reactions appear to be quite different [29].

2 Mechanism

As described above, Aponick and coworkers reported the addition of alcohol nucleophiles to allylic systems. Widenhoefer later reported the addition of amines [30] and Bandini reported the use of indoles as nucleophiles [31]. Detailed mechanistic studies on systems using both the alcohol and indole nucleophiles have appeared and the findings are described below. Throughout the remainder of this review, the mechanisms proposed by the original authors are presented, and many of the principles in this section are applicable throughout the chapter.

2.1 Mechanism of the Addition of Oxygen Nucleophiles to Allylic Alcohols

As described previously, a variety of mechanisms are possible for the metal catalyzed addition of nucleophiles to allylic systems. In the case of the gold-catalyzed addition

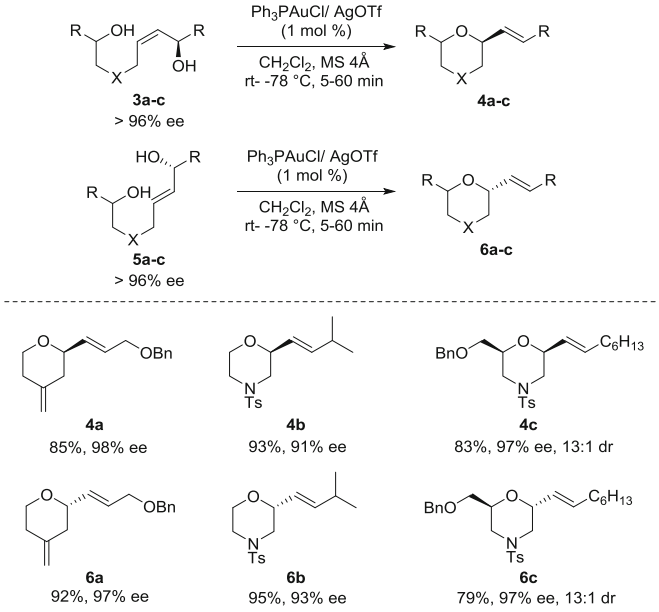

Scheme 2 Chirality transfer in the gold-catalyzed addition to allylic alcohols

of alcohols in a formal S_N2' sense, two observations were intriguing. First, the reactions proceed under conditions typically employed for alkynes and allenes instead of the more forcing conditions typical of gold-catalyzed olefin addition reactions. As seen in Scheme 1, the reactions are usually complete in minutes to 1 h at room temperature [26]. With olefins, the reactions typically require elevated temperatures for up to 48 h [21]. Second, the reaction proved to be highly stereoselective (Scheme 2) with the enantiomeric excess being transferred from the starting material, while *trans*-alkene products were always observed in our hands. It should be noted that there have now been reports of *cis*-olefin products [32, 33], but we consider these cases as more the exception than the rule.

These observations were suggestive of two possible mechanisms (Scheme 3). Since there are two pieces of stereochemical information embedded in the starting materials and products (absolute stereochemistry and olefin geometry) and these are known in both, information about the mechanism can be extracted. In these examples, the reaction must proceed by a *syn* addition/*syn* elimination or an *anti* addition/*anti* elimination mechanism for the stereochemistry to be correct (Scheme 3). If a *syn*/*anti* or an *anti*/*syn* mechanism is followed, either the absolute configuration of the product or the olefin geometry is incorrect. A mixture of products would also be expected for a concerted S_N2' mechanism and this was ruled out unless particular substrates are prone to ionization (contain a cation stabilizing group).

While it is well accepted that gold-catalyzed addition reactions occur via an *anti* addition mechanism, both the *anti* and *syn* mechanisms were explored

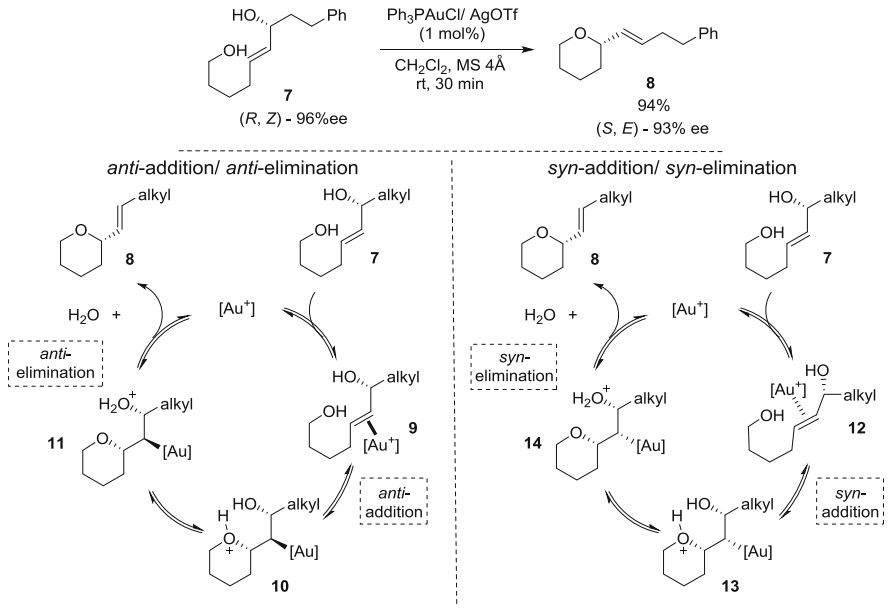

Scheme 3 Possible mechanisms of Au-catalyzed addition to allylic alcohols

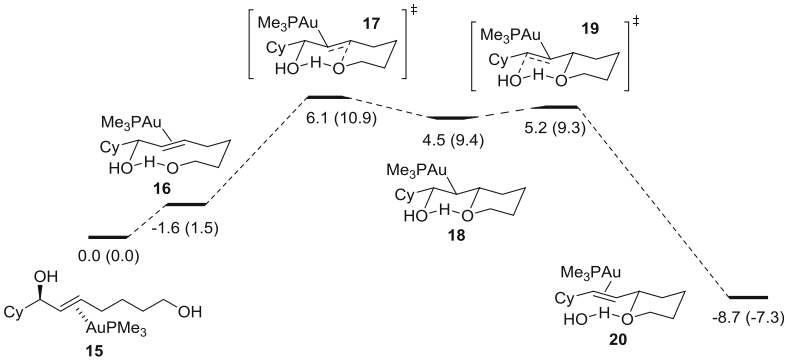

Scheme 4 Calculated reaction coordinate

experimentally and computationally by the Aponick, Ess, and coworkers [34]. It was found that the reaction does indeed follow an *anti* addition/*anti* elimination pathway (Scheme 4). Hydrogen bonding also appears to play a vital role in templating the reaction stereochemistry and obviating the need for intermolecular proton transfer. In earlier work, Widenhoefer had also suggested the importance of hydrogen bonding in amination reactions [35]. Essentially, this reaction proceeds under mild conditions because a pathway alternative to protodeauration is provided by the *anti* elimination of water.

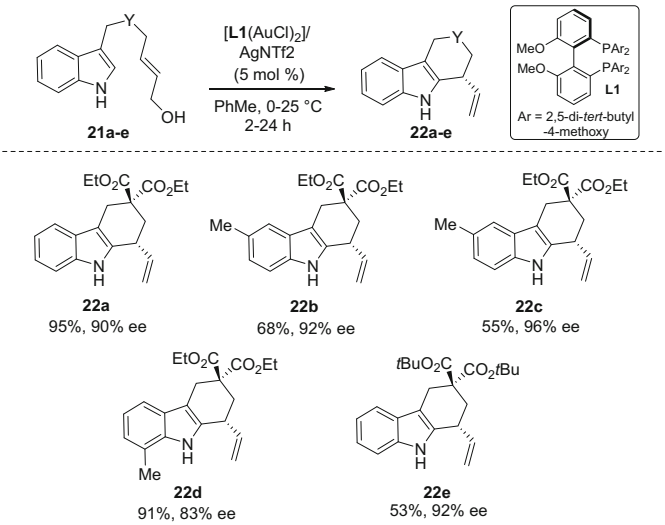

Scheme 5 Gold-catalyzed cyclization of indole nucleophiles

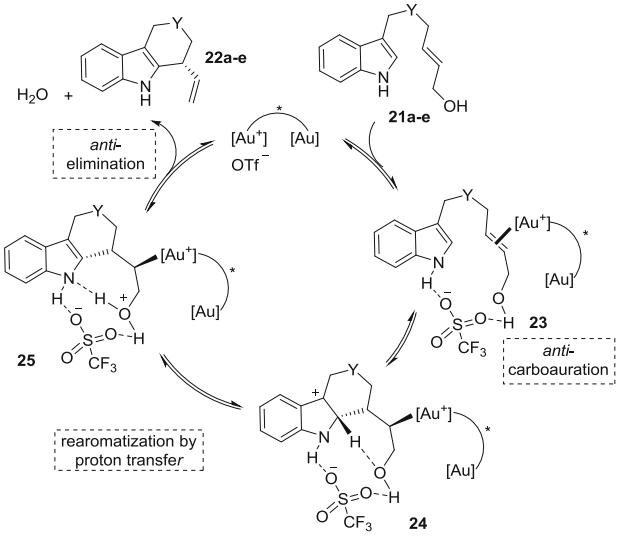

Scheme 6 Mechanism of gold-catalyzed nucleophilic addition by indoles

2.2 *Mechanism of the Addition of Carbon Nucleophiles to Allylic Alcohols*

In the case of carbon nucleophiles, the hydrogen bonding described as being crucial for the reaction is not possible, but Bandini and coworkers have been successful in explaining the mechanism, even in the absence of this hydrogen bonding. The

conditions for this reaction are shown in Scheme 5 and the reactions work quite well [31]. Indoles **21a–e** act as nucleophiles in this intramolecular reaction, delivering the products **22a–e** with high enantiomeric excess by using a chiral dinuclear bis (gold)phosphine-complex.

To explain the reactivity, based on calculations, the authors propose that the counterion is involved in proton shuttling (Scheme 6). They propose an initial *anti* carboauration with the triflate counterion templating the reaction by interaction with both the indole NH and the alcohol OH. Rearomatization and proton transfer then gives intermediate **25** and *anti* elimination of [Au]–OH provides the product [36]. Interestingly, the reaction provides the product with a variety of counterions including BF_4^-, SbF_6^-, and NTf_2^-.

3 Reactions of Allylic Alcohols

This section covers intra- and intermolecular gold(I)- and gold(III)-catalyzed dehydrative transformations of allylic alcohols which have appeared in the literature since 2011. There are generally two main pathways in which these reactions proceed: the formal S_N2' pathway, in which a gold-complex acts as a π-acidic late transition metal and is often involved in the aforementioned addition/elimination sequence and the cationic pathway, whereby a gold-complex acts as a Lewis acid to generate a stabilized allylic carbocation.

3.1 Intramolecular Reactions of Allylic Alcohols

The development of intramolecular gold-catalyzed dehydrative cyclization reactions of monoallylic diols has allowed for the rapid construction of functionalized saturated tetrahydropyran and tetrahydrofuran rings [16, 27]. Among the reactions of allylic and propargylic systems presented in this chapter, this class of reactions was the first to be developed [26]. These intramolecular catalytic processes encompass successful diastereoselective reactions [26], as well as transformations in which the chirality embedded in the substrate is fully transferred to the product [37].

More recently, Bandini and coworkers have employed a chiral bis(gold)phosphine-complex to perform an enantioselective gold-catalyzed cascade reaction targeting oxazino-indoles **27a–g** (Scheme 7) [38]. The reactions occurred under mild conditions, and among the chiral bisphosphine ligands studied, the (*R*)-DTBM-segphos gave the best results. The reaction tolerates a variety of substrates, delivering oxazinoindoles in good to excellent yields and enantioselectivities.

The cascade reaction begins with the formation of the indole moiety from substrates **26c** through a gold-catalyzed hydroamination reaction, placing the previously distal alcohol nucleophile in close proximity to the double bond [38] (Scheme 8). The second cyclization, which is inherently the enantiodetermining

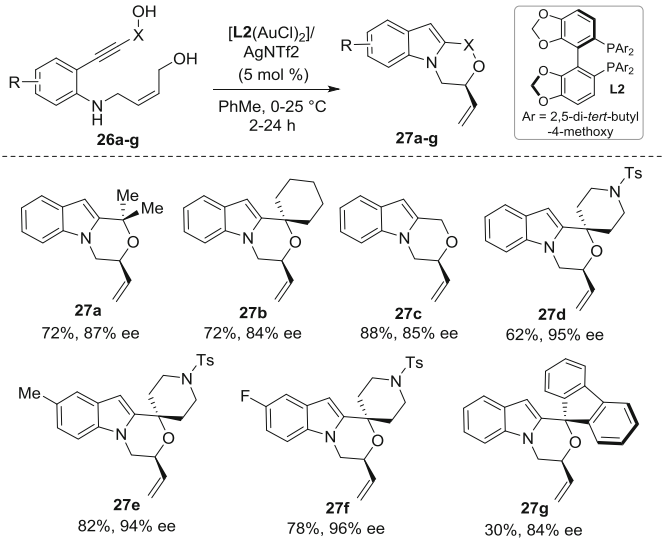

Scheme 7 Enantioselective gold-catalyzed cascade towards oxazinoindoles

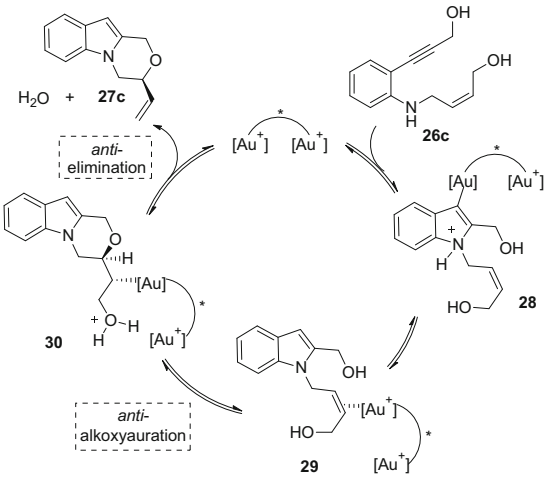

Scheme 8 Proposed catalytic cycle for the asymmetric synthesis of oxazino-indoles

step, is facilitated by the π-activation of the double bond by the chiral dinuclear gold-complex. The gold-catalyst and the pendant alcohol are believed to have an *anti* relationship in both the alkoxyauration and β-elimination steps which turns the catalyst over, and furnishes the desired oxazinoindoles **27** and water as the byproduct.

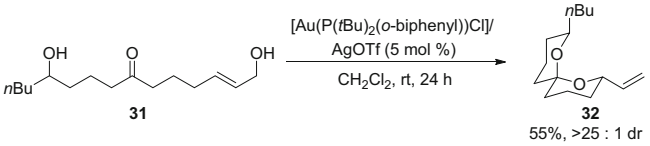

Scheme 9 Gold-catalyzed spiroketalization of monoallylic ketodiols

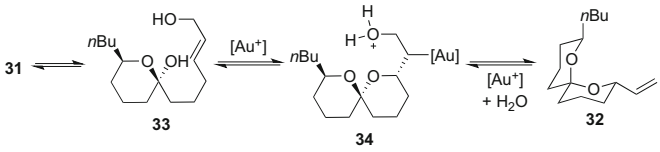

Scheme 10 Proposed pathway for the cyclization of monoallylic ketodiols

A gold-catalyzed cascade cyclization of allylic alcohols has been also successfully utilized by Aponick and coworkers in the synthesis of the [6,6]-spiroketal **31** (Scheme 9) [39]. Because of the biological relevance of spiroketal-containing molecules, several reports on metal-catalyzed synthesis of spiroketals have recently appeared [40], and these methods aim at complementing the well-known Brønsted-acid catalyzed spiroketalization of ketodiols [41]. In this report, Aponick and co-workers have employed allylic ketodiols **31** as precursors for the synthesis of vinylspiroketals **32**.

Mechanistically, Aponick and coworkers proposed that the in situ formed ketal **33** also undergoes the alkoxyauration/elimination sequence, forming two new stereocenters in very high diastereoselectivity (Scheme 10) [39]. This sequential spiroketal synthesis worked when Au(I)-complexes were employed, but Pd(II)-complexes proved to be superior catalysts, providing the products in higher yield. This reaction was later utilized in the synthesis of acortatarin A [42].

Robertson and coworkers have also utilized a dehydrative cyclization of an allylic alcohol in their total synthesis of (+)-isoaltholactone **40** (Scheme 11) [32]. In this synthesis, the tetrahydropyran moiety of the isoaltholactone was generated from the corresponding diastereomeric mixture of the monoallylic diols **36**. The gold-catalyzed dehydrative cyclization occurred smoothly, furnishing a diastereomeric mixture of tetrahydropyran-containing molecules **37**, **38**, and **39**, which were further elaborated to the natural product. The stereospecificity of the gold-catalyzed transformation was also studied with single diastereomers, suggesting that reactions of the *anti* diastereomers are more selective than the corresponding *syn* diols [32].

The importance of nitrogen-containing heterocycles such as pyrrolidine and piperidine derivatives in natural product synthesis has led the synthetic community to design stereoselective methods for their preparation [43]. In this context, Widenhoefer and coworkers showed that such azacyclic structures could be synthesized by gold-catalyzed dehydration of allylic alcohols containing an amine functionality [30]. More recently, two new complementary reports by the

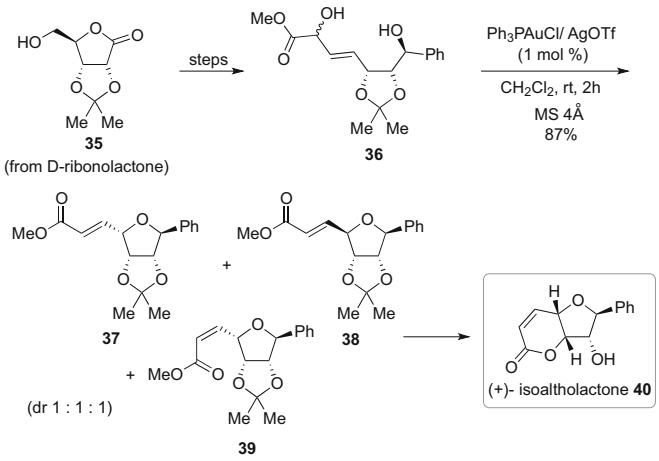

Scheme 11 Gold-catalyzed dehydrative cyclization in the total synthesis of (+)-isoaltholactone

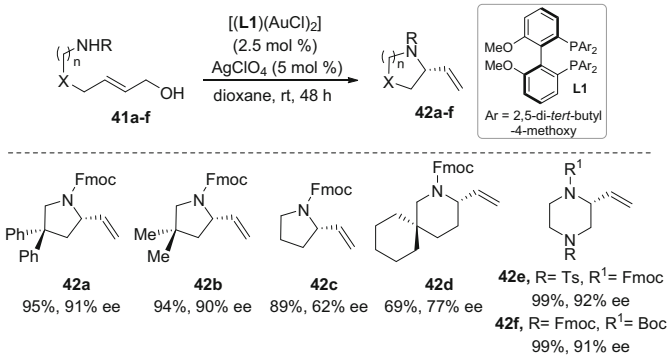

Scheme 12 Gold-catalyzed enantioselective synthesis of azacycles

Widenhoefer [33] and Aponick [44] groups have appeared on this topic, broadening the scope of preparation of substituted pyrrolidines and piperidines.

Widenhoefer and co-workers have elegantly demonstrated that axially chiral dinuclear bis(gold)phosphine-complexes could be employed for the asymmetric preparation of several azacycles **42a–f** (Scheme 12) [33]. The reactions were performed under mild conditions with various carbamates **41a–f**, furnishing the products **42a–f** in high yields, and in moderate to excellent enantioselectivities.

Similarly to Aponick and Ess's mechanistic proposal for the gold-catalyzed preparation of tetrahydropyrans and tetrahydrofurans [34], Widenhoefer and coworkers proposed an *anti* aminoauration, followed by an *anti* elimination step. The carbamate acts as a nucleophile at the nitrogen and the chiral environment created by the bisphosphine ligand dictates the face selectivity in the aminoauration step (Scheme 13).

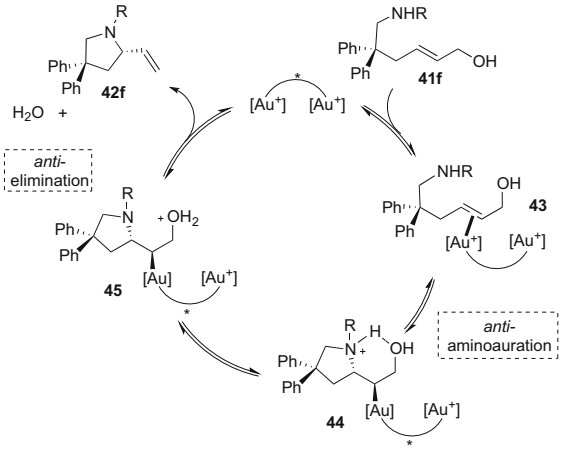

Scheme 13 Proposed catalytic cycle for the enantioselective gold-catalyzed synthesis of azacycles

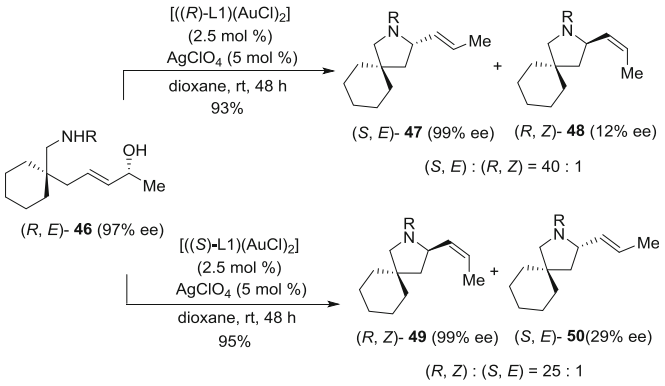

Scheme 14 Cyclization of enantiomerically enriched allylic alcohols

The mechanism hypothesis was supported by experiments with the chiral optically pure allylic alcohol **46**, which was submitted to the standard reaction conditions with two different enantiomers of the bisphosphine ligand (Scheme 14) [33]. The reaction employing the (*R*)-enantiomer of the ligand nearly exclusively afforded **47** (40:1 ratio of **47**:**48**), containing an (*S*)-stereocenter and an (*E*)-olefin. In contrast, the reaction with the (*S*)-enantiomer of the ligand almost exclusively afforded **49** (25:1 ratio of **49**:**50**), containing an (*R*)-stereocenter and a (*Z*)-olefin. This set of experiments demonstrated that the chirality of the ligand was responsible for the face selectivity in regard to the olefin addition (catalyst control), and that the olefin geometry in the final product is a consequence of a stereospecific and probably *anti* elimination pathway.

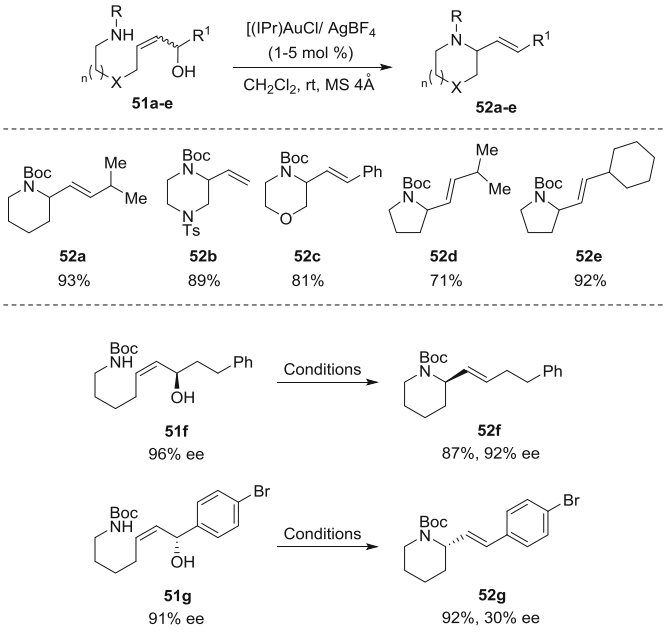

Scheme 15 Gold-catalyzed dehydrative cyclization towards azacycles

In order to expand the scope of the gold-catalyzed synthesis of azacycles, Aponick and coworkers have shown that carbamates and sulfonamides could be successfully employed in the reaction to deliver azacycles in high yields under very mild conditions (Scheme 15) [44]. Interestingly, it was demonstrated in this report that the chirality present in the substrate can be fully transferred to the product in the cases where an alkyl substituted allylic alcohol is utilized (**51f**); however, transfer of chirality was only partially successful when the compound **51g** containing an aryl substituent was employed.

It is probable that the chirality transfer in the alkyl substituted allylic alcohol **51f** results from the aforementioned *anti* aminoauration/*anti* elimination sequence (Scheme 16) [33]. In the cyclization of the aryl-substituted allylic alcohol **51g**, the loss of enantiomeric excess was attributed to a competing cationic mechanism, whereby the catalyst probably acts as a Lewis acid [44]. In fact, the transfer of chirality in aryl-substituted allylic alcohols is quite challenging and further development in this area is necessary for this transformation to be successfully accomplished.

Following the work on the synthesis of heterocycles by means of C–O and C–N bond formation, the Bandini group reported the use of carbon nucleophiles in gold-catalyzed intramolecular dehydrative cyclization of allylic alcohols. To accomplish this task, the authors have initially employed indole derivatives, which have been demonstrated to be suitable nucleophiles in this type of cyclization reaction as seen in Sect. 2.2 [31]. Moreover, Bandini and co-workers have demonstrated that

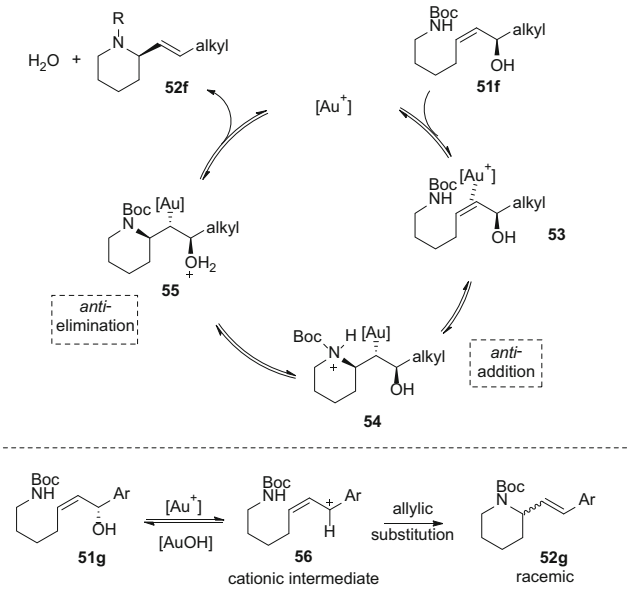

Scheme 16 Dual-pathways in the gold-catalyzed synthesis of azacycles

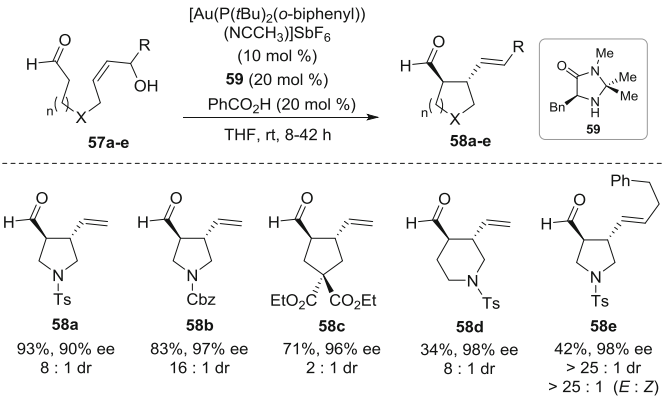

Scheme 17 Enamine catalysis meets gold-catalysis in the enantioselective α-allylic alkylation of aldehydes

enamine catalysis [45] and gold-catalysis could be combined for the enantioselective construction of a C–C bond, resulting in two new stereocenters via α-allylic alkylation of aldehydes (Scheme 17) [46]. In this report, chiral secondary amines were shown to be compatible with the reaction conditions, and a chiral enamine was generated from the aldehyde in situ. The formation of this chiral nucleophile allowed for the use of an achiral gold-complex in the asymmetric construction of the allylic stereocenter. In general, the reactions proceeded

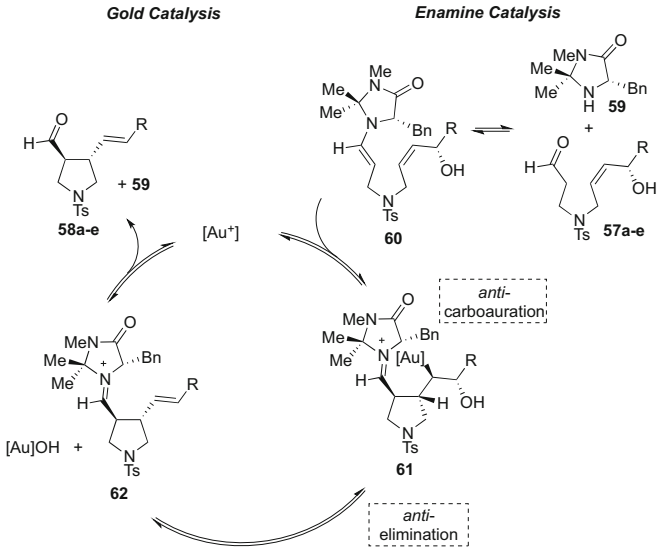

Scheme 18 Proposed pathway for the enantioselective α-allylic alkylation of aldehydes

smoothly, and the products **58a–e** were synthesized from the aldehydes **57a–e** in excellent yields and enantioselectivities, in good to excellent diastereoselectivities.

The proposed mechanism is comprised of two main catalytic cycles: the well-known enamine activation of carbonyl groups for asymmetric catalysis [45], and the catalytic cycle for gold-catalyzed dehydrative intramolecular cyclization of allylic alcohols (Scheme 18). The authors proposed that the condensation of the secondary amine **59** with the aldehyde generates the enamine **60**, which undergoes *anti* carboauration upon activation of the double bond by the cationic gold-complex, forming the *trans* ring system **61** [46]. Elimination then generates the (*E*)-olefin in the product, recycling the cationic gold-complex.

The intramolecular gold-catalyzed cyclization of allylic alcohols is a powerful method for the synthesis of very useful oxygen- and nitrogen-containing heterocycles, as well as carbocycles. Facile preparation of the substrates and mild reaction conditions are features of the cyclization reaction which should render it attractive for the preparation of complex natural products and biologically active molecules. Currently, there are many reports of highly diastereoselective and enantioselective reactions and the high functional group tolerance allows for application in a diverse variety of settings.

3.2 Intermolecular Reactions of Allylic Alcohols

Intermolecular palladium-catalyzed allylic alkylations – such as the Tsuji–Trost reaction – are well-documented processes [47], but, with minimal exceptions, a

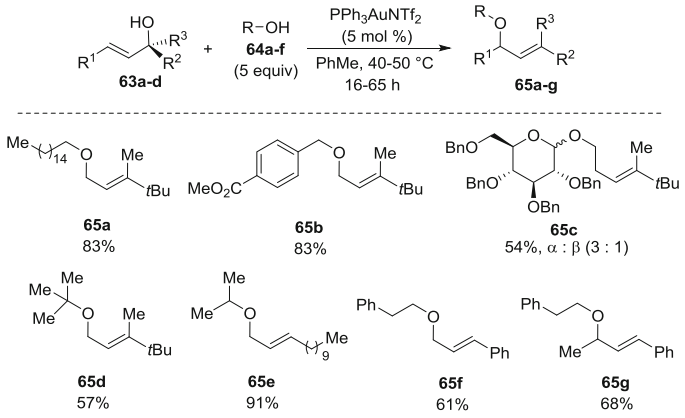

Scheme 19 Lee's gold-catalyzed dehydrative intermolecular allylic alkylation

good leaving group is required. Reactions catalyzed by other metals such as rhodium [48] and ruthenium [49], and seminal work from the Hartwig [50] and Carreira [51] groups on iridium-catalyzed intermolecular allylic alkylations, broadened the scope of this reaction. One particularly relevant advance is the ability to use poor leaving groups such as hydroxyl groups in which water is produced as the byproduct. At approximately the same time, the first intramolecular gold-catalyzed dehydrative transformations appeared [16] and the obvious next step was to develop intermolecular variants. In contrast to the Tsuji–Trost reaction, in these transformations the nucleophile and the electrophile are both alcohols, adding a degree of difficulty; nevertheless, the groups of Lee [52] and Widenhoefer [53] have disclosed the first intermolecular etherification of allylic alcohols.

Lee and coworkers demonstrated that primary, secondary, and tertiary alcohols are suitable nucleophiles for the gold-catalyzed intermolecular alkylation of several allylic alcohols, accomplishing an overall formal S_N2' reaction (Scheme 19) [52]. The reaction takes place with superstoichiometric amounts of the nucleophile, with isolated yields ranging from good to excellent, depending on the electrophile–nucleophile pair.

Widenhoefer expanded the scope of the gold-catalyzed intermolecular allylic alkylation and also provided insight into the reaction mechanism (Scheme 20) [53]. The reactions reported by Widenhoefer and coworkers were carried out at room temperature as opposed to 40–50°C, with yields comparable to those reported by Lee and coworkers [52].

Based on the previous work on chirality transfer in intramolecular gold-catalyzed dehydrations [37], the Widenhoefer group also explored the possibility of creating a process to generate non-racemic products whereby the chirality present in the allylic alcohol substrate could be transferred to the allylic ether product. To test the feasibility, the authors employed an enantioenriched allylic alcohol **69** in the cyclization (Scheme 21) [53]. Under the standard reaction conditions, the ether **70** was observed as the major product with the optical purity

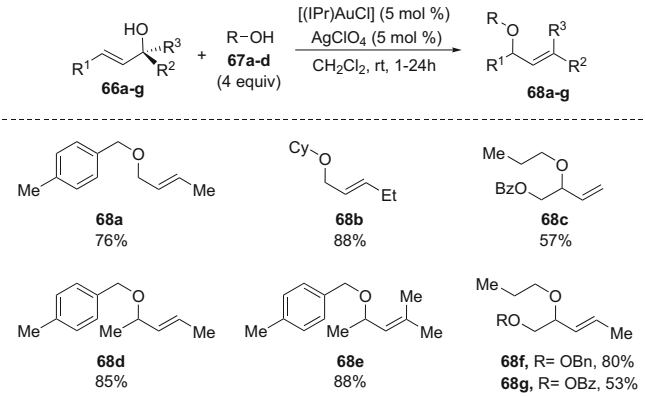

Scheme 20 Widenhoefer's gold-catalyzed intermolecular allylic alkylation

maintained. The *anti* alkoxyauration/*anti* elimination sequence would account for the stereospecificity of the reaction and hydrogen-bonding would lower the energy of the transition state in each step of the process [34]. Interestingly, the authors propose that the second major component of the reaction mixture, *trans*-olefin **72**, was most probably formed from the product **70**, since ethers may also be the leaving group in this reaction [54]. The enantiomeric excess was also maintained in this case. Further data supporting the author's hypothesis of an *anti* alkoxyauration/*anti* elimination sequence would be provided by use of (*Z*)-allylic alcohol **74** under the same conditions. This substrate should generate **75**, the enantiomer of **70**. Indeed, when **74** was subjected to the reaction conditions, compound **75** was furnished as the major product in the reaction. The second major product **77** was believed again to come from further reaction of **75** (Scheme 21) [53].

Having previously disclosed the gold-catalyzed etherification of allylic alcohols, Lee and coworkers have also shown that carbon nucleophiles could be successfully utilized in intermolecular gold-catalyzed dehydration reactions. More precisely, the authors employed a variety of phenol derivatives **79a**–**g** as nucleophiles, targeting the synthesis of polysubstituted chromans **81a**–**j** (Scheme 22) [55]. The reactions were carried out under similar conditions to those reported in the previous work [52], and several chromans were synthesized in good yields.

Mechanistically, Lee and co-workers proposed that the gold-complex simply acts as a Lewis acid in the reaction, creating a stabilized allyl carbocation, which is then attacked by the arene nucleophile via a Friedel–Crafts-type reaction. The reaction takes place at the *ortho* position of the arene, generating the intermediate **82** along with a molecule of water (Scheme 23) [55]. After the formation of the C–C bond, the cationic gold-complex or a source of proton activates the olefin, generating a tertiary carbocation. The carbocation is then trapped by the oxygen nucleophile, forming the C–O bond of the chroman.

In order to improve catalytic efficiency and reactivity in the gold-catalyzed intermolecular dehydrative allylic etherification, studies from the Lee and Crowley groups revealed that use of a 1,2,3-triazolylidine carbene ligand resulted in milder

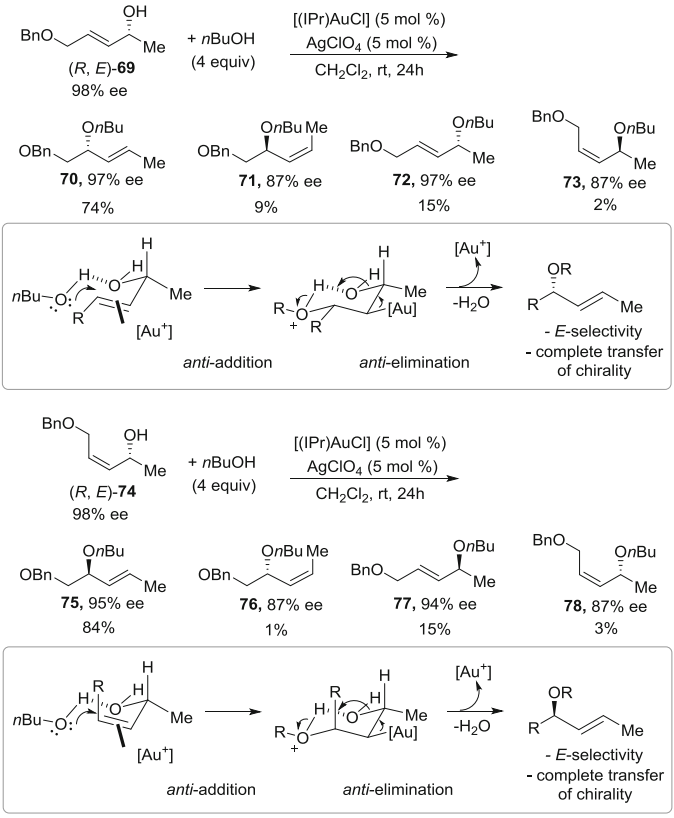

Scheme 21 Stereospecificity in gold-catalyzed intermolecular allylic alkylation

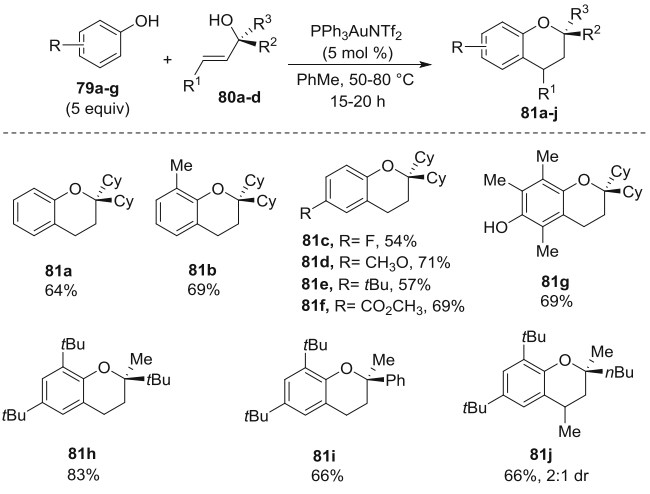

Scheme 22 Gold-catalyzed intermolecular dehydrative synthesis of chromans

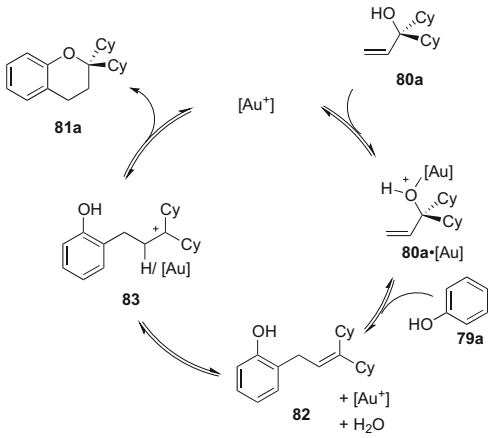

Scheme 23 Catalytic cycle of the gold-catalyzed intermolecular dehydrative synthesis of chromans

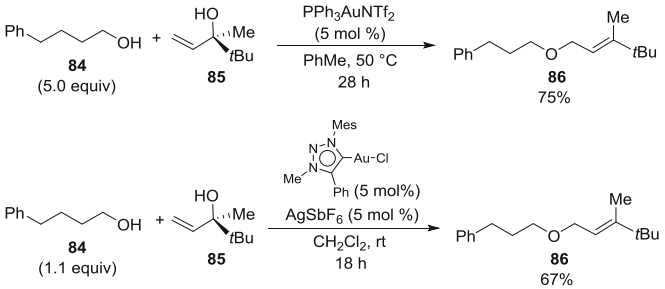

Scheme 24 1,2,3-Triazolylidine carbine ligand in gold-catalyzed intermolecular allylic alkylations

reaction conditions, improved regioselectivity, and eliminated the requirement for excess nucleophile (Scheme 24) [56].

In addition to the aforementioned reports on intermolecular reactions, Sierra and coworkers have shown that gold-catalyzed Nicholas reactions of allylic alcohols **87** and **90** were also feasible. The reactions take place under very mild conditions, tolerating different nucleophiles such as alcohols, arenes, and indoles (Scheme 25) [57]. This newly developed process minimized the formation of undesired elimination products generally observed under Brønsted-acid catalysis. Additionally, stereoselectivity was shown to be higher under gold-catalysis conditions in comparison to traditional Lewis acid catalysis. The reaction of the (*R*)-(−)-carvone-derived substrate **90** with benzyl alcohol gave a 4:1 ratio of products as opposed to 1.5:1 with BF_3·etherate (Scheme 25).

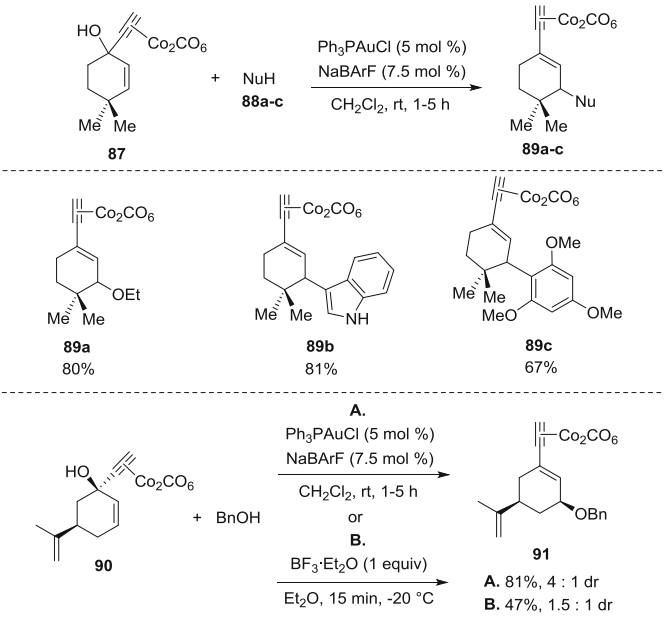

Scheme 25 The gold-catalyzed Nicholas reaction

Intermolecular gold-catalyzed allylic alkylation reactions with alcohol electrophiles are relatively new transformations. As a consequence, improvements in catalytic efficiency, as well as expansion of substrate scope regarding both electrophiles and nucleophiles, are probable subjects for future reports. The development of such processes would certainly complement the current synthetic methods for the preparation of interesting allylic building blocks, impacting the current state-of-the-art of the synthesis of natural products and other relevant molecules.

4 Reactions of Propargyl Alcohols

Over the past 3 years there has been an influx of publications on intra- and intermolecular gold(I)- and gold(III)-catalyzed dehydrative transformations of propargyl alcohols. In analogy to the reactions of allylic alcohols, either formal S_N2' or cationic pathway are often invoked to explain reaction outcomes. Although reactions of propargyl and allylic alcohols are mechanistically similar, these two types of reactions differ considerably on their synthetic target. As a consequence, gold-catalyzed dehydrations of propargyl alcohols are particularly interesting.

4.1 Intramolecular Reactions of Propargyl Alcohols

Gold-catalyzed intramolecular dehydrative reactions of propargylic alcohols appeared in the literature shortly after the first examples of the intramolecular reactions of allylic alcohols. The work of the Aponick [58] and Akai [59] groups on the gold-catalyzed synthesis of furans, pyrroles, and thiophenes, and Aponick's synthesis of monounsaturated spiroketals [60], gave rise to a series of reactions in which molecular complexity is increased from readily prepared starting materials. The reports of the Aponick and Akai groups were reviewed elsewhere [16] and are not detailed herein.

Bandini and coworkers have since shown that polycyclic fused indoles **93a–j** could be prepared via gold-catalyzed dehydrative cascade reactions (Scheme 26) [61]. The process involves an indole synthesis followed by C–O bond formation between the pendant alcohol and the propargylic carbon. The reaction furnished various indole derivatives in good yields and, in some cases, at ambient temperatures.

The catalytic cycle begins with the formation of the indole upon activation of the triple bond by the gold-complex [61], placing the pendant alcohol in proximity to the propargylic carbon (Scheme 27). For the construction of the second ring, the authors proposed formation of a benzylic carbocation, followed by nucleophilic attack of the terminal alcohol via S_N1 reaction.

Recently, Lipshutz and Krause have shown that the intramolecular gold-catalyzed synthesis of furans and pyrroles, as well as the synthesis of unsaturated spiroketals [58, 60], could be carried out in water in the presence of a surfactant (Scheme 28) [62]. To accomplish this task, the authors employed the TPGS-750-M surfactant, which is responsible for creating lipophilic nanomicelles in the reaction medium. In this work, syntheses of spiroketals **98a–b**, as well as furan and pyrrole derivatives **100a–g**, were accomplished in water in excellent yields and brief reaction times (Scheme 28). It is important to mention that dehydrative reactions are often carried out in the presence of dehydrating agents, such as molecular

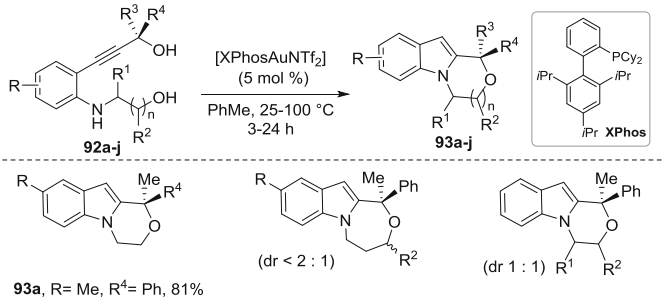

Scheme 26 Gold-catalyzed polycyclic fused indole synthesis

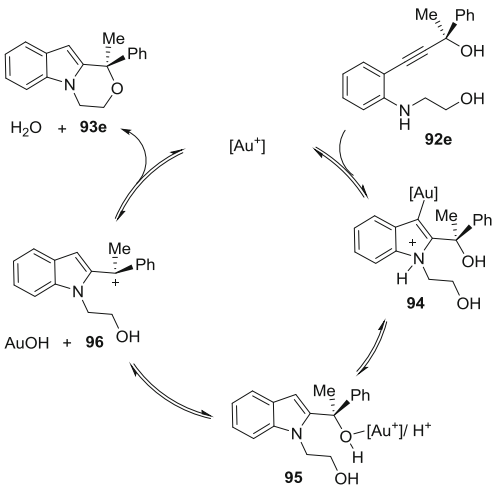

Scheme 27 Proposed catalytic cycle for the gold-catalyzed polycyclic fused indole synthesis

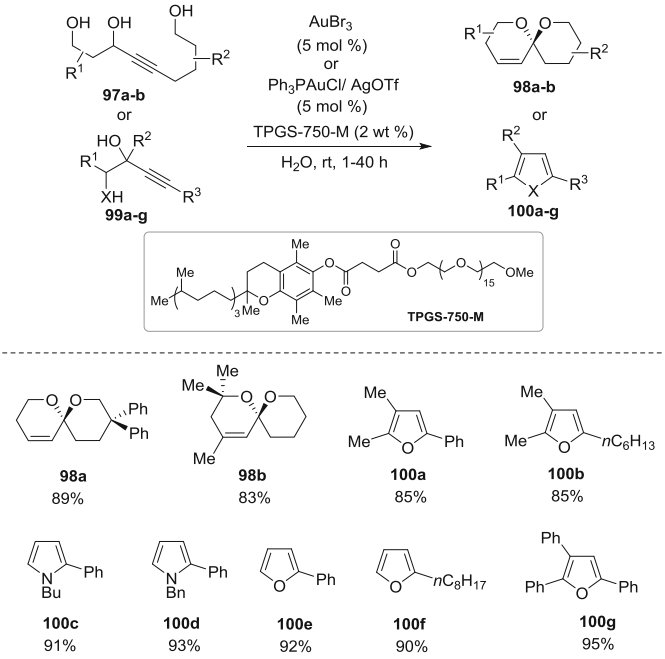

Scheme 28 Gold-catalyzed dehydrative cyclizations in water

sieves. In the micellar approach, water is generated inside the lipophilic core of the micelles and then moves to the outside of the micellar nanoparticle. The fact that dehydrative reactions can take place in water is remarkable, and this micellar approach has also been demonstrated on other important organic transformations

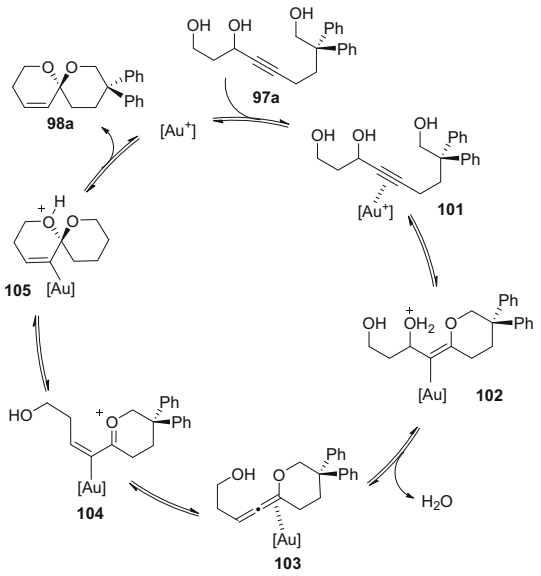

Scheme 29 Gold-catalyzed dehydrative synthesis of unsaturated spiroketals

[63], including those in which water-sensitive organometallic reagents are employed [64].

The mechanism of the gold-catalyzed synthesis of unsaturated spiroketals was proposed by Aponick and coworkers in their original publication [60]. Initially, the authors proposed activation of the triple bond by the gold-complex, followed by nucleophilic attack of the pendant alcohol via a 6-*exo* dig cyclization. In one of the possible mechanisms (Scheme 29), the vinyl gold intermediate **102** is formed, which undergoes elimination of water to form the key intermediate allenylether **103**. The intermediate **103** then undergoes the second cyclization, which can be catalyzed by gold or simply by a proton source to deliver the monounsaturated spiroketal **98a** and regenerating the catalyst.

As in the gold-catalyzed synthesis of spiroketals, in the synthesis of furan the vinyl-gold intermediate **107** is generated by nucleophilic attack of the pendant alcohol to the activated triple bond; however, in this case, the reaction probably proceeds via a 5-*endo* dig cyclization (Scheme 30) [58]. Finally, protodeauration and elimination of water furnishes the five-membered heteroaromatic **100e**.

Lamaty and coworkers have since demonstrated that the above-mentioned gold-catalyzed dehydrative furan synthesis could also be accomplished in poly (ethyleneglycol) matrix (PEG) (Scheme 31) [65]. During this study, the authors observed by transmission electronic microscopy that undesired gold(0)-containing nanoparticles were initially formed on the surface of the PEG matrix. To solve this problem, catalytic amounts of benzoquinone were used to oxidize the gold(0) back to the active gold(I) species. By using benzoquinone, the PEG matrix containing the

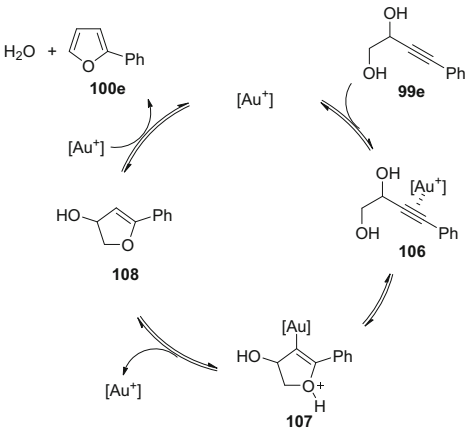

Scheme 30 Gold-catalyzed dehydrative synthesis of furans

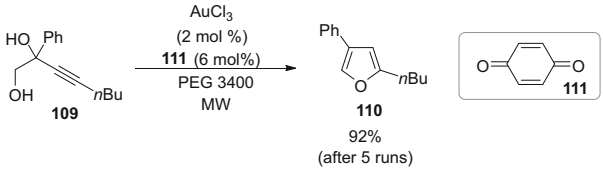

Scheme 31 Gold-catalyzed dehydrative furan synthesis in a PEG matrix

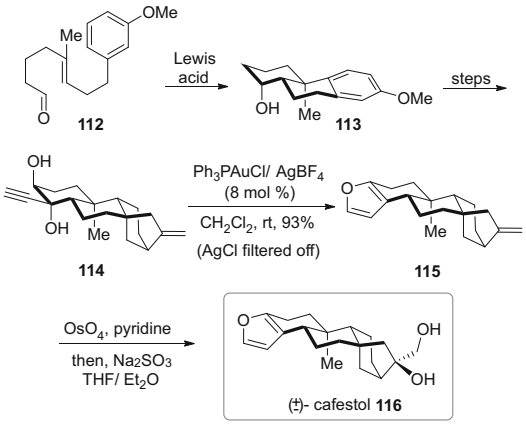

Scheme 32 Total synthesis of (±)-cafestol via a gold-catalyzed furan synthesis

gold-catalyst could be reutilized, and, even after five subsequent runs, the yield for the preparation of **110** did not decrease (Scheme 31) [65].

The gold-catalyzed dehydrative furan synthesis has also been elegantly explored by Hong and coworkers in the total synthesis of (±)-cafestol **116** (Scheme 32)

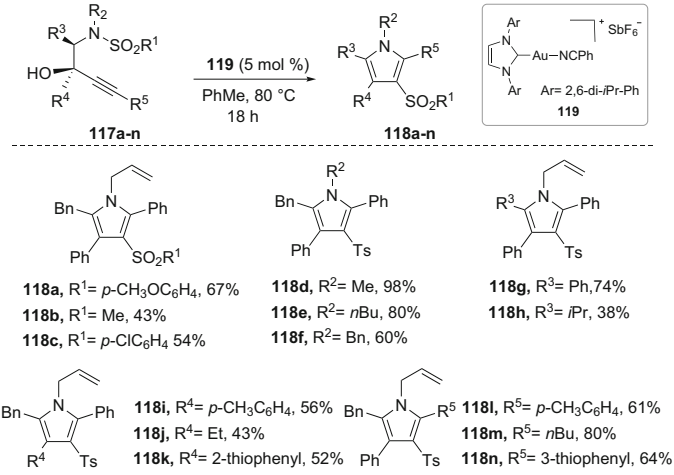

Scheme 33 Gold-catalyzed dehydrative 1,3-sulfonyl migration towards polysubstituted 3-sulfonyl-pyrroles

[66]. Inspired by the biosynthesis of cafestol [67], the authors synthesized the furan moiety in a late stage, as it is proposed in the biosynthetic pathway. The gold-catalyzed reaction proceeded smoothly to generate the desired advanced synthetic intermediate **115** in excellent yield. More interestingly, the authors mentioned that the presence of silver salts in the reaction triggered double-bond isomerization, forming the more stable tertiary *endo* olefin. To overcome this problem, the silver salt was filtered off prior to the gold-catalyzed reaction. After the furan synthesis, a dihydroxylation of the terminal olefin delivered the desired natural product **116** in a total of 20 steps from simple starting materials [66].

Chan and coworkers reported a gold-catalyzed dehydrative 1,3-sulfonyl migration towards sulfonyl substituted pyrroles. In this report, the authors have shown that propargyl alcohols bearing a sulfonamide group undergo 1,3-sulfonyl migration during the cyclization event, furnishing a variety of 3-sulfonyl pyrroles **118a–n** in moderate to good yields (Scheme 33) [68].

Similar to the pyrrole synthesis reported by Aponick [58] and Akai [59], the aminocyclization takes place to form the intermediate **120** (Scheme 34) [68]. In the absence of a proton source, the intermediate **120** undergoes a nitrogen to carbon 1,3-sulfonyl migration, generating the intermediate **121**, which is prone to aromatization.

Very recently, Chan and coworkers also demonstrated that α-carbonyl carbons are suitable nucleophiles for intramolecular gold-catalyzed dehydrative cyclizations of propargyl alcohols. Chan et al. reported a gold-catalyzed dehydrative benzannulation of hydroxy-oxoalkynoates **122a–g** to *o*-phenolic esters **123a–g** (Scheme 35) [69]. The reactions were carried out in the presence of the gold-complex **124** with 1 equiv. of acetic acid, with yields ranging from moderate to good.

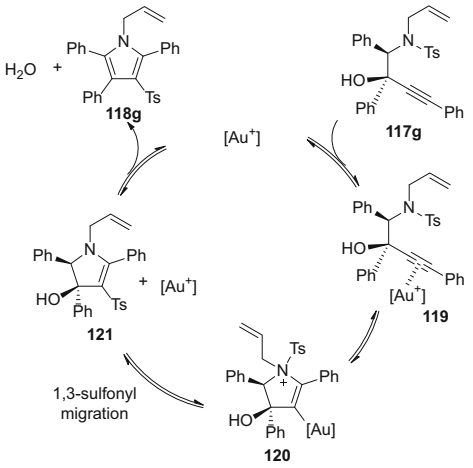

Scheme 34 Proposed pathway for the gold-catalyzed dehydrative 1,3-sulfonyl migration towards polysubstituted 3-sulfonyl-pyrroles

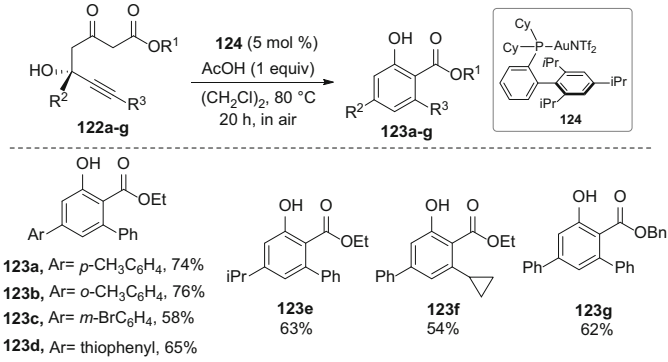

Scheme 35 Gold-catalyzed benzannulation towards *o*-phenolic esters

In terms of reaction mechanism, the authors proposed that the enol tautomer of the 1,3-dicarbonyl compound acts as a nucleophile and the activated triple bond as the electrophile to form **125** (Scheme 36) [69]. The vinyl gold intermediate **125** then undergoes protodeauration, furnishing **126**. Elimination of water and tautomerization from the intermediate **126** results in the formation of the final product **123e**. While this reaction is somewhat different mechanistically, the overall transformation would be categorized as a dehydrative transformation of an unsaturated alcohol.

The gold-catalyzed intramolecular dehydrative cyclization of propargyl alcohols is very effective for creating interesting heterocyclic compounds via structurally simple substrates. A variety of methods for synthesizing propargyl alcohols are

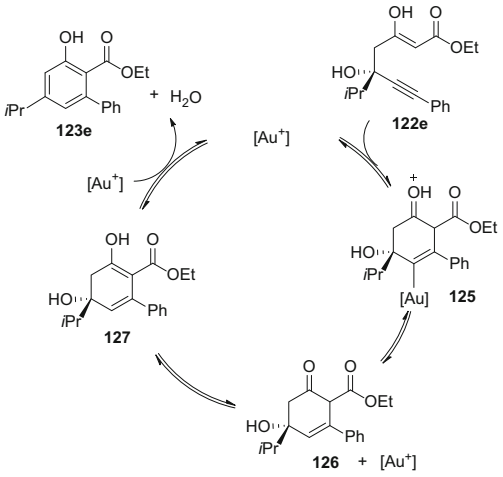

Scheme 36 Gold-catalyzed dehydrative benzannulation towards *o*-phenolic esters

available [70], and this is attractive for the design and development of new reactions in this area. To date, dehydrative reactions of propargyl alcohols are somewhat, although not exclusively, limited to the preparation of aromatic compounds. It is predicted that new methods for the construction of other interesting structural motifs are on the way.

4.2 Intermolecular Reactions of Propargyl Alcohols

The intermolecular S_N2' (or formal S_N2') gold-catalyzed dehydrative cyclization of propargyl alcohols is the most underdeveloped transformation covered here. A single report by Li and coworkers exemplifies how this type of reaction can be utilized for the preparation of useful polysubstituted allenes **130a–e**. Li et al. have shown that arenes **129a–d** undergo formal S_N2' reactions with propargyl alcohols **128a–e** catalyzed by gold(III)-complexes to form a variety of allenes in good to excellent yields (Scheme 37) [71].

Mechanistically, the authors proposed that the gold(III)-complex acts as a Lewis acid, forming the propargyl carbocation **133**, which undergoes Friedel–Crafts alkylation to form the C–C bond. Rearomatization delivers the final product **130a** along with a molecule of water, regenerating the active catalyst species (Scheme 38) [71].

As previously mentioned, intermolecular dehydrative reactions of propargyl alcohols have potential utility. It should be noted that direct substitution of the propargyl alcohol has been demonstrated in a variety of systems. This work has previously been reviewed and is not covered here [29, 73]. In contrast, the

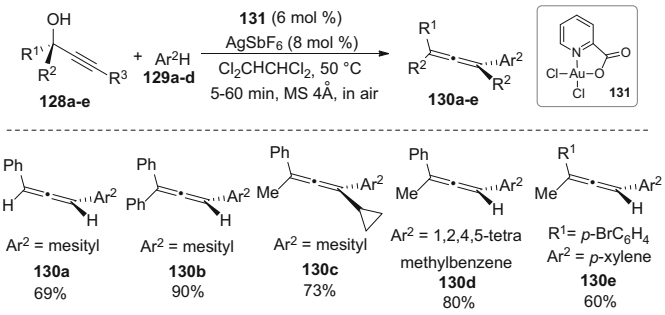

Scheme 37 Gold-catalyzed intermolecular dehydration of propargyl alcohols

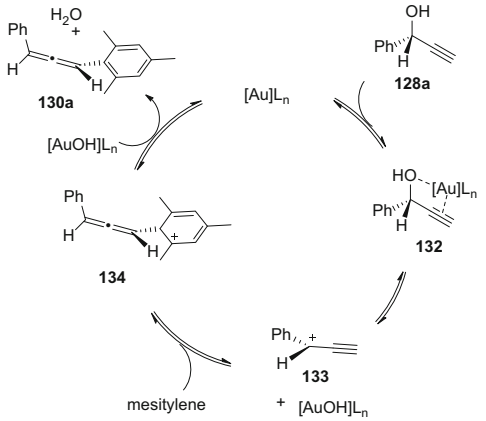

Scheme 38 Proposed catalytic cycle for the intermolecular gold-catalyzed reaction of propargyl alcohols

development of new reactivity, such as the allene formation seen here or asymmetric variants, may be the object of future research in this area.

5 Reactions of Benzyl Alcohols

This sections covers only examples of gold(I)- and gold(III)-catalyzed dehydrative reactions of benzyl alcohols which have appeared in the literature over the past 3 years. These reactions generally take place through Lewis acid-promoted ionization at the benzylic position. Among the topics included in this chapter, gold-catalyzed reactions of benzyl alcohols are the least developed, and intramolecular versions of this transformation are lacking. Nonetheless, interesting features can often be observed on these reactions, and this is reviewed herein.

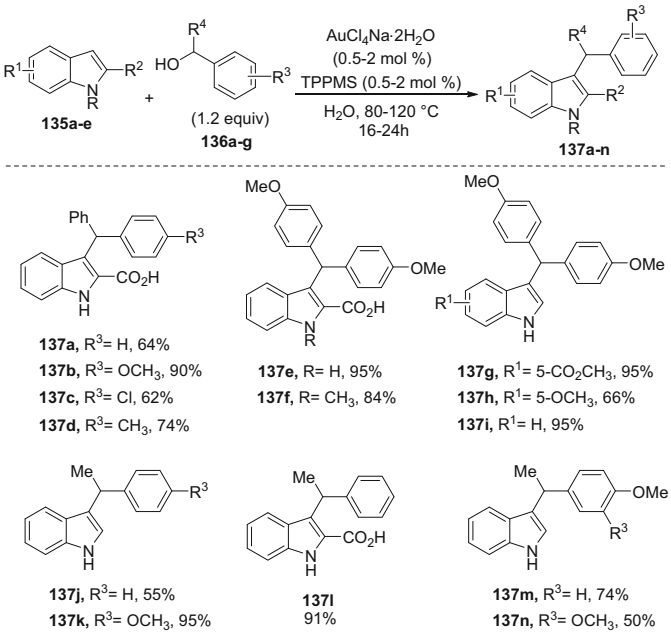

Scheme 39 Gold-catalyzed benzylation of indoles in water

5.1 Intermolecular Reactions of Benzyl Alcohols

Gold-catalyzed intermolecular dehydrative reactions of benzyl alcohols are powerful methods for the creation of C–C bonds at the benzylic position, as exemplified by Campagne and others [72, 73]. More recently, Hikawa and Azumaya demonstrated that various indole derivatives **135a–e** could be reacted with substituted benzyl alcohols **136a–e** to afford, upon dehydration, the functionalized indoles **137a–n** in moderate to excellent yields (Scheme 39) [74]. The reactions were carried out in water as the solvent at relatively high temperatures but with low catalyst loadings of both a gold(III)-salt and the water soluble ligand meta sulfonatophenyl-diphenylphosphine sodium salt (TPPMS).

Hikawa et al. have also utilized the same reaction conditions described above and demonstrated that anthranilic acid and *N*-methyl anthranilic acid have disparate reactivities [75] (Scheme 40). Under these conditions with benzyl alcohol electrophiles **140**, anthranilic acid undergoes *N*-benzylation to form aromatic benzyl amines **141**, while the methylated version of anthranilic acid **139** reacts at the *para* position of the aromatic ring to form **142** via Friedel–Crafts type benzylation.

The mechanism of the reaction involves formation of a benzylic carbocation upon Lewis acid activation by highly electrophilic gold(III) salts (Scheme 41) [74, 75]. The nucleophile then traps the carbocation, generating the C–C or C–N bond, depending on the nature of the nucleophile employed.

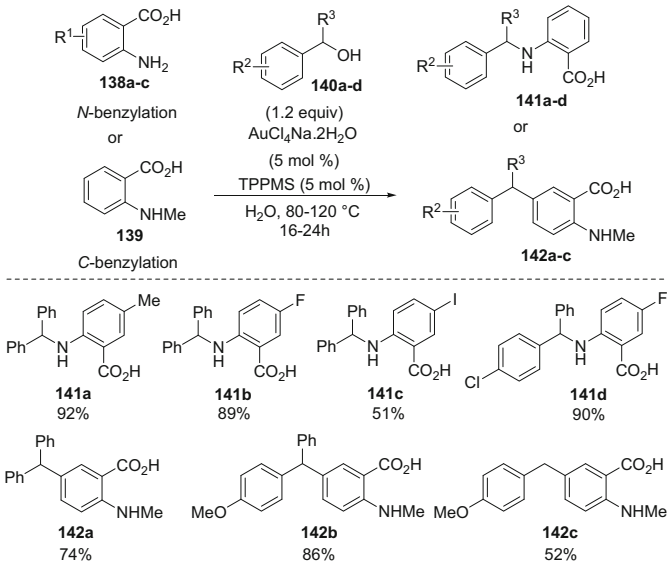

Scheme 40 *N*-Benzylation vs *C*-benzylation of anthranilic acid derivatives

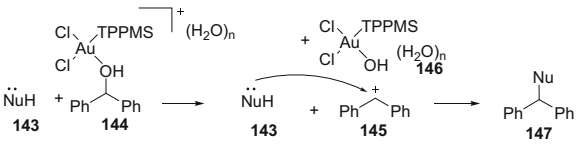

Scheme 41 Mechanism for the gold-catalyzed dehydrative benzylation reactions

Hanessian and coworkers have also reported a successful dehydrative benzylation of several arenes and sulfonamides catalyzed by gold(III) chloride. In this report, the authors have demonstrated that *syn*-benzyl alcohols **148a–f**, containing a homobenzylic nitro or azide groups, can react to produce *syn* substituted products **150a–f** in moderate to excellent diastereoselectivities (Scheme 42) [76].

While studying the reactivities of *syn* and *anti* derivatives **151** and **153**, respectively, the Hanessian group found that the reaction of the *syn* diastereomer **151** gave the *syn* product **154** in 1 h in good yields and diastereoselectivity, whereas reaction of the *anti* substrate **153** did not occur within the same time frame (Scheme 43) [76]. The authors analyzed the coupling constants between benzylic and homobenzylic protons to suggest that hyperconjugative interactions and steric effects are possibly responsible for the kinetic preference of the *syn* diastereomer to form the reactive benzylic oxocarbenium ion [76].

Gold-catalyzed benzylation reactions can be seen as synthetically useful transformations in which gold-complexes act mostly as a Lewis acid to generate

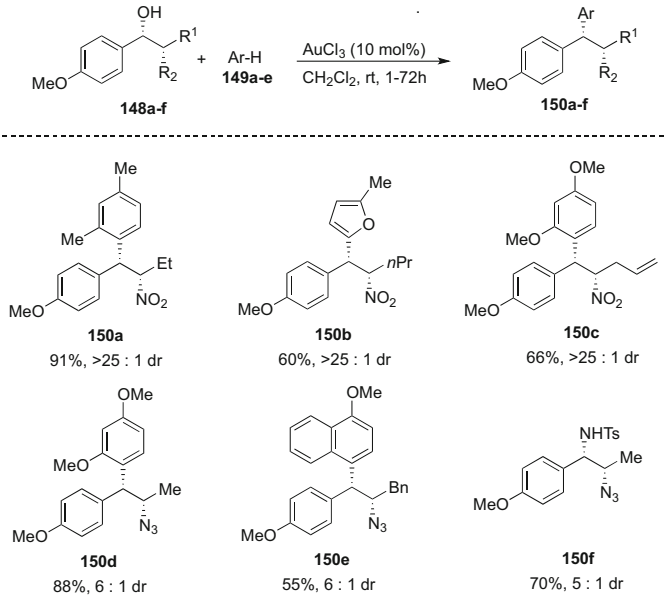

Scheme 42 Gold-catalyzed dehydrative *syn* alkylation of arenes and sulfonamides

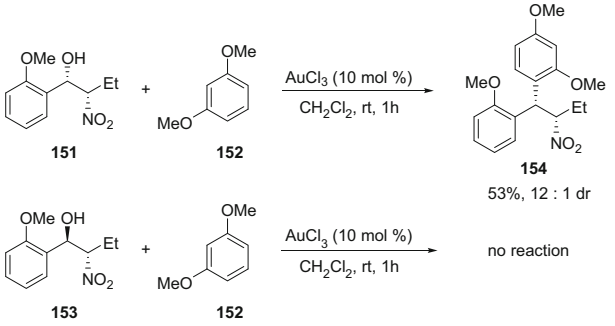

Scheme 43 Kinetic differentiation in the gold-catalyzed benzylic arylation

benzylic carbocations. This inherently complicates the system and is challenging for the development of stereoselective reactions; however, the work by Hanessian and coworkers demonstrated that highly diastereoselective processes can be achieved with proper substrate design. Furthermore, the use of carbon nucleophiles has been extensively studied in this context, but examples with other types of nucleophiles are encountered less frequently.

6 Conclusions and Outlook

The use of unsaturated alcohols in gold-catalyzed substitution reactions is a burgeoning research area. The foundation for significant advancements has been established and the impetus to do so is clear; the substrates are simple, the conditions are generally mild, the only byproduct is water, and the reactions can build complexity in a stereochemically-defined manner. In the coming years, catalyst design for intermolecular reactions can become more sophisticated and the reactions can probably be employed in increasingly more complicated settings for natural product and fine-chemical synthesis.

References

1. Hashmi ASK, Hutchings GJ (2006) Angew Chem Int Ed 45:7896–7936
2. Shapiro ND, Toste FD (2010) Synlett 5:675–691
3. Hashmi ASK (2014) Acc Chem Res 47:864–876
4. Zhang L (2014) Acc Chem Res 47:877–888
5. Wang Y-M, Lackner AD, Toste FD (2014) Acc Chem Res 47:889–901
6. Obradors C, Echavarren AM (2014) Acc Chem Res 47:902–912
7. Fensterbank L, Malacria M (2014) Acc Chem Res 47:953–965
8. Hashmi ASK (2013) Top Organomet Chem 44:143–164
9. Corma A, Leyva-Pérez A, Sabater MJ (2011) Chem Rev 111:1657–1712
10. Gorin DJ, Toste FD (2007) Nature 446:395–403
11. Teles JH, Brode S, Chabanas M (1998) Angew Chem Int Ed 37:1415–1417
12. Prati L, Rossi M (1998) J Catal 176:552–560
13. Fürstner A, Davies PW (2007) Angew Chem Int Ed 46:3410–3449
14. Fürstner A (2009) Chem Soc Rev 38:3208–3221
15. Fürstner A (2014) Acc Chem Res 47:925–938
16. Biannic B, Aponick A (2011) Eur J Org Chem 6605–6617
17. Muzart J (2008) Tetrahedron 64:5815–5849
18. Bandini M (2011) Chem Soc Rev 40:1358–1367
19. Rudolph M, Hashmi ASK (2012) Chem Soc Rev 41:2448–2462
20. Winter C, Krause N (2011) Chem Rev 111:1994–2009
21. Yang C-G, He C (2005) J Am Chem Soc 127:6966–6967
22. Liu L-P, Hammond GB (2012) Chem Soc Rev 41:3129–3139
23. Lalonde RL, Brenzovich WE Jr, Benitez D, Tkatchouk E, Keley K, Goddard WA III, Toste FD (2010) Chem Sci 1:226–233
24. Ketcham JM, Biannic B, Aponick A (2013) Chem Commun 49:4157–4159
25. Gómez-Suárez A, Gasperini D, Vummaleti SVC, Poater A, Cavallo L, Nolan SP (2014) ACS Catal 4:2701–2705
26. Aponick A, Li C-Y, Biannic B (2008) Org Lett 10:669–671
27. Ketcham JM, Aponick A (2013) Top Heterocycl Chem 32:157–186
28. Hirai Y, Terada T, Amemiya Y, Momose T (1992) Tetrahedron Lett 33:7893–7894
29. Debleds O, Gayon E, Vrancken E, Campagne J-M (2011) Beilstein J Org Chem 7:866–877
30. Mukherjee P, Widenhoefer RA (2010) Org Lett 12:1184–1187
31. Bandini M, Eichholzer A (2009) Angew Chem Int Ed 121:9697–9701
32. Unsworth WP, Stevens K, Lamont SG, Robertson J (2011) Chem Commun 47:7659–7661
33. Mukherjee P, Widenhoefer RA (2012) Angew Chem Int Ed 51:1405–1407

34. Ghebreghiorgis T, Biannic B, Kirk BH, Ess DH, Aponick A (2012) J Am Chem Soc 134:16307–16318
35. Mukherjee P, Widenhoefer RA (2011) Org Lett 13:1334–1337
36. Bandini M, Bottoni A, Chiarucci M, Cera G, Miscione GP (2012) J Am Chem Soc 134:20690–20700
37. Aponick A, Biannic B (2011) Org Lett 13:1330–1333
38. Chiarucci M, Mocci R, Syntrivanis L-D, Cera G, Mazzanti A, Bandini M (2013) Angew Chem Int Ed 52:10850–10853
39. Palmes JA, Paioti PHS, de Souza LP, Aponick A (2013) Chem Eur J 19:11613–11621
40. Palmes JA, Aponick A (2012) Synthesis 44:3699–3721
41. Brimble MA, Stubbing LA (2014) Top Heterocycl Chem 35:189–267
42. Borrero N, Aponick A (2012) J Org Chem 77:8410–8416
43. Thansandote P, Lautens M (2009) Chem Eur J 15:5874–5883
44. Ketcham JM, Cardoso FSP, Biannic B, Piras H, Aponick A (2013) Isr J Chem 53:1–9
45. Mukherjee S, Yang JW, Hoffmann S, List B (2007) Chem Rev 107:5471–5569
46. Chiarucci M, di Lillo M, Romaniello A, Cozzi PG, Cera G, Bandini M (2012) Chem Sci 3:2859–2863
47. Trost BM (2004) J Org Chem 69:5813–5837
48. Evans PA, Leahy DK, Andrews JW, Uraguchi D (2004) Angew Chem Int Ed 43:4788–4791
49. Onitsuka K, Okuda H, Sasai H (2008) Angew Chem Int Ed 47:1454–1457
50. Ueno S, Hartwig JF (2008) Angew Chem Int Ed 47:1928–1931
51. Roggen M, Carreira EM (2011) Angew Chem Int Ed 50:5568–5571
52. Young PC, Schopf NA, Lee A-L (2013) Chem Commun 49:4262–4264
53. Mukherjee P, Widenhoefer RA (2013) Chem Eur J 19:3437–3444
54. Biannic B, Ghebreghiorgis T, Aponick A (2011) Beilstein J Org Chem 7:802–807
55. Coutant E, Young PC, Barker G, Lee A-L (2013) Beilstein J Org Chem 9:1797–1806
56. Wright JR, Young PC, Lucas NT, Lee A-L, Crowley JD (2013) Organometallics 32:7065–7076
57. Valderas C, de la Torre MC, Fernandéz I, Muñoz MP, Sierra MA (2013) Organometallics 32:951–956
58. Aponick A, Li C-Y, Malinge J, Marques EF (2009) Org Lett 11:4624–4627
59. Egi M, Azechi K, Akai S (2009) Org Lett 11:5002–5005
60. Aponick A, Li C-Y, Palmes JA (2009) Org Lett 11:121–124
61. Chiarucci M, Matteucci E, Cera G, Fabrizi G, Bandini M (2013) Chem Asian J 8:1776–1779
62. Minkler SRK, Isley NA, Lippincott DJ, Krause N, Lipshutz BH (2014) Org Lett 16:724–726
63. Manabe K, Iimura S, Sun X-M, Kobayashi S (2002) J Am Chem Soc 124:11971–11978
64. Krasovskiy A, Duplais C, Lipshutz BH (2009) J Am Chem Soc 131:15592–15593
65. Spina R, Colacino E, Martinez G, Lamaty F (2013) Chem Eur J 19:3817–3821
66. Zhu L, Luo J, Hong R (2014) Org Lett 16:2162–2165
67. Fischbach MA, Clardy J (2007) Nat Chem Biol 3:353–355
68. Teo WT, Rao W, Koh MJ, Chan PWH (2013) J Org Chem 78:7508–7517
69. Teo WT, Rao W, Ng CJH, Koh SWY, Chan PWH (2014) Org Lett 16:1248–1351
70. Frantz DE, Fassler R, Carreira EM (2000) J Am Chem Soc 122:1806–1807
71. Xu C-F, Xu M, Yang L-Q, Li C-Y (2012) J Org Chem 77:3010–3016
72. Georgy M, Boucard V, Campagne JM (2005) J Am Chem Soc 127:14180–14181
73. Liu J, Muth E, Florke U, Henkel G, Merz K, Sauvageau J, Schwake E, Dyker G (2006) Adv Synth Catal 348:456–462
74. Hikawa H, Suzuki H, Azumaya I (2013) J Org Chem 78:12128–12135
75. Hikawa H, Suzuki H, Yokoyama Y, Azumaya I (2013) J Org Chem 78:6714–6720
76. Chénard E, Hanessian S (2014) Org Lett 16:2668–2671

Top Curr Chem (2015) 357: 95–132
DOI: 10.1007/128_2014_595

Published online: 7 February 2015

Gold-Catalyzed Domino Reactions

Véronique Michelet

Abstract Gold-catalyzed reactions have appeared to be highly attractive tools for chemists to promote novel transformations to prepare elaborated structures from simple starting materials. This chapter presents selected and original examples of domino processes in the presence of gold catalysts, highlighting reports implying hydration, hydroxylation, and hydroamination as key starting point for cascade transformations. Domino processes implying 1,*n*-enynes, asymmetric domino transformations, and applications of all the presented processes in total synthesis are presented.

Keywords Asymmetric catalysis · Domino process · Gold · Hydration · Hydroamination · Total synthesis

Contents

V. Michelet (✉)
PSL Research University, Chimie ParisTech – CNRS, Institut de Recherche de Chimie Paris, 75005 Paris, France
e-mail: veronique-michelet@chimie-paristech.fr

1 Introduction

Recent years have seen a myriad of new gold-catalyzed processes appear in the literature [1–22]. Among them, the domino processes ([23] and references therein, [24, 25]) have been a wide area of interest, addressing the challenge of atom and step economy. The definition of a domino reaction from Tietze is the formation of two or more bonds "which takes place under the same reaction conditions, without adding additional reagents and catalysts, and in which the subsequent reactions result as a consequence of the functionality formed in the previous step" [24]. Fogg and dos Santos added that domino processes are realized via a single catalytic mechanism [23]. In this chapter, the main contributions in the field of gold-catalyzed "simple" domino processes are highlighted, emphasizing the seminal reports and "easy to follow" pathways. Some too complicated cascade processes (more than three domino sequences) are not be presented, but some recent specific reviews have recently appeared in the literature [26–36]. The presentation focuses on two elemental steps (inter- and intramolecular pathways) which may start a domino process: hydroxylation and hydroamination steps. A second part is dedicated to 1,*n*-enyne rearrangement as the first step of the domino process [37–44]. The third part presents the gold-catalyzed asymmetric domino processes [42, 45–52] and some applications of the previously presented domino processes to the synthesis of natural products or biologically active ones [16, 53, 54].

2 Gold-Catalyzed Domino Reactions in the Presence of Oxygen and Nitrogen Nucleophiles

2.1 Domino Processes Implying a Hydration or Hydroxylation Step

Following the pioneer work of Fukuda and Utimoto [55, 56] on hydration of alkynes, several groups proposed domino processes implying a hydration step followed by a cyclization reaction. A representative example from the group of Zang and Hayashi is presented in (1) [57]. The catalytic system $(PPh_3)AuMe/CH_3SO_3H$ promoted the efficient hydrative cyclization of 1,6-diynes **1** leading to 3-methyl hex-2-enone derivatives **2** in good to excellent yield. The cyclization is proposed to proceed via an enol Au(I)–π-alkyne intermediate, which subsequently triggers the cyclization via a 6-*endo-dig* addition of the second alkynyl moiety. Protodemetalation followed by isomerization of the double bond leads to the α,β-unsaturated ketones. Similar reactivity is observed for substituted alkynes [58, 59], except that the cyclization occurs via a 5-*exo-dig* mode. This method was also efficiently applied to the synthesis of functionalized naphthalene derivatives [60] and functionalized furans [61].

Recently, a domino process involving an alkyne, an organoboronic acid, water, and Selectfluor was reported by Hammond, Xu and coworkers [62]. The addition/oxidative coupling/fluorination sequence afforded mixtures of α-fluoroketones **4/5** and **6/7** in excellent yields and good regioselectivity in the presence of, respectively, phenylboronic and 3-chlorophenylboronic acids – see (2) and (3). It should be noted that the participation of the benzoyl or acetate ester group was advocated to explain the regioselectivity. A cyclization/fluorination process was described in the case of β-hydroxy-α,α-difluoroynones [63].

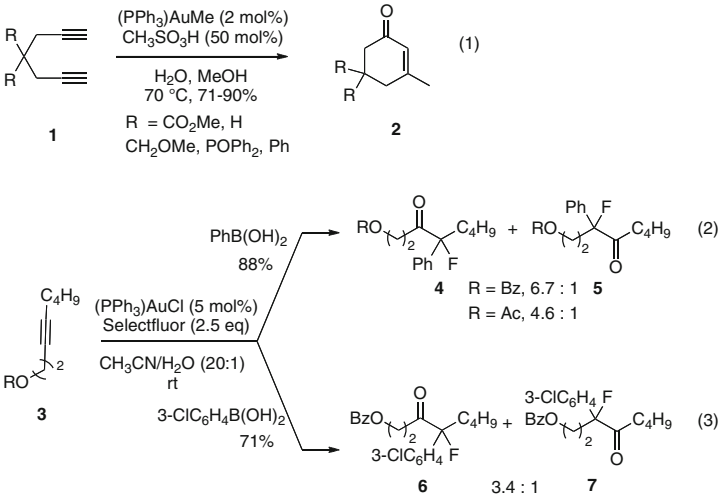

Teles' group originally reported a combined inter- and intramolecular reaction when subjecting propargylic alcohol **8** to a gold catalyst, this domino process implying two molecules of methanol as external nucleophile afforded the corresponding ketal **9** in 93% yield – see (4). This methodology has been the start of a very fruitful research area, where several groups studied a myriad of gold-catalyzed addition of alcohols to alkynes [64–70]. Intramolecular dihydroalkoxylation reactions of several functionalized bis(homopropargylic) diols **10** allowed, for example, the formation of strained bicyclic ketals **11** in good to excellent yields – see (5) [64]. It should be noted that mononuclear homogeneous gold catalyst derived from nitrogen acyclic carbene recently displayed extremely high turnover number (0.000001 mol%) in the synthesis of spiroketals [71]. The use of nitrogen acyclic carbene gold catalyst (NAC) led to highly substituted heterocyclic cages **13** in the presence of external nucleophiles such as amine [68]. The cyclization process proceeded by a multistep domino sequence, resulting in the creation of eight bonds – see (6).

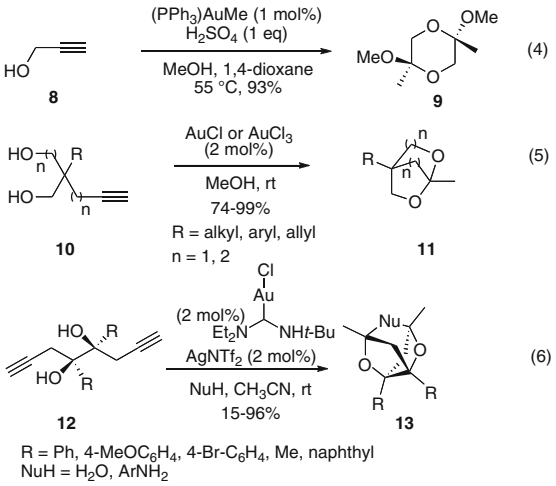

The group of Barluenga proposed a gold-catalyzed domino process where the formation of a carbon–oxygen bond is associated with the creation of a carbon–carbon bond [72, 73]. The gold(III)-catalyzed domino cycloisomerization/Prins-type cyclization of ω-alkynol **14** afforded eight-membered carbocycle **15** in 94% yield – see (7) – via an intermediate **16**, which is trapped by the remaining alkene. Similar intra- or intermolecular processes involving a hydroarylation step led to bicyclo[3.3.1]nonanes [74] and functionalized indoles, respectively [75]. Other domino processes were described implying a Diels–Alder reaction [76]. Domino epoxide-opening, 6-*exo*-cycloisomerization, and subsequent intermolecular nucleophilic addition to a double-bond sequence allowed a nice synthesis of ketals **18** – see (8) [77, 78]. The preparation of 3-oxabicyclo[3.1.0]hexanes **21** was described according to a three-component addition implying an intermolecular hydroalkoxylation of an alkyne **20** – see (9) [79] – via a stereoselective domino attack of alcohol on activated intermediate **22**, which therefore evolved towards the bicyclic adducts **21**.

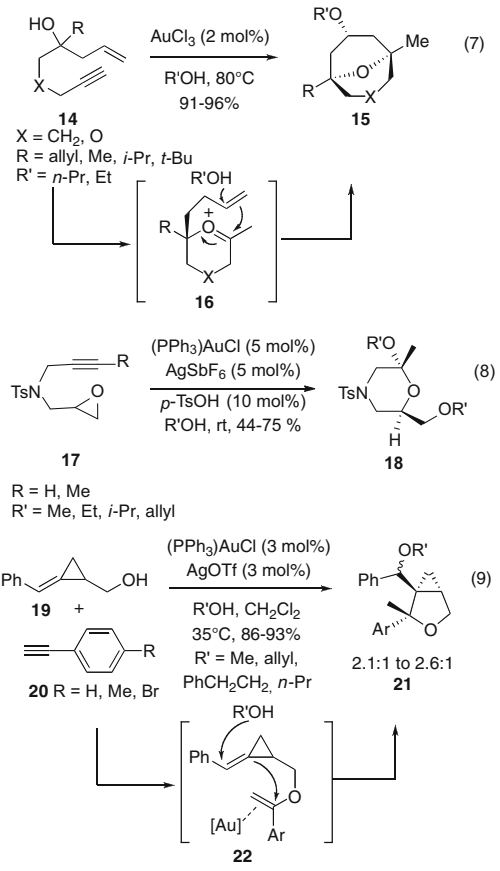

Other domino processes have been described with carbonyl derivatives. The group of Waser and allowed the cyclization/alkynylation of ketoallenes in the presence of hypervalent iodide reagents, leading to functionalized furans ([80] and references cited therein). The reactivity of propargylic esters, which are prone to gold-catalyzed 3,3-sigmatropic shift leading to allenyl esters and which can be trapped by other nucleophiles, has been a much studied area [81, 82]. The synthesis of 2,5-dihydrofurans **25** through a gold-catalyzed domino process was described starting from **23** via a 5-*endo-dig* cyclization of the alcohol moiety onto the in situ generated allenyl ester **24** [83, 84] – see (10). This methodology was also compatible with the preparation of functionalized tetrahydropyrans via a 6-*exo-dig* alkoxycyclization [85]. Nucleophiles other than alcohols may enter into the whole process, such as carbon nucleophiles as exemplified in (11) [86]. The synthesis of **27** occurred very smoothly at room temperature in 92% yield. The catalyst could be either a carbene-functionalized gold complex or a gold-hydroxide derivative [87].

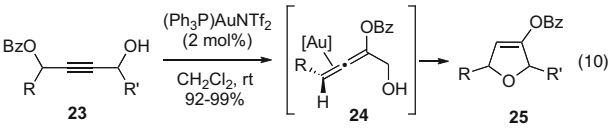

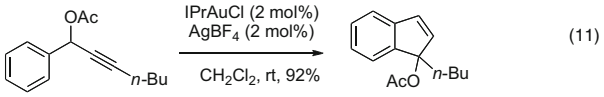

Interestingly, when an alkyne moiety is present in the substrate, a reverse selectivity may be observed, e.g., nucleophilic addition of the allenyl intermediate on the π-activated alkyne. The synthesis of aromatic ketones was described in the presence of a catalytic system consisting of Au(III) catalyst and triphenyphosphane – see (12) – or Au(I) system [88, 89]. The naphthyl derivative **29** was, for example, obtained in high isolated yield, most probably via the allenic-yne intermediate **30**. Interestingly, the alkyl-tethered 1,6-diynyl esters such as **31** had a different reactivity, a 1,5-sigmatropic acyl shift being observed during the domino process [90, 91]. One example is given in (13), but the scope of this domino 1,3-acyloxy migration/5-*exo-dig* cyclization/1,5- acyl migration of diynyl esters reaction is very broad and allowed the formation of highly functionalized δ-diketones. When propargyl propiolates were engaged in rearrangement processes [92, 93], the sigmatropic shift and cyclization steps may be followed by a nucleophilic addition of electron-rich aromatic rings or alcohols. Diyne **33** was efficiently transformed to α-pyrone **34** in 73% yield – see (14). Depending on the external nucleophile, other gold catalytic systems were optimized.

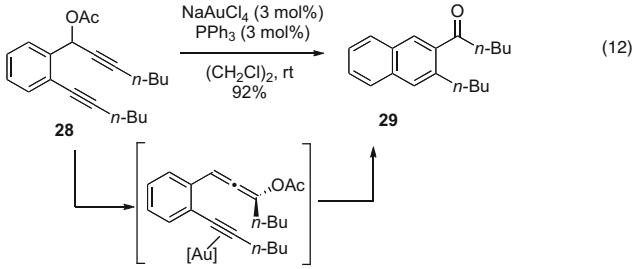

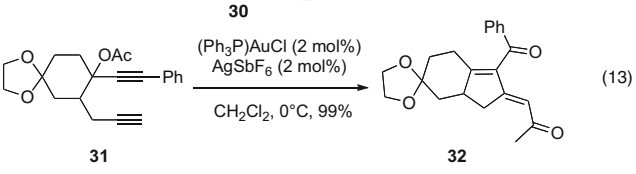

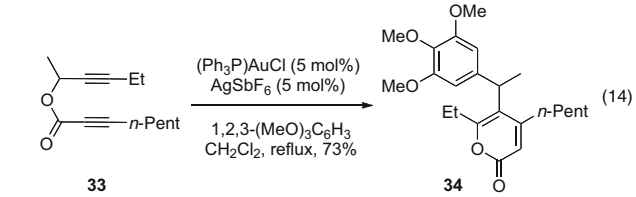

Other domino processes have been described involving a cycloaddition reaction after the 3,3-sigmatropic shifts of the propargyl ester. One key example was described by Zhang, who started from indolic derivatives such as **35** – see (15) [94]. Tetracyclic compounds such as **36** were obtained stereoselectively in the presence of cationic gold(I) catalyst. The vinylgold(I) **37**, resulting from a nucleophilic attack of the indolyl group on the allenyl ester, was advocated as a key intermediate and could react with the iminium moiety according to a [2 + 2] cycloaddition. Spirodindoles were recently obtained via a similar process [95].

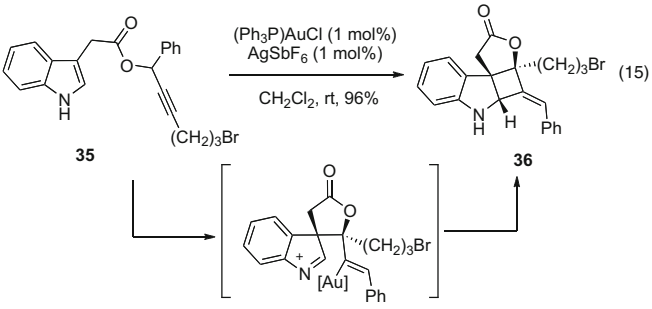

(15)

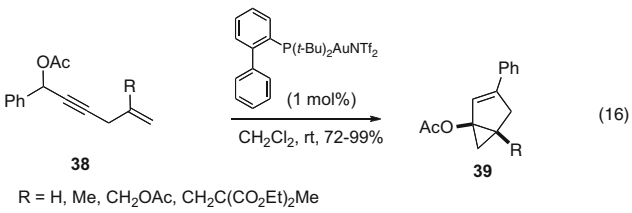

(16)

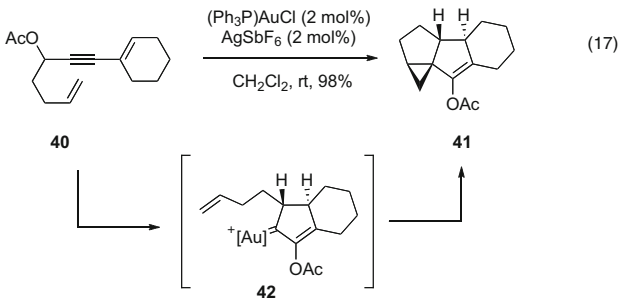

(17)

Other cycloaddition reactions have been observed during the study of similar domino processes. The preparation of bicyclo[3.1.0]hexenes **39** was, for example, disclosed starting from propargylic acetate **38** – see (16) [96]. The reaction allowed the presence of a chiral center and an excellent chirality transfer was achieved starting from an enantioenriched propargyl acetate. A formal [3 + 2] cycloaddition step was this time advocated during the domino process. The carbenic gold intermediate **42** was trapped by a remote alkenyl moiety, leading to tetracyclic derivative

41 starting from propargylic acetate **40** – see (17) [97, 98]. This atom-economical domino process relied on 3,3-rearrangement, metalla-Nazarov reaction, and electrophilic cyclopropanation and was supported by DFT calculations.

2.2 Domino Processes Implying a Hydroamination Step

Following the seminal work of Utimoto on gold-catalyzed intramolecular hydroamination of alkynes [99, 100], cascade intramolecular processes were described when functionalized alkynes were subjected to gold catalysts [101]. Aryl-annulated carbazoles **44** were, for example, prepared in a one-step procedure, starting from diynes **43**, via a 5-*endo-dig* hydroamination/6-*endo-dig* cycloisomerization sequence promoted by a catalytic amount of a cationic gold (I) complex – see (18) [102, 103]. A similar strategy, as previously described in the case of processes involving hydroalkoxylation reaction, implied a hydroamination/hydroarylation cascade via a subsequent activation of the *ortho* C–H bond of the aniline moiety. The group of Che described the synthesis of substituted 1,2-dihydroquinolines **47** starting from primary arylamines **45** and 2 equiv. of terminal alkynes **46** in the presence of a cationic carbine-type gold(I) catalyst – see (19) [104]. This method is very general, compatible with several groups, and occurs nicely under microwave conditions. The preliminary hydroamination step is most probably followed by the reaction of the generated enamine with a second molecule of alkyne to provide a propargylamine intermediate, which undergoes an intramolecular hydroarylation. Recently, Bertrand and coworkers extended the scope of this domino one-pot three-component access to heterocycles in the presence of secondary arylamines and two different alkynes [105]. The syntheses of pyrrolo[1,2-*a*]quinolines [106], pyrrolo[1,2-*a*]quinolin-1(*2H*)-ones [107], and pyrrolo- or indolo[1,2-*a*]quinoxalines [108, 109] were also possible according to a similar process.

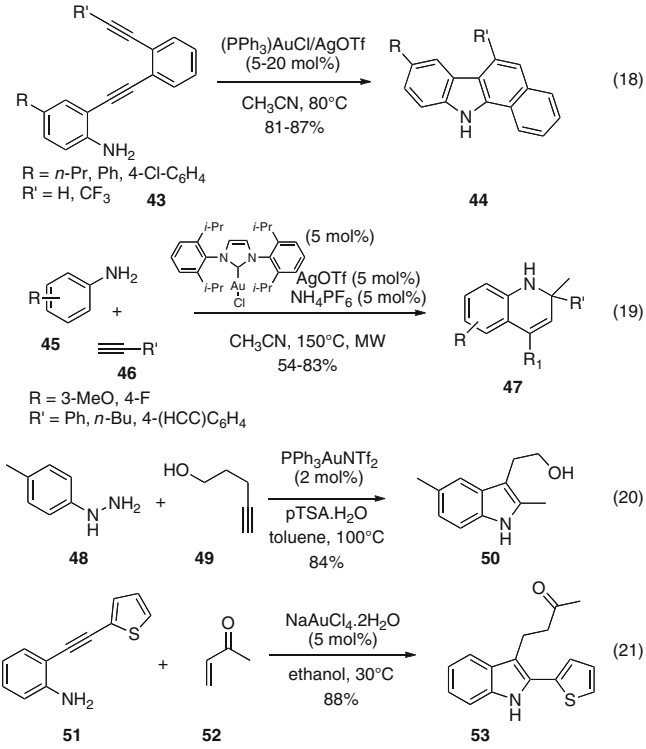

The reaction of a mixture of an arylhydrazine **48** and an alkyne **49** in the presence of a catalytic PPh_3AuNTf_2/*p*-TSA.H_2O system gave rise to a hydrohydrazination/Fisher indolization cascade, nicely affording the corresponding substituted indole **30** – see (20) [110] – in 84% yield. Several other analogues have been prepared according to this methodology. Other carbon-functionalized partners have been involved in the domino process, such as activated alkenes. The group of Arcadi proposed an alternative route to the synthesis of indoles via a sequential hydroamination cyclization/conjugate addition reaction of the 2-alkynylaniline **51** to the α,β-enone **52** – see (21) [111]. The mild reaction conditions allowed the formation of the 2,3-disubstituted indole **53** in 88% yield.

A very sophisticated cascade process was recently disclosed by Bandini and coworkers for the preparation of fused seven-membered ring azepino[1,2-*a*]indoles **55** [112]. The treatment of 2-(propargylicalcohol)anilines **54** with 5 mol% of [Au(IPr)Cl]/AgOTf allowed easy access to the polycyclic product **55** in 94% yield – see (22). The domino process implies a 5-*endo-dig* hydroamination/dehydration/cyclization step, cationic species **56** being a key intermediate. The tertiary alcohol moiety was found to be crucial for the whole success of the process. The introduction of electron-withdrawing groups on the aromatic rings was compatible with the methodology together with aryl and alkyl groups on the ketone and alcohol chains.

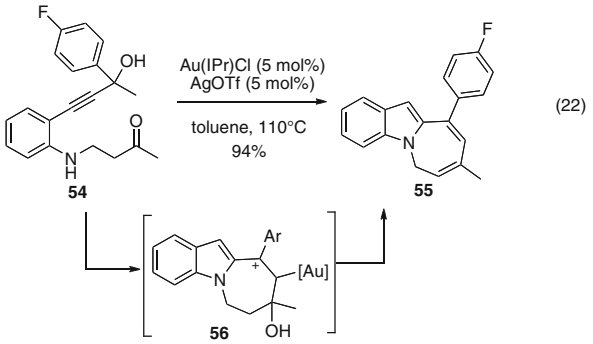

When two amino groups are present on the substrate, a domino double addition can occur and can lead to various *N*-heterocycles [109, 113]. A gold(I)-catalyzed Markovnikov's double addition of 2-aminobenzamide **57** or 2-(2-aminophenyl) benzimidazole **59** gave tetrahydroquinazolinone **58** or benzo[4,5]imidazo[1,2-*c*] quinazoline **60**, respectively, in very good yields – see (23) and (24).

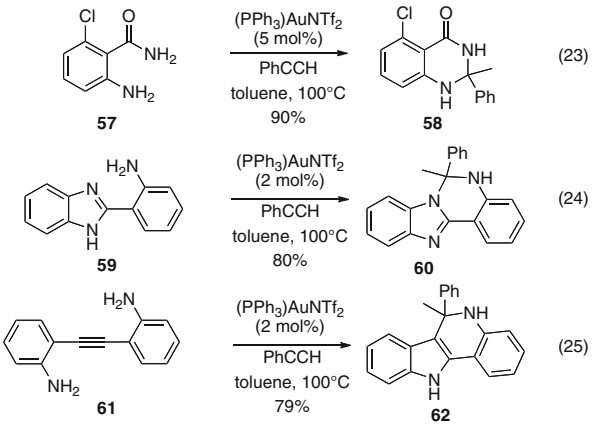

A mixture of phenylacetylene with a bisaniline alkyne **461** allowed a nice one-pot cascade reaction in the presence of $(PPh_3)AuNTf_2$ and thus provided the indolo [3,2-*c*]quinoline **62** in good yield – see (25). This methodology can also be used for the preparation of 1,5-benzodiazepines [114].

When primary amines were used in the presence of an excess of alkynes, a double hydroamination could take place via the formation of an enamine and according to the imine-enamine tautomerism [115]. The α,α′,*N*-triarylbienamines **64** were obtained in the presence of phenylacetylene and $(P(t\text{-}Bu)_3)AuNTf_2$ as a gold(I) complex – see (26). Other similar examples have been reported [116, 117] and allowed the synthesis of *N*-heterocycles such as pyrroles or pyrazoles derivatives via a two-step cascade inter- and intramolecular hydroamination sequence [61, 118–120]. The bulky cyclic (alkyl)(amino)carbene (CAAC)Au(I) catalyst

nicely promoted, for example, the synthesis of 4*H*-pyrazole **66** starting from hydrazine and diyne **65** – see (27).

Pyrrole derivatives, which are important building blocks in the heterocycle family, have been prepared via gold-catalyzed cascades [121, 122]. One typical example implied a gold(III)-catalyzed amination/hydroamination cascade of propargylic alcohols such as **67** in the presence of tosyl sulfonamide, affording the highly functionalized pyrrole **68** in 83% yield – see (28) [123]. This convenient approach was compatible with a large range of aryl, alkyl, and terminal alkynes and various substitutions on the allyl moiety. A similar approach was reported in the presence of a gold(I) catalyst [124].

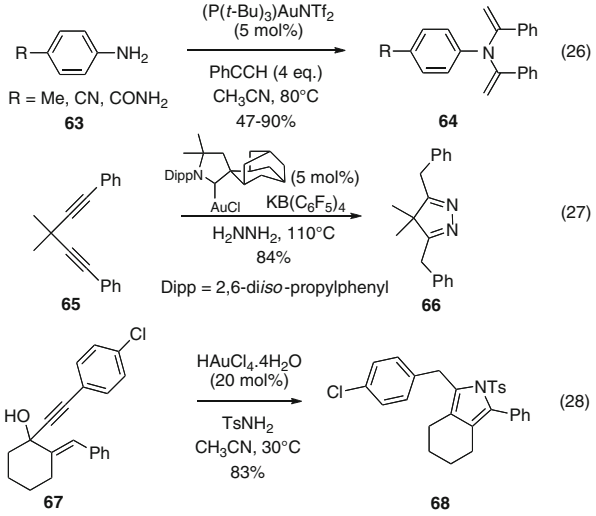

Following the pioneering work of the Gouverneur's group [63], cascade reactions implying hydroamination step have also been involved in fluorination processes. A seminal example was reported for the synthesis of fluorinated pyrazoles **70** by means of the aminofluorination reaction of alkynyl hydrazones **69** in the presence of Selectfluor as a source of electrophilic fluorine, a mineral base, and a catalytic amount of $(PPh_3)AuNTf_2$ – see (29) [125]. The protodeauration step was still found to be competitive, but the fluoro derivatives – see (21) – were this time obtained as major compounds. This methodology also gave rise to the preparation of fluorinated pyrrolidines and piperidines [126]. Other gold catalysts such as AuCl, $AuCl_3$, and $NaAuCl_4$ efficiently promoted the formation of 3,3-difluoro-2-substituted-3*H*-indoles from unprotected 2-alkynylanilines and Selectfluor under mild conditions without the use of any basic or acidic additive – see (30) [127, 128]. The 2-(arylethynyl)aniline **71** was, for example, transformed to the bis fluorinated adduct **72** via a domino gold(III)-catalyzed cyclization/electrophilic substitution sequence in 86% yield – see (30). This methodology was extended towards the synthesis of monofluorinated analogs such as **73** when less equivalent of Selectfluor

was used – see (31). It should be noted that domino gold-catalyzed rearrangement and fluorination of propargylacetates allowed the synthesis of α-fluoroenones [129].

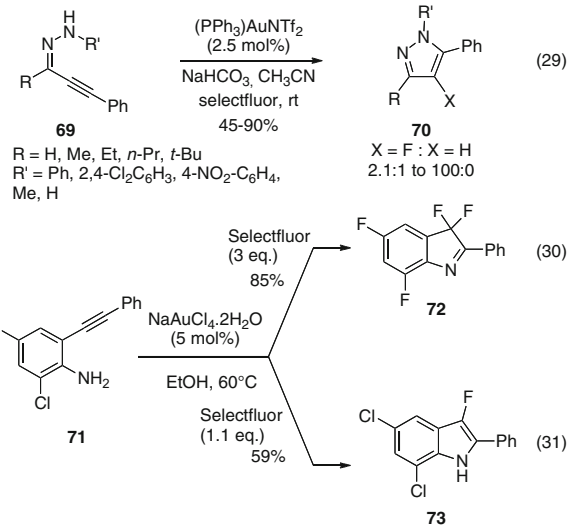

3 Gold-Catalyzed Domino Reactions of 1,*n*-Enynes

Cycloisomerization reactions of 1,*n*-enynes are one of the main transformations that have led to domino processes [37–44]. A general skeleton rearrangement picture is presented in Scheme 1: when subjected to gold-catalyzed reactions, 1,6-enynes **74** (the most studied substrates) are cyclized according to 5-*exo-dig* **75** and 6-*endo-dig* **76** cycloisomerization processes, leading to carbenoid intermediates. Then, depending on the reaction conditions (organometallic species and nucleophiles), several functionalized derivatives may be obtained such as **77**, **78**, **79**, and **80**. Selected examples are presented below.

The synthesis of carbo- and heterocycles implying the addition of water and alcohols was described in the presence of gold(I) catalysts [130–134] – see (32). Several catalytic systems based on gold have been found to be efficient for access to **81** from **74**, the gold(I) complexes being directly used [135] or generated by acid catalysis [136] or an Au(III)/Au(I) [137, 138] reduction process. The group of Toste et al. described a similar domino process for the preparation of vinylsilanes [139]. Intramolecular cyclizations of 1,6-enynes having a hydroxyl substituent on the alkene chain have also been described, leading to bicyclic derivatives [140, 141].

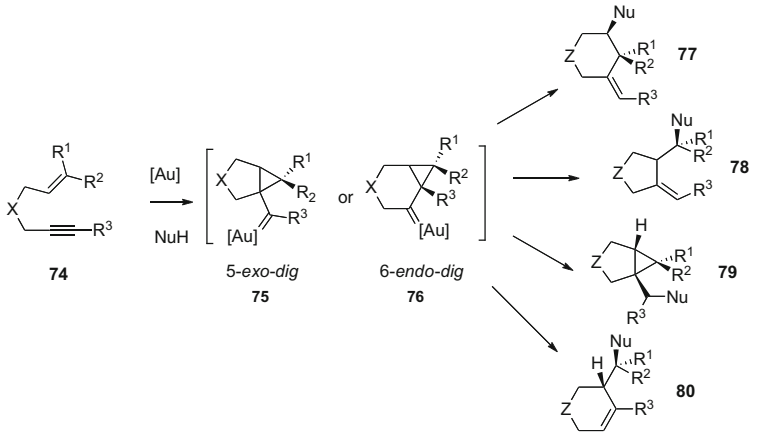

Scheme 1 General scheme for cycloisomerization of 1,6-enynes

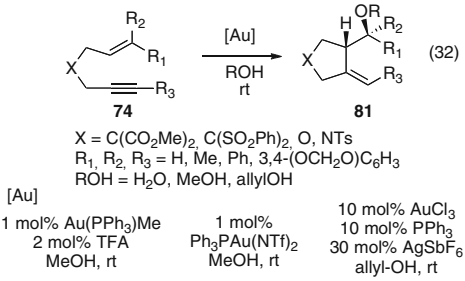

Apart from 1,6-enynes, few other substrates have been engaged in domino cycloisomerization/functionalization reactions such as 1,5- and 1,7-enynes.

The inter- [135] and intramolecular [142, 143] phenoxycyclization of 1,5-enynes was recently described in the presence of a gold catalyst – see (33). The enyne **82** was, for example, converted to the tetracyclic compound **83** in the presence of cationic gold(I) $Ph_3PAuNTf_2$ according to the 6-*endo-dig* process – see (33). When another unsaturation was present in the substrate, such as in **84**, two nucleophilic sites could be involved in the domino process – see (34) [144]. The group of Gagosz nicely showed that one parameter controlling the chemoselectivity was the dilution of the medium, the functionalized adduct **85** being isolated in 72% yield. The hydroxycyclization of 1,7-enyne **86**, substituted by a disulfonate moiety in position C-4, led to the alcohol **87** in 56% yield – see (35) [145]. The scope of this process was found to be quite limited as the hydration of the alkyne moiety was found to be competitive.

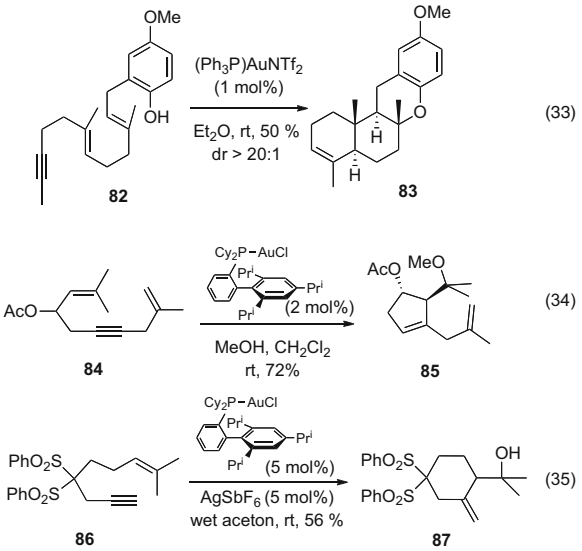

The intra- and intermolecular addition of nitrogen nucleophiles during the cycloisomerization of 1,6-enynes was based on the same concept [141, 144, 146].

When sulfoxides were used as external nucleophiles, an interesting reactivity, e.g., an oxidative rearrangement, was observed [147]. The use of *N*-heterocyclic gold(I) complex IPrAuCl, silver salt and diphenylsulfoxide promoted the formation of bicyclic adduct **89** in 90% yield – see (36). The reaction conditions were compatible with oxygen- or nitrogen-linked enynes. For unsubstituted alkene at the terminal position, an isomerization step occurred, and finally the whole process led to cyclopentene **90** in 85% yield.

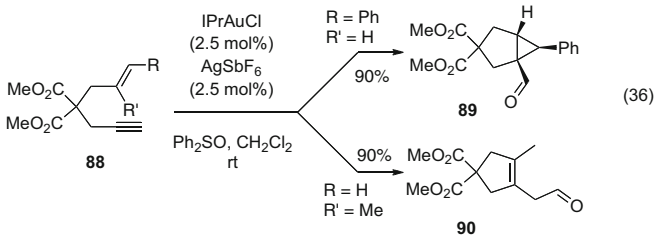

When carbonyl nucleophiles were used during the domino processes, an intermolecular addition of carbonyl compounds occurred, considering the process as a Prins rearrangement, where two C–C and one C–O bonds were assembled in a formal [2 + 2 + 2] alkyne/alkene/carbonyl cycloaddition [148]. The use of the catalyst system $Ph_3PAuCl/AgSbF_6$ and *o*-nitrobenzaldehyde promoted, for example, the synthesis of **92**, starting from **91** in 66% yield, via intermediate **93** – see (37). As previously observed with sulfoxide as nucleophile, the substitution of the alkene of the enyne was found to be crucial, as other derivatives such as dioxolanes [149] or

unsaturated pyranic bicycles [150] could be isolated. The domino cyclization associated with a Prins reaction was also described in an intramolecular manner for 1,6-enynes bearing a carbonyl moiety. The reaction of 1,6-enyne **94**, for example, gave oxatricyclic derivative **95** in 79% yield and 1,3-diene **96** in 10% yield [151]. Other catalysts than gold chloride were found to be efficient, but did not suppress the formation of diene.

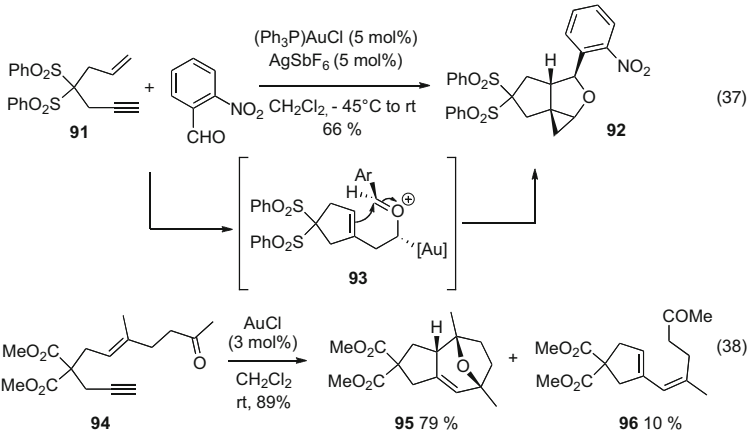

The domino rearrangement/functionalization of enynes has also been described in the presence of carbonated nucleophiles, such as alkenes, aromatic rings, and malonates.

Following Murai's work, the use of gold catalyst allowed the synthesis of polycyclic derivatives under milder conditions at room temperature [152]. Tetracyclic derivative **98** was, for example, obtained in 88% yield – see (39). Modifying the remote alkene position for the trapping step was compatible with the reaction conditions as shown in (40) [153, 154]. The preparation of tetracyclo[3.3.0.0^{2,8}.0^{4,6}]octane **100** was described efficiently starting from cyclohexadienyl substituted oxygen-tethered enyne **99**. The reaction conditions were amenable with other enynes such as nitrogen- and carbon-linked enynes. Similar domino processes have been described in the case of 1,5-enynes [155–158] and have been studied theoretically [159, 160]. The group of Echavarren proposed a remarkable catalytic system to perform such transformations in an intermolecular way [161]. In the presence of 5 equiv. of norbornene, the gold (I) complex IMesAuSbF$_6$ promoted, for example, the preparation of bicyclic adduct **102** in 73% yield – see (41).

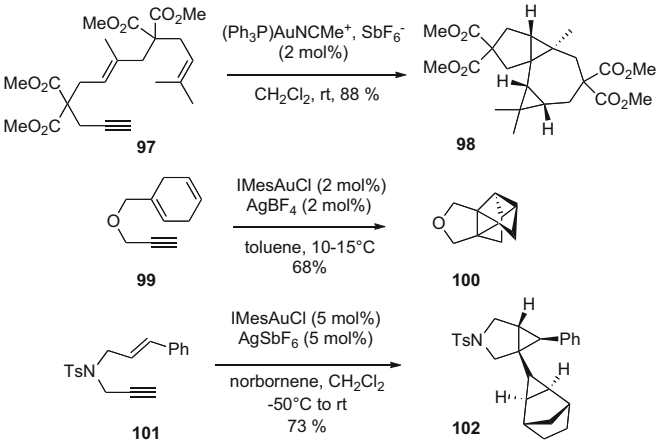

The electron-rich aromatic compounds can be involved in domino hydroarylation/cyclization processes in the presence of gold catalysts. Echavarren and co-workers disclosed the rearrangement of enynes, the alkyne function being substituted by an aromatic group [162, 163]. The synthesis of the tricyclic derivative **104** from the enyne **103** bearing a prenyl chain was efficiently realized in 94% yield – see (42). The synthesis of cyclopenta[b]naphthalenes was also possible according to the same process [164]. It is interesting to note that changing the reaction conditions, e.g., performing the reaction under microwave heating, authorized the *endo-dig* cyclization, which was followed by the isomerization of the alkene to the internal position. The gold-catalyzed transformation of **105** led to tricyclic adduct **106** in 93% yield – see (43). This latter reaction could also be obtained in the presence of tris(2,6-di-*tert*-butylphenyl)phosphite-based gold catalyst at room temperature. According to the same process, the cycloisomerization reaction implying an internal aromatic nucleophile linked onto the alkenyl moiety was disclosed [165]. The use of gold cationic catalyst afforded hexahydrophenanthrene **108** starting from **107** in excellent yields and a total stereoselectivity – see (44).

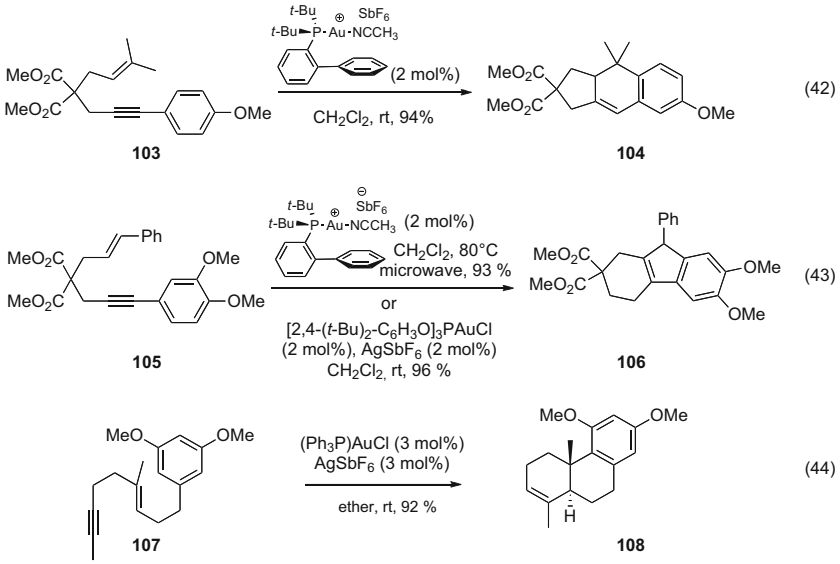

An intermolecular domino hydroarylation reaction/cyclization was also described, combining Ph_3PAuCl and silver salt $AgSbF_6$ in diethyl ether at room temperature [166, 167]. The introduction of electron-rich aromatic compounds, such as dimethoxybenzene, 4-bromo-1,3-dimethoxybenzene, or 1-methylindole, afforded the corresponding 5-*exo* adducts **110** (63–82% yield for **111–113**) in good to excellent yields – see (45). The process was found to be very similar to hydroxyl- and alkoxycyclization cascades. It was also amenable with 1,5-enynes as exemplified with the preparation of **115** – see (46) [134, 168].

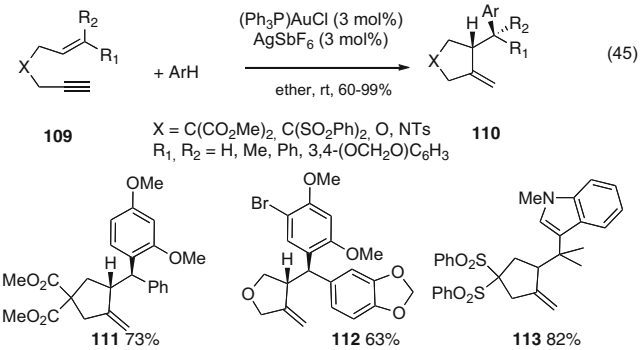

Remarkably, another domino process was found to be predominant when changing the gold catalyst [134, 168]. When the cationic gold complex [2,4-(*t*-Bu)$_2$C$_6$H$_3$O] PAuSbF$_6$ was reacted with enynes **116**, the major product obtained was the functionalized derivative **117**, resulting from the nucleophilic addition of the indole on the carbenoid intermediate – see (47). In the case of the nitrogen-linked derivative **116**, the azabicyclic derivative **119** was isolated in 50% yield – see (47). The 6-*endo* cyclization mode was found to be possible in the case of substituted 1,6-enyne **120**. The domino addition of 1-methylindole/ cycloisomerization reaction led to **121** in 73% yield – see (48).

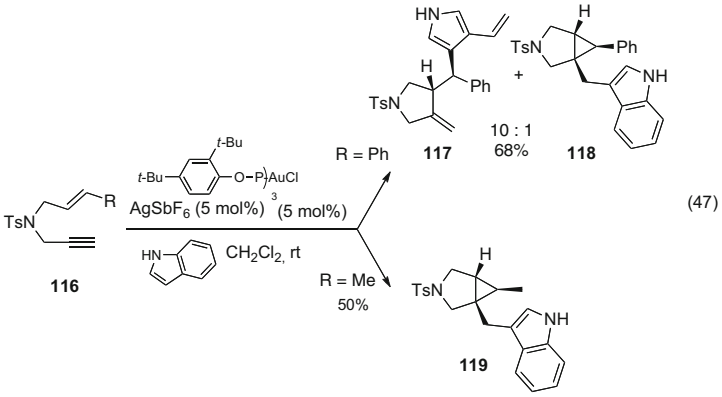

Few examples have been described so far in the presence of other carbon nucleophiles. The addition of allylsilane during the course of the cycloisomerization reaction of enyne **122** led to the formation of a carbon–carbon bond according to an SN_2' addition/cyclization [134], and functionalized sulfonated derivative **123** – see (49) – in 62% yield. The same reactivity was observed in the case of 1,3-dicarbonyl derivative dibenzoylmethane as external nucleophile. The corresponding five-membered ring derivative **124** was isolated in 84% yield. The reaction pattern was found to depend and vary upon the substitution and the nature of the enyne. In the case of nitrogen-tethered enyne **125**, a mixture of products **126** and **127** was obtained depending on the addition of the nucleophile, directly on the cyclopropyl intermediate or on the carbenoid specie – see (50). It should be noted that the use of IMesAuSbF$_6$ as catalyst gave functionalized cyclopropane **126** as the major product. The substitution of the alkynyl moiety, such as in compound **125** (R = Me), favored a domino 6-*endo* cyclization process/nucleophilic addition as the corresponding six-membered ring **128** was obtained in 75% yield.

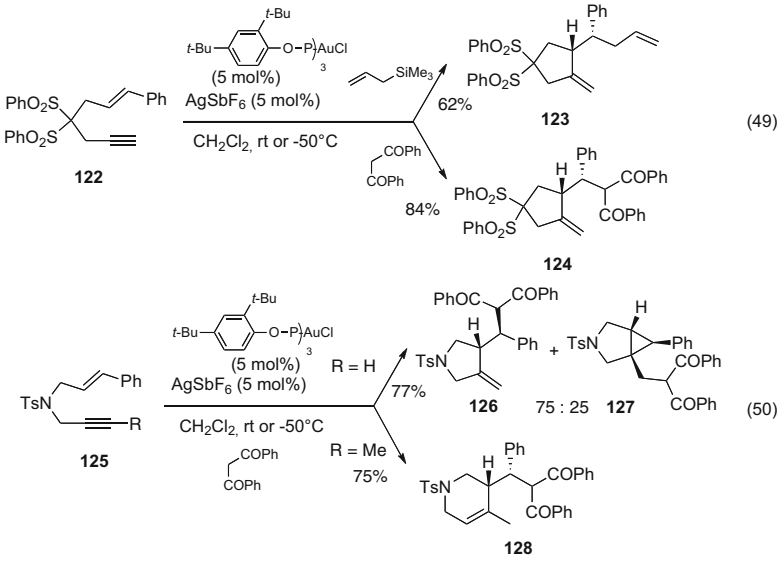

In the case of ene-diynes substrates, a recent Au(I)-catalyzed domino process has been described [169], giving rise to a highly efficient access to cyclobutene-fused azepines **130** – see (51). The authors proposed as intermediate the vinyl gold allyl cation **131**, coming from a 6-*endo-dig* cyclization of the enyne followed by the cleavage of the C–N bond. Removal of gold could generate the allenic species **132**, which would be transformed to the heterocycle **130** via a [2 + 2] cycloaddition. The scope of this transformation is quite broad as several aromatic-bearing electron-donating or -withdrawing groups as well as heterocycles were compatible, the resulting bicyclic heterocycles being isolated in moderate to good yield.

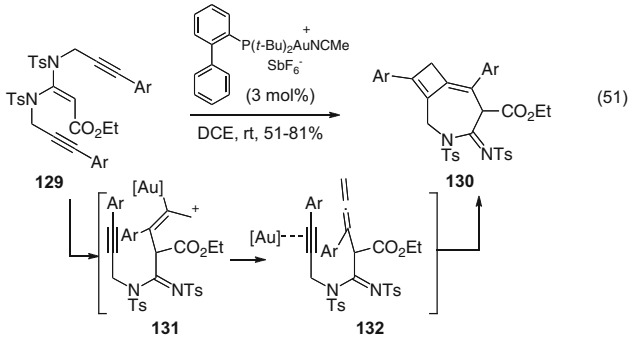

4 Asymmetric Gold-Catalyzed Domino Transformations

The enantioselective transformations employing gold catalysts have not flourished as fast as the gold-catalyzed transformations [42, 45–52]. Most of the examples rely on gold(I) linear chiral complexes, which make the control of stereogenic centers tricky.

Based on the synthesis of ring-fused tetrahydroazepines [170], Zhang and co-workers recently developed a remarkable process involving a redox-neutral domino cyclization/1,5-hydride shift/cyclization steps [171]. The use of bimetallic *(R)*-4-MeO-3,5-(*t*-Bu)$_2$-MeOBIPHEP(AuCl)$_2$ complex allowed the efficient preparation of furan-functionalized azepines such as **134**, which was isolated from **133** in 94% yield and 97% enantiomeric excess – see (52).

Trapping of an iminium intermediate was also possible in the case of indole-substituted derivatives bearing an alcohol group [172]. The synthesis of polycyclic indoline **137** was, for example, achieved via a chemo-, regio-, and stereoselective Au-catalyzed cascade hydroindolination/iminium trapping sequence in the presence of (*R*)-xylylBINAP-based bimetallic gold complex – see (53). The corresponding tricyclic derivative **137** was isolated in good yield and *ee*. This strategy could also be extended to the preparation of nitrogen-linked furoindolines.

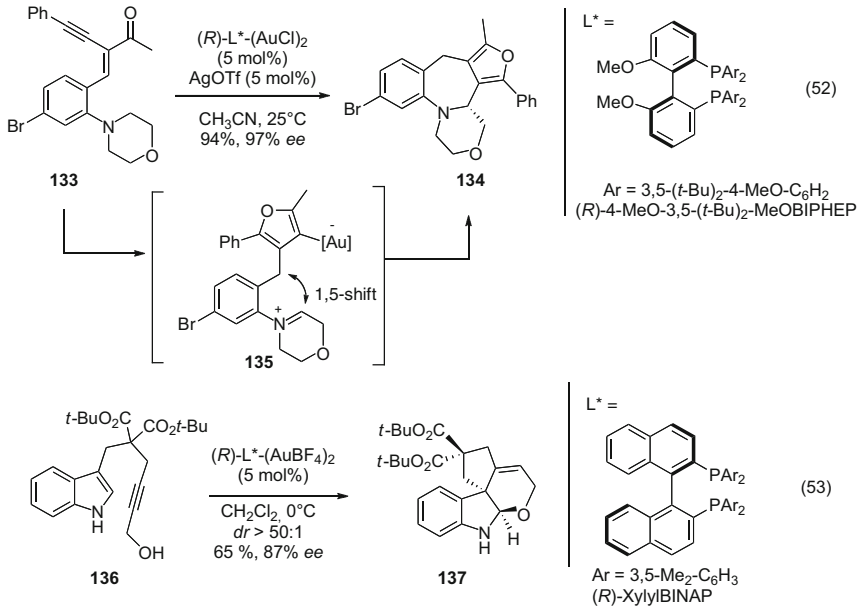

The synthesis of functionalized chiral furans has also been disclosed via domino processes, implying addition of oxygen nucleophiles such as nitrone **139**. Gold-catalyzed regiospecific 1,3-dipolar cycloaddition reactions led to furo[3,4-*d*][1, 2] oxazines such as **140** in good yields and enantiomeric excess [173, 174] – see (54).

A very careful optimization of the chiral ligand during this process showed the supremacy of chiral atropisomeric ligands derived from MeOBIPHEP or TUNEPHOS. The same team further developed similar methodology through an asymmetric [4 + 3] annulation of racemic 1-(1-alkynyl)cyclopropyl ketones such as **141** with nitrones such as **139** in high enantiomeric excesses [175] – see (55). The similar process implying [2 + 2 + 3] cycloaddition of nitrones was also reported [176].

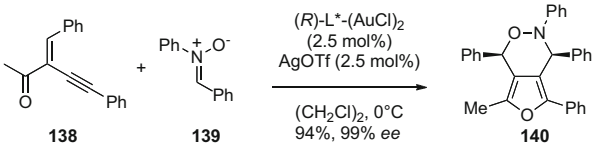

(54)

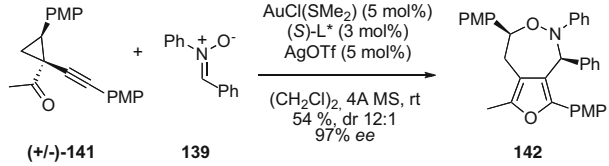

(55)

In the area of domino processes implying addition of carbonyl groups to alkynes, Slaughter's group reported a remarkable cascade process involving addition of alcohol and cycloisomerization steps starting from alkynyl-substituted benzaldehydes **143** [177–180]. The use of chiral sophisticated binaphthyl ligand with acyclic diaminocarbene was crucial for the formation of functionalized derivatives **144** in high enantiomeric excesses, presumably because of a specific conformation of the gold complex – see (56). This methodology was particularly efficient in the case of hindered alcohols and phenyl or *para*-tolyl groups at the alkynyl position. It should be noted that *n*-propyl-substituted adduct could also give the cyclic adducts in high *ee*, providing the fact that a chiral amine was introduced in place of the di-*iso*-propylamine moiety of the chiral ligand.

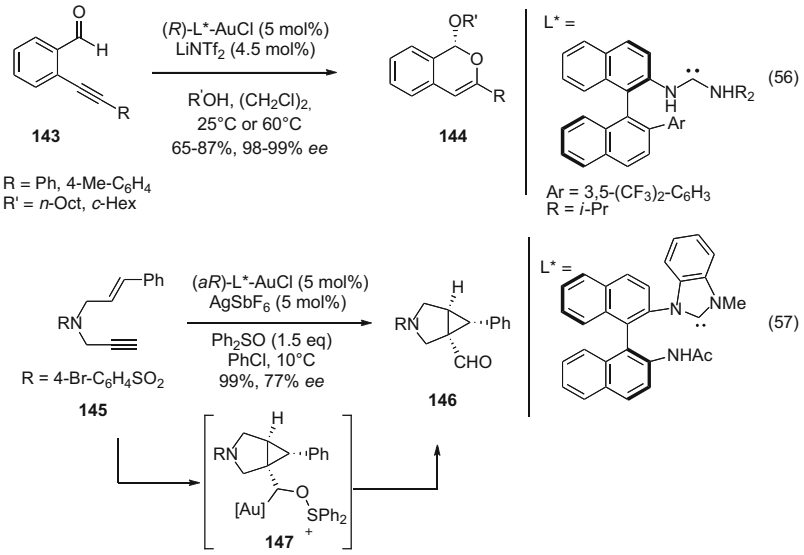

Another peculiar application of chiral atropisomeric carbene ligands has been reported by Shi's group [181]. The domino cyclization process of 1,6-nitrogen-linked enynes, employing diphenylsulfoxide as nucleophile (intermediate **147**), afforded the synthesis of bicyclic aldehydes. The enantiomeric excesses for most of the tested substrates were low to modest, the best result being obtained in the case of enyne **145** – see (57). The bicyclic aldehyde **146** was isolated in 99% yield and 77% *ee*.

Other oxygen-nucleophiles have been used in the asymmetric domino rearrangement of enynes. Several chiral ligands have been engaged in such transformations, as exemplified in (58), (59), and (60). Enyne **148** was transformed into ether **149** via a 5-*exo-trig* cycloisomerization mode and domino addition of methanol at the more substituted carbon of the alkene – see (58). The use of (*R*)-TolBINAP(AuCl)$_2$ [182], *(R)*-4-MeO-3,5-(*t*-Bu)$_2$-MeOBIPHEP [183, 184], or a chiral carbene [185] allowed the formation of **149** in good yields and enantiomeric excesses going from 72% to 94%. The structure of the enyne was a key parameter in such transformations, as the hydroxycyclization reaction of enyne **150** led to the corresponding alcohol **151** in 89% *ee* – see (59). The use of C2-symmetric NHC ligands was also possible in the presence of water, alcohol, or acetic acid as external nucleophiles, but led to modest *ee* [181, 186]. Apart from 1,6-enynes, the alkoxycyclization of 1,5-enynes such as **152** was recently described and allowed the formation of indenes such as **153** – see (60) [187].

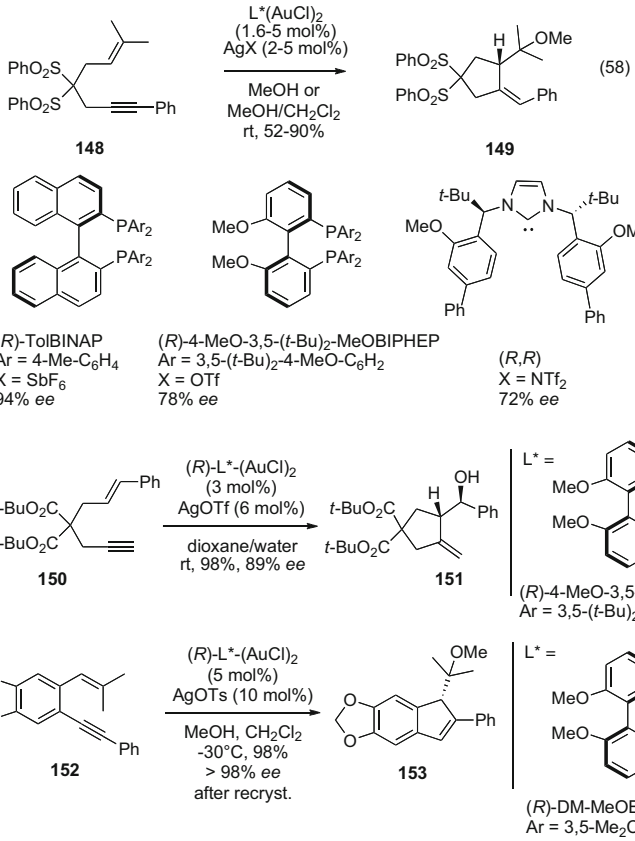

Intra- and intermolecular domino processes have also been disclosed. The Au(I)-catalyzed intramolecular domino 6-*exo* processes have been reported with phenols, carboxylic acids, and protected secondary amines as the internal nucleophile. In the presence of an atropisomeric-ligand-based chiral gold complex, the bicyclic derivative **155** was isolated in 96% yield and 93% *ee* [188] – see (61). The intermolecular reaction of alkene **156** with an alkyne **157** was recently described and afforded α,β-unsaturated δ-lactone **158** in good yield and enantiomeric excess – see (62) [189]. Another example was recently described implying oxoalkenes and allenamides, the whole process leading to oxa-bridged seven-membered ring derivatives in up to 92% *ee* [190].

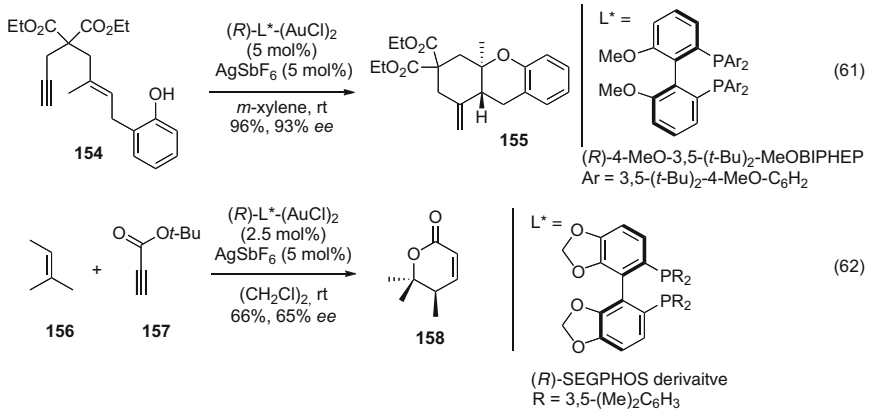

The domino processes involving enynes and external nucleophile were reported in the presence of electron-rich aromatic derivatives as carbon nucleophiles, according to either an inter- or an intramolecular way – see (63) and (64) [183, 184, 191]. The hydroarylation/cyclization reaction of enyne **159** led, for example, to the cyclic adduct **160** in 99% yield and 83% *ee* – see (63). A tricyclic derivative **162** was obtained according to a similar intramolecular process in 98% yield and 94% *ee* [188, 191]. These domino processes were extended to ene-allene cyclization and functionalization [192]. Interestingly, the best enantiomeric excesses were obtained in the presence of a mononuclear gold complex bearing a bulky phosphoramidite ligand. The cascade hydroarylation/ene-allene cycloisomerization reaction of **163** in the presence of 1,3,5-trimethoxybenzene resulted in the formation of pyrrolidine **164** in 73% yield and 97% *ee* – see (65).

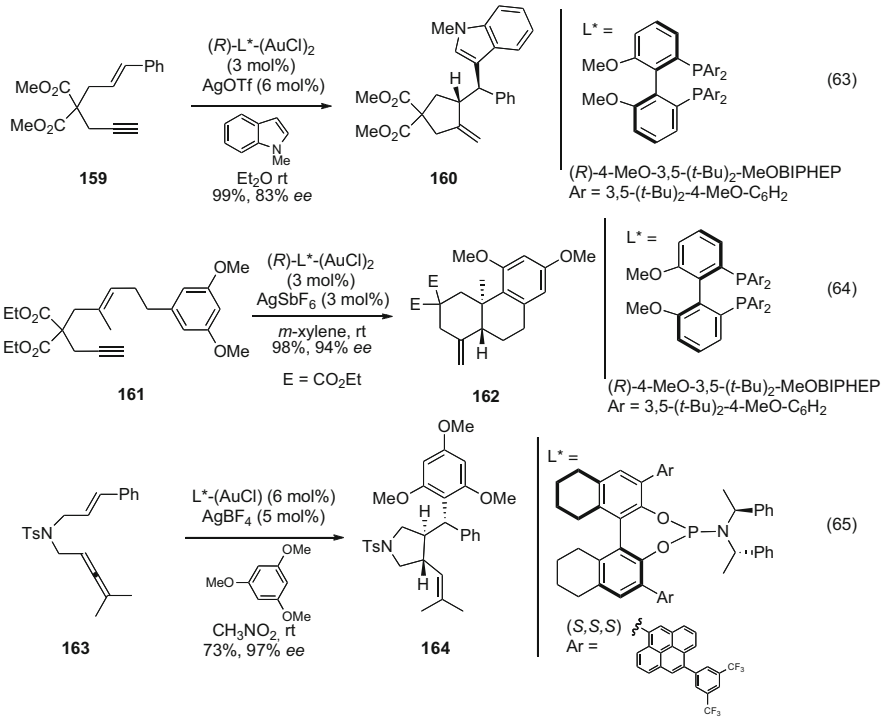

The case of cyclopropylidene-substituted alkyne was particularly remarkable as an unusual 6-*exo-dig* addition of the alkenyl moiety was obtained, the whole process being envisioned as a hydroarylation/cyclization cascade [193]. The stabilized allylic cation **167** was advocated and involved in a Nazarov-type electrocyclization reaction leading to the tetracyclic derivative **166** – see (66). During their development of gold-catalyzed synthesis of phenols, the group of Hashmi described the domino formation of functionalized phenol **168** by the addition of furanyl group to alkyne [194]. The addition of carbon nucleophile – see (67) – was completely chemoselective via intermediates **170** and **171** and the best enantiomeric excess (55% *ee*) was obtained in the presence of (*R*)-4-MeO-3,5-(*t*-Bu)$_2$-MeOBIPHEP-based bimetallic gold complex. The authors proposed carbene intermediate **170** (resulting from a classical enyne type rearrangement) and arene oxide **171**. Several other systems employing atropisomeric, ferrocenyl-type, and phosphoramide chiral ligands were tested but did not give better results.

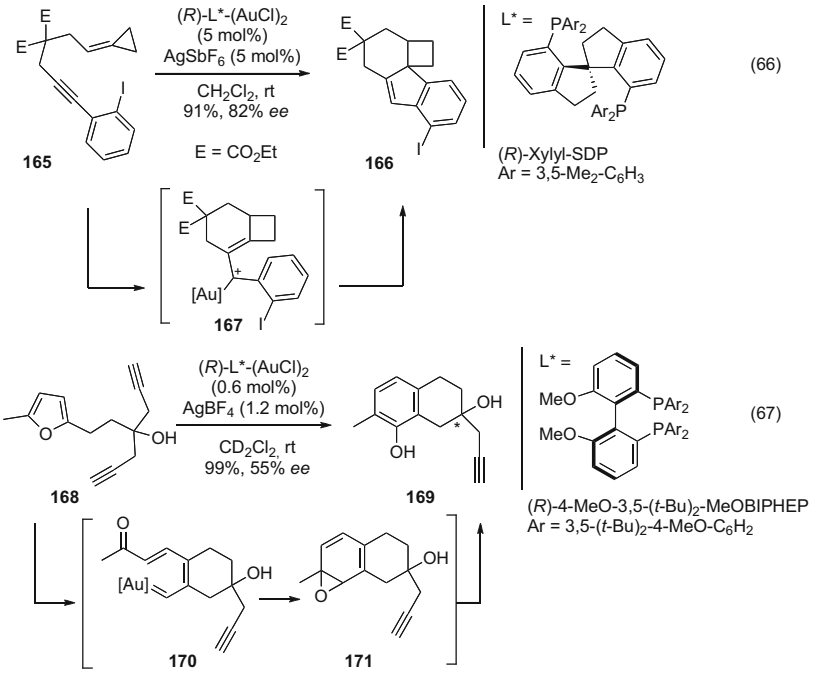

An original domino process implying a cycloisomerization and amination reaction was recently disclosed in the literature [195]. The reaction of various 2-(alkynyl) phenylboronic acids **172** with diazene **173** afforded enantiomerically-enriched heteroaryl atropisomers **174** in good yields and fair to good *ee*s – see (68). The addition of the boronic acid to the activated alkyne moiety would lead to a vinyl chiral gold complex which would attack the diazene. The chirality was found to be stable at room temperature.

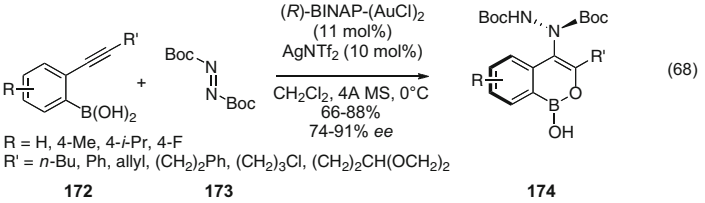

5 Applications to the Synthesis of Natural Products

Gold-catalyzed domino processes have been described for the synthesis of natural products or biologically active products. The gold-catalyzed hydration step was involved in the cascade sequence for the preparation of the piperidine core of alkaloid (+)-andrachcinidine (Scheme 2) [196]. The addiction of water on alkyne **175** was followed by the elimination of methanol leading to α,β-unsaturated ketone

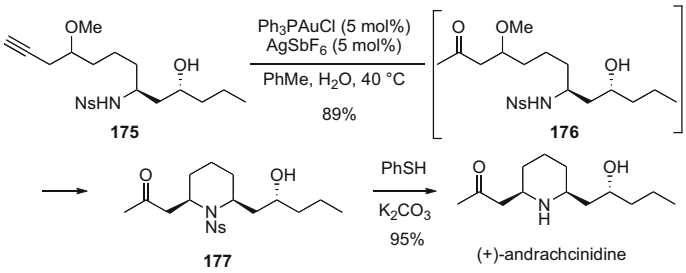

Scheme 2 Synthesis of (+)-andrachcinidine

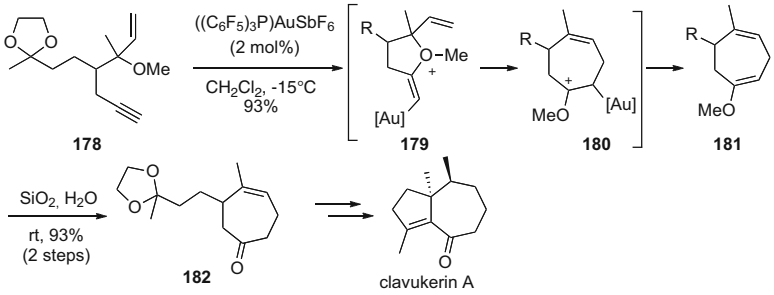

Scheme 3 Synthesis of clavukerin A

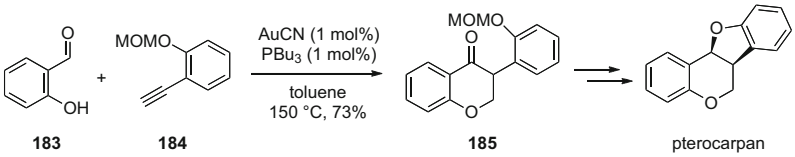

Scheme 4 Synthesis of pterocarpan

as intermediate. Then the 1,4-addition of the amine allowed the easy access to the piperidine core **177**, which, upon one deprotection step, afforded the natural product.

A cyclization/sigmatropic rearrangement cascade step was used in the formal synthesis of racemic clavukerin A [197]. The seven-membered ring of the natural product (Scheme 3) was cleanly obtained via a gold-catalyzed 5-*exo*-*dig* cyclization of alkyne **178** to form the oxonium ion **179**, which evolved to enol ether **181** via a [3,3]-sigmatropic rearrangement. The unstable enol ether **181** was quickly transformed to ketone **182**, precursor of the natural product.

A synthesis of racemic natural product pterocarpan was also described via a gold (I)-catalyzed cascade starting from phenol **183** and alkyne **184** [198] (Scheme 4). The authors proposed an oxidative addition of CH bond of aldehyde leading to an acyl Au(III) hydride (followed by a hydrometalation step) or a gold–carbene

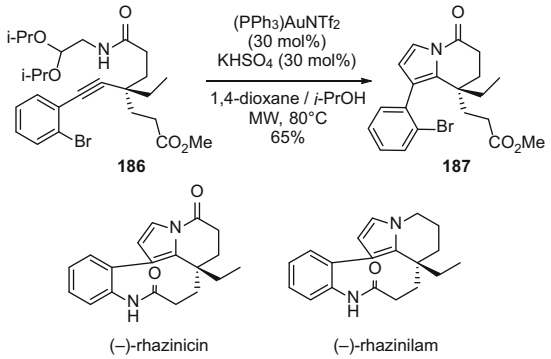

Scheme 5 Gold-catalyzed key step in the syntheses of (−)-rhazinicin and (−)-rhazinilam

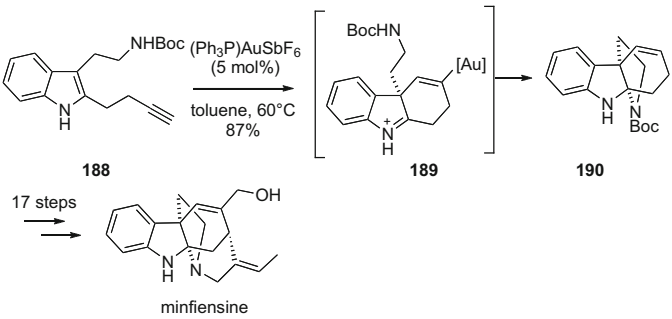

Scheme 6 Synthesis of minfiensine

intermediate to explain such a process. The alkoxylation step would occur on the enone and would therefore nicely give an access to isoflavanone derivatives, pterocarpan being obtained in two steps from **185**.

The total synthesis of (−)-rhazinilam and (−)-rhazinicin was very recently described in the presence of gold(I) catalyst [199] (Scheme 5). The gold-catalyzed cascade double cyclizations of the functionalized derivative **186** allowed the formation of the bicyclic indolizinone moiety **187**, which could then be transformed to the desired natural products in three to five steps.

The hydroamination step could be placed on a second plan when indole was present in the starting material as exemplified by the formal total synthesis of minfiensine [200] (Scheme 6). Hydroarylation reactions have also been utilized in domino processes. The 6-*endo-dig* cyclization of alkyne **188** led to tetracyclic structure **190** via an iminium derivative **189** in the presence of a gold(I) cationic catalyst in 87% yield. This strategy allowed the formation of other very elaborated tetracyclic moieties.

The 5-*exo-dig* amination of azido alkyne **191** was recently described as the key step for formal synthesis of the anti-tumor agent 7-methoxymitosene (Scheme 7) [201]. The authors proposed a gold carbene intermediate **193**, which would be formed from a dicationic intermediate **192** via a 4π electrocyclic ring closure. An

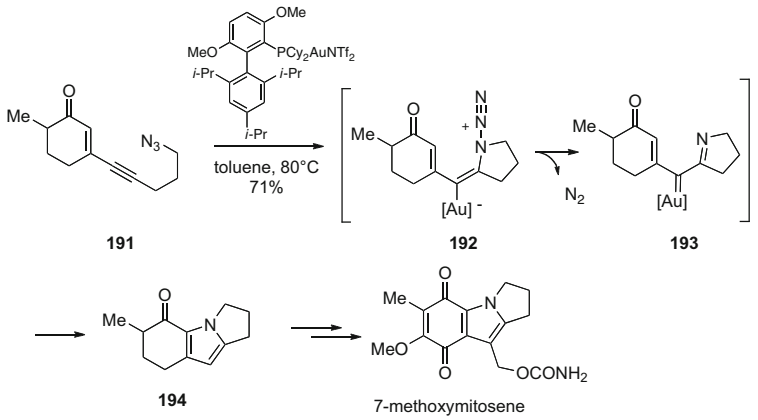

Scheme 7 Synthesis of 7-methoxymitosene

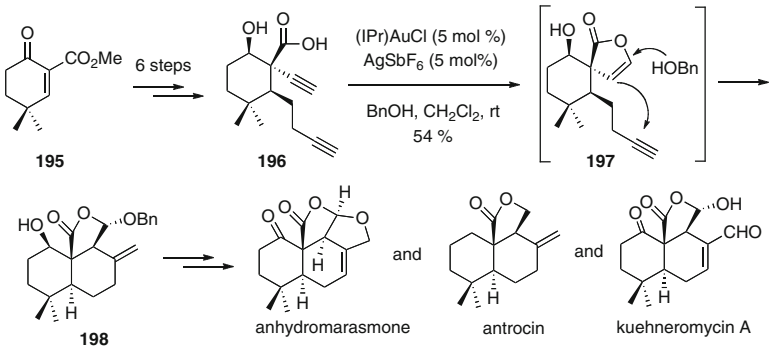

Scheme 8 Syntheses of drimane-type terpenoids

isomerization and protodeauration would lead to the corresponding pyrrole **194**, precursor of the natural product via a seven-step sequence.

Apart from hydration and hydroamination, the involvement of hydrocarboxylation in cascade sequences has also led to natural products such as drimane-type terpenoids (Scheme 8) [202]. A remarkable gold-catalyzed domino reaction of 1,7-diynes allowed the synthesis of lactone **197**, via a 5-*endo-dig* hydrocarboxylation of diyne **196**. The tricyclic core of the natural products was built via a subsequent gold-catalyzed enyne cyclization mediated by an external alcohol. Overall, this cascade process allowed the formation of five new bonds, two rings, and two stereocenters.

The reactivity of propargylic esters such as **199** was also developed towards total synthesis, implying domino processes (Scheme 9). The main issues concerned 1,3- and 1,2-acyl migrations leading to a gold carbenic species, which may then be involved in another process [81]. The synthesis of $\Delta^{(9,12)}$-capnellene was, for example, described via an 1,3-acyl transfer cascade [98]. The gold-activated allene

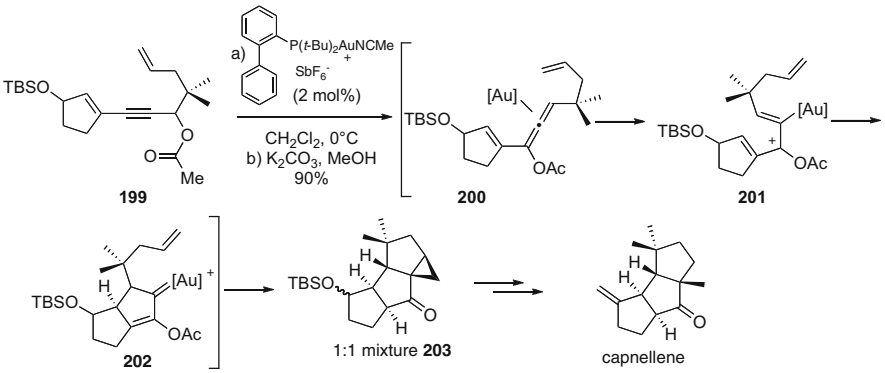

Scheme 9 Synthesis of capnellene

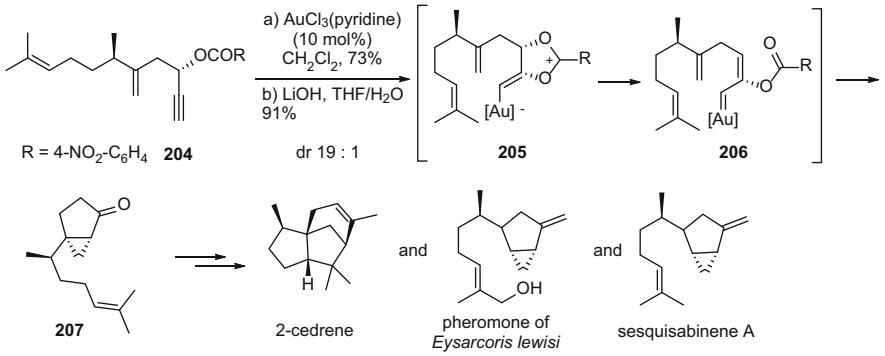

Scheme 10 Synthesis of sesquiterpenes

200 evolved to a vinyl gold species **201** via an isomerization process, the formation of the carbene species **202** via a Nazarov cyclization being followed by a cyclopropanation reaction. The triquinane backbone **203** of the natural product was then obtained in a complete stereoselective manner.

A remarkable example implying gold-catalyzed 1,2-acyl shift cascades concerned the synthesis of terpenoids such as sesquiterpenes [203–205] (Scheme 10). The gold carbene specie was formed via a gold-catalyzed 1,2-acyl addition to alkyne, producing a zwitterion **205** as a key intermediate. A similar cyclopropanation step afforded a key intermediate **207**, which could be easily transformed to 2-cedrene and insect pheromone.

Other rearrangements implying enynes as starting material have been applied for the total synthesis of natural products, such as the enyne-Pinacol cascade [206] (Scheme 11). The group of Toste described the easy access to ventricosene, a novel sesquiterpene triquinane natural product [193]. The 1,6-enyne **208** was transformed to tricyclic adduct **210** in 87% yield, via a *6-exo* mode of cyclization, the vinylaurate **209** being advocated as the key intermediate.

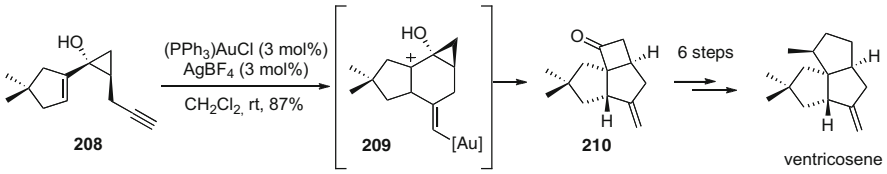

Scheme 11 Synthesis of ventricosene

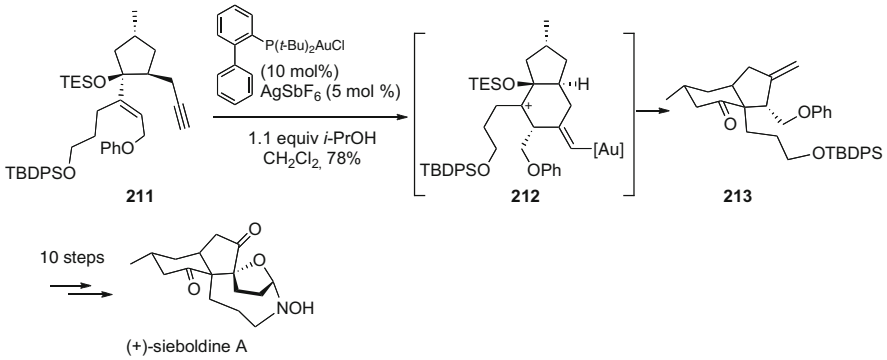

Scheme 12 Synthesis of (+)-sieboldine A

The Overman's group later proposed a very efficient synthesis of (+)-sieboldine A via a classical cycloisomerization process of enyne **211**, followed by a stereospecific Pinacol 1,2-shift (intermediate **212**), generating a ring-expanded ketone **213** [207] (Scheme 12).

The carbocationic intermediates could also be trapped by carbonyl derivatives, known as the Prins rearrangement. Echavarren as well as Ma and coworkers independently described the synthesis of (−)-englerin A according to the same cascade process, but starting from a different functionalized enyne [208, 209] (Scheme 13). The oxatricyclic derivative **216** was obtained in the presence of $IPrAuSbF_6$ as the catalyst starting from enyne **215**, which was prepared in eight steps from geraniol **214**. This methodology could be applied to other natural products such as pubineroid B and (–)-englerin B, using a similar methodology [210]. The other approach relied on the synthesis of allylic alcohol **218** from (*R*)-citronellal **217**. A simple gold catalyst such as AuCl allowed the clean formation of oxatricyclic adduct **219** in moderate yield, the latter being transformed to (–)-englerin A in nine steps.

The synthesis of jungianol was a particularly spectacular and unusual example of transformation of furan derivatives to phenols [211] (Scheme 14). This gold-catalyzed cascade started from alkyne **220**, which, upon activation with $AuCl_3$, was transformed to bicyclic phenol **223**, via presumably a carbonic specie **221** and the epoxide **222**.

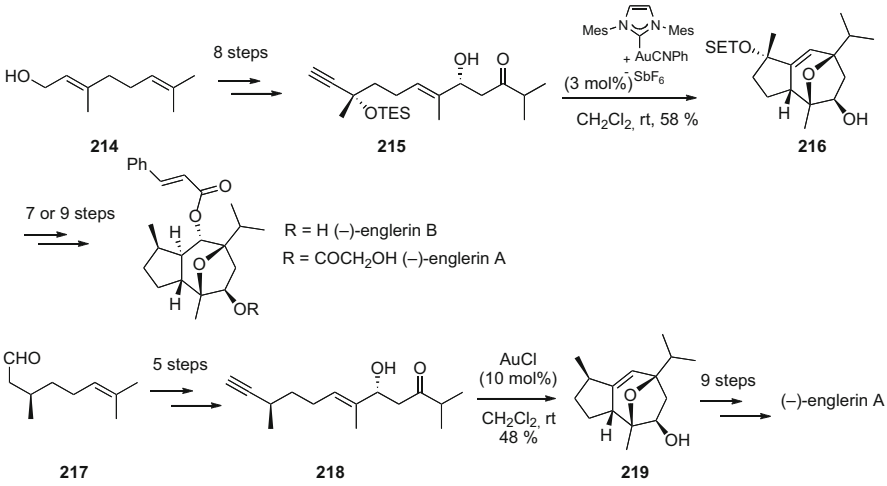

Scheme 13 Syntheses of (−)-englerins A and B

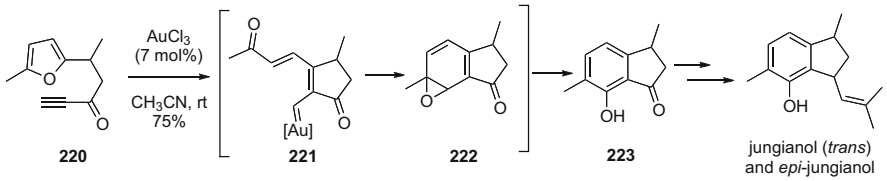

Scheme 14 Syntheses of jungianol derivatives

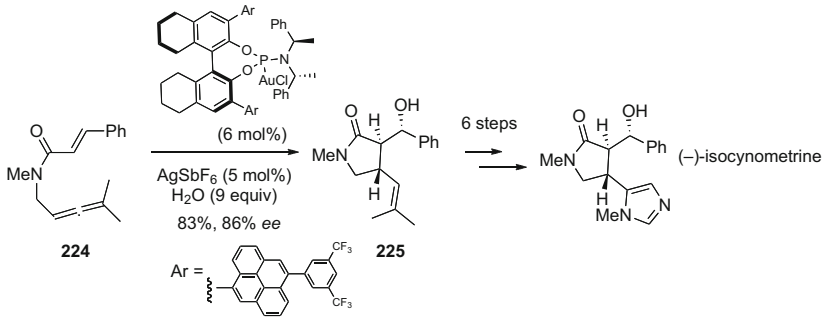

Scheme 15 Synthesis of (−)-isocynometrine

Cycloisomerization of ene-allene **224** in the presence of a chiral extremely hindered phosphoramidite-functionalized gold complex allowed the asymmetric synthesis of (–)-isocynometrine [192] (Scheme 15). The 5-*exo-trig* cyclization was accompanied by the addition of water in a domino process and led to cyclic amide **225** in good yield and enantiomeric excess. Further transformation afforded the natural product in six steps.

6 Conclusion

Gold-catalyzed domino processes have emerged as highly valuable tools to access complicated molecular architecture from simple precursors. As shown in this review, the activation of alkynes and allenes (generated from specific substrates or not) by gold complexes is generally followed by multiple bond formations which can lead to acyclic and carbo- or heterocyclic compounds. The emergence of asymmetric domino processes shows that chemists are able to identify and control important features in enantioselective reactions. Moreover, the remarkable and selective activities of tailor-made gold catalysts have encouraged the synthetic community to apply methodologies to natural products or biologically active derivatives. Further investigations in this area should provide us with novel and original domino rearrangements.

References

1. Hashmi ASK, Toste FD (eds) (2012) Modern gold catalyzed synthesis. Wiley-VCH, Weinheim
2. Toste FD, Michelet V (eds) (2014) Gold catalysis: an homogeneous approach. Imperial College Press, London
3. Obradors C, Echavarren AM (2014) Chem Commun 50:16
4. Hashmi ASK (2010) Angew Chem Int Ed 49:5232
5. Hashmi ASK, Bührle M (2010) Aldrichim Acta 43:27
6. Shapiro ND, Toste FD (2010) Synlett 675
7. Das A, Abu Sohel SM, Liu R-S (2010) Org Biomol Chem 8:860
8. Abu Sohel SM, Liu R-S (2009) Chem Soc Rev 38:2269
9. Nevado C (2010) Chimia 64:247
10. Fürstner A (2009) Chem Soc Rev 38:3208
11. Arcadi A (2008) Chem Rev 108:3266
12. Patil NT, Yamamoto Y (2008) Chem Rev 108:3395
13. Li Z, Brouwer C, He C (2008) Chem Rev 108:3239
14. Shen HC (2008) Tetrahedron 64:3885
15. Skouta R, Li C-J (2008) Tetrahedron 64:4917
16. Hashmi ASK, Rudolph M (2008) Chem Soc Rev 37:1766
17. Muzart J (2008) Tetrahedron 64:5815
18. Gorin DJ, Sherry BD, Toste FD (2008) Chem Rev 108:3351
19. Hashmi ASK (2007) Chem Rev 107:3180
20. Fürstner A, Davies PW (2007) Angew Chem Int Ed 46:3410
21. Gorin DJ, Toste FD (2007) Nature 446:395
22. Liu L-P, Hammond GB (2012) Chem Soc Rev 41:3129
23. Fogg DE, dos Santos EN (2004) Coord Chem Rev 248:2365
24. Tietze LF (1996) Chem Rev 96:115
25. Poli G, Giambastiani G, Heumann A (2000) Tetrahedron 56:5959
26. Muratore ME, Homs A, Obradors C, Echavarren AM (2014) Chem Asian J. doi:121002/asia.201402395, 9:3066
27. Obradors C, Echavarren AM (2014) Acc Chem Res 47:902
28. Xie J, Pan C, Abdukader A, Zhu C (2014) Chem Soc Rev 43:5245

29. Huang H, Zhou Y, Liu H (2011) Beilstein J Org Chem 7:897
30. Lopez F, Mascarenas JL (2011) Beilstein J Org Chem 7:1075
31. Hopkinson MN, Gee AD, Gouverneur V (2011) Chem Eur J 17:8248
32. Zhang D-H, Tang X-Y, Shi M (2014) Acc Chem Res 47:913
33. Garayable D, Nevado C (2012) ACS Catal 2:1462
34. Umland KD, Kirsch SF (2013) Synlett 24:1471
35. Ohno H (2013) Isr J Chem 53:869
36. Qian D, Zhang J (2014) Chem Rec 40:280
37. Belmont P, Parker E (2009) Eur J Org Chem 35:6075
38. Lee SI, Chatani N (2009) Chem Commun 45:371
39. Jimenez-Nunez E, Echavarren AM (2008) Chem Rev 108:3326
40. Michelet V, Toullec PY, Genet J-P (2008) Angew Chem Int Ed 45:7427
41. Zhang L, Sun J, Kozmin S (2006) Adv Synth Catal 348:2271
42. Fairlamb IJS (2004) Angew Chem Int Ed 43:1048
43. Lloyd-Jones G (2003) Org Biomol Chem 1:215
44. Buisine O, Aubert C, Malacria M (2002) Chem Rev 102:813
45. Bongers N, Krause N (2008) Angew Chem Int Ed 47:2178
46. Widenhoefer RA (2008) Chem Eur J 14:5382
47. Sengupta S, Shi X (2010) ChemCatChem 2:609
48. Pradal A, Toullec PY, Michelet V (2011) Synthesis 43:1501
49. Marinetti A, Jullien H, Voituriez A (2012) Chem Soc Rev 41:4884
50. Watson IDG, Toste FD (2012) Chem Sci 3:2899
51. Wang Y-M, Lackner AD, Toste FD (2014) Acc Chem Res 47:889
52. Patil NT (2012) Chem Asian J 7:2186
53. Krause N, Aksin-Artok O, Asikainen M, Breker V, Deutsch C, Erdsack J, Fan H-T, Gockel B, Minkler S, Poonoth M, Sawama Y, Sun T, Volz F, Wintert C (2012) J Organomet Chem 704:1
54. Fürstner A (2014) Acc Chem Res 47:925
55. Fukuda Y, Utimoto K (1991) J Org Chem 56:3729
56. Fukuda Y, Utimoto K (1991) Bull Chem Soc Jpn 64:2013
57. Zhang C, Cui D-M, Yao L-Y, Wang B-S, Hu Y-Z, Hayashi T (2008) J Org Chem 73:7811
58. Sperger C, Fiksdahl A (2009) Org Lett 11:2449
59. Sperger C, Strand LHS, Fiksdahl A (2010) Tetrahedron 66:7749
60. Lian J-J, Liu R-S (2007) Chem Commun 43:1337
61. Kramer S, Madsen JLH, Rottländer M, Skrydstrup T (2010) Org Lett 12:2758
62. Wang W, Jasinski J, Hammond GB, Xu B (2010) Angew Chem Int Ed 49:7247
63. Schuler M, Silva F, Bobbio C, Tessier A, Gouverneur V (2008) Angew Chem Int Ed 47:7927
64. Antoniotti S, Genin E, Michelet V, Genêt J-P (2005) J Am Chem Soc 127:9976
65. Liu L-P, Hammond GB (2009) Org Lett 11:5090
66. Aponick A, Li C-Y, Palmes JA (2009) Org Lett 11:121
67. Paito PHS, Ketcham JM, Aponick A (2014) Org Lett. doi:10.1021/ol5024954, 16:5320
68. Hashmi ASK, Bührle M, Wölfle M, Rudolph M, Wieteck M, Rominger F, Frey W (2010) Chem Eur J 16:9846
69. Liu B, De Brabander K (2006) Org Lett 8:4907
70. Belting V, Krause N (2006) Org Lett 8:4489
71. Blanco Jaimes MC, Bçhling CRN, Serrano-Becerra JM, Hashmi ASK (2013) Angew Chem Int Ed 52:7963
72. Barluenga J, Diéguez A, Fernández A, Rodríguez F, Faňanás FJ (2006) Angew Chem Int Ed 45:2091
73. Barluenga J, Fernández A, Diéguez A, Rodríguez F, Faňanás FJ (2009) Chem Eur J 15:11660
74. Barluenga J, Fernández A, Satrustegui A, Diéguez A, Rodríguez F, Faňanás FJ (2008) Chem Eur J 14:4153
75. Ferrer C, Amijs CHM, Echavarren AM (2007) Chem Eur J 13:1358

76. Barluenga J, Calleja J, Mendoza A, Rodríguez F, Fañanás FJ (2010) Chem Eur J 16:7110
77. Dai L-Z, Qi M-J, Shi Y-L, Liu X-G, Shi M (2007) Org Lett 9:3191
78. Balamurugan R, Kothapalli RB, Thota GK (2011) Eur J Org Chem 1557
79. Tian G-Q, Shi M (2007) Org Lett 9:4917
80. Li Y, Brand JP, Waser J (2013) Angew Chem Int Ed 52:6743
81. Marion N, Nolan SP (2007) Angew Chem Int Ed 46:2750
82. Marco-Contelles J, Soriano E (2007) Chem Eur J 13:1350
83. Buzas A, Istrate F, Gagosz F (2006) Org Lett 8:1957
84. Yeom HS, Yoon S-J, Shin S (2007) Tetrahedron Lett 48:4817
85. De Brabander JK, Liu B, Qian M (2008) Org Lett 10:2533
86. Marion N, Diez-Gonzalez S, de Frémont P, Noble AR, Nolan SP (2006) Angew Chem Int Ed 45:3647
87. Gaillard S, Slawin AMZ, Nolan SP (2010) Chem Commun 46:2742
88. Oh CH, Kim A, Park W, Park DI, Kim N (2006) Synlett 17:2781
89. Oh CH, Kim A (2007) New J Chem 31:1719
90. Leboeuf D, Simonneau A, Aubert C, Malacria M, Gandon V, Fensterbank L (2011) Angew Chem Int Ed 50:6868
91. Fensterbank L, Malacria M (2014) Acc Chem Res 47:953
92. Luo T, Schreiber SL (2007) Angew Chem Int Ed 46:8250
93. Luo T, Schreiber SL (2009) J Am Chem Soc 131:5667
94. Zhang L (2005) J Am Chem Soc 127:16804
95. Modha SG, Kumar A, Vachani DD, Jacobs J, Sharma SK, Parmar V, Van Meervelt L, Ven der Eycken EV (2012) Angew Chem Int Ed 51:9572
96. Buzas A, Gagosz F (2006) J Am Chem Soc 128:12614
97. Lemiere G, Gandon V, Cariou K, Fukuyama T, Dhimane AL, Fensterbank L, Malacria M (2007) Org Lett 9:2207
98. Lemiere G, Gandon V, Cariou K, Hours A, Fukuyama T, Dhimane AL, Fensterbank L, Malacria M (2009) J Am Chem Soc 131:2993
99. Fukuda Y, Utimoto K, Nozaki H (1987) Heterocycles 25:297
100. Fukuda Y, Utimoto K (1991) Synthesis 23:975
101. Sperger CA, Fiksdahl A (2010) J Org Chem 75:4542
102. Hirano K, Inaba Y, Watanabe T, Oishi S, Fujii N, Ohno H (2010) Adv Synth Catal 352:368
103. Hirano K, Inaba Y, Takasu K, Oishi S, Takemoto Y, Fujii N, Ohno H (2011) J Org Chem 76:9068
104. Liu XY, Ding P, Huang J-S, Che C-M (2007) Org Lett 9:2645
105. Zeng X, Frey GD, Kinjo R, Donnadieu B, Bertrand G (2009) J Am Chem Soc 131:8690
106. Liu X-Y, Che C-M (2008) Angew Chem Int Ed 47:3805
107. Zhou Y, Feng E, Liu G, Ye D, Li J, Jiang H, Liu H (2009) J Org Chem 74:7344
108. Liu G, Zhou Y, Lin D, Wang J, Zhang L, Jiang H, Liu H (2011) ACS Comb Sci 13:209
109. Patil NT, Lakshmi PGVV, Singh V (2010) Eur J Org Chem 4719
110. Patil NT, Konala A (2010) Eur J Org Chem 6831
111. Alfonsi M, Arcadi A, Aschi M, Bianchi G, Marinelli F (2005) J Org Chem 70:2265
112. Cera G, Piscitelli S, Chiarucci M, Fabrizi G, Goggiamani A, Ramón RS, Nolan SP, Bandini M (2012) Angew Chem Int Ed 51:9891
113. Patil NT, Kavthe RD, Raut VS, Shinde VS, Sridhar B (2010) J Org Chem 75:1277
114. Qian J, Liu Y, Cui J, Xu Z (2012) J Org Chem 77:4484
115. Leyva-Pérez A, Cabrero-Antonino JR, Cantín Á, Corma A (2010) J Org Chem 75:7769
116. Zhang Y, Donahue JP, Li C-J (2007) Org Lett 9:627
117. Leyva A, Corma A (2009) Adv Synth Catal 351:2876
118. Lavallo V, Frey GD, Donnadieu B, Soleilhavoup M, Bertrand G (2008) Angew Chem Int Ed 47:5224
119. Kinjo R, Donnadieu B, Bertrand G (2011) Angew Chem Int Ed 50:5560
120. Duan H, Sengupta S, Petersen JL, Akhmedov NG, Shi X (2009) J Am Chem Soc 131:12100

121. Harrison TJ, Kozak JA, Corbella-Pané M, Dake GR (2006) J Org Chem 71:4525
122. Demir AS, Emrullahoglu M, Buran K (2010) Chem Commun 46:8032
123. Shu X-Z, Liu X-Y, Xiao H-Q, Ji K-G, Guo L-N, Liang Y-M (2008) Adv Synth Catal 350:243
124. Lu Y, Fu X, Chen H, Du X, Jia X, Liu Y (2009) Adv Synth Catal 351:129
125. Qian J, Liu Y, Zhu J, Jiang B, Xu Z (2011) Org Lett 13:4220
126. Simonneau A, Garcia P, Goddard J-P, Mouriès-Mansuy V, Malacria M, Fensterbank L (2011) Beilstein J Org Chem 7:1379
127. Arcadi A, Pietropaolo E, Alvino A, Michelet V (2013) Org Lett 15:2766
128. Arcadi A, Pietropaolo E, Alvino A, Michelet V (2014) Beilstein J Org Chem 10:449
129. De Haro T, Nevado C (2011) Chem Commun 47:248
130. Méndez M, Paz Muñoz M, Echavarren AM (2000) J Am Chem Soc 122:11549
131. Méndez M, Paz Muñoz M, Nevado C, Cárdenas DJ, Echavarren AM (2001) J Am Chem Soc 123:10511
132. Paz Muñoz M, Méndez M, Nevado C, Cárdenas DJ, Echavarren AM (2003) Synthesis 18:2898
133. Nevado C, Charruault L, Michelet V, Nieto-Oberhuber C, Paz Muñoz M, Méndez M, Rager M-N, Genêt J-P, Echavarren AM (2003) Eur J Org Chem 706
134. Amijs CHM, López-Carrillo V, Raducan M, Pérez-Galán P, Ferrer C, Echavarren AM (2008) J Org Chem 73:7721
135. Buzas AK, Istrate FM, Gagosz F (2007) Angew Chem Int Ed 46:1141
136. Nieto-Oberhuber C, Muñoz MP, Buñuel E, Nevado C, Cárdenas DJ, Echavarren AM (2004) Angew Chem Int Ed 43:2402
137. Genin E, Leseurre L, Toullec PY, Genêt J-P, Michelet V (2007) Synlett 18:1780
138. Chao C-M, Toullec PY, Michelet V (2009) Tetrahedron Lett 50:3719
139. Horino Y, Luzung MR, Toste FD (2006) J Am Chem Soc 128:11364
140. Nieto-Oberhuber C, Paz Muñoz M, López S, Jiménez-Nuñez E, Nevado C, Herrero-Gómez E, Raducan M, Echavarren AM (2006) Chem Eur J 12:1677
141. Zhang L, Kozmin SA (2005) J Am Chem Soc 127:6962
142. Toullec PY, Blarre T, Michelet V (2009) Org Lett 11:2888
143. Buzas A, Istrate F, Le Goff XF, Odabachian Y, Gagosz F (2009) J Organomet Chem 694:515
144. Böhringer S, Gagosz F (2008) Adv Synth Catal 350:2617
145. Cabello N, Rodriguez C, Echavarren AM (2007) Synlett 11:1753
146. Leseurre L, Toullec PY, Genêt J-P, Michelet V (2007) Org Lett 9:4049
147. Witham CA, Mauleón P, Shapiro ND, Sherry BD, Toste FD (2007) J Am Chem Soc 129:5838
148. Schelwies M, Dempwolff AL, Rominger F, Helmchen G (2007) Angew Chem Int Ed 46:5598
149. Schelwies M, Moser R, Dempwolff AL, Rominger F, Helmchen G (2009) Chem Eur J 15:10888
150. Escribano-Cuesta A, López-Carillo V, Janssen D, Echavarren AM (2009) Chem Eur J 15:5646
151. Jiménez-Núñez E, Claverie CK, Nieto-Oberhuber C, Echavarren AM (2006) Angew Chem Int Ed 45:5452
152. Nieto-Oberhuber C, López S, Muñoz MP, Jiménez-Núñez E, Buñuel E, Cárdenas DJ, Echavarren AM (2006) Chem Eur J 12:1694
153. Kim SM, Park JH, Choi SY, Chung YK (2007) Angew Chem Int Ed 46:6172
154. Sim SH, Lee SI, Park JH, Chung YK (2010) Adv Synth Catal 352:317
155. Mainetti E, Mouries V, Fensterbank L, Malacria M, Marco-Contelles J (2002) Angew Chem Int Ed 41:2132
156. Cariou K, Mainetti E, Fensterbank L, Malacria M (2004) Tetrahedron 60:9745
157. Marco-Contelles J, Arroyo N, Anjum S, Mainetti E, Marion N, Cariou K, Lemière G, Mouriès V, Fensterbank L, Malacria M (2006) Eur J Org Chem 4618
158. Moreau X, Hours A, Fensterbank L, Goddard J-P, Malacria M, Thorimbert S (2009) J Organomet Chem 694:561
159. Marco-Contelles J, Soriano E (2006) J Mol Struct: THEOCHEM 761:45

160. Marco-Contelles J, Soriano E (2009) Acc Chem Res 42:1026
161. López S, Herrero-Gómez E, Pérez-Galán P, Nieto-Oberhuber C, Echavarren AM (2006) Angew Chem Int Ed 45:6029
162. Nieto-Oberhuber C, López S, Echavarren AM (2005) J Am Chem Soc 127:6178
163. Nieto-Oberhuber C, Pérez-Galán P, Herrero-Gómez E, Lauterbach T, Rodriguez C, López S, Bour C, Rosellón A, Cárdenas DJ, Echavarren AM (2008) J Am Chem Soc 130:269
164. Yeh M-CP, Tsao W-C, Lee B-J, Lin T-L (2008) Organometallics 27:5326
165. Pradal A, Chen Q, Faudot dit Bel P, Toullec PY, Michelet V (2012) Synlett 23:74
166. Toullec PY, Genin E, Leseurre E, Genêt JP, Michelet V (2006) Angew Chem Int Ed 45:7427
167. Leseurre L, Chao C-M, Seki T, Genin E, Toullec PY, Genet J-P, Michelet V (2009) Tetrahedron 65:1911
168. Amijs CHM, Ferrer C, Echavarren AM (2007) Chem Commun 43:698
169. Nayak S, Ghosh N, Sahoo AK (2014) Org Lett 16:2996
170. Zhou G, Zhang J (2010) Chem Commun 46:6593
171. Zhou G, Liu F, Zhang J (2011) Chem Eur J 17:3101
172. Cera G, Chiarucci M, Mazzanti A, Mancinelli M, Bandini M (2012) Org Lett 14:1350
173. Liu F, Yu Y, Zhang J (2009) Angew Chem Int Ed 48:5505
174. Liu F, Qian D, Li L, Zhao X, Zhang J (2010) Angew Chem Int Ed 49:6669
175. Zhang Y, Zhang J (2012) Chem Commun 48:4710
176. Gawade SA, Bhunia S, Liu R-S (2012) Angew Chem Int Ed 51:7835
177. Handa S, Slaughter LM (2012) Angew Chem Int Ed 51:2912
178. Raubenheimer HG (2012) Angew Chem Int Ed 51:5042
179. Barbazanges M, Fensterbank L (2012) ChemCatChem 4:1065
180. Slaughter LM (2012) ACS Catal 2:1802
181. Wang W, Yang J, Wang F, Shi M (2011) Organometallics 30:3859
182. Muñoz MP, Adrio J, Carretero JC, Echavarren AM (2005) Organometallics 24:1293
183. Chao C-M, Genin E, Toullec PY, Genêt JP, Michelet V (2009) J Organomet Chem 694:538
184. Pradal A, Chao C-M, Vitale MR, Toullec PY, Michelet V (2011) Tetrahedron 67:4371
185. Banerjee D, Buzas AK, Besnard C, Kündig EP (2011) Organometallics 30:6303
186. Matsumoto Y, Selim KB, Nakanishi H, Yamada K-I, Yamamoto Y, Tomioka K (2010) Tetrahedron Lett 51:404
187. Martinez A, Garcia-Garcia P, Fernandez-Rodriguez MA, Rodriguez F, Sanz R (2010) Angew Chem Int Ed 49:4633
188. Sethofer SG, Mayer T, Toste FD (2010) J Am Chem Soc 132:8276
189. Yeom HS, Koo J, Park HS, Wang Y, Liang Y, Yu Z-X, Shin S (2012) J Am Chem Soc 134:208
190. Faustino H, Alonso I, Mascarenas J, Lopez F (2013) Angew Chem Int Ed 52:6526
191. Chao C-M, Vitale MR, Toullec PY, Genêt J-P, Michelet V (2009) Chem Eur J 15:1319
192. González AZ, Benitez D, Tkatchouk E, Goddard WA III, Toste FD (2011) J Am Chem Soc 133:5500
193. Sethofer SG, Staben ST, Hung OY, Toste FD (2008) Org Lett 10:4315
194. Hashmi ASK, Hamzié M, Rominger F, Bats JW (2009) Chem Eur J 15:13318
195. Guo R, Li K-N, Zhu H-J, Fan Y-M, Gong L-Z (2014) Chem Commun 50:5451
196. Jung HH, Floreancig PE (2007) J Org Chem 72:7359
197. Cheong JY, Rhee YH (2011) Beilstein J Org Chem 7:740
198. Skouta R, Li C-J (2007) Tetrahedron Lett 48:8343
199. Sugimoto K, Toyoshima K, Nonaka S, Kotaki K, Ueda H, Tokuyama H (2013) Angew Chem Int Ed 52:7168
200. Liu Y, Xu W, Wang X (2010) Org Lett 12:1448
201. Yan Z, Xiao Y, Zhang L (2012) Angew Chem Int Ed 51:8624
202. Shi H, Fang L, Tan C, Shi L, Zhang W, Li C, Luo T, Yang Z (2011) J Am Chem Soc 133:14944
203. Fehr C, Galindo J (2006) Angew Chem Int Ed 45:2901

204. Fürstner A, Hannen P (2006) Chem Eur J 12:3006
205. Fürstner A, Schlecker A (2008) Chem Eur J 14:9181
206. Baskar B, Bae HJ, An SE, Cheong JY, Rhee YH, Duschek A, Kirsch SF (2008) Org Lett 10:2605
207. Canham SM, France DJ, Overman LE (2010) J Am Chem Soc 132:7876
208. Jiménez-Núñez E, Molawi K, Echavarren AM (2009) Chem Commun 45:7327
209. Zhou Q, Chen X, Ma D (2010) Angew Chem Int Ed 49:3513
210. Molawi K, Delpont N, Echavarren AM (2010) Angew Chem Int Ed 49:3517
211. Hashmi ASK, Ding L, Bats JW, Fischer P, Frey W (2003) Chem Eur J 9:4339

Top Curr Chem (2015) 357: 133–166
DOI: 10.1007/128_2014_593

Published online: 27 Februay 2015

Gold π-Complexes as Model Intermediates in Gold Catalysis

Amanda C. Jones

Abstract Homogeneous gold catalysis has emerged as a powerful method for activating hydrocarbon double and triple bonds. Methodology development and computational studies have blossomed in the past 20 years. In contrast, experimental exploration of mechanisms and structure-reactivity relationships has gained traction only in the past 5 years. Recent developments in the synthesis of organometallic intermediates have revealed exciting new details about the mechanisms of gold catalysis. Central to these studies are the structure and reactivity of gold π-complexes. Following successes in structurally characterizing these key structures, advancements are gradually being made in placing them in the context of an overall catalytic cycle. As a result, a research field has emerged which is rich with potential for continued discovery and catalyst improvement.

Keywords π-System (alkene/alkyne/allene) activation · Gold catalysis · Ligand effects · Mechanism · Reactivity

Contents

A.C. Jones (✉)
Wake Forest University, Salem Hall, Box 7486, Winston-Salem NC 27109, United States

1 Introduction and Early Observations

Homogeneous gold catalysis has emerged as a powerful method for activating hydrocarbon double and triple bonds toward nucleophilic addition and involvement in selective skeletal rearrangements (for some reviews see [1–5]). The utility of gold catalysis is evident in the explosion in the number of new methods over the last two decades [6], and more recently in its increased use in total synthesis [7, 8] and asymmetric processes [9, 10]. Gold catalysts are attractive for their high activity, corresponding mild reaction conditions, and general compatibility for one-pot multi-step processes (tandem chemistry). Gold catalysts also mediate transformations traditionally carried out with toxic mercury salts, offering a greener alternative for use in industrial and academic settings [5]. Because simple protic acids (H^+) have been implicated in a number of supposedly "gold-catalyzed" processes, there are weighty financial implications for determining the specific role of gold [11]. Furthermore, while gold catalysts are efficient at facilitating an astonishing array of complex transformations, catalyst decomposition and relatively high catalyst loadings pose a challenge for industrial-scale development [12]. Although methodology development and computational studies have far out-paced experimental exploration of mechanisms and structure-reactivity relationships, recent developments in the synthesis of cationic π-complexes and organogold compounds have revealed exciting new details about the nature of the catalysts and the structures of reaction intermediates. As a result, a research field has emerged which is rich with potential for continued discovery and catalyst improvement [13–16].

The prototypical first step in a number of gold-catalyzed processes is the coordination of gold to a C–C double or triple bond to generate an activated π-complex. Reports on the isolation and characterization of such complexes have steadily grown in number over the past 5 years and excellent reviews by Widenhoefer [17], Schmidbaur [18], and Dias [19] have already detailed the progress in this area. Although some of the work covered by those reviews is also summarized here, the main focus of the current review is on those studies that have specifically linked π-complexes with distinct reactivity observations. Following the successes in structurally characterizing gold π-complexes, advancements are gradually being made in placing these structures in the context of an overall catalytic cycle. Since the most widely used ligands in the synthetic arena are phosphines and N-heterocyclic carbenes (NHCs), this review is limited to the discussion of reports which utilize those particular scaffolds.

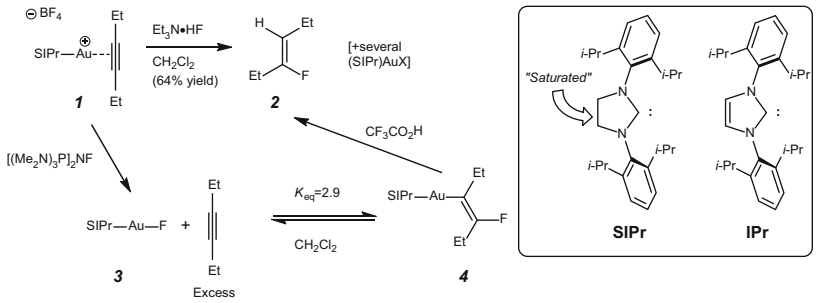

Fig. 1 Sadighi's seminal report of gold(I) alkyne reactivity, 2007

One of the earliest syntheses of a gold(I) π-complex in the context of modern catalytic methods was reported in 2007 by Sadighi and co-workers [20]. Their report is noteworthy both for its isolation of a cationic gold alkyne and its observation of corresponding reactivity (Fig. 1). Attempts to engage alkyne complex **1** in reaction with a soluble fluoride source led predominantly to displacement of the alkyne to generate gold fluoride complex **3**. However, when 3-hexyne was treated with independently synthesized **3**, equilibrium was observed which indicated intermediacy of a gold alkyne complex and subsequent attack by fluoride to generate vinyl gold complex **4**. The equilibrium was measured quantitatively by adding 3-hexyne to solutions of **3** in CD_2Cl_2 at room temperature and lies on the side of the vinyl gold. The *trans* stereochemistry of gold and fluorine in complex **4** suggests this process goes by an outer sphere mechanism (attack on the coordinated alkyne from the side opposite of the metal). Crystals of vinyl gold **4** were obtained and characterized and underwent protodemetalation upon treatment with trifluoroacetic acid to generate alkene **2**. These observations were used to develop conditions for a gold-catalyzed alkyne hydrofluorination and are an excellent early demonstration of mechanistically driven design and corroboration of a full gold catalytic cycle.

In the following year, Bertrand et al. reported an important advance in hydroamination chemistry, namely the direct addition of ammonia to alkynes and allenes utilizing a bulky cyclic (alkyl)(amino)carbene ligand (CAAC) (Fig. 2) [21]. They also independently synthesized the presumed gold alkyne intermediate **6**, and found that its treatment with the NH_3 nucleophile resulted in quantitative displacement to form the gold ammonia complex **7**. The stability imparted by the strongly donating carbene ligand is probably a key factor in the success of these reactions, which require high temperatures (>100°C). Such harsh conditions are presumably required to overcome an unfavorable equilibrium to generate the requisite activated π-complex (further discussion below). What such studies underscore is that, in many gold-catalyzed reactions, the nucleophile involved in the reaction probably coordinates more strongly than the π-system being activated. A number of studies, therefore, have sought to establish a quantitative scale of binding affinity towards gold. Nevertheless, if the kinetic reactivity of the coordinated complex is high enough, reactions take place even if its concentration is low.

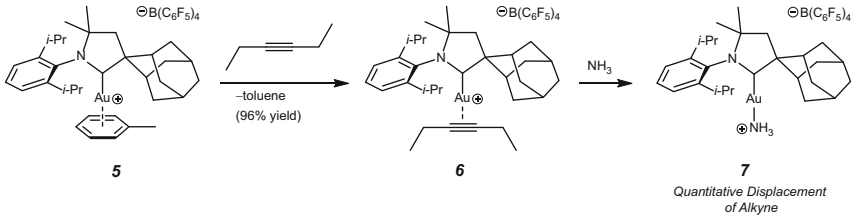

Fig. 2 Bertrand's observations on gold(I)-catalyzed hydroamination, 2008

2 Structure of Gold(I) π-Complexes

Solution evidence for a cationic gold(I) norbornadiene complex with an N-heterocyclic carbene (NHC) ligand and PF_6^- counterion was found by Nolan and co-workers, but over time the complex degraded to a unique digold complex with a bridging PF_4^- ion [22]. Shortly after, Widenhoefer prepared a series of analogous NHC gold(I) alkene complexes [23]. Key to the successful isolation of the latter complexes was the use of the now ubiquitously employed SbF_6^- counterion. This minor procedural modification has led to many successful π-complex syntheses, including: phosphine gold(I) alkenes by Widenhoefer [24, 25] and Russell [26]; phosphine gold(I) dienes by Widenhoefer [27] and Russell [28, 29]; phosphine gold(I) allenes by Widenhoefer [30, 31]; phosphine gold(I) enol ethers by Jones [32]; phosphine gold(I) enamines by Jones [33], Fürstner [34] and Maier [35]; phosphine gold(I) alkynes by Widenhoefer [36] and Russell [37]; and NHC gold(I) alkynes by Fürstner [38]. As research progresses in this area, the focus is beginning to shift from synthetic and structural characterization of π-complexes toward an understanding of their discrete reactivity and appearance in catalytic cycles.

2.1 General Structure Features of Alkenes

Gold(I) forms linear two-coordinate π-complexes with alkenes, alkynes, and allenes. Cationic gold's ability to activate multiple bonds for subsequent nucleophilic attack can be attributed to its electron deficiency, thus rendering π-systems electrophilic upon coordination. In addition to this simple inductive argument, the activation process is also thought to rely on the ability of the metal to "slip" to one end of the multiple bond, generating a positive charge at the other [39]. Accordingly, a higher degree of ground state slippage may correspond to a more electrophilic complex and higher degree of reactivity. Despite a plethora of experimental support for the higher electrophilicity of complexes with electron-poor ligands, there has not been any direct correlation with π-complex structure, mainly because of the challenge of characterizing π-complexes with such ligands (further details below). Comparison of ground-state slippage in a variety of complexes with strong

donor ligands has been determined from solid state data, and it has shown that the substituents on the donor π-system are among the dominant factors contributing to the extent of slippage. Several methods to quantify slippage have been used. The original characterization by Eisenstein and Hoffman determined the relative distance the metal was displaced from the center of the double bond [39]. Widenhoefer, in his recent review, compared the distances between the gold and the two ends of the π-system: the greater the slippage, the greater the difference between these two distances [17]. Alternatively, Jones et al. proposed a slightly modified scale where they defined 100% slippage to correspond to a geometry where the Au–C–C angle is 90° and the gold is situated directly above one end of the double bond (η^1 coordination) and 0% slippage to correspond to where the gold center is equidistant from the two carbons (η^2 coordination) [32]. In the latter method, the distance *d* (Fig. 3) is compared to half the length of the C–C bond, whereas in the Eisenstein/Hoffman method it is compared to the full length, making those numbers span half the scale. An even simpler approach is to look solely at the Au–C–C angle, which would be expected to max out at around the 109° angle of an sp^3 hybridized carbon. Because this angle is dependent on both the slippage and the alkene–gold distance, and because of the large errors associated with angles in crystal structures, this method must be used with care. We use it here to highlight the qualitative spectrum of slippage.

This continuum has been examined in great detail for coordinating double bonds, mainly because of the great variety of possible substituents (Fig. 4). The angle increases steadily on going from monosubstituted to disubstituted to oxygen- to nitrogen-substituted alkenes. In an electron-rich enediamine complex reported by Fürstner (**16a,** L=PPh_3), the distortion is so great it may no longer be appropriately called a π-complex [34]. The even wider angle observed in the (t-Bu)$_2$(o-biphenyl)P analogue (**16c**) does not appear to be an inherent ligand effect, but rather an artificial one imposed by ligand interaction with the aromatic imidazolium ring [33]. Otherwise, incorporation of the *o*-biphenyl substituent in phosphines appears to do little to alter the structure of a coordinated alkene; the distortion and bond lengths in coordinated methoxypropene are nearly identical whether (tBu)$_3$P or (tBu)$_2$(o-biphenyl)P is used (**14b** and **14c**). In contrast, the rates of intermolecular alkene exchange are significantly altered. Exchange is more facile when (tBu)$_3$P is used, and thus it is proposed that the biphenyl ring represents a steric hindrance,

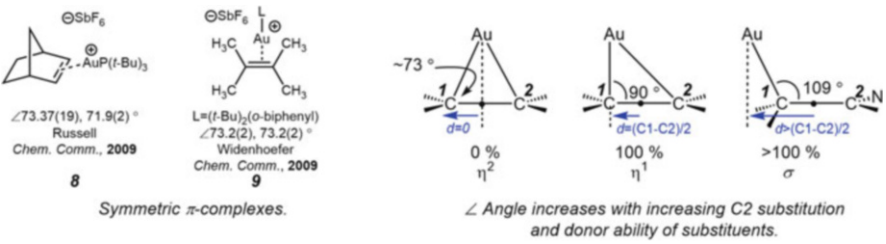

Fig. 3 Continuum of slippage; from symmetric η^2-π-complex to σ-complex

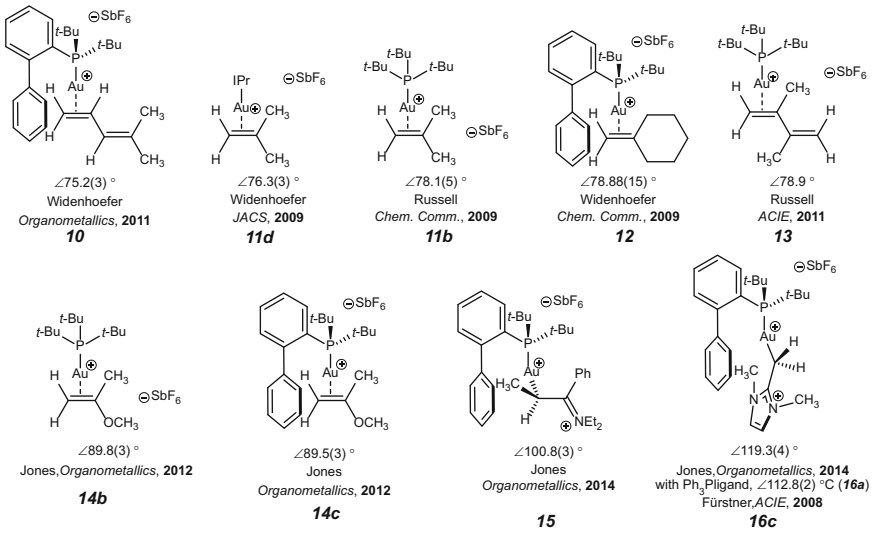

Fig. 4 Representative gold(I) alkene π-complexes and distortion in coordination mode as indicated by Au–C–C angles. (Drawings not meant to be fully accurate representations of geometry)

rather than an electronic one [32]. The distortion in a gold(I) coordinated alkene featuring the *I*Pr ligand is statistically equivalent to that seen in one employing a phosphine ligand (see **11d** vs **11b**) [23]. The ligand exchange is more facile in **11b** compared to **11d**, and in combination with equilibrium binding constants, the data points to the greater electrophilicity of the cationic gold phosphine fragment and the stronger donating character of the *I*PrAu$^+$ fragment. This effect is not, however, reflected in the solid state structure [17].

In going from enol ether to enamine complexes, a significant change was seen in the solution behavior of the complexes. After wide success in preparing hydrocarbon alkene, alkyne, and allene complexes, structural characterization of gold (I) enamines was limited prior to 2014. Bertrand et al. observed a highly substituted gold-coordinated enamine from a stoichiometric intramolecular alkyne amination reaction (NMR characterization only) [40], and Che detected a gold(I) enamine intermediate by mass spectrometry [41]. Besides Fürstner's atypical triphenyl phosphine gold enediamine (**16a**, atypical in that it does not represent a common amination intermediate) [34], the structures had not been fully characterized. The first structural details were reported by Zhdanko and Maier [35] and then elaborated on by Jones et al. [33]. In addition to exhibiting highly distorted or "slipped" coordination modes (Au–C–C angles $> 90^{\circ}$, Figs. 4 and 5), rapid rotation on the NMR timescale of the formal enamine C=C double bond was observed. For enamines **17** and **18**, the formerly distinct vinyl Hs become a single peak upon coordination to gold (Fig. 5a, a doublet from coupling to phosphorus). Solid state structures, however, show these protons to be in different environments. In low-temperature ^{1}H NMR spectra of **19**, they resolve to the ABX pattern expected

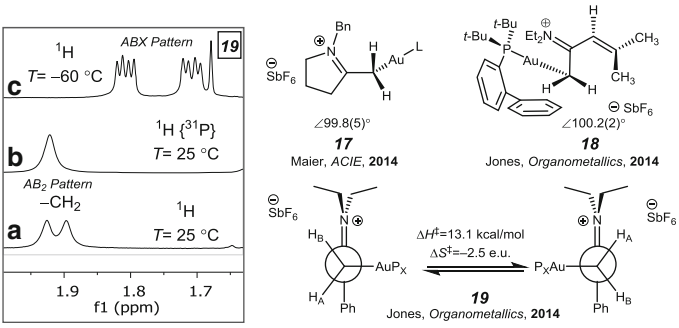

Fig. 5 Structurally characterized gold(I) enamines and dynamic behavior.[1]H NMR spectra (**a**) of **19** ($P_x = (t\text{Bu})_2(o\text{-biphenyl})P$ inCD_2Cl_2, 300 MHz) and (**b**) with ^{31}P decoupling and (**c**) at −60°C (500 MHz). NMR spectra reprinted with permission from [33]. Copyright 2014 American Chemical Society

for two diastereotopic protons. Variable temperature ^{1}H NMR spectra were simulated by Jones et al. and activation parameters were measured for the bond rotation process; the barrier is comparable to that measured for the electronically restricted C–C bond rotation in tetrabromobutane [42]. Thus, distortion in these complexes is so great as to diminish significantly the double bond character in the parent enamine.

This observation raises the possibility of *E*/*Z* isomerization in enamines, an issue important to mechanistic discussions about gold-catalyzed alkyne aminations. Most important to the discussion is the nature of the coordinated propiophenone enamine **15**, which showed a similar level of distortion as the less substituted **17** and **18**. See Sect. 3.2 below for further discussion.

2.2 *Digold Coordination Modes*

Since the 1980s it has been understood that dispersion forces enhanced by strong relativistic effects on the outer electrons of gold ions lead to a gold–gold attraction known as "aurophilicity." Such gold–gold interactions are estimated to have binding energies in the range of 5–15 kcal/mol ([43] and references therein), and provide the driving force for aggregation of gold cations with pre-catalysts and catalytic organogold intermediates to generate digold coordination complexes.

It has long been known that gold acetylides can be synthesized using terminal acetylenes and strong bases [44]. In 2007, during their studies on the reactivity of CAAC gold catalysts, Bertrand and co-workers found that enamines were basic enough to mediate the transformation from π-complex to acetylide (e.g., **20** → **21**, Fig. 6) [45]. When excess cationic gold is around, further coordination of the triple bond can be observed as seen in complex **23b** isolated by Russell and co-workers [37]. In 2011, Widenhoefer and co-workers and Garcia and Corma et al. both

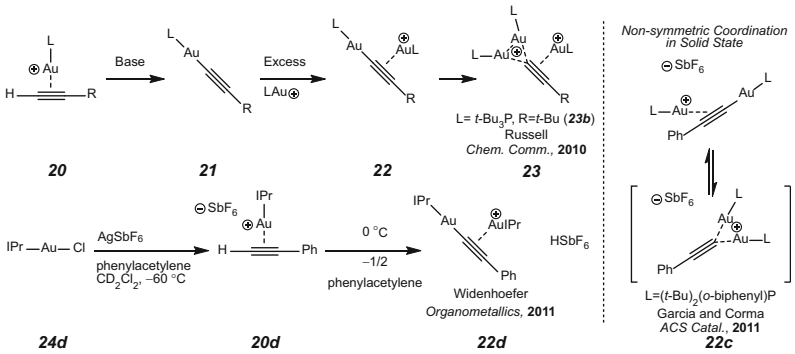

Fig. 6 Conversion of gold(I) π-complexes to acetylide and σ,π-acetylide complexes

showed that, in the presence of cationic gold, conversion from gold acetylide to diaurated complex (**20** → **22**) is in fact spontaneous to generate an equivalent of acid [46, 47]. These complexes are, thus, remarkably resistant to protodemetalation. Solid state structures reveal non-identical ligands, while NMR spectroscopic data reveal a fast exchange of ligand signals, presumably a result of chemical equilibration through a symmetric structure. The asymmetry in the solid state led these to be called σ,π-acetylides to reflect the different ways the gold units are coordinated.

In 2009, Gagné and co-workers made the unexpected discovery that the resting state for a gold(I)-catalyzed allene hydroarylation was a geminally diaurated vinyl gold intermediate (**28a**), a structure that can be formally considered a vinyl gold π-complex (Fig. 7) [48]. Fürstner et al. synthesized model complexes (**26a**, **27a**) by transmetalation of vinyl boronate precursors[49] and then Maier et al. prepared a series of digold complexes from the intramolecular cyclization of alkynyl alcohols (e.g., **25c**) [50]. Solution spectroscopic data supported symmetric structures (plane of π-system cutting orthogonally through the digold-ligand plane), and this was confirmed by X-ray crystallography in **26a** and **27a**. In contrast, when switching to the more sterically demanding $(o\text{-tol})_3$P ligand, a different coordination mode was observed by Weber and Gagné [51]. The geometries in complex **28e** are such that the vinyl gold is essentially unperturbed and it is truly a vinyl gold π-complex. The Au–C–C angle is narrower than expected for a terminally disubstituted alkene (Au–C–C = 78–79° in isobutylene and exomethylene cyclohexane complexes, see Fig. 4), and although this may be a ligand effect (no other π-complexes with the $(o\text{-Tol})_3$P ligand have been characterized in the solid state), it is probably a result of aurophilic attraction between the two metal centers. Following the discovery of *gem*-digold complexes in the context of catalytic reactions, a number of reports on their synthesis and structural characterization have been published [52, 53].

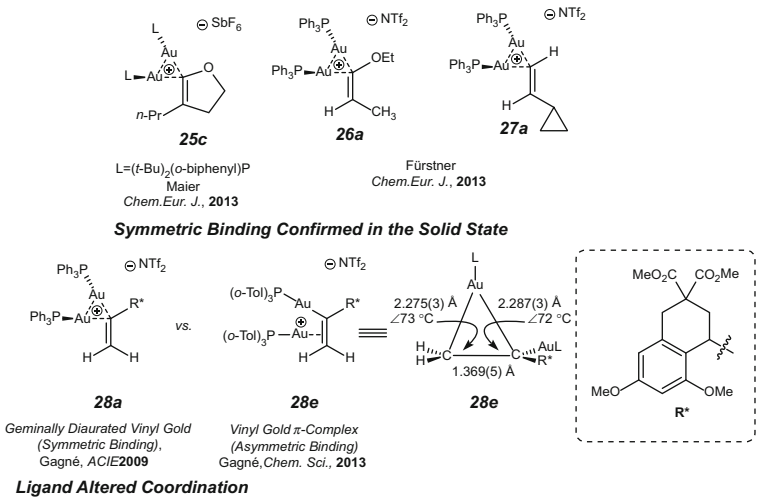

Fig. 7 *gem*-Digold coordination in vinyl systems

2.3 Importance of Ligand and Complex Decomposition

Except for an early report by Toste [54] and for Fürstner's enediamine **16a** [34], no π-complexes examined in the solid state contained aryl phosphine ligands, and in particular, strong donor ligands (e.g., *tert*-butyl phosphines and NHCs) have generally facilitated π-complex isolation. A detailed solution study by Widenhoefer et al. clarified the challenges associated with trying to isolate complexes without the strongly stabilizing donor ligands [55]. Although a series of complexes could be prepared and characterized by NMR spectroscopy in CD_2Cl_2 at −78°C, warming the solutions to ≥ −20°C resulted in rapid decomposition to the bis(phosphine) complex **30** (Fig. 8). The latter complex is well understood to be catalytically inactive and its formation under catalytic conditions may obfuscate mechanism studies and be the root cause of inefficient reactions [56].

Complexes with *p*-methylstyrene, cyclohexadiene, 3-hexyne, and the allenes 3-methyl-1,2-butadiene and 1,7-diphenyl-3,4-heptadiene were prepared. The syntheses were found to be sensitive to reaction stoichiometry, and this was explored in detail for the preparation of **29**. If a deficiency of alkene was used, the complex was generated alongside an unknown gold species with which, however, no ligand or alkene exchange processes were detected. If, however, a deficiency of silver was used, the predominant species was the bridging chloride complex, **31** (Fig. 9). The alkene 2-methyl-2-butene does not coordinate strongly enough to displace a significant amount of Ph_3PAuCl. Although triphenylphosphine gold π-complexes have been purportedly observed during mechanism and solution studies, it is quite possible that this byproduct was present instead.

Digold complexes with bridging halides are well known [57–59] and in 2006 Hashmi and co-workers showed that they are catalytically active [60]. In 2013,

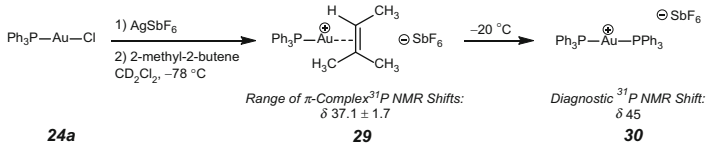

Fig. 8 Destructive decomposition product observed during Ph_3P gold(I) π-complex syntheses

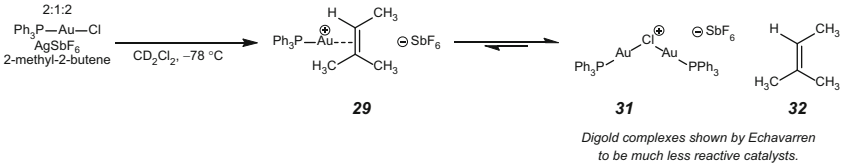

Fig. 9 Competitive coordination of L–Au–Cl

Echaverren et al. performed simple reactivity studies to show that $[(LAu)_2Cl]SbF_6$ (when L=(*t*Bu)$_2$(*o*-biphenyl)P) is significantly less reactive than the commonly used acetonitrile catalyst, $[LAu(NCMe)]SbF_6$ [61]. The bridged dimers were generated when halide abstraction with silver was done in the absence of substrate, even when the Au/Ag ratio was 1:1. If the substrate is capable of cleaving the dimer, the reactivity is not impacted. If the substrate is incapable, then significantly inhibited reaction rates are anticipated. This led to the practical recommendation by the authors that, when using the LAuCl/AgX combination, the silver salt should be added last, after substrate/LAuCl premixing, to minimize the formation of the chloride-bridged gold complexes. The use of silver to generate cationic complexes is common in catalysis, and the sensitivity to mixing procedure (to which chemists do not always pay close attention) could explain some of the unexpected "silver effects" observed in the literature [62]. Others have shown that gold halides can be a trap for silver, as mixed gold–silver halides have also been isolated [63, 64].

The $^{-}NTf_2$ and ^{-}OTf counteranions coordinate more strongly than 2-methyl-2-butene by factors of 4 and 6, respectively. Even at −90°C, distinct signals for coordinated alkene and free alkene were not observed in the ^1H or ^{13}C NMR spectra, indicating very rapid exchange between the complexes. The rate of intermolecular alkyne exchange was measured for $[Ph_3PAu(3\text{-hexyne})]SbF_6$; as has been typically observed with gold(I) complexes, the data is consistent with an associative exchange mechanism [17]. The activation barrier to intermolecular exchange of 3-hexyne is ≥6 kcal/mol lower than the corresponding barriers in (*t*Bu)$_2$(*o*-biphenyl)P complexes. This is presumed to reflect both the less hindered steric environment and a weaker bond to gold.

Hammond, Xu et al. [65] performed XPS and NMR spectroscopic studies to understand better the decomposition pathway to $(Ph_3P)_2Au^+$ (**30**). They found that the coordination of π-donors accelerates the process. Solutions of $Ph_3PAuOTf$ are relatively stable in solution (no appearance of bis(phosphine)gold after 10 h), while addition of cyclohexene appears to trigger the decomposition and the rate of

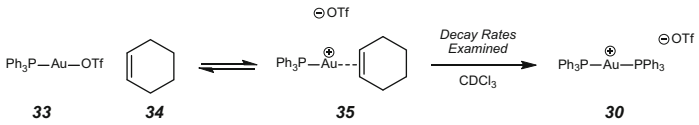

Fig. 10 Alkene induced decay of cationic gold to the inactive bisphosphine cation

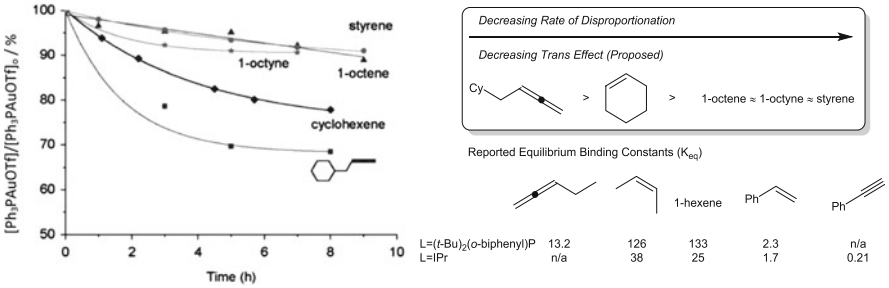

Fig. 11 Decay of $(Ph_3P)AuOTf$ in the presence of alkene/alkyne/allene and known corresponding structural data. Data plot reproduced with permission from [65]. Copyright 2014 Wiley. Equilibrium constants measured relative to $NCAr_F$ (3,5-trifluoromethylbenzonitrile) [23, 24, 31, 46]

decomposition increases with increasing concentration of cyclohexene (Fig. 10). Further studies support a disproportion mechanism. A number of additives were also screened in the presence of cyclohexene to determine the impact on the decomposition process; water alone does not facilitate decomposition, but in the presence of cyclohexene the alkene-initiated decomposition is much faster. The presence of coordinating counteranions significantly slowed the decomposition ($^{-}NTf_2$ was more effective than ^{-}OTf), while decomposition was more facile when the "non-coordinating" SbF_6^{-} counteranion was used. Heterocycles and heteroatom donors such as benzotriazole and HMPA impeded the decomposition, as well as acetonitrile, when used as solvent.

Rates of decay were also sensitive to the identity of the π-system donor (Fig. 11). The authors propose displacement of the phosphine ligand by a *trans* effect; strong *trans* donation of the alkyne/allene/alkene is proposed to displace temporarily the stabilizing phosphine ligand from gold and the resultant gold undergoes disproportionation more readily. Ligand-free AuCl/AgOTf solutions displayed rapid decomposition and confirmed the importance of the ligand in stabilizing gold. This control experiment supported the conclusion that ligand loss is a key step in the decomposition process.

In the absence of full structural details on Ph_3P gold complexes, there does not appear to be enough structural/mechanistic data to corroborate this hypothesis specifically. One might propose that trends in *trans* influence would correlate with trends in equilibrium binding constants, but the experimental results, based on K_{eq} values with other ligands, do not support this. Further studies in this important area are required to understand these trends.

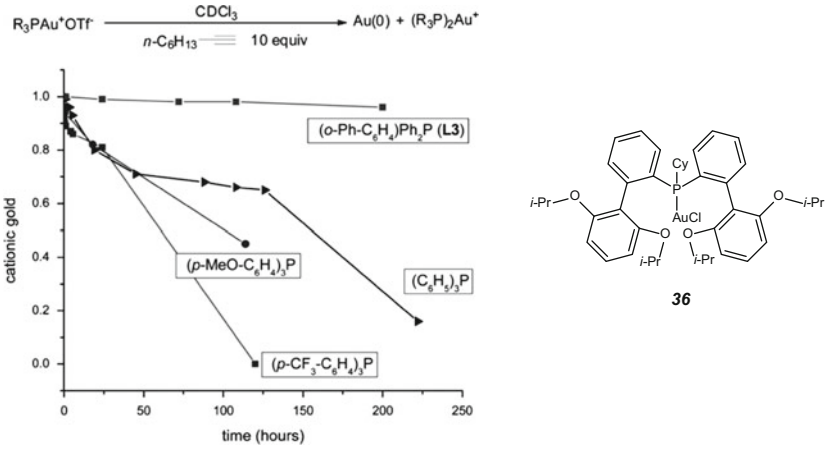

Fig. 12 Ligand steric and electronic effects on the decay of cationic gold ($R_3PAuOTf$). Kinetic plots reprinted with permission from [66]. Copyright 2012 American Chemical Society

Based on their observation that coordination of unsaturated compounds (alkyne/allene/alkene) is the key factor in catalyst decomposition, the authors predict that mechanisms with gold π-complex resting states display faster decomposition rates and thus lower turnover numbers, whereas mechanisms without these resting states display higher turnover numbers. An important steric component has been observed as well; addition of a biphenyl substituent on the phosphine also leads to slower decomposition [66]. This has led to the development by Hammond and co-workers of a highly active bis(biphenyl)phosphine gold pre-catalyst (**36**) (Fig. 12) [67].

These studies all point to the importance of solvent, counterion, and ligand in the design of improved catalysts. For example, Shi et al. developed $(Ph_3P)Au(triazole)^+$-based catalysts which show highly enhanced thermal stability [68, 69]. Thus, improvements need not solely be made based on changes to the ligand.

2.4 Relative Coordination Strength

Maier et al. performed a detailed solution study to determine explicitly the affinity of a series of compounds toward cationic gold [70]. In combination with other experimental studies, a wide scale has been established (Fig. 13). These trends are important to mechanistic discussions which include postulates about counteranion effects and competition between nucleophile and reaction substrates. One noteworthy observation is the high affinity of acetonitrile compared to simple hydrocarbon π-substrates. The commonly used triflate counterion also competes for coordination with hydrocarbon alkenes and alkynes. Electron-rich substrates (enol ethers, amines, enamines) create strong complexes. The methanol nucleophile is at the low end of the scale, while amine nucleophiles are at the high end. For aminations,

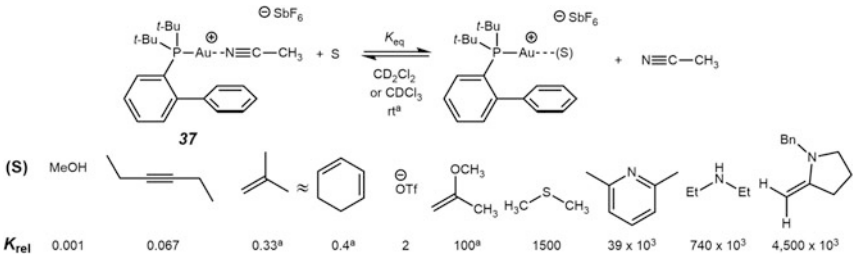

Fig. 13 Binding constants relative to acetonitrile. [a]Measured at –65°C [24, 32, 35, 70]

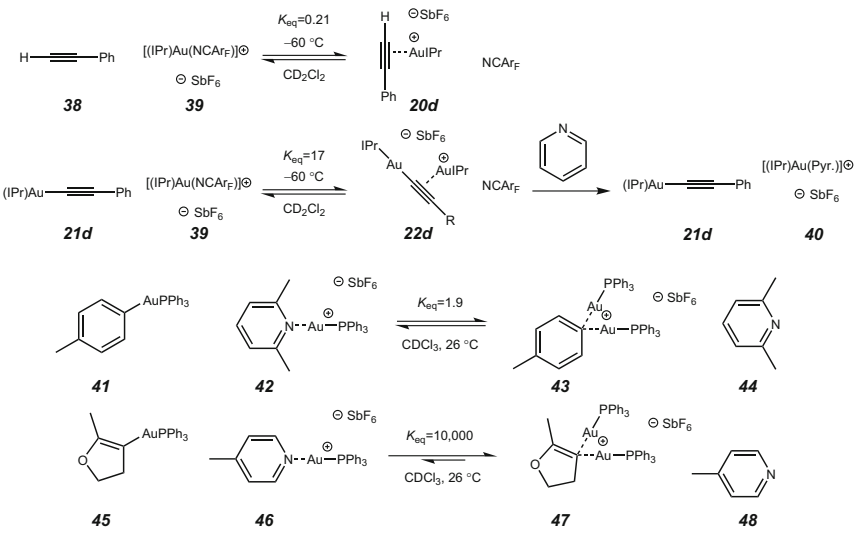

Fig. 14 Select binding affinities of vinyl gold and gold acetylides

inhibition by reaction nucleophile is a significant factor, whereas in hydrations it may not be.

Expanding this further, a series of experiments have determined the affinity of vinyl gold and acetylide gold species to cationic gold and they consistently show stronger affinities than their proton counterparts (Fig. 14). In the case of vinyl or aryl systems, they can be placed at the far end of the affinity scale shown in Fig. 13 [46, 71]. Gagné studied *gem*-digold formation in solution for a series of triphenyl phosphine gold(I) aryl compounds and determined the following trends: (1) electron-rich aryl compounds show a higher propensity for forming *gem*-digold species; (2) digold formation is more favored with less coordinating counterions ($^-NTf_2$ less coordinating than $^-OTs < {}^-OCOCF_3$); and (3) *gem*-digold formation inhibits rates of protodemetalation [72]. The higher propensity to form *gem*-digold structures with the enol ether-derived vinyl golds or electron-rich aryls is not surprising and

parallels the higher coordination strength of electron-rich moieties to cationic gold shown in Fig. 13. Mechanistic studies have generally shown that the *gem*-diaurated species do not react directly (see below), so these are expected to be catalyst reservoirs in many reactions.

In their work characterizing *gem*-digold intermediates from alkynol cyclization reactions (e.g., **47**), Maier and Zhdanko showed that electron-poor phosphines lead to less stable *gem*-digold complexes than electron-rich phosphines, although this trend can be reversed if sterically bulky ligands are used [71]. Thus $(t\text{Bu})_2(o\text{-biphenyl})\text{P}$ has a lower propensity for *gem*-digold formation than Ph_3P. Diaurated species derived from the latter ligand are thermodynamically more stable than those with the $(t\text{Bu})_2(o\text{-biphenyl})\text{P}$ ligand; however they are also more labile as evidenced by the presence of a single set of signals in the ^{1}H NMR spectra for mixtures containing both vinyl($AuPPh_3$) and vinyl$(AuPPh_3)_2^+$. Complexes with the $(t\text{Bu})_2(o\text{-biphenyl})\text{P}$ ligand are less stable (form to a lesser extent), *and* less labile; they display distinct NMR signals for the *gem*-digold and uncoordinated gold. Tuning the ligand to minimize the formation of *gem*-digold species may be key to optimizing alkyne activation reactions.

2.5 Ion-Pairing in Cationic Gold(I) π-Complexes

Zuccaccia, Belpassi, Macchioni, and Tarantelli have extensively used NOE and pulsed field gradient spin-echo NMR spectroscopic techniques to determine the nature of ion pairing in cationic gold(I) π-complexes. They have combined this work with computational studies of the potential energy surfaces and Coulomb potential of the ions, which helps identify the locus of positive charge and thus explains the location of counterions. Their recent review has highlighted the ability to use ligand structure to tune the distribution of cationic charge in gold(I) π-complexes [73]. Following a survey of triarylphosphine and NHC gold alkene and alkyne complexes, they were able to draw some general conclusions about ligand effects on the ion-pair interactions. Three main orientations were identified from the data (Fig. 15).

When L is a poorly donating ligand such as triphenylphosphine, the counterion approaches mainly opposite gold, on the side of the alkene/alkyne as in **C**. This reflects the great electron-withdrawing power of the ligand and leads to an enhanced π-acidity that localizes positive charge on the coordinated π-system. In

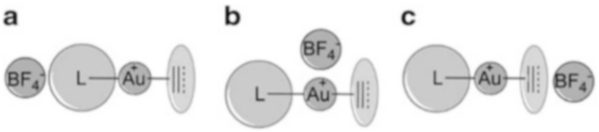

Fig. 15 Important ion-pair orientations in cationic gold π-complexes. Figure reproduced with permission from [73]. Copyright 2013 Wiley

contrast, use of the strongly donating *I*Pr ligand results in ion-pair structures with less specific interactions, and the counteranion shows a propensity to orient itself near the backbone of the ligand, as in **A**. This relative "blocking" of the π-substrate in **C** appears to be consistent with the higher sensitivity of gold(I) chemistry to counterion effects when phosphines are used. Their further work in this area has shown that the interactions can be finely tuned, depending upon the electronic and steric properties of the ligands [74, 75].

3 Reactivity and Formation of Gold(I) π-Complexes

Following these successes in characterizing important π-complex intermediate structures, research has been directed toward understanding their role in catalytic cycles. One point of discussion is the inherent reactivity and electrophilicity of a gold-coordinated π-system. Although an increasing number of kinetic studies have shed important light on the various mechanistic steps of gold-catalyzed reactions, this simple process has rarely been measured independent of such other steps. A second important point of discussion is the turnover of the organogold intermediates formed following π-complex reactivity either by protodeauration or other processes.

3.1 Kinetics of Nucleophilic Attack on π-Systems

After Sadighi's seminal studies confirming *both* π-complex generation *and* π-complex reactivity (see Fig. 1), another early "proof" of gold involvement in π-activation chemistry was Hammond's isolation of a vinyl gold generated by intramolecular allene cyclization (Fig. 16) [76]. Since then, vinyl gold intermediate observation has proven to be rather straightforward, and a number of other cases have been reported which provide experimental confirmation of the π-activation step in reactions with alkynes and allenes [77–79]. Although vinyl gold **50** is unusually stable, control experiments with isolated vinyl gold intermediates have in general supported the feasibility of the protodemetalation pathway, confirming true gold catalysis in alkyne and allene activations. All complexes isolated support the *anti* mode of nucleophilic attack (for further discussion, see below).

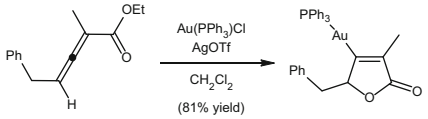

49 **50**

Fig. 16 Another early "proof" of gold-mediated π-activation

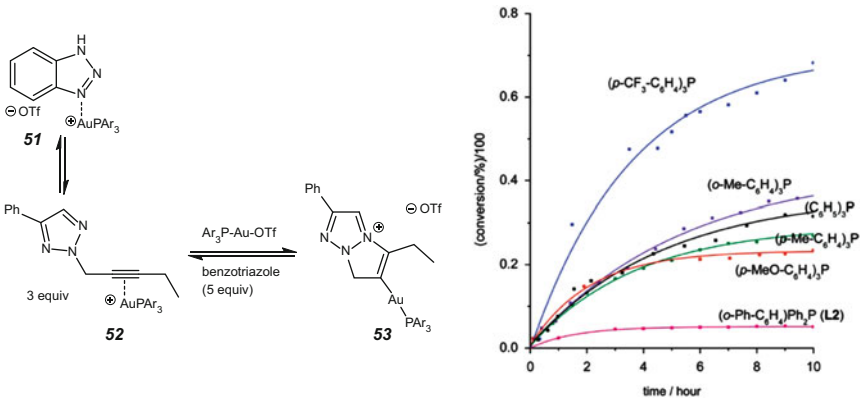

Fig. 17 Direct measure of ligand effect on alkyne activation. Kinetic plots reprinted with permission from [66]. Copyright 2012 American Chemical Society

In 2012, Xu and co-workers performed a broad kinetic study of the elementary processes associated with activation of alkynes and this included a survey of ligand effects on protodemetalation and nucleophilic attack [66]. In one series of experiments they examined the cyclization of triazole **52** to generate the inherently stable vinyl gold **53** (Fig. 17) [80]. This is a way to isolate the specific mechanistic step of nucleophilic attack on the alkyne and separate it from the protodemetalation step. It was observed that intramolecular attack on a variety of alkynes is too fast to measure and so the reaction rates were tempered by addition of excess benzotriazole. Thus the equilibrium between coordinated triazole and alkyne must also be considered when interpreting the kinetic results and this makes explaining the observed trends more difficult. Finally, the reaction is reversible and so the reaction rates are also influenced by the thermodynamic stabilities of the vinyl gold products. The electron-poor $(p\text{-}CF_3C_6H_4)_3P$ gives the best conversion and fastest initial rate. In an allenyl ester rearrangement also examined (where substrate-catalyst inhibition is negligible and π-activation is more clearly rate-determining), there was a clear trend toward increasing rates with increasing electron-withdrawing character in the ligand.

Analogous experimental confirmation for gold(I) activation of alkenes was provided by Toste et al. in 2010, and it remains the only such example [81]. In this study, treatment of alkenes containing pendant nitrogen nucleophiles (e.g., urea such as **54**, or carbamate, amide, amine) with the trigold oxo species $[(Ph_3PAu)_3O]BF_4$ in the presence of external base (Et_3N) yielded alkyl gold complexes such as **55** (Fig. 18). Similar to the alkyne cyclization above, the rate was enhanced by arylphosphine ligands with electron-withdrawing substituents. A significant result of this work is that treatment of the alkyl gold with acid leads not to protodemetalation, but instead to reversion to the starting alkene. Although this work confirms the gold cation's alkene π-activating capabilities, it calls into question the ability of these alkyl gold intermediates to turnover under catalytic conditions. Use of deuterium-labeled alkene and examination of the $^3J_{HH}$ coupling constants supported *anti*-addition of the nucleophile.

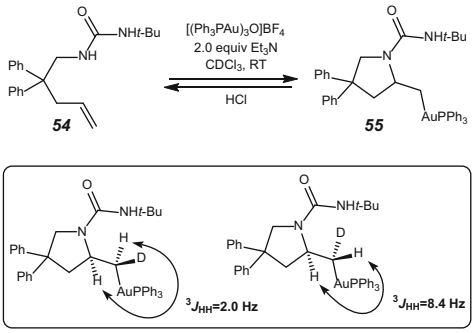

Fig. 18 Isolation of an alkyl gold complex confirms gold's alkene π-activating capability

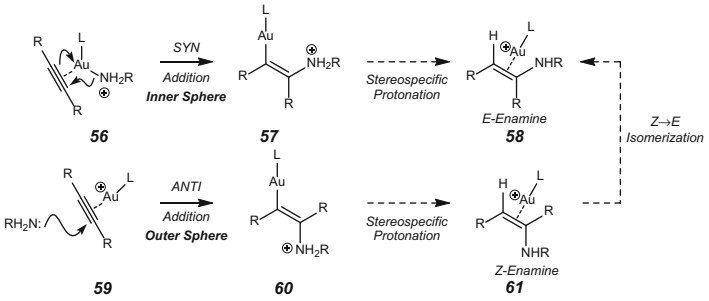

Fig. 19 Representative mechanisms for π-activation and implications for alkyne amination stereochemistry

3.2 Role in Amination Mechanism Studies

Some of the earliest reports on gold-catalyzed alkyne activation proposed inner sphere or *syn* insertion mechanisms, although by 2014 most experimental data, including the vinyl and alkyl gold complexes described above, supported outer sphere or *anti*-addition mechanisms. In the stereoselective hydroamination of internal alkynes reported by Stradiotto and co-workers, selective observation of *E*-enamine products could be rationalized by a *syn* addition, followed by stereospecific protonation. Because protonation was shown to be stereospecific in the case of a simple triphenylphosphine vinyl gold [82], this reaction was considered for some time to be a possible substrate-specific exception to the *anti*-mechanism. However, *E–Z* isomerization could also explain the observed results (Fig. 19).

Bertrand and co-workers examined alkynamine **62**, specifically proposing that the relative geometry of alkyne and amine would be ideal for observing a tricoordinated intermediate such as **56**. Instead, enamine complex **63** was isolated (one of the first) (Fig. 20) [40]. In an effort to shut down the cyclization and favor isolation of the pre-coordinated intermediate, tertiary amine **64** was prepared and the ammonium vinyl gold **65** was unexpectedly isolated. For **62,** syn insertion is

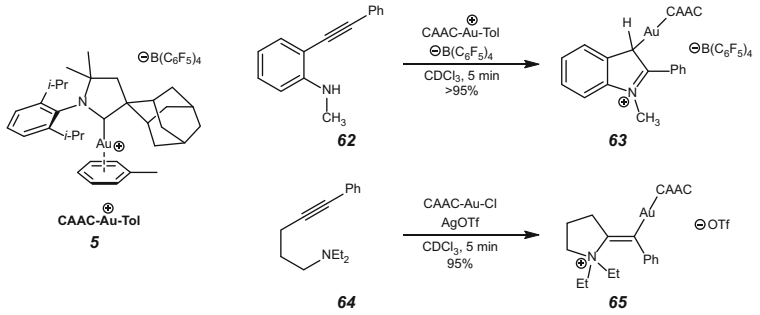

Fig. 20 Confirmation by Bertrand of the outer sphere/*anti*-addition mechanism in intramolecular alkyne aminations

geometrically improbable, but for **64** it is possible, and the *trans* relationship between Au and N clearly implicates the *anti* mode of attack. Around the same time, Hashmi isolated a vinyl gold analogous to the non-protonated precursor to **63** [78]. In light of the known strength of amine coordination compared to alkyne coordination (see Fig. 13), the isolation of **65** in particular directly implicates the feasibility of generating reactive concentrations of coordinated alkyne followed by *anti*-attack of the amine.

Technically this does not rule out the possibility of an inner sphere mechanism in the case of *intermolecular* additions, although such a significant mechanism change seems improbable. The structural observations by Maier [35] and Jones [33] showed definitively in the case of geminally disubstituted enamines (see Fig. 5) that coordination to gold results in significant loss of double bond character in the enamine leading to facile bond rotation. *E*/*Z* isomerization would be mediated by just such a process, although the aforementioned results do not definitively confirm a corresponding rotational ease when additional substitution is introduced.

Evidence in support of facile isomerization is as follows (Fig. 21). When the disubstituted propiophenone enamine **66** (a mixture of *E* and *Z* isomers) is treated with gold, only a single stereochemically defined isomer is generated (stereochemistry defined in the solid state). Close examination of *E*/*Z* ratios indicated that *both* isomers reacted with gold to form the coordinated complex **15** and that both isomers could be regenerated upon displacement from gold. Because the *E* isomer already predominates, these experiments required measuring fairly small differences in *E*/*Z* ratio, although variations in that ratio appeared to support some kinetic preference for reaction *and* regeneration of the *E* isomer. The isomerization process is dependent on both the activation barrier to generate the less stable complex (which is probably quite high) and the rates of displacement from gold (which in some cases was observed to be quite slow). Further work is required to quantify the energetics of these steps.

Interestingly, the coordination strength of enamines shows a much higher sensitivity to substitution than other alkenes [33]. This feature drives the isomerization of initially formed enamines in alkynamine cyclization reactions [33, 35]. Zhdanko

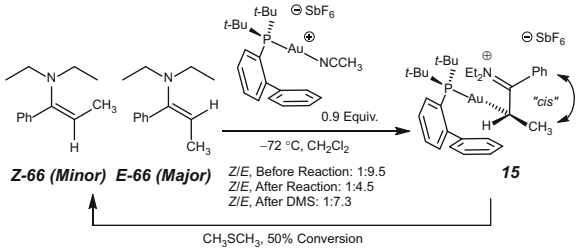

Fig. 21 Evidence in support of *E*/*Z* isomerization. Figure reproduced with permission from [33]. Copyright 2014 American Chemical Society

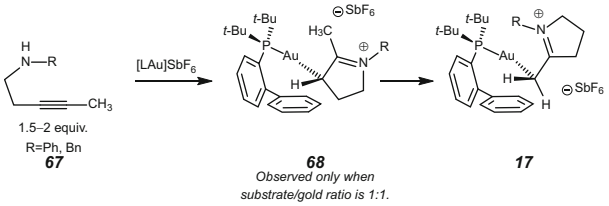

Fig. 22 Enamine isomerization in alkynamine cyclization. When R=Ph, conditions are LAuCl/$NaSbF_6$ in THF. When R=Bn, conditions are [LAu(acetonitrile)]SbF_6 in $CDCl_3$. L=(tBu)$_2$(o-biphenyl)P [33, 35]

and Maier showed that this isomerization (**68** → **17**) is dependent upon ligand exchange processes (Fig. 22). That is, if the alkyne/gold ratio is 1:1 the initially formed isomer can be observed. Only when the enamine is displaced by some other coordinating moiety does the isomerization happen. The data supported a simple acid-catalyzed mechanism for the isomerization.

3.3 Geminally Diaurated Acetylides

Geminally diaurated acetylides are increasingly being considered to play a role in influencing reaction kinetics and progress. A full picture of their proposed involvement in catalytic cycles is not drawn here because it has been covered elsewhere [14, 83, 84]. Briefly stated, extensive experimental and computational evidence has supported a new mode of "dual activation." Although direct nucleophilic attack on the σ,π-acetylide was originally proposed, this has not been supported by continuing studies (Fig. 23).

It has been shown repeatedly that reaction selectivities can be controlled by steering the reaction to proceed through pre-formed *gem*-digold acetylides. In Corma and Garcia's original report, [2+2] alkene/alkyne cycloaddition proceeded cleanly and selectively when pre-formed *gem*-digold acetylides were used as catalysts, while poor selectivities were shown to be a result of the acid generated

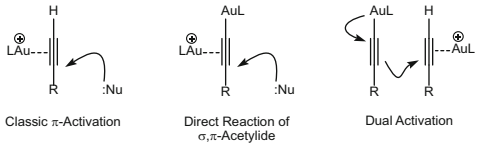

Fig. 23 Possible reaction modes for gold-coordinated terminal acetylenes

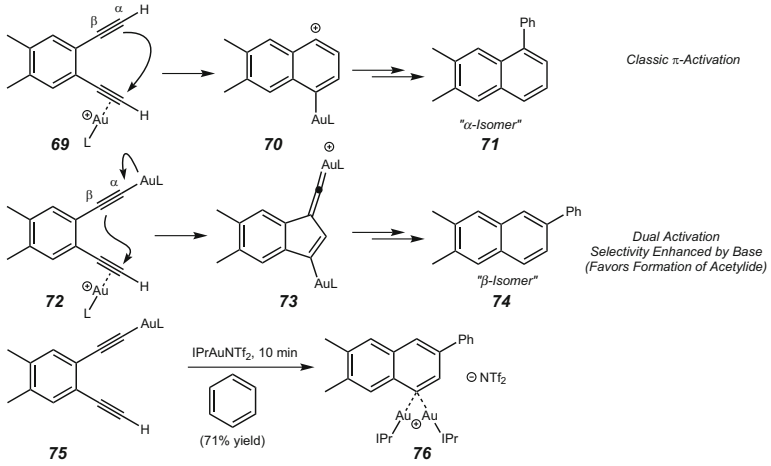

Fig. 24 Selectivity control in gold-catalyzed naphthalene synthesis

by initial *gem*-digold formation (see above, Fig. 6) [47]. Additionally, in a diyne cyclization reported by Hashmi and co-workers, a mixture of isomers was initially formed and mechanistic studies supported two different pathways involving the two modes of activation ("classic" vs "dual") (Fig. 24) [85]. When acetylide **75** was pre-formed and treated with a second equivalent of cationic gold, clean conversion to a single isomer was observed, *gem*-digold **76**. This experiment suggests that the β-isomer **74** arises specifically from a pathway involving a gold acetylide. The nature of that pathway, particularly the intermediacy of gold vinylidenes such as **73**, is mainly corroborated by trapping experiments. In other work by Hashmi and co-workers, a model heteroatom stabilized allenylidene has been prepared, but such structures have otherwise not been structurally verified [86].

Interestingly, *anti*-Markovnikov attack on a gold-coordinated acetylide is implied by the mechanistic models for both pathways in Hashmi's naphthalene synthesis. In contrast, the pre-generation of a *gem*-digold acetylide was correlated with a selectivity switch between Markovnikov and *anti*-Markovnikov addition in a gold-catalyzed alkyne amination. In work by Medio-Simón and co-workers, ethynylphenyl urea **78** was treated with various gold(I) catalysts (Fig. 25) [87]. Either dihydroquinazolinone **77** was generated as the major product by the "classic" or expected Markovnikov addition or else indole **79** by an *anti*-Markovnikov pathway. While use of the *I*Pr ligand gave predominantly the

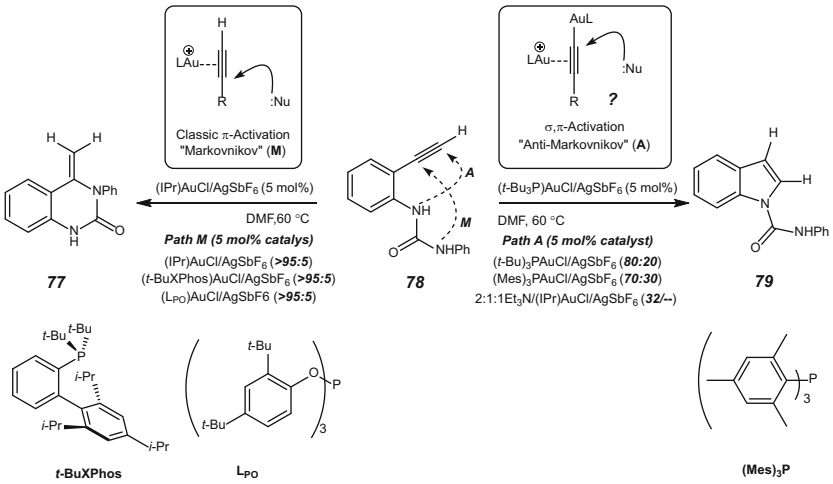

Fig. 25 Selectivity switch in an intramolecular alkyne hydroamination

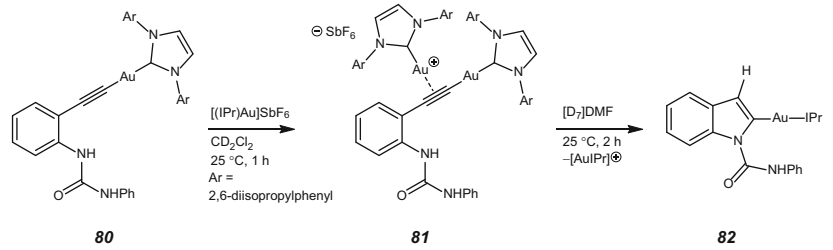

Fig. 26 Hydroamination selectivity through the digold acetylide

Markovnikov product, the pathway could be diverted to the *anti*-Markovnikov product by adding triethylamine. This led the authors to propose a competition between a classic π-activation mode (nucleophilic addition to a gold-coordinated acetylene) and the alternative α,π-gold-activation mode (nucleophilic addition involving a *gem*-digold acetylide).

Deuterium labeling experiments strongly support the conclusion that the normal mode of Markovnikov addition proceeds prior to formation of the *gem*-digold acetylides (no loss of terminal deuterium). However, the observation that neither acetylide **80** nor digold acetylide **81** cyclizes spontaneously seems inconsistent with the proposal that the *gem*-digold acetylides are "dually" activated (Fig. 26). The reaction could be triggered by addition of DMF to **81** or DMF and cationic gold to **80**. The authors propose a steric argument for explaining the ligand-based selectivity differences. The bulky substituents on the *I*Pr ligand, they propose, may interact more significantly with the alkyne substituents and lead to a higher distortion toward the terminal end, thus accelerating the Markovnikov addition. With phosphines such as $(t\text{Bu})_3\text{P}$, however, the steric bulk is located farther away from the alkyne. Distortion is then proposed not to be as significant, and the cyclization

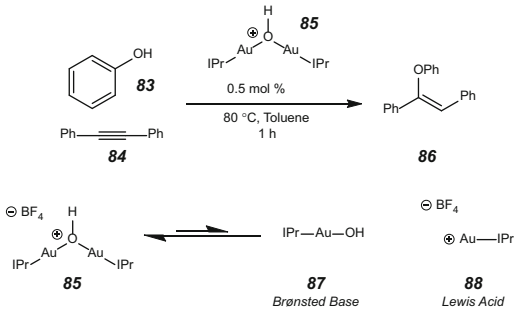

Fig. 27 Proposed dual activation mediated by digold hydroxide **85**

proceeds slowly enough to allow competitive formation of the *gem*-digold acetylide. Irrespective of reaction path, a second-order dependence on catalyst concentration was determined. A more detailed exploration of ligand effects and further mechanism studies is required to understand fully the role of DMF and the specific mode of dual activation. However, the ability to control reaction pathway based on either forming or avoiding *gem*-digold intermediates is sure to be a very powerful tool.

In a somewhat related manner, Nolan and co-workers have proposed another way to think about the cooperativity of two gold cations [88]. In their optimization of the hydrophenoxylation of alkynes they proposed that reaction efficiency could be improved by a dual activation based on both enhancing the strength of the nucleophile *and* enhancing the electrophilicity of the alkyne. This proposal required the use of digold hydroxide **85**, which under appropriate conditions can be considered both a Brønsted base (**87**) and a Lewis acid (**88**). The Lewis acid portion can activate the π-system; the Brønsted basic unit can deprotonate phenol and generate a stronger nucleophile (anionic phenoxide) (Fig. 27).

Under catalytic conditions with **85**, the hydrophenoxylation reaction proceeds with better yield and under milder conditions compared to earlier reports. When the gold alkyne π-complex was isolated and treated with the phenol nucleophile, only a small yield of phenyl ether **86** was generated (Fig. 28). When gold phenoxide **90** was treated with diphenylacetylene, no reaction was observed. When phenoxide **90** and acetylene complex **89** were combined, an equilibrium was established between digold phenoxide **91**, free acetylene, and *gem*-digold **92** (tentatively assigned). Productive addition to the alkyne was confirmed by addition of water, which slowly led to the enol ether product and regeneration of catalyst **85**. These observations supported the necessity of both modes of activation. Continued study of dual activation should continue to be an area of active and productive research.

3.4 Geminally Diaurated Vinyl Species

After their seminal discovery of the *gem*-diaurated vinyl gold resting state in an allene hydroarylation (see Fig. 7, structure **28a**) [48], Gagné and Widenhoefer

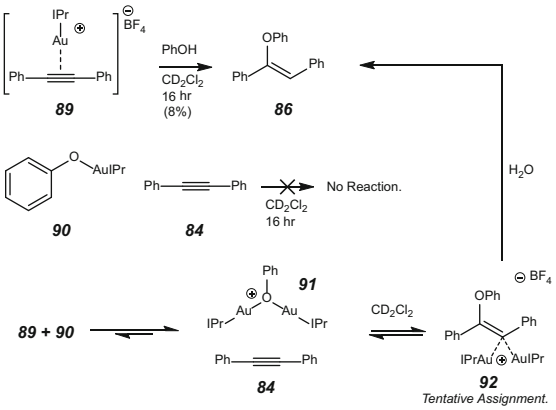

Fig. 28 Control studies in support of dual activation. Both "cationic" gold and "basic" gold appear to be required for productive reaction

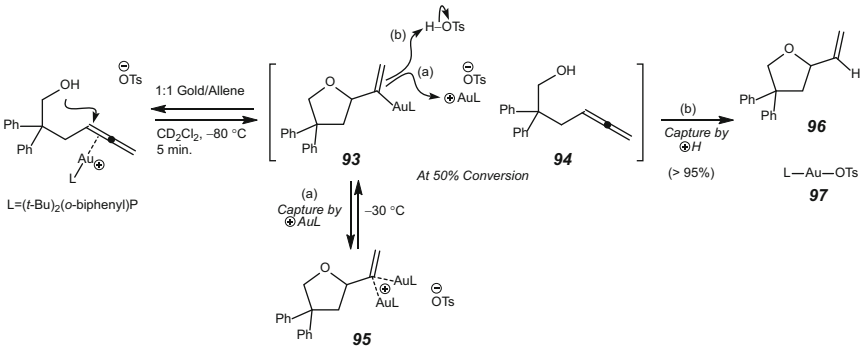

Fig. 29 Control studies to support the reversibility of intramolecular hydroalkoxylation and mechanistic involvement of vinyl *gem*-digold intermediates

collaborated to analyze mechanistically an intramolecular allene hydroalkoxylation (Fig. 29) [89]. Under stoichiometric conditions and at low-temperature, allene **94** undergoes facile cyclization. Rapid formation of *gem*-digold **95** (at 50% remaining starting alcohol) indicates that capture of vinyl gold **93** by cationic gold (pathway a) is significantly faster than capture by the equivalent of acid formed from the reaction (pathway b). When the solution containing **95** was warmed to −30°C, the final ether product **96** was generated in high yield. Studies under catalytic conditions show that *gem*-digold **95** persists throughout the reaction as the only organometallic species, indicating it is the catalyst resting state. Treatment of vinyl gold **93** with HOTs at low temperature generated the same mixture of **94** and **95**, indicating that the initial nucleophilic addition is reversible! Protonation experiments on vinyl gold **93** at room temperature led to rapid formation of ether **96**. Strikingly, a zero-order dependence on [HOTs] and no kinetic isotope effect ($k_H/k_D = 0.9$) suggest that the reaction proceeds through fast formation of the *gem*-digold intermediate **95** followed by rate-limiting dissociation back to the reactive vinyl gold. Further deuterium

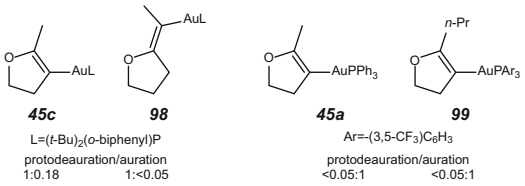

Fig. 30 Ligand effect on protodeauration/auration competition

labeling experiments under catalytic conditions (where the concentrations of gold and acid are much lower) indicated that *most* of the catalyst turnover avoids formation of the *gem*-digold complex **95**, which solidifies its assignment as an off-cycle reservoir. Additionally, protodeauration is not terribly efficient; nearly 80% of vinylgold **93** undergoes cycloreversion prior to protodeauration.

Several papers have shown that *gem*-digold complexes are off-cycle intermediates which do not protodemetalate or otherwise react directly [71, 90]. Zhdanko and Maier have performed extensive analysis on the alkyne hydroalkoxylation mechanism, and this work has provided additional experimental information to help control the involvement of this key gold-inhibition pathway [91]. The competition between protodeauration and auration was sensitive to both the electronics and sterics of the ligand (Fig. 30). For example when $(t\text{Bu})_2(o\text{-biphenyl})\text{P}$ was used, protonation outcompeted auration in the reaction of enol ether-derived vinyl gold complexes(**45c** and **98**). When electron-withdrawing ligands such as Ph_3P and Ar_3P ($Ar = 3,5\text{-}(CF_3)_2C_6H_3-$) were used, diauration outcompeted protonation. This was consistent with their earlier observations on the thermodynamic stabilities of *gem*-digold compounds. Their kinetic studies also confirmed that *gem*-digold complexes are not active π-acids either (they cannot directly activate alkynes).

To complicate things further, formation of *gem*-digold intermediates results in a corresponding release of an equivalent of acid. In the case of an intermolecular addition, when electron-poor ligands are used, acid formation can produce an increase in reaction efficiency despite the production of a less-active gold reservoir. Other experimental observations suggest that, under catalytic conditions, the counterplay between the two processes (protodeauration/auration) may also be highly sensitive to counterions or other additives. For example, Hammond and Xu and co-workers have shown that the reactivity of gold-catalyzed reactions can be enhanced by using additives that facilitate proton transfer, thus presumably accelerating the protodeauration step [92]. Enhancement of counteranion basicity has also been shown by Zhdanko and Maier to increase the rate of nucleophilic addition, and this may also play a role in improving overall reaction efficiency [93].

3.5 Enyne Cycloisomerization

The cycloisomerization of enynes has been examined extensively by Echavarren and co-workers and a strong theoretical and mechanistic framework has been

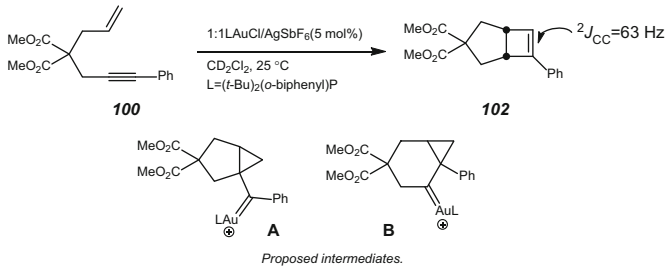

Fig. 31 Proposed intermediates in enyne cycloisomerization

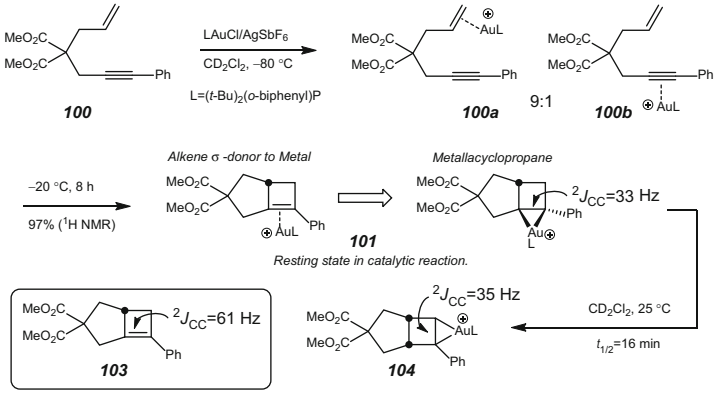

Fig. 32 First organometallic intermediate observed in an enyne cycloisomerization

established to account for ligand effects on reaction selectivities [4]; however, none of the proposed organometallic intermediates had been observed until a 2013 report by Brooner, Brown, and Widenhoefer [94]. Under catalytic conditions, enyne **100** is transformed to cyclobutene **102**, and cyclopropyl gold carbenes **A** and **B** have been proposed as possible intermediates (Fig. 31).

When the reaction was done with stoichiometric (tBu)$_2$(o-biphenyl)PAuCl/$AgSbF_6$ and monitored by ^{1}H NMR spectroscopy at $-80°C$ in CD_2Cl_2, at first only the precursor gold alkene and alkyne π-complexes were observed (**100a** and **100b**) (Fig. 32). This corroborated early spectroscopic studies by Echavarren which showed preferential binding to the alkene [95]. The alkene was favored over the alkyne by a ratio of 9:1, which is fully consistent with the now well-established binding affinities (see Fig. 13). At $-20°C$, after 8 h the mixture was converted completely to the highly strained gold-coordinated fused cyclobutene **101**. Its most striking feature was the diminished C–C coupling constant of the coordinated double bond ($^2J_{CC} = 33$ Hz) compared to the non-coordinated double bond ($^2J_{CC} = 61$ Hz). This indicates a significant change in hybridization from sp^2 to sp^3 and suggests that **101** should be characterized as a metallacyclopropane. This contrasts with the bonding normally observed in gold(I) alkene complexes where the π-system acts mainly as a σ-donor and metal to π* back-bonding is not generally

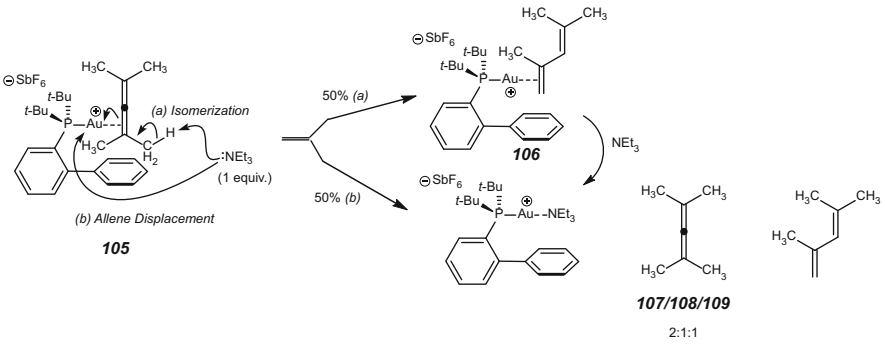

Fig. 33 Spontaneous allene to diene isomerization

considered a major contributor. The difference in binding can be attributed to the strain associated with cyclobutene **102**. Upon warming, coordinated alkene **101** isomerizes to **104**. Based on the $^2J_{CC}$ coupling constant, it also displays metallacyclopropane character.

3.6 Allene Isomerization and Racemization

Following detailed reports on the structure of phosphine gold(I) allene complexes [30, 31], Widenhoefer et al. showed that the highly substituted tetramethylallene complex spontaneously isomerizes in solution to the corresponding 2,4-dimethyl-1,3-pentadiene complex (**105** → **106**) (Fig. 33) [96]. The process could also be induced by exogenous base. Addition of triethylamine resulted in formation of a 2:1:1 mixture of triethylamine complex, allene and diene. This indicates that the triethylamine acts *both* as a Lewis base (displacing the allene from gold) *and* as a Brønsted base, removing an allenylic proton to initiate isomerization. Both processes compete kinetically with each other, and the 1:1 ratio of products suggests nearly identical rates for each.

The intermediacy of vinyl gold species **110** is implied by these observations, although it was not directly observed (Fig. 34). It is interesting that in the presence of the strongly basic triethylamine this presumed species can apparently still protodemetalate to form the final diene product. Triethylamine is routinely used to shut down protodemetalation and thus facilitate observation of organogold intermediates (see Fig. 18 and [77]).

Attempts to exploit this observation to develop conditions for catalytic isomerization were met with moderate success: PhN=O, DBU, 2,6,-di-*t*Bu-pyridine, and 2,2,6,6-tetramethylpiperidine used at 10 mol% in dioxane with 5 mol% of (*t*Bu)$_2$(*o*-biphenyl)PAu(N≡C–CH$_3$)SbF$_6$ at 60°C gave <5% conversion after 16 h, while *N*-methylpyrrolidinone and *N*,*N*-dimethylaniline gave 20% and 35% yields of diene, respectively (Fig. 35). In parallel work, however, Zhang and

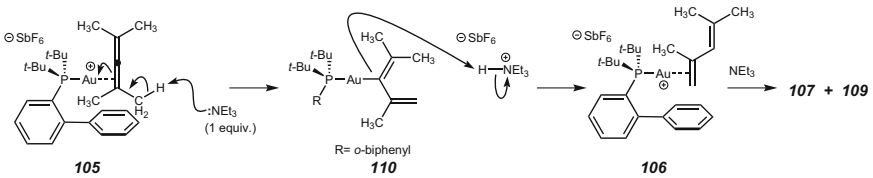

Fig. 34 Possible mechanism in amine-mediated allene isomerization

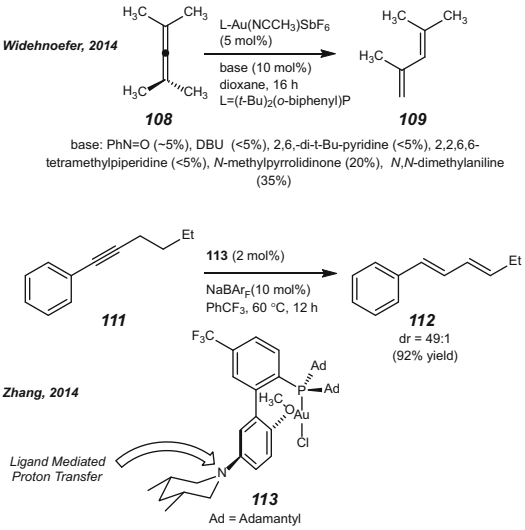

Fig. 35 Gold-catalyzed multiple bond isomerizations

co-workers reported a gold-catalyzed alkyne-to-diene isomerization, which presumably proceeds through a gold allene intermediate (allene to diene isomerization was confirmed independently) [97]. Their reaction utilized a uniquely designed bifunctional pre-catalyst (**113**) and is proposed to be facilitated by ligand-mediated deprotonation and protonation. The ligand was specifically designed to combine both highly π-acidic gold (by use of the *p*-CF_3 group), a rigid framework for proton transfer (adamantyl worked better than cyclohexyl), and a strongly basic amine (piperidine over dimethylamino).

Harris, Nakafuku, and Widenhoefer expanded on previous allene structural studies [30, 31]with a mechanistic study of gold-catalyzed racemization (Fig. 36) [98]. A series of Hammet studies were performed to determine the electronic nature of the process. Electron-withdrawing groups on the aromatic substituent in aryl-1,2-butadienes (**114**) decrease the rate of racemization, and the strength of this trend was similar for Ph_3P and (tBu)$_2$(o-biphenyl)P ligands. Electron-withdrawing groups on the aromatic substituent in 1-aryl-3-phenylpropadienes (**115**) also decrease the rate, but the influence was less strong, an observation consistent with the inherent higher delocalization of charge in the more substituted system. Finally,

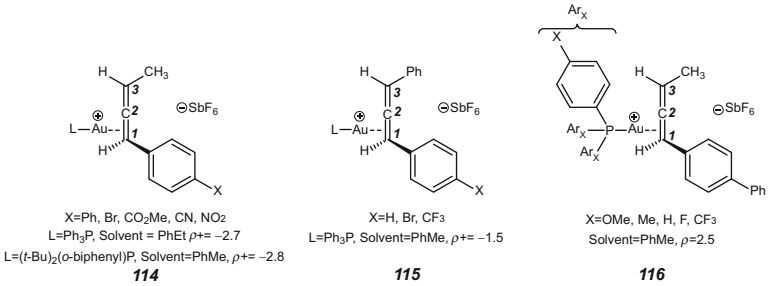

Fig. 36 Racemization rates examined and corresponding Hammett data

racemization rates when using *para*-substituted triarylphosphines (as in **116**) were significantly enhanced upon going from electron-donating groups to electron-withdrawing groups on the ligand.

Finally, an important solvent effect was observed which correlated with solvent polarity. Racemization rates for 1-aryl-1,2-butadienes (**114**) in toluene ($\varepsilon = 2.38$) were similar to those in ethylbenzene ($\varepsilon = 2.41$). In contrast, significant increases of $\geq$36 times and $\geq$50 times in chlorobenzene ($\varepsilon = 5.62$) and 1,2-dichloroethane ($\varepsilon = 10.36$), respectively, were observed. All these data support a mechanism that involves significant transfer of electron density away from the allene and onto the phosphine ligand. Further kinetic analysis supported a mechanism that involves turnover-limiting unimolecular conversion to an achiral allylic cation.

4 Progress in Gold(III) Chemistry

Generally, catalysis based on gold(III) has been ligand-free, and this has hampered isolation of directly relevant mechanistic intermediates. Recent successes in the area show the promise of future progress. For example, after Hashmi confirmed protodemetalation in vinyl gold(I) compounds generated from acetylenic amides [77], Ahn and co-workers were intrigued to observe oxidized products instead when gold(III) was used [99]. They thus pursued the isolation of analogous gold(III) intermediates. Treatment of butynyl benzamide **117** with $AuCl_3$ in CD_3CN yielded a 2:1 mixture of monovinyl gold **118** and divinyl gold **119** (Fig. 37). Both compounds are resistant to protodemetalation, and **119** forms dimer **120** on standing. These results highlight the higher stability of organogold(III) compounds in the presence of acid. In contrast to reactions with gold(I), no added base is required to halt the reaction of organogold intermediates formed. Finally, the structures provide analogous support for the outer sphere/*anti*-addition mechanism, even with gold (III).

Tilset and co-workers reported the first solid state characterization of a gold(III) π-complex, that of cyclooctadiene [100]. This report closely followed the first solution characterization of gold(III) alkene complexes (**122**) reported by

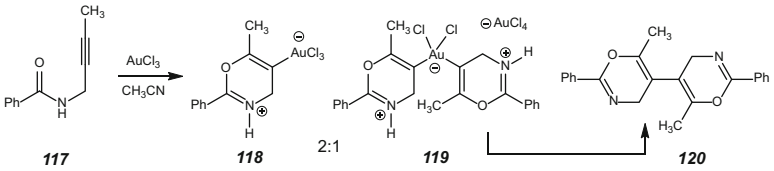

Fig. 37 *Anti*-addition and vinyl gold formation from gold(III) catalysts. Both characterized in the solid state

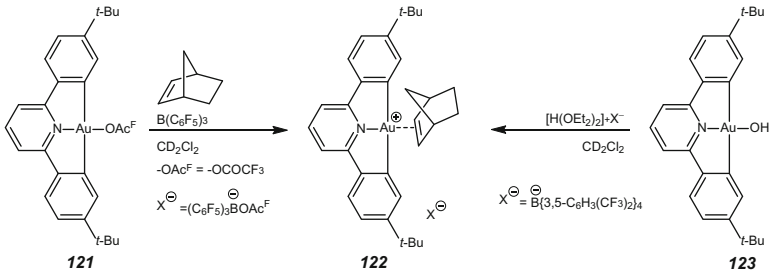

Fig. 38 Two routes to prepare gold(III) alkene complexes [101]

Bochmann and co-workers [101]. The complexes could be prepared by protonolysis of a gold alkyl compound [100], protonolysis of a gold hydroxide such as **123** [101], or by acetate abstraction from **121** [101], all in the presence of the desired alkene (Fig. 38). In the latter work, the presence of a bis(aryl)pyridine ligand was important for preventing pathways involving reductive elimination.

When **121** was allowed to react directly with ethylene in CD_2Cl_2, quantitative insertion into the Au–O bond was observed to give the alkyl gold complex **124** (Fig. 39). Interestingly, the structure was corroborated by isolation of crystalline material showing association with a polymeric ribbon of silver trifluoroacetate molecules. In further efforts to obtain crystallographic information on the π-complex itself, another synthesis was explored. When the corresponding gold (III) chloride complex **127** was treated with $AgSbF_6$ in the presence of norbornene, alkyl gold complex **128** was isolated unexpectedly, presumably from adventitious addition of water and protodemetalation of the aryl ligand C-bond. This complex is strikingly similar to complex **126** prepared previously by Cinellu and co-workers from a bipyridine gold oxo complex [102]. Addition of water upon heating has also been observed with a bipyridine gold(III) complex in the presence of propylene [103].

Tilset and co-workers further examined the acetate insertion discussed above. In their work, an analogous addition was observed for a related 2-*p*-tolylpyridine gold (III) diacetate complex (**129** → **130**) (Fig. 40) [104]. The reaction is selective; ethylene formally inserts opposite the substituent with the weaker *trans* effect (nitrogen), even though the acetate opposite the substituent with the stronger *trans* effect (carbon) was shown to be more labile. They found significant rate

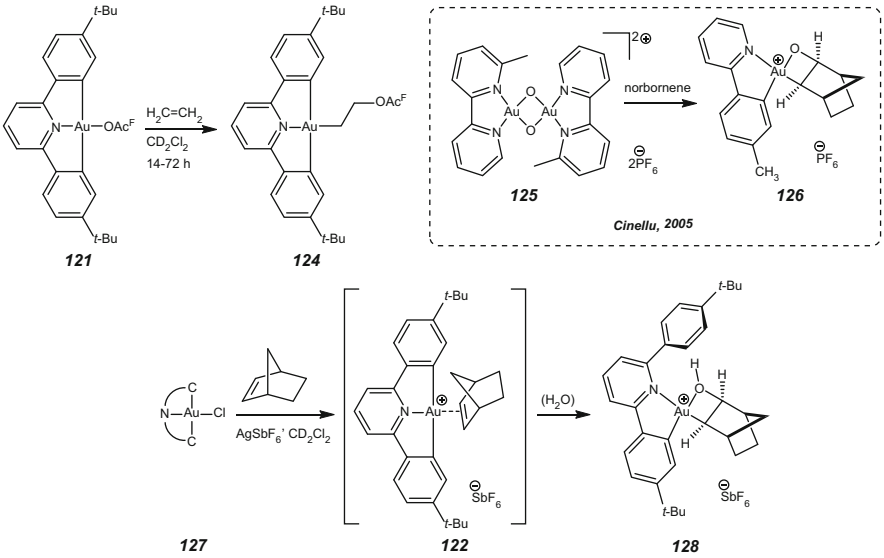

Fig. 39 Addition reactions of gold(III) alkenes. C–N–C=2,6-bis(4-*t*BuC_6H_3)$_2$pyridine dianion

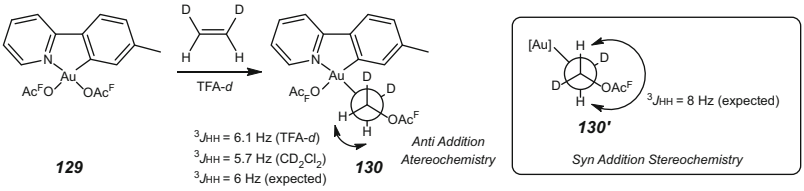

Fig. 40 Stereochemistry of acetate addition to gold(III) alkene

acceleration when the reaction was performed in trifluoroacetic acid (reaction in 5 min vs $\geq$14 h). When the reaction was carried out in trifluoroethanol (TFE-d_3), the corresponding trifluoroethylether alkyl gold complex was generated, suggesting a process involving external nucleophilic addition of solvent to an intermediate gold(III) alkene complex. When *cis*-1,2-dideuterioethylene was used, a single stereoisomer was formed. The coupling constant observed between the two alkyl protons was in the range expected for the stereochemistry corresponding to *anti* addition, supporting the proposal of outer sphere nucleophilic attack on coordinated ethylene.

In combination with computational studies, the general consensus in the literature appears to broadly favor outer sphere mechanisms for both gold(I) and gold (III) activation chemistry. The exceptional isolation of two *syn* oxyaurated intermediates (**126** and **128**, Fig. 39) from reactions with norbornene requires a closer look, but may be driven more by the unique properties imparted by strain in that alkene. Finally, no catalytic turnover, even with strong triflic acid, has been

observed, revealing again the high stability of organogold(III) intermediates to protonolysis.

5 Summary/Outlook

In summary, the past decade has seen the establishment of reliable procedures for the syntheses of π-complexes with strong donor ligands (phosphines and NHCs). That has in turn led to a better understanding of catalyst decomposition and pre-catalyst activation by halide abstraction. With these insights, π-complex isolation with a broader variety of ligands should soon become achievable. In turn, π-complex *reactivity* studies are providing crucial details on the varied mechanistic processes (substrate-catalyst inhibition, inhibition through off-cycle digold structures, modulation of reactivity by counterion, ligand, solvent) and these insights can surely empower chemists to improve broadly selectivity and efficiency in gold catalysis, and thus take full advantage of the unique reactivity features it has to offer. Finally, new structural insights into gold(III) chemistry facilitated by the development of stabilizing ligands add to this understanding, and the corresponding avenues opening increase the diversity of possible selective reaction pathways.

Acknowledgments This work was supported in part by the National Science Foundation, Award Award#1352296.

References

1. Fürstner A, Davies PW (2007) Angew Chem Int Ed 46:3410–3449
2. Gorin DJ, Sherry BD, Toste FD (2008) Chem Rev 108:3351–3378
3. Li Z, Brouwer C, He C (2008) Chem Rev 8:3239–3265
4. Jiménez-Núñez E, Echavarren AM (2008) Chem Rev 108:3326–3350
5. Arcadi A (2008) Chem Rev 108:3266–3325
6. Hashmi ASK (2005) Angew Chem Int Ed 44:6990–6993
7. Hashmi ASK, Rudolpha M (2008) Chem Soc Rev 37:1766–1775
8. Rudolpha M, Hashmi ASK (2012) Chem Soc Rev 41:2448–2462
9. Pradal A, Toullec PY, Michelet V (2011) Synthesis 10:1501–1514
10. Sengupta S, Shi X (2010) ChemCatChem 2:609–619
11. Rosenfeld DC, Shekhar S, Takemiya A, Utsunomiya M, Hartwig JF (2006) Org Lett 8:4179–4182
12. Kumar M, Hammond GB, Xu B (2014) Org Lett 16:3452–3455
13. Hashmi A, Stephen K (2010) Angew Chem Int Ed 49:5232–5241
14. Hashmi ASK (2014) Intermediates and elementary reactions in gold catalysis. In: Gade LH, Hofmann P (eds) Molecular catalysts: structure and functional design. Wiley, Weinheim
15. Liu L-P, Hammond GB (2012) Chem Soc Rev 41:3129–3139
16. Obradors C, Echavarren AM (2014) Chem Commun 50:16–28
17. Brooner REM, Widenhoefer RA (2013) Angew Chem Int Ed 52:11714–11724
18. Schmidbaur H, Schier A (2010) Organometallics 29:2–23

19. Dash C, Dias VR (2014) Synthesis and reactivity of gold-olefin complexes. In: PATAI's chemistry of functional groups. Wiley, New York
20. Akana JA, Battacharyya KX, Müller P, Sadighi JP (2007) J Am Chem Soc 129:7736–7737
21. Lavallo V, Frey GD, Donnadieu B, Soleilhavoup M, Bertrand G (2008) Angew Chem Int Ed 47:5224–5228
22. de Frémont P, Marion N, Nolan SP (2009) J Organomet Chem 694:551–560
23. Brown TJ, Dickens MG, Widenhoefer RA (2009) J Am Chem Soc 131:6350–6351
24. Brown TJ, Dickens MG, Widenhoefer RA (2009) Chem Commun 6451–6453
25. Brooner REM, Widenhoefer RA (2012) Organometallics 31:768–771
26. Hooper TN, Green M, McGrady JE, Patel JR, Russell CA (2009) Chem Commun 3877–3879
27. Brooner REM, Widenhoefer RA (2011) Organometallics 30:3182–3193
28. Sanguramath RA, Hooper TN, Butts CP, Green M, McGrady JE, Russell CA (2011) Angew Chem Int Ed 50:7592–7595
29. Sanguramath RA, Patra SK, Green M, Russell CA (2012) Chem Commun 48:1060–1062
30. Brown TJ, Sugie A, Dickens MG, Widenhoefer RA (2010) Organometallics 29:4207–4209
31. Brown TJ, Sugie A, Leed MGD, Widenhoefer RA (2012) Chem Eur J 18:6959–6971
32. Zhu Y, Day CS, Jones AC (2012) Organometallics 31:7332–7335
33. Sriram M, Zhu Y, Camp AM, Day CS, Jones AC (2014) Organometallics 33:4157–4164
34. Fürstner A, Alcarazo M, Goddard R, Lehmann CW (2008) Angew Chem Int Ed 47:3210–3214
35. Zhdanko A, Maier ME (2014) Angew Chem Int Ed 53:7760–7764
36. Brown TJ, Widenhoefer RA (2011) J Organomet Chem 696:1216–1220
37. Hooper TN, Green M, Russell CA (2010) Chem Commun 46:2313–2315
38. Flügge S, Anoop A, Goddard R, Thiel W, Fürstner A (2009) Chem Eur J 15:8558–8565
39. Eisenstein O, Hoffmann R (1981) J Am Chem Soc 103:4308–4320
40. Zeng X, Kinjo R, Donnadieu B, Bertrand G (2010) Angew Chem Int Ed 49:942–945
41. Liu X-Y, Guo Z, Dong SS, Li X-H, Che C-M (2011) Chem Eur J 17:12932–12945
42. Roberts JD, Hawkins BL, Bremser W, Borcic S (1971) J Am Chem Soc 93:4472–4479
43. Raubenheimer HG, Schmidbaur H (2014) J Chem Ed 91:2024–2036
44. Cross RJ, Davidson MF (1986) J Chem Soc Dalton Trans 411–413
45. Lavallo V, Frey GD, Kousar S, Donnadieu B, Bertrand G (2007) Proc Natl Acad Sci U S A 104:13569–13573
46. Brown TJ, Widenhoefer RA (2011) Organometallics 30:6003–6009
47. Grirrane A, Garcia H, Corma A, Álvarez E (2011) ACS Catal 1:1647–1653
48. Weber D, Tarselli MA, Gagné MR (2009) Angew Chem Int Ed 48:5733–5736
49. Seidel G, Lehmann CW, Fürstner A (2010) Angew Chem Int Ed 49:8466–8470
50. Zhdanko A, Maier ME (2013) Chem Eur J 19:3932–3942
51. Weber D, Gagné MR (2013) Chem Sci 4:335–338
52. Gómez-Suárez A, Dupuy S, Slawin AMZ, Nolan SP (2013) Angew Chem Int Ed 52:938–942
53. Heckler JE, Zeller M, Hunter AD, Gray TG (2012) Angew Chem Int Ed 51:5924–5928
54. Shapiro ND, Toste FD (2008) Proc Natl Acad Sci 105:2779–2782
55. Brooner REM, Brown TJ, Widenhoefer RA (2013) Chem Eur J 19:8276–8284
56. Wang ZJ, Benitez D, Tkatchouk E, Goddard WA, Toste FD (2010) J Am Chem Soc 132:13064–13071
57. Schmidbaur H, Hamel A, Mitzel NW, Schier A, Nogai S (2002) Proc Natl Acad Sci U S A 99:4916–4921
58. Hamel A, Mitzel NW, Schmidbaur H (2001) J Am Chem Soc 123:5106–5107
59. Bayler A, Bauer A, Schmidbaur H (1997) Chem Ber 130:115–118
60. Hashmi ASK, Blanco MC, Kurpejović E, Frey W, Bats JW (2006) Adv Synth Catal 348:709–713
61. Homs A, Escofet I, Echavarren AM (2013) Org Lett 15:5782–5785
62. Wang D, Cai R, Sharma S, Jirak J, Thummanapelli SK, Akhmedov NG, Zhang H, Liu X, Petersen JL, Shi X (2012) J Am Chem Soc 134:9012–9019

63. Zhu Y, Day CS, Zhang L, Hauser K, Jones AC (2013) Chem Eur J 19:12264–12271
64. Weber SG, Rominger F, Straub BF (2012) Eur J Inorg Chem 2012:2863–2867
65. Kumar M, Jasinski J, Hammond GB, Xu B (2014) Chem Eur J 20:3113–3119
66. Wang W, Hammond GB, Xu B (2012) J Am Chem Soc 134:5697–5705
67. Malhotra D, Mashuta MS, Hammond GB, Xu B (2014) Angew Chem Int Ed 53:4456–4459
68. Duan H, Sengupta S, Petersen JL, Akhmedov NG, Shi X (2009) J Am Chem Soc 131:12100–12102
69. Chen Y, Yan W, Akhmedov NG, Shi X (2010) Org Lett 12:344–347
70. Zhdanko A, Ströbele M, Maier ME (2012) Chem Eur J 18:14732–14744
71. Zhdanko A, Maier ME (2013) Organometallics 32:2000–2006
72. Weber D, Jones TD, Adduci LL, Gagné MR (2012) Angew Chem Int Ed 51:2452–2456
73. Zuccaccia D, Belpassi L, Macchioni A, Tarantelli F (2013) Eur J Inorg Chem 2013:4121–4135
74. Ciancaleoni G, Biasiolo L, Bistoni G, Macchioni A, Tarantelli F, Zuccaccia D, Belpassi L (2013) Organometallics 32:4444–4447
75. Ciancaleoni G, Belpassi L, Tarantelli F, Zuccaccia D, Macchioni A (2013) Dalton Trans 42:4122–4131
76. Liu L, Xu B, Mashuta MS, Hammond GB (2008) J Am Chem Soc 130:17642–17643
77. Hashmi ASK, Schuster AM, Rominger F (2009) Angew Chem Int Ed 48:8247–8249
78. Hashmi ASK, Ramamurthi TD, Rominger F (2010) Adv Synth Catal 352:971–975
79. Zhu Y, Yu B (2011) Angew Chem Int Ed 50:8329–8332
80. Chen Y, Wang D, Petersen JL, Akhmedov NG, Shi X (2010) Chem Commun 46:6147–6149
81. LaLonde RL, Brenzovich WE Jr, Benitez D, Tkatchouk E, Kelley K, Goddard WA III, Toste FD (2010) Chem Sci 1:226–233
82. Hashmi ASK, Ramamurthi T, Rominger F (2009) J Organomet Chem 694:592–597
83. Hashmi ASK (2014) Acc Chem Res 47:864–876
84. Gómez-Suárez A, Nolan SP (2012) Angew Chem Int Ed 51:8156–8159
85. Hashmi ASK, Braun I, Rudolph M, Rominger F (2012) Organometallics 31:644–661
86. Hansmann MM, Rominger F, Hashmi ASK (2013) Chem Sci 4:1552
87. Gimeno A, Cuenca AB, Suárez-Pantiga S, de Arellano CR, Medio-Simón M, Asensio G (2014) Chem Eur J 20:683–688
88. Oonishi Y, Gómez-Suárez A, Martin AR, Nolan SP (2013) Angew Chem Int Ed 52:9767–9771
89. Brown TJ, Weber D, Gagné MR, Widenhoefer RA (2012) J Am Chem Soc 134:9134–9137
90. Tang Y, Li J, Zhu Y, Li Y, Yu B (2013) J Am Chem Soc 131:18396–18405
91. Zhdanko A, Maier ME (2014) Chem Eur J 20:1918–1930
92. Wang W, Kumar M, Hammond GB, Xu B (2014) Org Lett 16:636–639
93. Zhdanko A, Maier ME (2014) ACS Catal 4:2770–2775
94. Brooner REM, Brown TJ, Widenhoefer RA (2013) Angew Chem Int Ed 52:6259–6261
95. García-Mota M, Cabello N, Maseras F, Echavarren AM, Pérez-Ramírez J, Lopez N (2008) Chemphyschem 9:1624–1629
96. Brown TJ, Robertson BD, Widenhoefer RA (2014) J Organomet Chem 758:25–28
97. Wang Z, Wang Y, Zhang L (2014) J Am Chem Soc 136:8887–8890
98. Harris RJ, Nakafuku K, Widenhoefer RA (2014) Chem Eur J 20:12245–12254
99. Egorova OA, Seo H, Kim Y, Moon D, Rhee YM, Ahn KH (2011) Angew Chem Int Ed 123:11648–11652
100. Langseth E, Scheuermann ML, Balcells D, Kaminsky W, Goldberg KI, Eisenstein O, Heyn RH, Tilset M (2013) Angew Chem Int Ed 52:1660–1663
101. Savjani N, Roşca D-A, Schormann M, Bochmann M (2013) Angew Chem Int Ed 52:874–877
102. Cinellu MA, Minghetti G, Cocco F, Stoccoro S, Zucca A, Manassero M (2005) Angew Chem Int Ed 44:6892–6895
103. Rezsnyak CE, Autschbach J, Atwood JD, Moncho S (2013) J Coord Chem 66:1153–1165
104. Langseth E, Nova A, Tråseth EA, Rise F, Øien S, Heyn RH, Tilset M (2014) J Am Chem Soc 136:10104–10115

Top Curr Chem (2015) 357: 167–212
DOI: 10.1007/128_2014_585

Published online: 18 December 2014

Aurophilicity in Gold(I) Catalysis: For Better or Worse?

Dieter Weber and Michel R. Gagné

Abstract This book chapter discusses the effects of aurophilicity on gold catalysis. First, a brief historic account of aurophilicity in organogold chemistry is given, focusing on the pioneering results which set the stage for its association with catalytic intermediates (gold vinyl and gold aryl complexes); this is followed by an introduction to cationic gold(I) as an electrophilic catalyst, and the first isolation of organogold intermediates from catalysis. In the main section, the growing number of reports observing aurophilic interactions in catalysis or illustrative model systems is reviewed in a non-comprehensive tutorial way. The effects of aurophilicity are discussed in the following structures: (1) the geminal diauration of $C(sp^2)$-atoms; (2) geminal diauration of other atoms; (3) σ-π-diauration of terminal alkynes. It is apparent that in most cases efficient catalysis is hindered by aurophilic effects as less active aggregates tend to be formed from more active species $[LAu]^+$, but there are a growing number of reports using aurophilicity as a driving force to access new reactivity and selectivity.

Keywords Aurophilicity · Geminal diauration · Gold acetylide complexes · Gold aryl complexes · Gold catalysis · Gold vinyl complexes · Mechanistic proposals · Organogold chemistry · σ-π-Diauration

D. Weber (✉)
Max-Planck-Institut für Kohlenforschung, Kaiser-Wilhelm-Platz 1, 45470 Mülheim an der Ruhr, Germany
e-mail: dweber@kofo.mpg.de

M.R. Gagné
Department of Chemistry, Caudill and Kenan Laboratories, The University of North Carolina at Chapel Hill, Chapel Hill, NC 27599-3290, USA

Contents

1 Introduction

1.1 A Brief Historic Account of Aurophilicity in Organogold Chemistry

Long before gold complexes were identified as promising homogenous catalysts (early 1990s), a variety of organogold(I) compounds were synthesized and studied (for representative reviews, see [1, 2]). For example, the *Nesmeyanov Institute of Organoelement Compounds of Russian Academy of Sciences* began its studies on "univalent" organogold(I) complexes in 1970 and published more than 100 articles on this topic in Russian and other chemistry journals. The synthesis of alkyl-, alkenyl-, alkynyl-, cyclopropyl-, benzyl-, allyl-, aryl-, cyclopentadienyl-, cymantrenyl-, and ferrocenylgold(I) complexes was described and their reactivity studied. These seminal studies were carried out by Nesmeyanov, Grandberg, and Baukova [3–6]. Other main contributors to this research field were the research groups of contemporaries such as Puddephatt ([7–9] and references therein), Schmidbaur ([10, 11] and references therein), and Kochi [12–17], and shortly thereafter by Gimeno [18], Laguna ([19] and references therein), and many others ([20, 21] and references therein, [22, 23]). Schmidbaur in particular highlighted organogold(I) complexes as tending to form multinuclear aggregates in both their solid state and in solution, and coined the terms *aurophilic bonding* or *aurophilicity*, which describe weak attractive forces between two gold centers comparable in strength to hydrogen bonding (5–10 kcal mol^{-1}) [24]. Aurophilic bonding is characterized by an Au–Au distance of 2.8–3.5 Å in X-ray crystal structures. This wide range is a consequence of the mutual approach of two gold centers being characterized by a relatively flat energy profile [11, 25]. Because other closed shell metals have revealed similar behavior, the general terms *metallophilicity* and *metallophilic bonding* were also introduced [26].

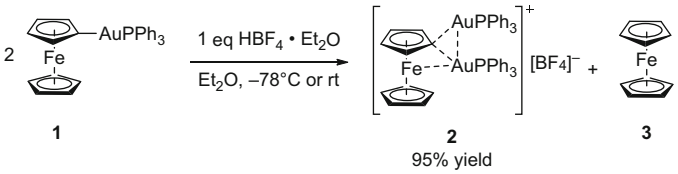

Scheme 1 Synthesis of geminally diaurated gold complex $[Fc(AuPPh_3)_2]^+[BF_4]^-$

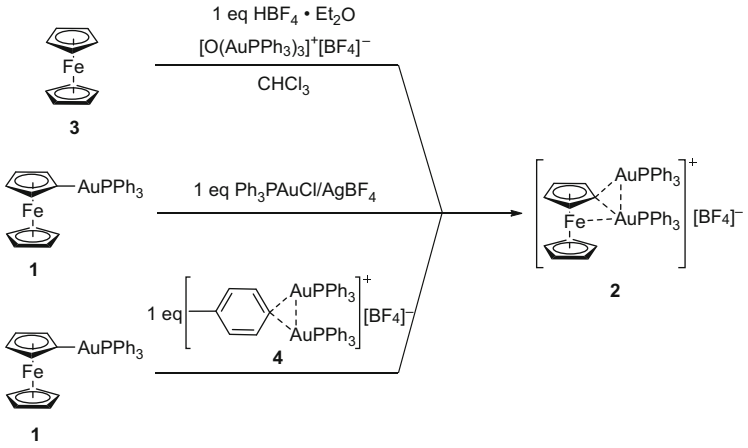

Scheme 2 Synthetic pathways for $[Fc(AuPPh_3)_2]^+[BF_4]^-$ via alternative generations of $[Ph_3PAu]^+[BF_4]^-$

Nesmeyanov and Grandberg were among the first to identify this characteristic effect of gold while studying the reactivity of the ferrocenylgold(I)-complex $FcAuPPh_3$ (**1**) with the Brønsted acid HBF_4 (Scheme 1) ([27] and references therein). Treating this species with HBF_4 led to the formation of the geminally diaurated complex $[Fc(AuPPh_3)_2]^+[BF_4]^-$ (**2**), which could be isolated as a white precipitate in 95% yield, and characterized by X-ray diffraction analysis and NMR.

The structure of $[Fc(AuPPh_3)_2]^+[BF_4]^-$ (**2**) revealed a hyperconjugated $C(sp^2)$-atom with an Au_2C-three-center-two-electron (3c-2e) bond [3–6]. The connectivity was stabilized by an aurophilic interaction between the two gold(I) atoms and a second metallophilic bond between one gold(I) atom and the low spin iron(II) center of ferrocene. ^1H NMR signals of the diaurated Cp-ring exhibited large downfield shifts relative to the monogold complex (shifting from $\delta = 3.90$, 4.16 ppm to $\delta = 4.17$, 5.43 ppm upon diauration) and the diastereotopic phosphine ligands revealed two resonances at $\delta = 36.4$ and $\delta = 38.2$ ppm (^{31}P NMR). ^{13}C NMR data were not reported.

Later studies by the same group showed that $[Ph_3PAu]^+$ accompanied by the low coordinating $[BF_4]^-$ anion was the reactive gold species which intercepts the neutral monogold species to form dinuclear gold complexes. In this way, digold $[Fc(AuPPh_3)_2]^+[BF_4]^-$ (**2**) was accessible in several related ways (Scheme 2).

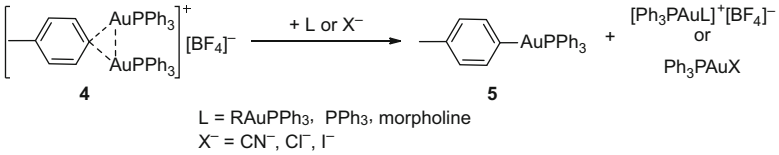

Scheme 3 Characteristic reactivity of digold complexes with abstracting ligands L or anions X^-

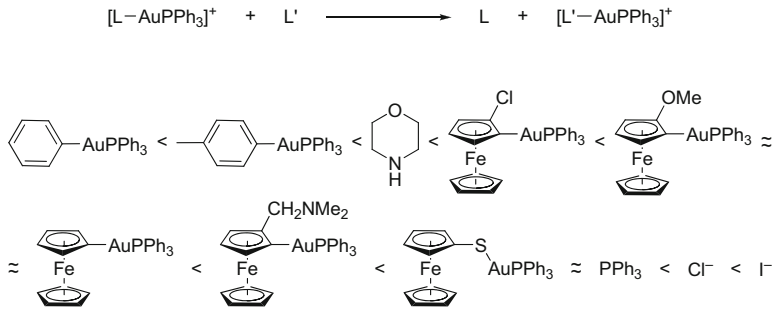

Scheme 4 Donor strength of ligands measured by competitive $[Ph_3PAu]^+$ exchange

Ferrocene **3** could be converted to the digold species by direct auration with a mixture of $[O(AuPPh_3)_3]^+[BF_4]^-$ and HBF_4 ([28] and references therein). Other pathways included the reaction of $FcAuPPh_3$ (**1**) with in situ generated $[Ph_3PAu]^+[BF_4]^-$ (by the metathesis reaction of Ph_3PAuCl and $AgBF_4$) and the addition of a different digold, e.g. $[4\text{-Me-}C_6H_4\text{-}(AuPPh_3)_2]^+[BF_4]^-$ (**4**) which bound $[Ph_3PAu]^+$ less strongly than **1**.

An alternative method to characterize diaurated gold complexes was their innate reactivity. Nesmeyanov and Grandberg demonstrated that one $[Ph_3PAu]^+$ unit was efficiently abstracted from $[4\text{-Me-}C_6H_4\text{-}(AuPPh_3)_2]^+[BF_4]^-$ (**4**) by a variety of coordinating ligands L or anions X^- yielding the corresponding monogoldaryl **5** and $[Ph_3PAuL]^+[BF_4]^-$ or Ph_3PAuX species, respectively (Scheme 3).

Competitive $[Ph_3PAu]^+$ unit transfer from digold $[L–AuPPh_3]^+$ to another ligand L' was used to determine the donor strength of ligands; these studies showed that more basic C–Au σ-bonds had a stronger affinity for cationic gold (Scheme 4). Interestingly, C–Au σ-bonds competed with the ligating ability of morpholine, a secondary amine.

The concept of aurophilicity and the generation of hyperconjugated carbon atoms were investigated in detail by Schmidbaur as well. The synthesis of unusual complexes demonstrated how enabling aurophilic interactions could be for stabilizing oligomeric structures. For example, the sum stabilization of multiple aurophilic contacts (Au–Au distance 3.003 Å) was impressively demonstrated by the synthesis of $[(Ph_3PAu)_6C]^{2+}[MeOBF_3]_2^-$, an octahedrally coordinated carbon center (Scheme 5) [29].

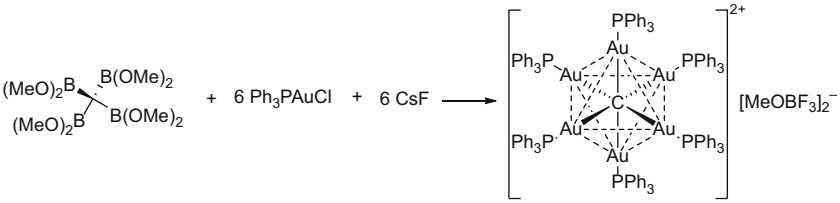

Scheme 5 Synthesis of $[(Ph_3PAu)_6C]^{2+}[MeOBF_3]_2^-$

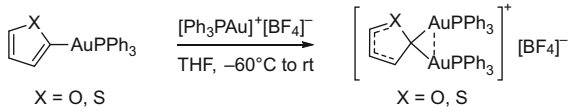

Scheme 6 Synthesis of geminally diaurated furanyl (50% yield) and thiophenyl cations (63% yield)

Schmidbaur also studied the spectroscopic properties of dinuclear gold aryl complexes. Mono- and digold complexes of the heteroaromatic furan and thiophene were synthesized and structurally characterized by X-ray analysis (Scheme 6) [30].

Upon diauration the phosphine chemical shifts in the ^{31}P NMR changed in both examples from $\delta \approx 44$ ppm to $\delta \approx 36$ ppm. While ^{13}C NMR spectra showed a characteristic doublet for the *ipso*-carbon of the monogold species, the same carbon was not detected in digold complexes. Difficulties in detection were attributed to the quadrupolar moment of gold. These data confirmed the findings of Grandberg and Nesmeyanov.

It was expected that vinylgold(I) complexes would express similar attributes to Schmidbaur's heteroaryl species as both contained a $C(sp^2)$–Au σ-bond. The first synthesis of a gold vinyl species was reported by Nesmeyanov and Grandberg in 1972, who synthesized the parent vinyl $CH_2{=}CH{-}AuPPh_3$ from Ph_3PAuCl and vinylmagnesium bromide [31]. In a later study, the reactivity of $CH_2{=}CH{-}AuPPh_3$ with $HBF_4{\bullet}Et_2O$ was investigated and the formation of an unstable digold vinyl $[CH_2{=}CH(AuPPh_3)_2]^+[BF_4]^-$ proposed. Even though no crystallographic evidence or other structural confirmation was provided, the tentative formation of $[CH_2{=}CH(AuPPh_3)_2]^+[BF_4]^-$ was indicated by IR data and its similar reactivity to related digold complexes [32].

1.2 Gold Catalysis is Electrophilic Catalysis

The development of late transition metal-catalyzed cross coupling reactions to form new C–C bonds is a terrific illustration of the power of metal-catalyzed processes in synthetic chemistry. These palladium mediated transformations, which typically cross-couple a carbon-nucleophile with a carbon-electrophile, was awarded the

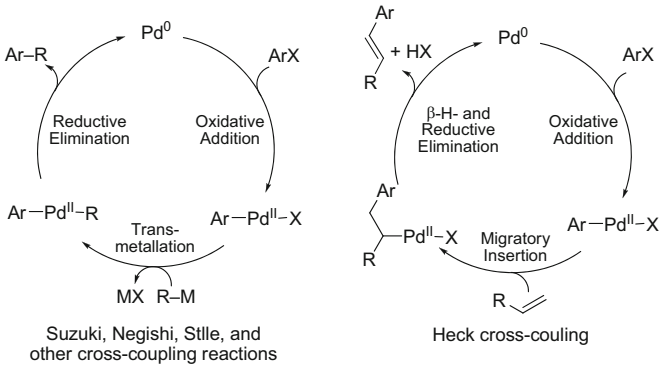

Scheme 7 Representative reaction steps in catalytic cycles for palladium-catalyzed cross-coupling reactions

Nobel Prize in 2010 ([33, 34]; R. F. Heck did not provide his Nobel lecture in text format). Proposed Pd(0)/Pd(II) catalytic cycles feature five basic steps, which themselves may consist of multiple elementary reactions: (1) oxidative addition, (2) reductive elimination, (3) migratory insertion, (4) β-elimination, and (5) transmetalation (Scheme 7).

Facilitating these reaction steps requires flexibility in the oxidation state and coordination number of the metal center. Because palladium exhibits low RedOx energy barriers between its Pd(0) and Pd(II) states, and because of its flexible coordination sphere, it is most often the metal of choice in cross-coupling chemistry.

In comparison, gold is a third row late transition metal which displays significantly higher RedOx energy barriers, and thus suffers from inhibited oxidative addition and reductive elimination sequences in a hypothetical Au(I)/Au(III) cycle [35–37]. Additionally, gold generally does not engage in β-elimination or migratory insertion processes [38, 39], which is demonstrated by the isolation and thermal stability of numerous gold alkyl complexes (for representative examples of gold alkyl complexes, see [40–42] and references therein), further inhibiting Au(I)/Au(III) cycles from operating. Out of the five basic late-transition metal reactions, gold complexes easily undergo transmetalation reactions; for example, organolithium ([43]; see also [30]), Grignard reagents [3–6], organoboron [44, 45], and organomercury compounds [3–6] easily transfer their organic groups to LAuCl species, and organogold complexes transfer to other transition metals such as Pd ([46–49] and references therein), even enabling dual Au/Pd catalysis (for pioneering examples, see [50–52]). Other basic reaction steps typically attributed to late-transition metal catalysts require additional driving forces with gold (for illustrative examples, see [53–60] and references therein).

The catalytic activity of gold complexes is rooted in another phenomenon. As a third row late transition metal, gold exhibits not only strong relativistic effects ([61, 62] and references therein) but also strongly feels the lanthanide contraction.

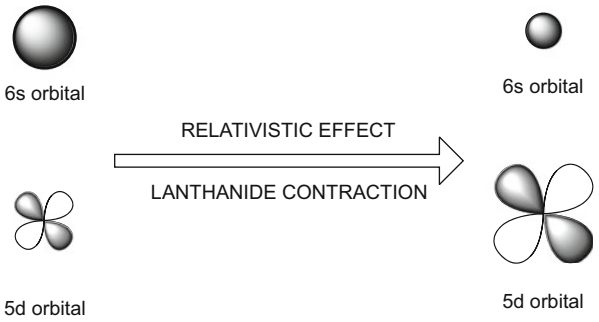

Fig. 1 Effects of relativity and lanthanide contraction on outer-shell orbitals of gold

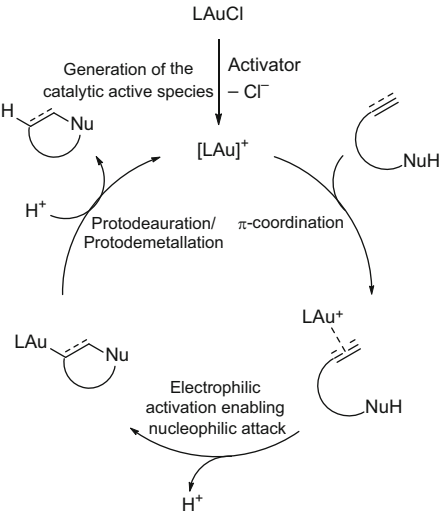

Scheme 8 Typically proposed reaction steps in gold(I) catalytic cycles

Both effects significantly decrease the size and energy level of the 6s orbital, while increasing the size and energy levels of the 5d orbitals (Fig. 1).

This effect alters the electron density around the metal center, which increases its π-acidity (empty 6s orbital) and π-backbonding (occupied 5d orbitals) ability in the Dewar–Chatt–Duncanson model [63–65]. As a result, ligand-supported cationic gold(I) acts as an electrophilic soft π-Lewis acid capable of activating C–C multiple bonds (alkynes, allenes, and alkenes) for nucleophilic attack to form new C–C, C–O, C–N, and other bonds ([64, 66–81]; see also [64, 65, 82]).

Typical mechanistic proposals of gold-catalyzed processes include the following basic reaction steps (Scheme 8). First, the catalytically active cationic species has to be generated from an inactive gold chloride precursor. Once generated, this species activates the C–C multiple bond of alkynes, allenes, and alkenes towards intra- or intermolecular nucleophilic attack, which is typically outersphere and *anti* selective (a representative report supporting anti-selective addition is [83]. Another study demonstrated that Au–Si σ bonds add *syn*-selective to alkynes [84]). The formation

of the desired C–Nu bond leads to a cationic gold(I) vinyl (if starting from allenes or alkynes) or gold(I) alkyl intermediate (if starting from an alkene), which is converted to a neutral intermediate through proton loss. The proton reenters the catalytic cycle to cleave the intermediary Au–C σ-bond and thus turns the catalytic cycle over, yielding the final product and regenerating the catalytically active cationic gold species.

A feature which has enhanced the power of gold catalysis has been the great (and also unexpected) molecular complexity which can be achieved in gold-catalyzed reactions as, in addition to the simple electrophilic catalysis outlined above, complex rearrangements are possible, many of which are proposed to involve cationic gold carbenoid intermediates (for representative reactions, see [85]. For recent evidence for gold carbenes, see [86–88]. For isolated model complexes, see [89, 90]). The soft Lewis acidic character of gold(I) not only activates C–C multiple bonds for catalysis but also contributes to the feasibility of most gold-catalyzed reactions in ambient bench top conditions which do not require extensive solvent purification or an air-free atmosphere.

Gold-catalyzed transformations can be broken down into the following categories: nucleophilic functionalization reactions on C–C multiple bonds (for representative examples, see [91, 92]), cycloisomerization reactions (for representative examples, see [93] and references therein), cycloadditions (for representative examples, see [94–96]), or sigmatropic rearrangements (for representative examples, see [97]) of polyunsaturated substrates, and, most recently, also cross-coupling reactions [53–60] using external strong oxidants to facilitate RedOx reactions on the gold center (the division of gold-catalyzed reactions into these categories stems from the review articles [98, 99]). All of these reactions significantly expand the synthetic toolbox of organic chemists who have taken advantage of the unique features of gold-catalyzed transformations to construct complex structural architectures found in natural products and medicinally important compounds ([100]; see also [101] and references therein).

1.3 Limitations/Challenges of Gold Catalysis

Despite its recent success, gold catalysis retains several limitations. The development of new specific reactions has often suffered from unpredictability in outcome as small changes in substrate or catalyst architecture can severely affect the course of the reaction ([101]. We experienced this unpredictability in our own laboratory, where an attempted polyolefin cyclization of alkylidene cyclopropanes resulted in an unexpected Cope rearrangement. For the leading reference, see [102]). While this risk is manageable in academic research (or perhaps even welcome) this issue would be detrimental to industrial applications or those wherein late stage intermediates (i.e. natural product synthesis) are subjected to gold chemistry as specific reliable transformations are critical in these scenarios.

Other obstacles for the industrial application of gold catalysis are catalyst stability and recyclability, which often result in higher catalyst loadings (>5 mol%). As the centuries have demonstrated, gold has a significant preference for its neutral oxidation state. Once a ligand-stabilized catalytically active cationic gold species $[LAu]^+$ is generated and exposed to organic unsaturated substrates, catalyst decomposition can often be observed by the formation of colloidal gold, which is identifiable by a dark violet, sometimes even black, color (strong σ donor ligands, such as N-heterocyclic carbenes augment the stability of cationic Au(I) species [103, 104]). Eventually a metallic gold mirror is formed on the glass wall. Both "metallic" states are considered to be catalytically less active or inactive because of their lower electrophilic character in comparison to cationic gold(I) complexes. The synthesis of homogenous gold catalyst precursors from metallic gold are always multistep processes,[1] which can be impractical and costly as recycling measures.

A third obstacle hindering the broad application of gold catalysis is the intrinsic property of gold(I) complexes preferring linear dicoordination geometries and subsequent consequences for the development of asymmetric reaction variants. Positioning the chiral information far from the substrate binding site, additionally separated by a gold atom, significantly hinders chirality transfer. There have been major efforts to overcome the intrinsic challenge of asymmetric gold(I) catalysis [105], for example the use of chiral counteranions [106], gold complexes stemming from bidentate phosphine ligands, which include two gold centers [107], and mononuclear phosphoramidite gold complexes [108, 109]. Even though these approaches have been found to be successful in a variety of benchmark reactions, they have often suffered from substrate specificity, again contributing to the unpredictability of gold catalysis.

The price of gold is often used as an argument for why gold catalysis has found limited application in industrial settings. Of course, lower purchase costs are always preferred, and while price is always an important consideration, other expensive metals have proven invaluable in facilitating chemistry in the industrial setting (rhodium is used, for example, in quite a few technical processes, for example hydroformylation [110], the Monsanto acetic acid process [111], and the Eastman chemical company acetic anhydride process [112]). Price thus seems to be a secondary issue. If a gold complex could catalyze the right reactions, operate at appropriately low catalyst loadings, and be sufficiently stable and recyclable, industry would most likely adopt them. Likewise, if gold catalysis had a predictable reaction outcome, or if a broadly applicable asymmetric ligand were designed which effectively transferred chiral information in transformations with broad substrate scope, medicinal and synthetic chemists would include gold catalytic steps in more retrosynthetic analyses. Therefore, it seems that the root of the limited application of gold catalysis in industry lies more in technical than financial limitations.

[1] Metallic gold is first oxidized to Au(III) species, e.g., by aqua regia. In a second step, the addition of sulfides reduces gold(III) to a (sulfide)Au(I)Cl complex, which can then be ligated with the desired ligand.

2 First Detailed Mechanistic Studies of Gold-Catalyzed Reactions Including the Isolation of Organogold Intermediates

2.1 Motivation for Detailed Mechanistic Studies in Gold Catalysis

The above-mentioned limitations of substrate specificity, uncertainty of reaction outcome, and issues related to catalyst stability and recyclability are at least partially because of a lack of a detailed understanding of gold-catalyzed processes. This knowledge gap, of course, was self inflicted and resulted partially from an imbalance in the development of new reactions and the experimental verification of the numerous plausible mechanistic proposals. Although this situation has significantly improved, early mechanistic efforts focused extensively on isotope labeling studies, with the identification of viable gold-containing intermediates conspicuously absent. In some cases this led chemists to question whether gold salts were truly catalytically active species as gold electrophiles were known to generate protons from a variety of reactions with substrate or traces of water, which could operate as an alternative electrophilic catalyst (therefore, it is crucial to run control experiments to distinguish gold catalysis from potential Brønsted acid catalysis; see [113]; for an illustrative example of Brønsted acid catalysis initiated by cationic gold, see [114]; for a review of the isolobality of H^+ and Au^+, see [115]). In 2007, this lack of a mechanistic understanding of gold-catalyzed processes was pointed out in a comprehensive review by Hashmi, which stated [116]:

> "there exists no direct proof for most intermediates shown in the mechanistic proposals" and "in most cases, it is still unknown what the active [catalyst] species really looks like".

Most intermediates in mechanistic schemes of gold-catalyzed reactions were primarily based on early findings in organogold chemistry and computational modeling. Ours and other research groups therefore made the decision to pursue fundamental mechanistic examinations, and we chose to focus on a seemingly simple gold-catalyzed reaction which we had previously developed. These efforts led to the detection of gold-containing intermediates formed during catalysis, their isolation, and a probing of their reactivity and their role in gold catalysis.

2.2 Triad of Studies Supporting the Viability of Gold Vinyl Intermediates in Gold Catalysis

The first report of isolated gold vinyl intermediates came out of the Hammond lab in 2008 [82]. While investigating the reactivity of allenoate **6**, two products were obtained; the expected γ-lactone **7** in 56% yield, and a minor component, which was found to be the neutral gold vinyl **8** (Scheme 9). It was obtained in good yield (68%

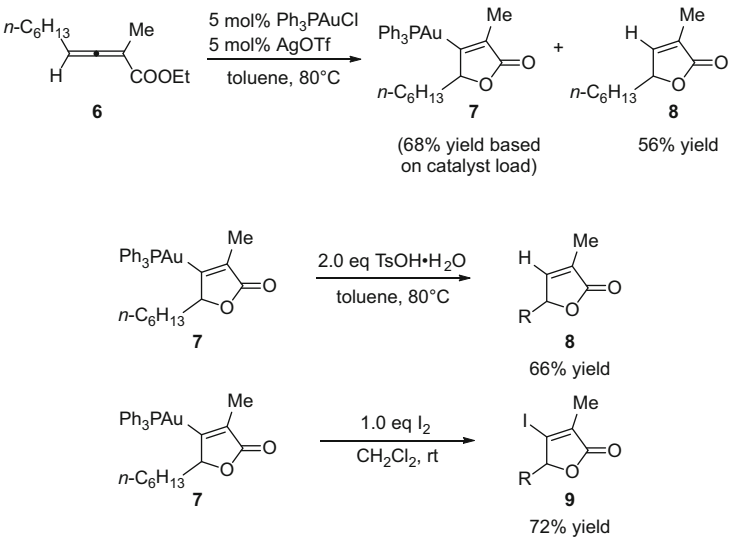

Scheme 9 Isolation of gold vinyl **7** from the gold-catalyzed reaction of allenoate **6** to γ-lactone **8** and its reactivity with TsOH•H_2O and I_2 to **8** and **9**, respectively

based on catalyst load) depending on the amount of catalyst subjected to reaction conditions.

Gold vinyl **7** could be intentionally isolated in an 85% yield from a stoichiometric reaction. It was stable and tolerated flash chromatography on silica gel. Single crystal X-ray structures gave structural proof for an Au–C σ-bond, and reactivity studies showed that this bond reacted with electrophiles. Protodemetalation with 2 equiv. of the Brønsted acid TsOH•H_2O gave **8** while the iodinated γ-lactone **9** was obtained when gold vinyl **7** was reacted with 1 equiv. of iodine. The combined data strongly suggested that gold vinyl complexes of type **7** were reaction intermediates in the gold-catalyzed transformation of allenoates to γ-lactones.

Shortly thereafter, Gagné reported the isolation of a gold vinyl intermediate from the intramolecular hydroarylation of allenes (Scheme 10) [117]. Preliminary studies identified $Ph_3PAuNTf_2$ as a convenient source of $[Ph_3PAu]^+$ for mechanistic studies as it did not require in situ activation of Ph_3PAuCl with silver salts [118]. Unexpectedly, the ^{31}P NMR spectrum of an in situ catalytic reaction showed two sharp peaks in a 1:1 ratio at $\delta \approx 36$ ppm. This observation was not only inconsistent with the expected catalyst resting states of the mechanistic proposal, the neutral gold vinyl ($\delta = 43$–45 ppm) and/or $[Ph_3PAu]^+$ ($\delta \approx 30$ ppm); it also appeared in stark contrast to the gold vinyl precedence of Hammond. After suppressing protodemetalation and arresting catalytic turnover by the addition of 2,6-di-*tert*-butyl pyridine (DTBP), it was found that 2 equiv. of $Ph_3PAuNTf_2$ were necessary to consume all of allene **10**.

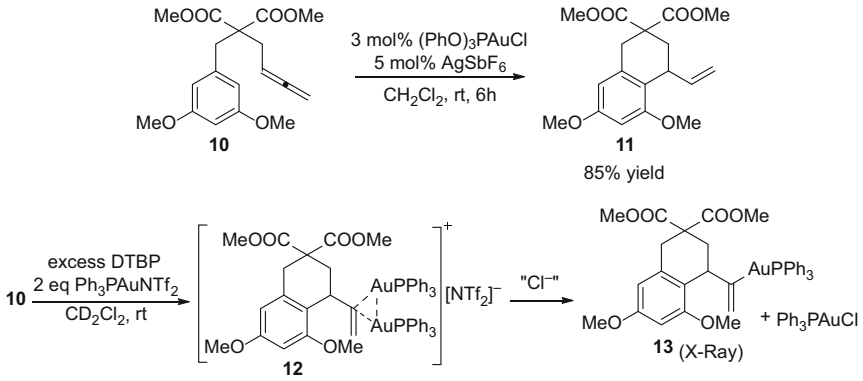

Scheme 10 Gold-catalyzed intramolecular hydroarylation of allene **10** to vinyl tetralin **11** and the isolation of gold vinyl intermediates **12** and **13**

The ^{1}H NMR data pointed clearly towards the generation of a single carbocyclic fragment which integrates 1:2 to the aromatic PPh_3 signals. ^{31}P NMR data always showed two characteristic $\delta \approx 36$ ppm signals, independent of the amount of gold catalyst added, additionally pointing to the incorporation of 2 equiv. of $AuPPh_3$ per carbocycle. Filtering a solution of the unknown intermediate through a plug filled with neutral alumina, which was later found to be contaminated with chloride, resulted in a modified NMR spectrum. The spectroscopic data of this new intermediate suggested close similarities in the vinyl region of the ^{1}H NMR to the previously isolated gold vinyl complexes ($\delta = 5.62$ and 4.97 ppm). The ^{31}P NMR spectrum showed two signals in a 1:1 ratio at $\delta = 43.0$ and 32.1 ppm matching the originally expected gold vinyl intermediate **13** and catalyst precursor Ph_3PAuCl, respectively. Fractional crystallization in diethyl ether at room temperature removed the Ph_3PAuCl, and slow evaporation of a methanol solution of an enriched sample of gold vinyl **13** gave single crystals suitable for X-ray analysis, and confirmed the structure of gold vinyl **13**.

Crystallization of digold **12** proved to be difficult and was never achieved (instead, decomposition products were crystallized; these complexes have already been reported in other studies [119, 120]). The literature precedence for multinuclear gold aryl structures in particular and aurophilic interactions in general as summarized in Sect. 1.1.1 (Grandberg, Nesmeyanov [3–6, 27], and Schmidbaur [30], etc.),[2] suggested that the isolated intermediate was a geminally diaurated vinyl compound, where the second (Ph_3PAu^+ engages the gold vinyl moiety **12** in a bridging three-center-two-electron mode stabilized by Au–Au interaction. The phosphines in such a chiral structure are diastereotopic and account for the inequivalent resonances in the ^{31}P-NMR. Despite the lack of an absolute structural confirmation, this formulation has stood the test of time and multiple investigations.

[2] Fruitful discussions with A. Stephen K. Hashmi should be acknowledged at this point.

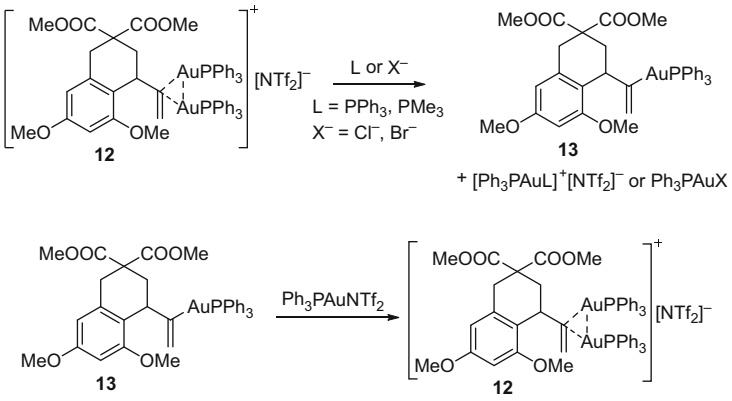

Scheme 11 Interconversion of intermediates **12** and **13**

The isolation of **13** and **12** provided a rare opportunity to study the reactivity of gold-containing reaction intermediates. Paralleling the characteristic digold reactivity established by Nesmeyanov, Grandberg, and Schmidbaur, compound **12** extruded $[Ph_3PAuL]^+$ or Ph_3PAuX and **13** upon reaction with a ligand L or anion X^- which had stronger coordinating ability than **13**, such as phosphines or halides (Scheme 11) [3–6, 30]. Similarly, **13** could be converted to **12** by the addition of $Ph_3PAuNTf_2$, a process that presumably competes favorably with protodeauration under catalytic conditions.

Comparative protodemetalation studies were conducted with **13** and **12** to gain a better understanding of this proposed key step in gold catalysis. Compound **13** readily reacts with stoichiometric quantities of HX (X=OAc, Cl, NTf_2) to yield exclusively **11** and the expected gold(I) by-product Ph_3PAuX ([121, 122]). When only 0.5 equiv. of $HNTf_2$ was added, clean conversion to a mixture of **12** and **11** occurred. Interestingly, the addition of *excess* DTBP•$HNTf_2$ ($pK_a(H_2O) = 4.95$; $pK_a(DMSO) = 0.90$) (for an explanation of the great difference between $pK_a(H_2O)$ and $pK_a(DMSO)$ of DTBP, see [123]) to **13** caused instant conversion to a 1:1 mixture of **12** and **11** (Scheme 12) (Weber and Gagné, unpublished results).

The reactivity of **12** with Brønsted acids differed greatly from that of **13**. Treatment with excess acetic acid ($pK_a = 4.76$) left **12** untouched, while **13** immediately protodeaurated to **11** (Scheme 13). Digold **12** was also unreactive with α-bromo-acetic acid ($pK_a = 2.86$) (for 12 h), and only traces of **11** were observed with excess HTFA ($pK_a = -0.25$). However, complete protodeauration of **12** was observed with the stronger acids $HNTf_2$ and HCl.

To demonstrate that compounds **13** and **12** were viable reaction intermediates, their reactivity was probed with allene **10**. Although **12** and **13** were unreactive with **10**, they could each be activated with $HNTf_2$ to give $Ph_3PAuNTf_2$ (Scheme 14). The subsequent conversion of **10** to **11** indicated that both, **12** and **13** were catalytically competent. Interestingly, monitoring by ^{31}P NMR showed **12** as the catalyst resting state in both reactions (two signals at $\delta \approx 36$ ppm).

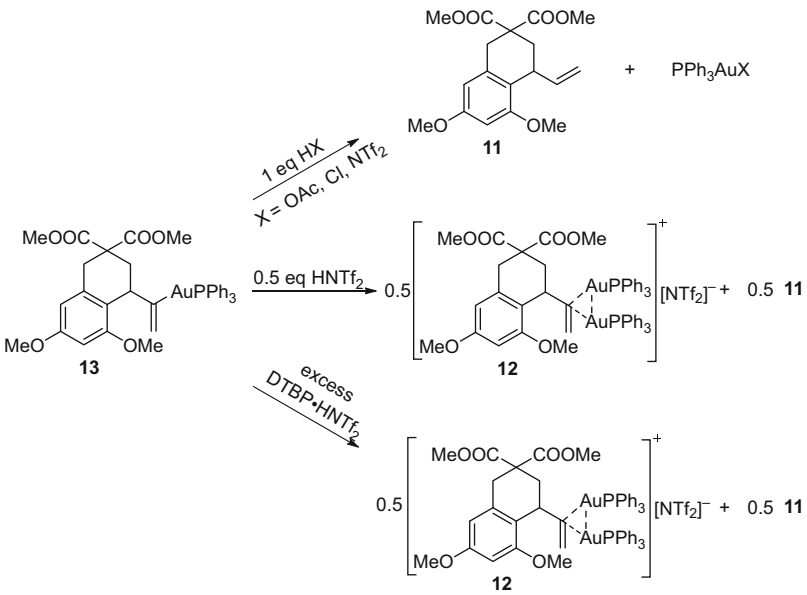

Scheme 12 Reactivity of **13** with Brønsted acids to **11** and/or **12**

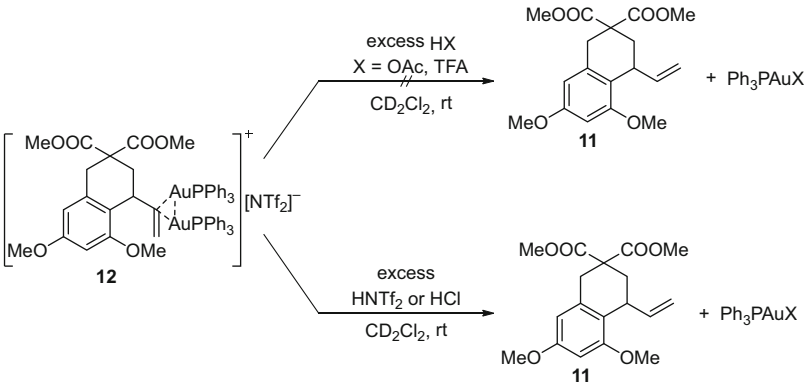

Scheme 13 Reactivity of **12** with Brønsted acids

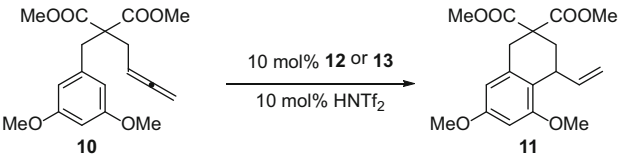

Scheme 14 Activation of intermediates **12** or **13** with $HNTf_2$ to serve as catalysts in the conversion of **10** to **11**

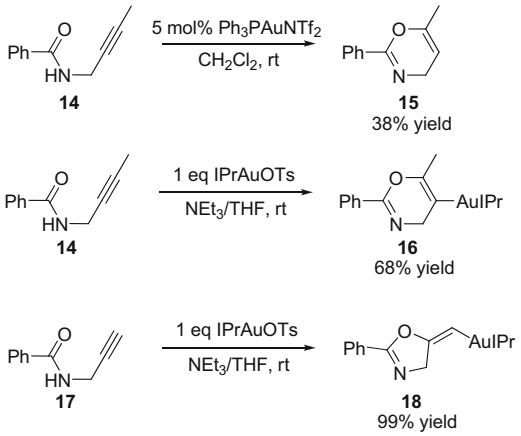

Scheme 15 Isolation of 6-*endo-dig* and 5-*exo-dig* cyclized gold vinyl intermediates **16** and **18**, respectively

These results clearly indicated that complexes **12** and **13** were each viable intermediates in the intramolecular hydroarylation of allenes, which meant that the originally proposed mechanistic scheme was not incorrect, just incomplete, as it now required the addition of an additional digold structure. From experimental work on the isolated intermediates, it is clear that the bridged vinyl **12** is considerably more stable than monogold vinyl **13**, and it appeared to sequester the key Lewis acidic species $[Ph_3PAu]^+$ more quickly than the latter promoted allene activation. Although **12** was less reactive with Brønsted acids than **13**, both could be activated by $HNTf_2$ to generate catalytically active $[Ph_3PAu]^+$. Therefore, the role of **12** was not yet clear under true catalytic conditions.

The third milestone in the isolation of gold vinyl intermediates was reported by Hashmi. While studying the sluggish 6-*endo-dig* cyclization of propargyl amide **14** to the six-membered heterocycle **15** with 5 mol% $Ph_3PAuNTf_2$, only 38% of the desired product was obtained after a long reaction time (6 days, Scheme 15) ([124]; with Nolan's IPrAuOH catalyst 5-*exo-dig* cyclization could be selectively achieved with internal alkynes; see [125]). A closer look at in situ NMR spectra pointed towards the formation of a byproduct whose concentration increased as the catalyst loading increased. Suspecting the formation of a gold vinyl species, the reaction conditions were optimized for its formation. This required changing the gold species, adding NEt_3 as a base, and running the stoichiometric reaction of **14** with IPrAuOTs in THF to allow isolation of the gold vinyl **16** in a 63% yield. Using propargyl amide **17** featuring a terminal alkyne under the same conditions led to 5-*exo-dig* cyclized gold vinyl **18** (99% yield). Upon the addition of aqueous acetonitrile, both isolated gold vinyl species **16** and **18** readily protodemetalated to the corresponding organic product. The isolation of gold vinyl complexes **16** and **18** comprised the first isolation of reaction intermediates from a gold-catalyzed reaction of alkynes [126].

The successful isolation of gold vinyl intermediates by Hammond, Gagné, and Hashmi sparked a general interest in mechanistic studies of gold-catalyzed reactions. Each paper validated gold vinyl intermediates in mechanistic proposals and

described ways to detect, capture, and isolate them. As a result, there has been a surge of reports on isolated gold vinyl and gold alkyl intermediates. These studies have been reviewed elsewhere ([127–129] and references therein).

3 Recent Findings of Aurophilicity in Gold Catalysis and Relevant Model Complexes

The Gagné work provided the first experimental support for the presence of aurophilic interactions in gold(I) catalysis (prior computational work suggested the existence of aurophilic interactions in gold catalysis, but no experimental support was provided [130]), and even though the precise role of this intermediate remained unclear, it demonstrated the necessity of mechanistic studies in gold catalysis and to question the completeness of mechanisms which proposed gold vinyl intermediates and ignored the importance of aurophilic interactions. This section discusses observations of aurophilic and other metallophilic interactions, which stabilize the formation of gold aggregates on hyperconjugated carbon- and heteroatoms. Combining the knowledge of gold catalysis and organogold chemistry has enhanced the complexity of functional catalytic pathways [131, 132] and continued the fascination expressed by Schmidbaur with aurophilicity [62].

First, we review the gold community's growing interest in the geminal diauration of C(sp^2)-atoms. With a greater awareness of the existence of aurophilicity in gold chemistry, several research groups have uncovered their presence in multiple catalytic transformations. Second, the geminal diauration of other X-atoms (X=O, S, Cl, Br, I, N, H) is briefly overviewed, and in a third section, σ-π-diaurated acetylides are presented as there has been a growing number of recent reports in this area, which is also relevant to gold catalysis. This book chapter gives lead references, but it shouldn't be considered as being comprehensive.

3.1 Geminal Diauration of C(sp^2)-Atoms

Shortly after our initial findings on geminally diaurated gold vinyl intermediate **12**, we reported in 2009 that electrophilic $[Ag]^+$ could also compete with $[Ph_3PAu]^+$ to form a hetero geminally dimetalated species **19** (Scheme 16) [133]. In situ observations of catalysis indicated that the actual resting state of the catalyst depended on the silver to gold ratio, with compound **19** being observed as the catalyst resting state under conditions of excess Ag^+, while at low Ag^+ concentrations, the silver free digold resting state **12** dominated.

The structure of **19** was not elucidated, but NMR spectroscopy, mass spectrometry, reactivity data, and comparison to an X-ray structure of a related Au–Ag complex published by Laguna and others pointed to a geminally dimetalated

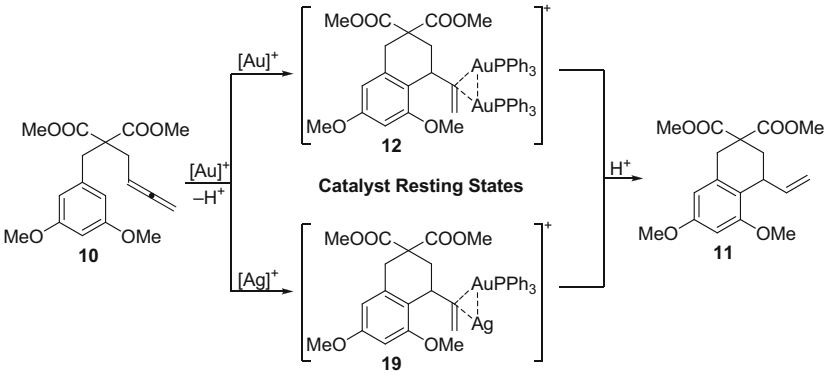

Scheme 16 In the presence of $[Ag]^+$ complex **19** was observed as an alternative catalyst resting state to **12** in the reaction of **10** to **11**

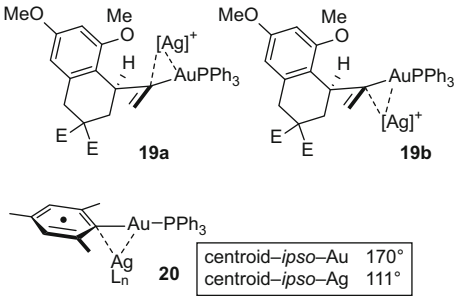

Fig. 2 Structural proposal of **19** based on Laguna's Au–Ag complex **20**

Au–Ag complex where the $[Ag]^+$ binds to the vinyl carbon of a minimally perturbed gold vinyl **13** (Fig. 2). In such a scenario, the three-center-two-electron interaction was not equal and the stronger C–Au bond dominated the structure. Although this new resting state did not affect the reaction outcome, it does retard the reaction kinetics in comparison to the gold-only situation. This study showed that even if the reactants were untouched by $[Ag]^+$, silver ions could still influence gold-catalyzed reactions by intercepting key organogold intermediates to form dinuclear intermediates with their own unique reactivity, which may rationalize so-called $[Ag]^+$ effects in gold catalysis [134, 135].

Supporting the validity of geminally diaurated vinyl species, Fürstner published in 2010 the efficient synthesis of geminally diaurated vinyl complexes from a vinyl borane and $Ph_3PAuNTf_2$, of which two were structurally characterized by X-ray diffraction analysis (Scheme 17) [136]. In compound **21** the two gold atoms are bound symmetrically to the same C-atom. The conceivable alternative mode, wherein only one $[LAu]^+$ fragment was σ-bonded, while the second one engaged in a side-on π-coordination, did not substantially contribute to the ground-state structure of **21**. As a consequence, the former C=C bond of the vinyl borane had

Scheme 17 Synthesis of gem-diaurated complexes **21** and **22** from vinyl boranes $Ph_3PAuNTf_2$

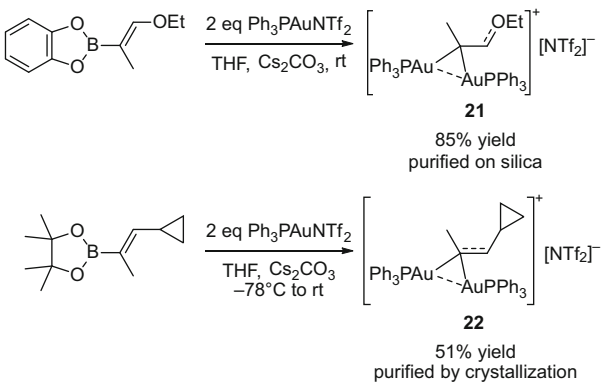

lost much of its double-bond character and confirmed the build-up of considerable charge density at the carbon oxygen bond. In the extreme, this could be interpreted as an oxocarbenium cation flanked by a diaurated sp^3-carbon center. The pattern of the bond lengths in the backbone of **22** was strikingly different, and reflected a C=C double bond which was fairly close to a regular olefin. Hence, complex **22** was more adequately described by a three-center two-electron bonding motif rather than as a cation flanked by a *gem*-dimetalated center, as was the case in **21**. The distinctly different character of **21** and **22** showed that the charge density resulting from the second auration step could either be "kept within" the resulting Au_2C-entity or shifted to an adjacent position if a sufficiently stabilizing heteroelement was present. This surprising modularity in the bonding character suggested that *gem*-diauration might occur in many structural environments of different chemical nature. Informative were observations that monoaurated species could not be obtained, even with an equimolar ratio of any vinyl borane and $Ph_3PAuNTf_2$, consistent with an efficient interception of the gold vinyl by $[Ph_3PAu]^+$. In contrast, the poorer electrophile Ph_3PAuBr led exclusively to the monogold vinyl complexes.

In the same year, Blum studied the kinetic basicity of monogold aryl and vinyl complexes, by competition protodemetalation experiments [137]. The relative rates of protodemetalation spanned approximately 2.2 orders of magnitude, with Hammond vinyl (discussed in Sect. 1.2.2) [82] possessing a very low kinetic basicity. Since geminal diauration and protodemetalation were viewed as competing and mechanistically related processes, this low basicity could explain why the Hammond vinyl does not form geminally diaurated complexes, even in the presence of excess $Ph_3PAuNTf_2$ (Weber and Gagné, unpublished results).

In 2012, Gagné studied the electronic and counterion effects on the geminal diauration of gold aryl complexes as models for the less stable gold vinyls [138]. Using averaging signals in ^1H NMR spectra the equilibrium of digold to monogold complex could be calculated as a function of counterion and aryl ligand (Scheme 18). In addition, the effect of Brønsted acids (protodemetalation) on such mixtures could be investigated as well.

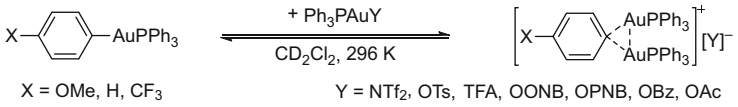

Scheme 18 Counterion and aryl ligand effects were determined in the equilibrium of monogold aryl, Ph_3PAuY, and digold aryl complexes (*TFA* trifluoroacetate, *OONB* *o*-NO_2-benzoate, *OPNB* *p*-NO_2-benzoate)

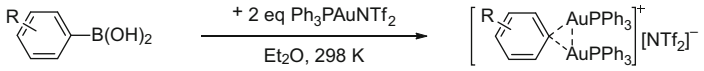

Scheme 19 Synthesis of geminally diaurated arenes from arylboronic acids and $Ph_3PAuNTf_2$

These studies established a number of important reactivity principles of relevance to catalytic activity and speciation: (1) electron-rich aryl (and thus vinyl) ligands had a heightened propensity to form less reactive digold structures, (2) digold formation was more favorable for the less coordinating counterions (which was also influenced by Brønsted acids), and (3) exogenous gold salts could affect the rate of fundamental processes such as protodemetalation even though they did not appear in the balanced equation. Each of these scenarios is commonly encountered in gold(I) catalysis. For example, point (1) explained why the isolable electron-deficient Hammond vinyl rested (and was isolated) in a monomeric form, while the gold vinyl generated by the hydroarylation of allenes rested (and was isolated) in the digold form. These results additionally illuminated the challenges of developing highly efficient multi-step catalysts. To maximize substrate activation, one typically aimed for the least coordinating anions, and while this almost certainly maximized the initiation step of a catalytic cycle, point (2) demonstrated that these more activated $[LAu]^+$ ions were also more apt to intercept gold vinyl intermediates and generate more stable, less reactive, digold intermediates (e.g., for protodemetalation). These results helped provide a rationale for the inevitable search for catalysts which balanced the competing demands of efficiently circumnavigating a catalytic cycle.

Gray reported the general synthesis of *gem*-diaurated aryl species bearing phosphine ligands to enable access to these species for further studies [139]. Optimizing the methodology developed by Fürstner, arylboronic acids efficiently react with an electrophilic (phosphine)gold(I) cation source (2 equiv. of $Ph_3PAuNTf_2$) in ether, producing a series of air- and moisture-stable solids (Scheme 19).

Key was the use of diethyl ether as a solvent, which led to the precipitation of the digold complex, an observation also noted by Grandberg and Nesmeyanov [27]. The isolated solids were stable at room temperature, but decomposed within days in solution. The reaction tolerated a range of boronated substrates. Isolation of these species demonstrated the stability of *gem*-diaurated arenes, and their plausibility as resting states in gold-catalyzed transformations of olefins and alkynes.

In a collaborative effort, Widenhoefer and Gagné studied the mechanism of the intramolecular hydroalkoxylation of hydroxy-allene **23** to vinyl THF **24** in detail,

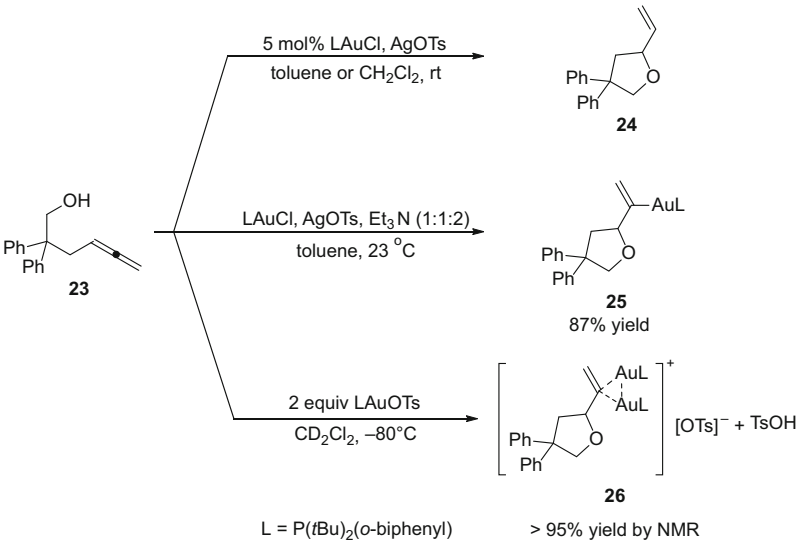

Scheme 20 Isolated gold intermediates **25** and **26** from the intramolecular hydroalkoxylation of allene **23** to vinyl THF **24**

and were able to comment on where digold species fit into the catalytic scheme (Scheme 20) [140]. Lalic reported the observation of a monogold resting state, probably caused by the use of stronger coordinating counteranions [141]. From the stoichiometric reaction of **23** with [(*t*Bu)$_2$(*o*-biphenyl)]PAuOTs formed in situ in the presence of NEt_3 in toluene at r.t., the monogold vinyl **25** was obtained in 87% yield. Full conversion to digold **26** was detected, when the stoichiometric reaction of **23** with 2 equiv. of $Ph_3PAuOTs$ was followed at –80 °C by NMR. Digold **26** was clearly distinguishable from monogold **25** by ^1H and ^{31}P NMR. In catalytic studies, digold **26** was identified as the catalyst resting state, but no single crystals suitable for structural analysis by X-ray diffraction were obtained.

Through kinetic isotope effect (KIE) studies and isotope labeling experiments of gold intermediates in catalysis, an off-cycle role for the digold was determined for the intramolecular hydroalkoxylation of allenes. When isolated monogold vinyl **25** was reacted with AcOH and its isotopomer AcOD at room temperature, a KIE of 3.2 was measured, demonstrating the direct involvement of H^+ in the rate determining step. In contrast, the protodemetalation of digold-vinyl **26** with TsOH or TsOD at 5 °C, revealed a KIE of 0.9, suggesting that digold dissociation was the rate-limiting step in this reaction. When catalytic reactions of **23** and its O-deuterated isotopomer were monitored by ^1H NMR at –20 °C (5 mol% $Ph_3PAuOTs$), a large kinetic isotope effect was revealed (KIE = 5.3), which suggested that protodemetalation of in situ formed monogold was the likely turnover limiting step, despite the digold resting state. These studies further demonstrated that C–O bond formation (electrophilic activation of the allene for

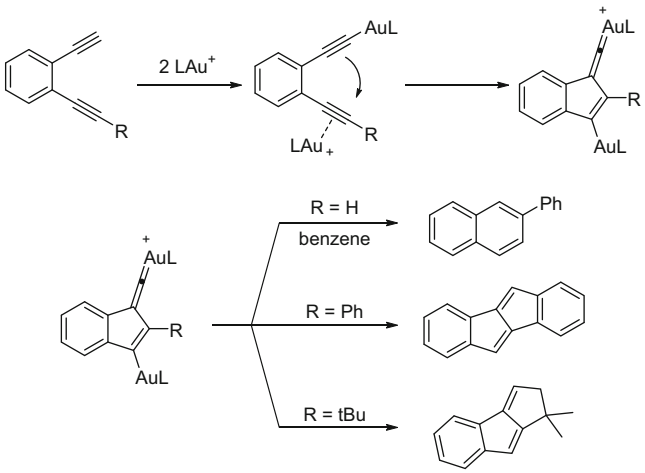

Scheme 21 Dual gold activation of 1,2-dialkynyl benzenes to highly reactive gold vinylidene intermediates, which insert into aromatic and aliphatic C–H bonds

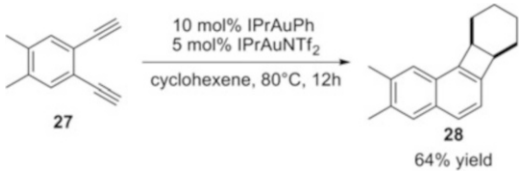

Scheme 22 Gold-catalyzed conversion of a 1,2-dialkynyl **27** with cyclohexene to **28**

nucleophilic attack by the hydroxyl group) was reversible under catalytic conditions, and hence could not be stereochemistry determining (with chiral catalysts).

While studying the reactivity of 1,2-dialkynyl benzenes for possible domino reactions with external nucleophiles, the benefit of dual gold activation catalysis was convincingly demonstrated by Hashmi [142, 143]. After the formation of a σ-gold acetylide complex, which did not require the addition of a base, the second alkyne is activated by a second $[LAu]^+$ unit, cyclization onto which leads to the formation of a highly reactive gold vinylidene intermediate (Scheme 21).

This reactive intermediate is capable of inter- or intramolecular reactions with C(sp^2)–H and C(sp^3)–H bonds to form selectively β-naphthalene derivatives [144], dibenzopentalenes [145], or benzofulvenes ([146]. The synthesis of iodofulvenes was also reported [147]) depending on the substitution pattern of one alkyne. Non-activated double bonds were also suitable reaction partners for the intermediary gold vinylidene as well and yielded cyclobutane derivatives **28** (Scheme 22) [148].

Furthermore, selective γ-C(sp^3)–H activation was reported in a process proposed to proceed via a preferred competing carbene mechanism instead of the gold vinylidene pathway [149, 150]. Via this route, indanothiophenes, dibenzothiophenes, benzofurans, and fluorenothiophenes were accessible (Scheme 23). Stoichiometric experiments gave further mechanistic insight. In all reactions the

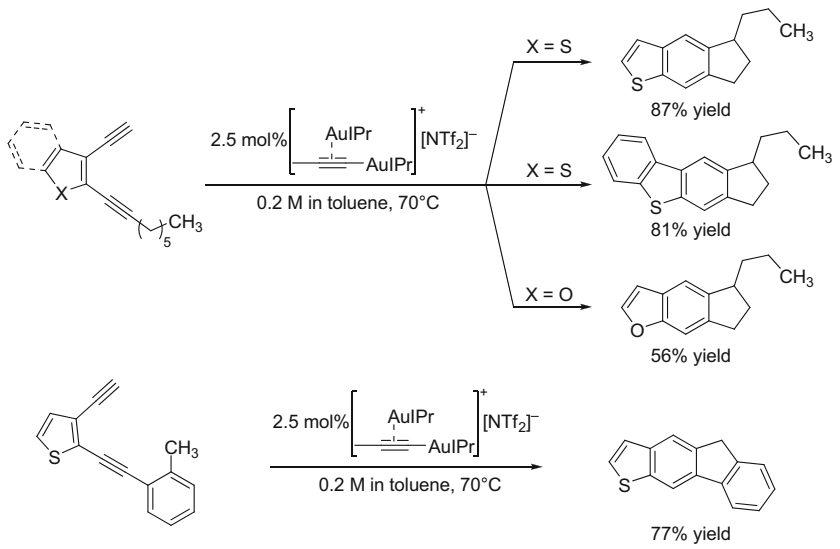

Scheme 23 C–H bond insertion of an intermediary gold carbene stemming from dual gold activation of 1,2-dialkynyl arenes

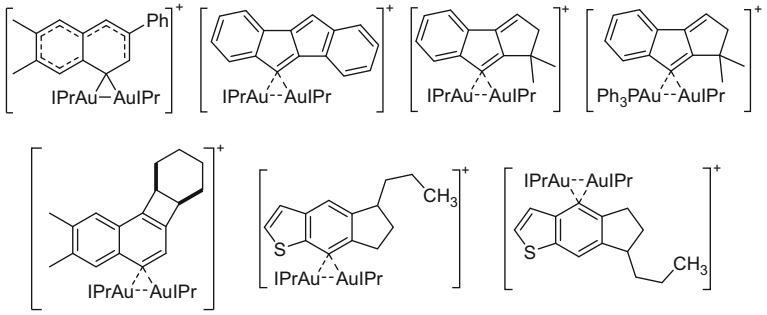

Fig. 3 G*em*-diaurated species obtained from mono-σ-gold acetylides of 1,2-dialkynyl arenes and $LAuNTf_2$ (L=IPr, PPh_3)

treatment of isolated gold acetylide complexes with a stoichiometric amount of $LAuNTf_2$ (L=IPr, PPh_3) resulted in the formation of the corresponding *gem*-diaurated species. Moreover, these species were active catalyst precursors and were also the observable catalyst resting states in dual gold activated transformations (Fig. 3). These studies reported the first *gem*-diaurated species bearing NHC ligands.

Recently, Yu and coworkers developed a new glycosylation protocol with glycosyl *ortho*-alkynylbenzoates as donors and a gold(I) complex as catalyst [151]. The frequent occurrence of anomerization of the glycosyl *ortho*-alkynylbenzoates prompted mechanistic studies ([152]; for recent reports on sugar anomerization, see [153, 154] and references therein), which revealed a propensity of the cationic gold

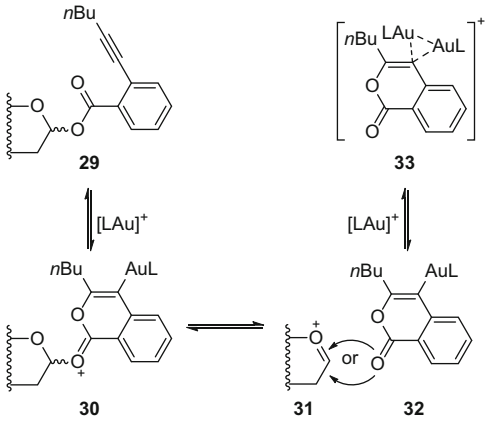

Scheme 24 Reversible fragmentation of glycosyl *ortho*-alkynylbenzoates to mono- and digold vinyl complexes upon exposure to $[LAu]^+$

vinyl intermediate to fragment reversibly and compromise the anomeric center (Scheme 24). This catalyst additionally rests at a digold structure (**33**).

First, $[LAu]^+$ activated the C≡C triple bond of the glycosyl *ortho*-alkynylbenzoate **29** for intramolecular nucleophilic attack of the benzoyl oxygen. The resulting 1-glycosyloxy-isochromenylium-4-gold(I) complex **30** readily converted to the sugar oxocarbenium **31** and isochromen-4-gold(I) complex **32**. Geminally diaurated complex **33** was found to be in equilibrium with monogold vinyl **32**. Reversible nucleophilic addition of **31** and **32** gave rise to an anomeric mixture of vinyl gold(I) glycosyloxypyrylium **30**, which underwent reversible C–O bond formation to give alkyne **29**. Through these steps, the anomerically pure compounds eventually equilibrated to thermodynamic mixtures.

While developing a gold-catalyzed cyclization of 1,6-diyne-4-en-3-ols (such as **34**) to stannylated naphthalene derivatives (such as **35**), which included a stannyl transfer reaction from 2-tributylstannyl furan, Liu and coworkers found that 2-tributylstannyl furan reacted with Echavarren's catalyst $[\{(t\text{Bu})_2(o\text{-biphenyl})\}PAuNCMe]^+[SbF_6]^-$ to a geminally diaurated species (Scheme 25) [155].

The corresponding monogold complex was not observed. Interestingly, compound **36** was also catalytically active. Its formation demonstrated the feasibility of direct tin to cationic gold transmetalations, suggesting that electrophilic $[SnBu_3]^+$ might stem from this reaction, which could intercept the Au–C σ-bond of gold vinyl intermediates and lead to the stannylated final product **35**.

Nolan has illustrated that Gray's methodology failed with the less electrophilic NHC-ligated gold source $IPrAuNTf_2$ ([156]; $IPrAuNTf_2$ was reported by Gagosz [157]). Reaction optimization demonstrated that *gem*-diaurated NHC species were obtained under mild and straightforward reaction conditions in excellent yields when $[(IPrAu)_2(\mu\text{-}OH)]^+[BF_4]^-$ was used in CH_2Cl_2 at r.t. (Scheme 26) [158, 159]. This protocol proved efficient for a wide range of phenyl derivatives bearing EWG, EDG, and sterically demanding substituents, as well as for vinyl and heteroaromatic species. The same conditions were also used to synthesize σ-π-diaurated acetylides from terminal alkynes in high yield.

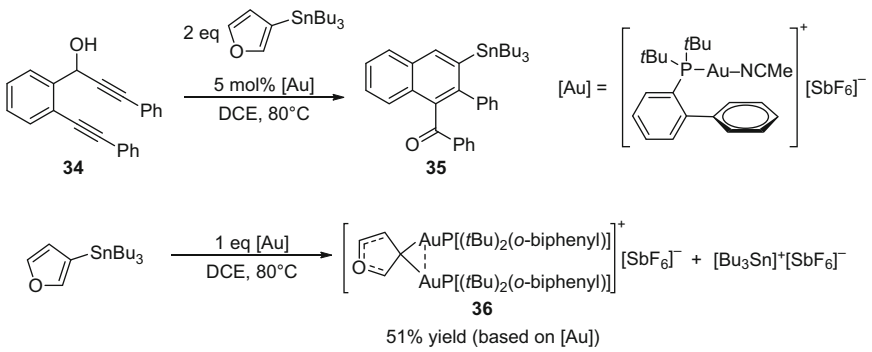

Scheme 25 Tin to gold transmetalation generating gem-diaurated species **36** and $[Bu_3Sn]^+$ as potential tin source for the stannylation of **34** to **35**

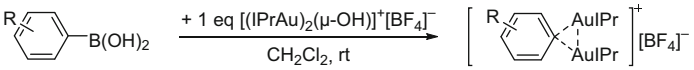

Scheme 26 Synthesis of *gem*-diaurated arenes from arylboronic acids and $[(IPrAu)_2(\mu\text{-}OH)]^+[BF_4]^-$

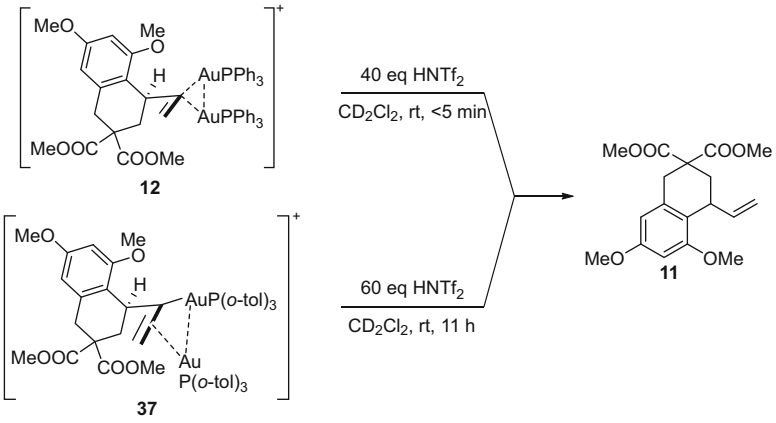

Scheme 27 Distinguishable reactivity of digold intermediate **37** with an alternative σ-π-diauration mode and *gem*-diaurated **12** with the Brønsted acid $HNTf_2$

While investigating the effect of different phosphine ligands in the gold-catalyzed intramolecular hydroarylation of allene **10** to **11**, Gagné reported an X-ray diffraction study of a single crystal of a digold intermediate synthesized from **10** and 2 equiv. of $(o\text{-tolyl})_3PAuNTf_2$ [160]. Instead of the expected geminal diaurated species (observed with PPh_3 as the ligand on cationic gold), σ-π-diauration was discovered as the dominant binding mode, but only with bulky phosphine ligands, such as P(*o*-tolyl)$_3$ or P(mesityl)$_3$ (Scheme 27).

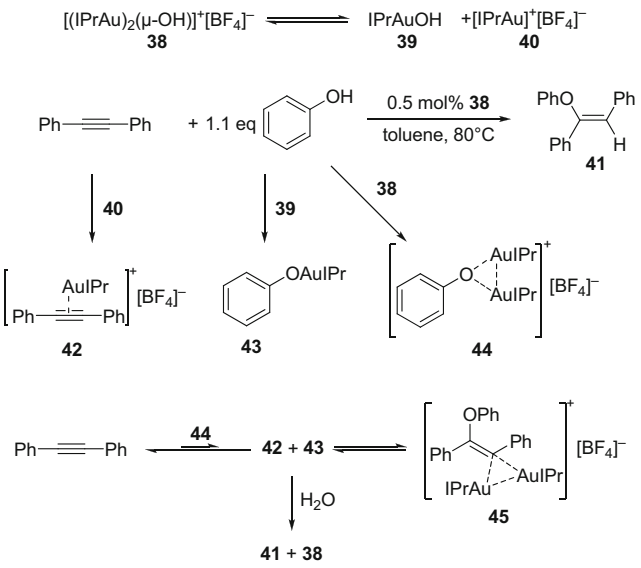

Scheme 28 Concept and detected intermediates in the hydrophenoxylation of 1,2-diphenylethyne

The digold complexes **12** and **37** diverged in their reactivity with the non-coordinating strong acids $HNTf_2$. Reacting **12** with ~40 equiv. of $HNTf_2$ gave complete conversion in less than 5 min to **11**, while complete consumption of **37** (to multiple decomposition products) with ~60 equiv. of $HNTf_2$ took nearly 11 h. This difference in acid sensitivity indicated that the σ-π-binding mode significantly diminished the propensity for protonolysis. The stability of **37** towards Brønsted acids was not entirely unreasonable given the direct engagement of the π-unit in coordinating the second $[(o\text{-}Tol)_3PAu]^+$ unit. Similar observations were reported with σ-π-diaurated acetylide complexes.[3] The uniquely broad and asymmetric signal shapes of the σ-π-structure in the ^{31}P NMR spectrum contrasted the sharp resonances observed with less bulky catalysts, and in addition to the different coupling constants in the ^1H NMR, and their divergent reactivity with excess $HNTf_2$, it was proposed that the σ-π-diaurated structure of **37** was not representative of the binding mode of previously isolated **12**.

Recently, Nolan reported the hydrophenoxylation of 1,2-diphenylethyne using $[(IPrAu)_2(\mu\text{-}OH)]^+[BF_4]^-$ (**38**) as catalyst, leading to the high yield synthesis of various aryl vinyl ethers with good regioselectivities [161]. The dinuclear catalyst **38** was considered to liberate a mixture of a Lewis acidic ($IPrAuBF_4$, **39**) and a Brønsted basic (IPrAuOH, **40**) form of the catalyst, which achieved their enhanced catalytic activity through a cooperative mechanism (Scheme 28).

[3] See reports by Widenhoefer, Hashmi, Corma, and others in Sect. 1.3.3.

Catalyst **39** was proposed to react with phenol to generate gold phenoxide **43** while catalyst **40** served to activate the 1,2-diphenylethyne for nucleophilic attack by **43**, which led to hydrophenoxylated alkyne **41**. Mechanistic investigation under anhydrous conditions suggested that phenol reacted with **38** to form diaurated **44**. In addition, 1,2-diphenylethyne reacted reversibly with **44** to give a mixture of **42** and **43**, which were in equilibrium with the geminally diaurated gold vinyl complex **45**. Attempts to isolate **45** were not successful because once the excess alkyne was removed from the mixture, a new equilibrium between digold phenoxide **44**, 1,2-diphenylethyne, and *gem*-digold complex **45** was established, further supporting the hypothesized equilibrium. Water addition to this mixture led to complete conversion to the final product **41** and catalyst **38**. The role of digold phenoxide **44** and the *gem*-diaurated complex **45** could not be determined in a catalytic setting, but their formation was postulated under anhydrous condition.

Along the same line, Roithova reported a dual gold activation mechanism for the intermolecular methanol addition to 1-phenylpropyne using $[Me_3PAu]^+[SbF_6]^-$ generated in situ (2.5 mol% Me_3PAuCl and 3.0 mol% $AgSbF_6$) as the catalyst [162]. Experimental data suggest that a *gem*-diaurated intermediate was directly formed by $[Me_3PAu]^+$ activation of the C≡C triple-bond for nucleophilic attack by the gold methanolate complex $Me_3PAuOMe$.

Insightful contributions were reported by Maier and Zhdanko in a series of studies on the mechanism of the hydroalkoxylation of alkynes, specifically focusing on the formation and catalytic role of *gem*-diaurated complexes. It was demonstrated that several enol ether derived diaurated species were directly obtained from various cationic gold(I) catalysts and alkynols by using proton sponge as the base (Scheme 29) [163]. Geminally diaurated species were also found to form from the intermolecular hydroalkoxylation of alkynes in methanol when DTBP or proton sponge is present. Bulky ligands (e.g., P[(*t*Bu)$_2$(*o*-biphenyl)]) did not preclude the formation of diaurated species, and alternative gold sources, such as the diaurated oxonium salt $[(LAu)_2(\mu\text{-}OH)]^+$, could also be used. The parallels of the described synthetic route to the *gem*-diaurated complexes to the proposed catalytic method of

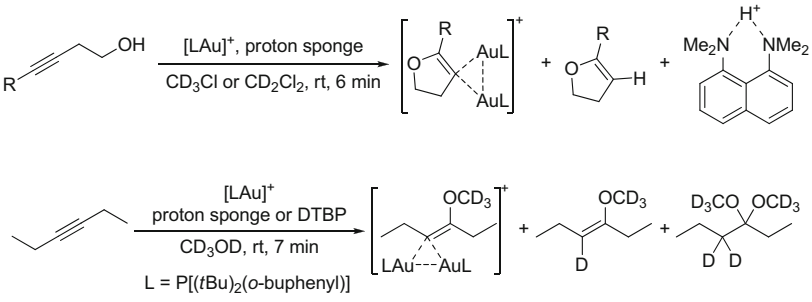

Scheme 29 Synthesis of *gem*-diaurated species from an intra- and intermolecular hydroalkoxylation of alkynes in the presence of a base

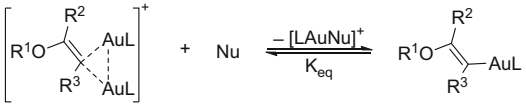

Scheme 30 Determination of stability of *gem*-diaurated species using nucleophiles Nu as competitive $[LAu]^+$ binders

C–O bond formation (with protodemetalative catalytic turnover being arrested with added base) suggested the involvement of such diaurated species in the standard catalytic hydroalkoxylation process.

Several enol ether-derived geminally diaurated complexes were accessible, which prompted Maier to measure quantitatively their stability towards nucleophiles. Using comparative binding data (K_{eq}) which probed the energetics of $[LAu]^+$ binding to the gold enol ether moiety (Scheme 30), it was found that the stability of *gem*-digold complexes was directly influenced by the electronic and steric properties of the enol ether moiety and ligand L ([164]; the binding affinities of nucleophiles was previously determined [165]). In general, electron-rich ligands and electron-donating substituents on the enol ether moiety were beneficial for digold formation unless the steric properties of these groups were prohibitive. Based on the quantitative data, it was estimated that digold complexes with PPh_3 were approximately 1,000 times more stable than with P[(*t*Bu)$_2$(*o*-biphenyl)]. Given the inhibitory effect of diaurated species in catalysis, this provided at least a partial explanation for why catalysts with the JohnPhos ligand outperformed PPh_3 in many hydroalkoxylation reactions.

Perhaps most impressive from this dataset is the realization that the $[LAu]^+$ unit binds to gold vinyl intermediates by a factor of 10^6–10^9 (!) stronger than an alkyne substrate, explaining how thermodynamically favored diauration of monogold vinyl intermediates significantly affects catalysis. It should be noted that enol ether-derived geminally diaurated species were generally more stable than other alkene-derived complexes which lacked the stabilizing oxygen atom, in large part because of the stabilizing contribution of an oxocarbenium resonance structure (see results by Fürstner mentioned above). However, on the flip-side, this also meant that the likelihood of observing *gem*-diaurated intermediates was significantly higher in alkyne hydroalkoxylation reactions than those reactions not generating enol ether-derived gold vinyl intermediates.

Recently, Maier and Zhdanko gained insight into each of the elementary steps of the alkyne hydroalkoxylation catalytic cycle, including the role of *gem*-diaurated species [166]. Through kinetic protonolysis experiments with geminally diaurated complexes, a nucleophile-assisted dissociative pathway was concluded, wherein the nucleophile breaks the digold into a monogold vinyl complex which is subsequently prone to protodemetalating instead of the alternative direct S_E2 pathway (Scheme 31). This conclusion confirmed earlier findings by Widenhoefer and Gagné described above. The authors additionally suggested that fast protodeauration ensured that an equilibrium between digold and monogold was never established, which meant that the conversion of diaurated complexes into vinyl gold species should be considered as an irreversible rate-limiting step.

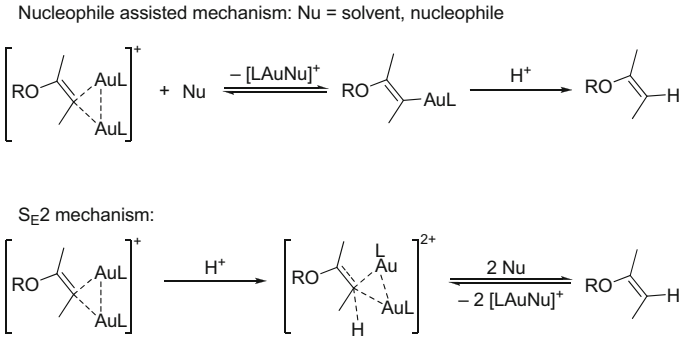

Scheme 31 Possible mechanisms for the protodemetalation of *gem*-diaurated complexes isolated by Maier

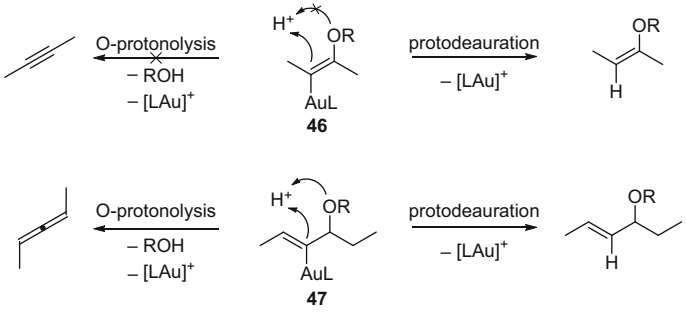

Scheme 32 Rationale for competing O-protonolysis in the protodeauration of gold vinyl complexes **46** and **47**

Studying the reactivity of enol ether-derived monogold vinyl species with acids revealed that these complexes were more susceptible to protodeauration than complexes lacking the enol ether functionality. The conjugate acid of proton sponge in $CDCl_3$ or MeOD was sufficiently acidic to cleave the Au–C σ-bond of these complexes. Surprisingly, immediate protodemetalation was also observed in methanol, unless strong electron-withdrawing groups or adequate π-conjugators (alkene, arene) were installed.

In earlier results, Widenhoefer and Gagné reported cycloreversion (reversible C–O bond formation) of an isolated gold vinyl complex upon exposure to Brønsted acids, which was not the case for Maier's monogold compounds. This difference in behavior was ascribed to the position of the oxygen in the molecule. A strongly stabilizing mesomeric effect of oxygen in Maier's complex **46** makes carbon the preferred site for protonation. Since this conjugation is lacking in **47**, a cyclorevertive oxygen protonation is preferred (Scheme 32).

The catalytic scenario where product-yielding protodeauration of monogold vinyl complexes competes with an unproductive geminal diauration was also

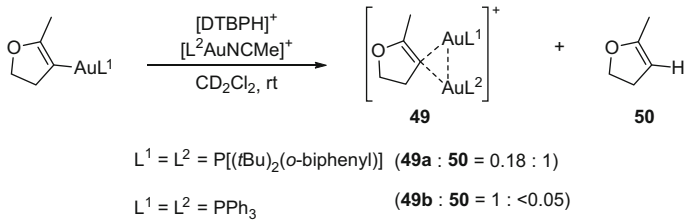

Scheme 33 Competition experiment if gold vinyl complexes with Brønsted acid $[DTBPH]^+$ and gold cation $[LAuNCMe]^+$ to protodemetalated product **50** or *gem*-diaurated complex **49**, respectively

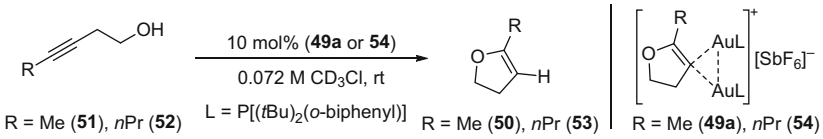

Scheme 34 Cross-over experiments of alkynols **51** or **52** with catalysts **49a** or **54** to **50** or **53**, respectively

mimicked by Maier (Scheme 33). For example, treating a gold vinyl complex with a mixture of $[DTBPH]^+[OTf]^-$ and $[LAuNCMe]^+[SbF_6]^-$ showed that the sterically hindered electron-rich P[(*t*Bu)$_2$(*o*-biphenyl)] ligand favored protodeauration to **50** over geminal diauration to **49a** whereas PPh_3 preferred digold formation to **49b**. It is thus obvious that, with a sufficiently clear mechanistic picture, complex observations can be adequately rationalized, if not used predictively.

Diaurated species were also investigated as suitable catalysts for the intramolecular hydroalkoxylation of alkynes. When alkynes **51** or **52** were reacted with 5 mol% of digold species **54** or **49a**, respectively, sluggish catalytic turnover to **50** or **53** was observed (Scheme 34). These cross-over experiments clearly showed that the geminally diaurated enol ether does not exchange with the one formed in the catalytic transformation. The kinetic isolation of the catalyst precursor indicated that all catalytic activity actually stemmed from traces of free $[LAu]^+$ which consumed all substrate before the new diaurated species could form. When a digold complex with decreased stability and hence faster deauration (in comparison to **49a** or **54**) was used as catalyst, higher catalytic activity was observed. These data point to the diaurated species themselves not being active catalysts, but through a ligand-exchange the deauration process can populate the catalytic cycle with enough free $[LAu]^+$ to turn over the starting material completely.

By monitoring the catalyst resting states (^{31}P and ^1H NMR) three mechanistic scenarios were realized for the gold-catalyzed hydroalkoxylation of alkynes (Scheme 35): (1) immediate and complete conversion of the catalyst precursor to the diaurated resting state, (2) exclusive monogold vinyl resting state, and (3) multiple catalyst resting states, including a *gem*-diaurated species. These scenarios were illustrated by experiments as follows. (1) Alkynol **51** converts to **55** with the catalyst $[Ph_3PAuNCMe]^+[SbF_6]^-$ in CD_3OD, and the formation of the **49b** resting state is

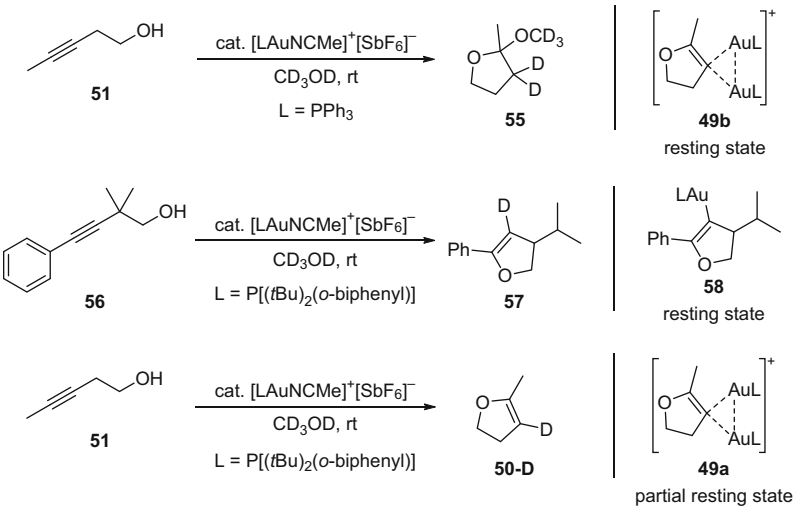

Scheme 35 Different reaction conditions for the observation of complete, partial, or no *gem*-digold resting state

complete and immediate. Because formation of **49b** was accompanied by the generation of an equimolar amount of strong acid ($HSbF_6$), the Brønsted acid catalyzes the conversion of **50** to **55**. (2) When the sterically demanding substrate **56** was combined with bulky catalyst [{(tBu)$_2$(o-biphenyl)}PAuNCMe]$^+$[SbF_6]$^-$, **57** was smoothly formed without any trace of the digold structure; the monogold vinyl **58** is the observed catalyst resting state. (3) When alkynol **51** is cyclized with the bulkier and more basic catalyst [{(tBu)$_2$(o-biphenyl)}PAuNCMe]$^+$[SbF_6]$^-$, an initial kinetic "burst" period ensues for the formation of product **50-D** while the catalyst slowly shifts to the digold resting state **49a**. During the "burst" period, cationic gold [LAu]$^+$ and monogold vinyl were detected and are likely to be responsible for the rapid catalytic rates.

The role of anions was separately investigated by Zhdanko and Maier for this reaction [167]. It was suggested that anion effects during electrophilic activation or protodeauration outweighed effects in digold formation (at least in methanol).

Since our initial observation of a geminally-diaurated resting state in the intramolecular hydroarylation of allenes, these complexes have been detected as intermediates in numerous catalytic processes. It appears that the hyperconjugation of carbon atoms leading to geminally diaurated complexes, a process driven by aurophilicity, is not limited to singular examples or special cases in the literature and should not be considered an anomaly in gold-catalyzed processes. It is clear that they are viable structures in any reaction proceeding via a neutral gold vinyl intermediate, especially when that vinyl group is relatively electron rich. The role of geminally diaurated complexes has been studied in detail for the hydroalkoxylation of alkynes and allenes. Whether lessons learnt from these reactions are generally applicable by the community remains to be evaluated.

3.2 Geminal Diauration of Other Atoms

As this section discusses, geminal diauration is not limited to carbon atoms. Other atoms can be hyperconjugated by $[LAu]^+$ units and cause aggregates to form. A brief overview of leading and recent reports is given with a focus on the activation of gold precatalysts with Ag salts.

In 1979, Uson and coworkers reported the synthesis and isolation of several bridged $[(Ph_3PAu)_2(\mu\text{-}X)]^+[Y]^-$ species where X = Cl, SCN, N_3 with Y = ClO_4, and X = Cl, Br, I, SCN with Y = BF_4. These complexes have a long history in the coordination chemistry of gold (Scheme 36) [168]. The perchlorato complexes were synthesized by reacting equimolar amounts of $[Ph_3PAu]^+[ClO_4]^-$ and Ph_3PAuX (X = Cl, SCN, N_3), while the $[(Ph_3PAu)_2(\mu\text{-}X)]^+[BF_4]^-$ complexes were accessible by the reaction of $AgBF_4$ with 2 equiv. of Ph_3PAuX (X = Cl, Br, I, SCN).

A $[(IPrAu)_2(\mu\text{-}H)]^+[OTf]^-$ species was reported by Tsui [169] in 2008 and was produced by reacting IPrAuH with electrophilic $[IPrAu]^+[OTf]^-$ (Scheme 37). Shortly thereafter, Jean and Le Floch isolated a Xantphos derivative of $[(LAu)_2(\mu\text{-}H)]^+[OTf]^-$ from a reaction of $[LAu]^+[OTf]^-$ with $HSiMe_2Ph$ using their bulky XDPP ligand ([170]; for a similar report, see [171]). Most recently, Widenhoefer reported the formation of $[(LAu)_2(\mu\text{-}H)]^+[BF_4]^-$ with L = P[(*t*Bu)$_2$(*o*-biphenyl)] as a by-product, while studying the reactivity of $HSiEt_3$ with a cationic gold carbenoid which lacked heteroatom stabilization [172].

More recently, Nolan reported two routes to the isolation of $[(IPrAu)_2(\mu\text{-}OH)]^+[Y]^-$ with Y = BF_4, OTf, NTf_2, FABA,[4] and SbF_6 (Scheme 38) [164, 165]. Subjecting a solution of IPrAuOH in benzene to aqueous HBF_4 solution gave rise to $[(IPrAu)_2(\mu\text{-}OH)]^+[BF_4]^-$ after 4 h (90% yield). Alternatively, a suspension of $[IPrAuNCMe]^+[BF_4]^-$ in water directly yielded $[(IPrAu)_2(\mu\text{-}OH)]^+[BF_4]^-$ after 72 h in 96% yield. These complexes were suggested to form readily in water-inclusive gold-catalyzed reactions and were additionally highlighted as being catalyst precursors free of silver and acid [173].

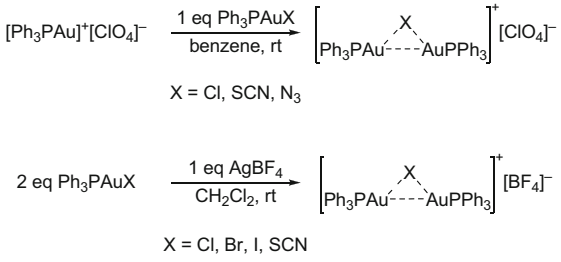

Scheme 36 Synthesis of μ-bridged geminally diaurated complexes stabilized by aurophilic interactions

[4] FABA = tetrakis(pentafluorophenyl)borate.

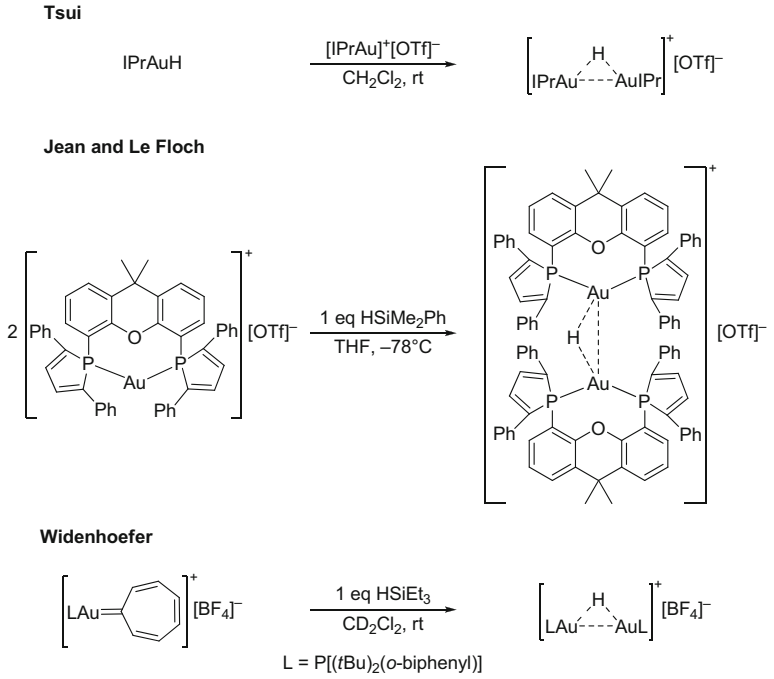

Scheme 37 Synthesis of *gem*-diaurated hydride complexes stabilized by aurophilic interactions

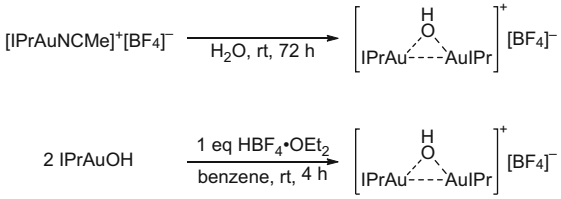

Scheme 38 Synthesis of *gem*-diaurated hydroxide complexes stabilized by aurophilic interactions

The Yu group supported this notion of Nolan as they detected several polynuclear gold hydrates stabilized by aurophilic interactions while studying gold-catalyzed reactions in aqueous media [174]. Several complexes were crystallographically characterized, demonstrating that phosphine-bound $[LAu]^+$ units form O-bridged complexes as well (Fig. 4). Starting from the monogold water $[Ph_3PAuOH_2]^+[OTf]^-$ two tetranuclear complexes and the known trinuclear $[(Ph_3PAu)_3O]^+$ were obtained ([175, 176]; see also [122]). Further reactivity studies of similar complexes $Ph_3PAuNTf_2$, $[LAu\text{-triazole}]^+[SbF_6]^-$ [177], and $[LAuNCMe]^+[SbF_6]^-$ revealed a lower affinity for hydrolysis, while $[Ph_3PAu]^+[BF_4]^-$ and $[Ph_3PAu]^+[SbF_6]^-$ readily hydrolyzed to aggregates (for an additional reference, see [178]).

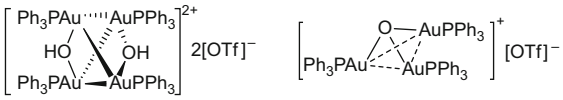

Fig. 4 Crystallographically characterized polynuclear gold hydrates

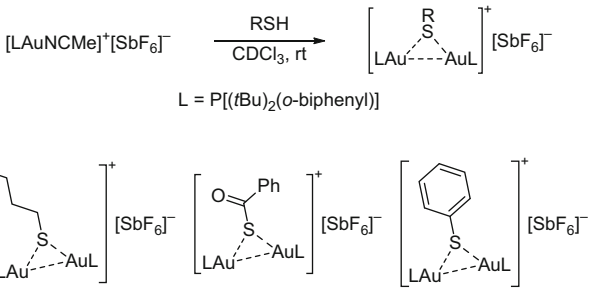

Scheme 39 Synthesis of *gem*-diaurated thiolate complexes stabilized by aurophilic interactions

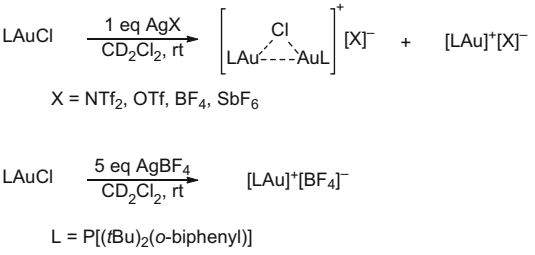

Scheme 40 Isolation of *gem*-diaurated chloride complexes from in situ activation of gold chloride catalyst precursors with silver salts

Sulfur bridged species of the type $[(LAu)_2(\mu\text{-}SR)]^+[SbF_6]^-$ were isolated and structurally characterized by Lee (Scheme 39) [179]. Even though these species were in equilibrium with $[LAu]^+$ and monogold thiolate, the presence of H^+ was required to release enough free $[LAu]^+$ to engage in catalysis, demonstrating that thiols inhibit gold-catalyzed reactions (for more reports of thiolate bridged aggregates see [180–183]).

In 2013, Echavarren reported the surprising isolation of $[(LAu)_2(\mu\text{-}Cl)]^+[Y]^-$ species where weak stabilizing aurophilic interactions were evident (Scheme 40) ([184]. The same complex was reported by Widenhoefer while studying the reactivity of cationic π-complexes [185]. Schmidbaur demonstrated that $[(\{(t\text{Bu})_2(o\text{-biphenyl})\}PAu)_2(\mu\text{-}Cl)]^+[Y]^-$ species dimerized to a tetranuclear adduct, although dissociation back to the monomer was observed in CH_2Cl_2 solution [186, 187]). These complexes were obtained from reactions of $[(t\text{Bu})_2(o\text{-biphenyl})]PAuCl$ precursor and an equimolar amount of AgX ($X = NTf_2$, OTf, BF_4, SbF_6) in CD_2Cl_2. Unless 5 equiv. of AgOTf was used for activation, mixtures of the bridged dimer

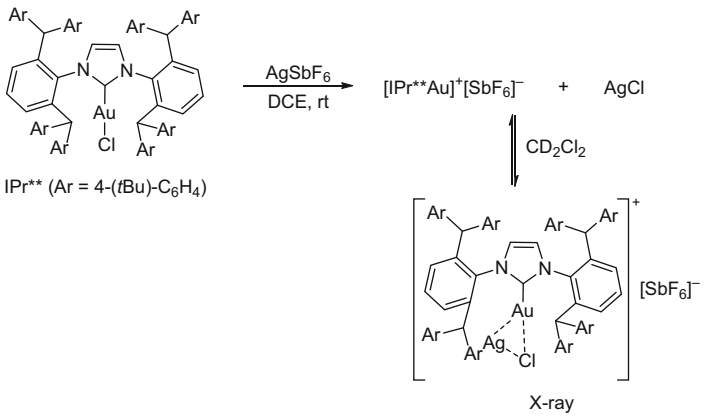

Scheme 41 Isolation of chloride bridged Au–Ag complex

and desired monomer were obtained. The robust chloride-bridged dinuclear gold (I) complexes were demonstrated to be significantly less active in catalysis than cationic complexes $[\{(t\text{Bu})_2(o\text{-biphenyl})\}\text{PAu(NCMe)}]^+[\text{X}]^-$. The order of addition of the silver salt (before or after organic substrate) was illustrated to have a significant effect on reactivity. When the substrate was unable to cleave the chloride bridge efficiently, slower reactions rates and varying yields were observed. Such phenomena could also contribute to so-called "silver effects" in gold catalysis.

Simultaneously, Jones reported the isolation of the same complexes [188]. In addition, a chloride bridged Au_2–Ag aggregate was isolated, pointing towards a non-innocent role of AgCl in the activation process. This role was supported by reports from Straub when a mixed Au–Ag complex featuring auroargentophilic interactions was isolated (Scheme 41) [189]. Activating the super-bulky IPr**AuCl complex with $AgSbF_6$ in DCE gave rise to a mixture of $[\text{IPr**Au}]^+[SbF_6]^-$ and AgCl, which was in equilibrium with chloro-bridged $[(\text{IPr**Au})\text{Ag}(\mu\text{-Cl})]^+[SbF_6]^-$.

3.3 σ-π-Diauration of Acetylenes

In this section the facile formation σ-π-diaurated acetylides from terminal alkynes is presented. These complexes form under catalytic and stoichiometric conditions with the help of aurophilic stabilization.

When Russell studied the synthesis of cationic η^2-complexes of gold [190, 191], it was reported that alkyne **59** reacted with $[(t\text{Bu})_3\text{PAu}]^+[SbF_6]^-$ depending on the reaction time either to the desired complex **60** or to a surprising dicationic trinuclear π-species **61** (Scheme 42) ([192]; for another report of aggregated σ-π-diaurated complexes, see [193]). The formation of the dicationic complex **61** was rationalized as follows. The electropositive silicon atom in complex **60** facilitates an η^2 to η^1 slippage of the gold fragment towards the $\equiv\text{CSiMe}_3$ carbon, which enhances its

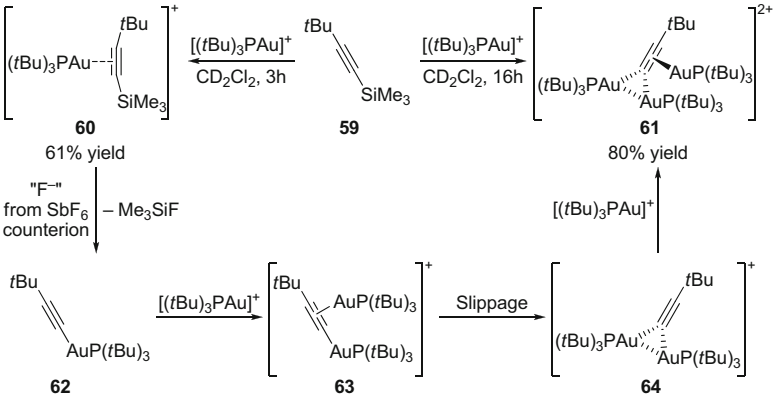

Scheme 42 Route towards the unexpected isolation of dicationic trinuclear gold complex **61**

susceptibility towards nucleophilic attack by adventitious F^- which stems from the counteranion decomposition (similar reactivity of $Me_3Si–C{\equiv}C–Ph$ has been reported [194]). The resulting neutral σ-acetylide complex **62** then coordinates a second gold unit to its π-system to yield σ-π-diaurated acetylide **63**. The X-ray structure of **63** suggested that the bridging gold cation was slipped by 15% towards the acetylide carbon carrying the σ-bonded gold unit (probably caused by aurophilicity). Additional slippage in the same direction led to the geminally diaurated intermediate **64**, which π-coordinates an additional $[(tBu)_3PAu]^+$ unit to form the observed product **61**. Interestingly, a solution of complex **61** gave only one singlet at $\delta = 100$ ppm (^{31}P NMR), suggesting either a rather different solution structure or one that rapidly exchanges the terminal and bridging gold units.

Shortly after, Corma and Leyva-Pérez reported a σ-π-bisfunctionalization of terminal alkynes using $[(tBu)_3PAu]^+[NTf_2]^-$ as a catalyst, suggesting an intermediary role of η^1,η^2-digold complexes in catalysis [195]. These catalytic implications were supported in a separate study by the isolation of σ-π-diaurated species, which could also be used as catalysts for the intermolecular [2 + 2] cycloaddition of phenylacetylene **65** and α-methyl-styrene **66** to cyclobutene **67** (Scheme 43) [196, 197]. For the general use of σ-π-diaurated species as gold catalysts, see [198]. Using P[$(tBu)_2$(*o*-biphenyl)] and other bulky Buchwald type-ligands on gold, σ-π-diaurated complexes of phenylacetylene such as **70** were accessible. When isolated **70** was used as catalyst, **67** was obtained as the major product. In contrast, employment of $[\{(tBu)_2(o\text{-biphenyl})\}PAuNCMe]^+[SbF_6]^-$ led to significant amounts of undesired acid derived products (**68** and **69**), as σ-π-diauration to **70** was accompanied by strong acid formation ($HSbF_6$).

Parallel reports by Widenhoefer showed that $[IPrAu]^+[SbF_6]^-$ generated in situ reacts with **65** to form a thermally unstable non-isolable cationic η^2-complex **71** at low temperatures (–60 °C) (Scheme 44) [199]. Raising the temperature of the solution of **71** to 0 °C led to exclusive decomposition to a σ-π-diaurated acetylide complex **72** matching Bertrand's observation that π-bound gold-units could migrate

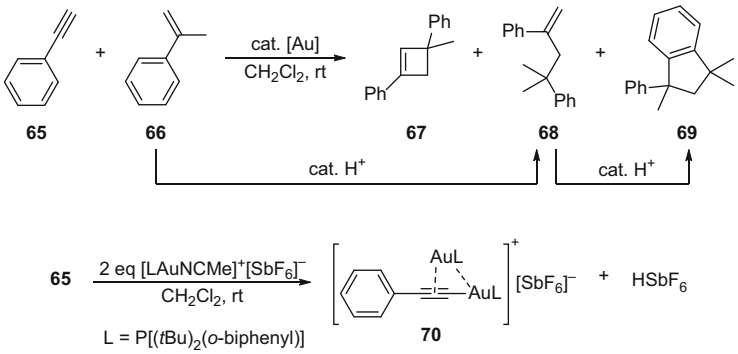

Scheme 43 Detection of σ-π-diaurated intermediate **70** in the conversion of alkyne **65** and styrene **66** to cyclobutene **67**

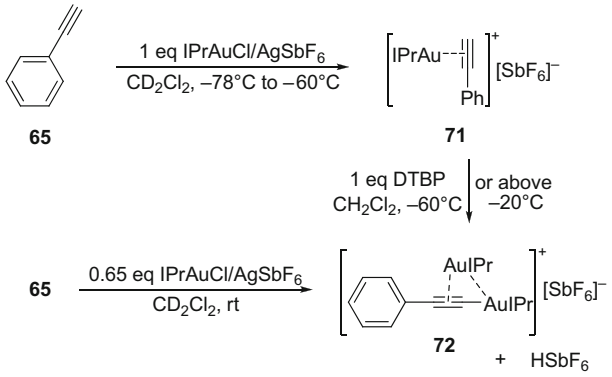

Scheme 44 Pathways to σ-π-diaurated complex **72**

to σ connectivity [200]. This π-σ-migration of **71** to **72** was facilitated by the addition of DTBP, which enabled the reaction to proceed at –60 °C.

Alternatively, the direct synthesis of **72** was achieved from the reaction of IPrAuCl, $AgSbF_6$, and **65** in a 0.65:0.65:1 ratio, respectively, at room temperature. Although the $[IPrAu]^+$ fragments of complex **72** resided in nonequivalent environments, the room-temperature ^1H and ^{13}C NMR spectra displayed resonances corresponding to a single type of $[IPrAu]^+$ group which neither broadened nor resolved at −60 °C. These observations pointed to facile σ-π-interconversion of the two chemically inequivalent $[IPrAu]^+$ groups on the NMR time scale, probably proceeding via a symmetric *gem*-digold complex in which both gold atoms were bound symmetrically to the terminal acetylenic carbon, a three-center two-electron bond stabilized by aurophilic interactions. The facile formation of **72** in the absence of a base had to be accompanied by the generation of the strong Brønsted acid $HSbF_6$. These results not only suggested an intermediary role of σ-π-diaurated

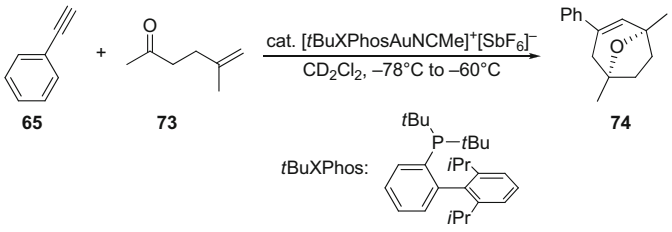

Scheme 45 [2+2+2] Cycloaddition of terminal alkynes and oxoalkenes to 8-oxabicyclo[3.2.1] oct-3-ene **74**

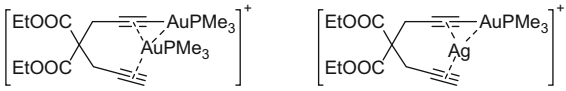

Fig. 5 Examples of calculated structures of digold and Au–Ag acetylide complexes of dialkynes

acetylide complexes in gold-catalyzed transformations involving terminal alkynes, but also pointed towards the appropriate consideration of Brønsted acid involvement in catalysis.

An off-cycle role of σ-π-diaurated species was proposed by Fensterbank, Gandon, and Gimbert in their experimental and computational study of the cycloisomerization of 1,6-enynes. It was confirmed that gold acetylides had a high affinity for a second gold complexation, but both species appeared to be non-reactive in the catalytic cycle and were not directly responsible for the formation of geminally diaurated complexes in this reaction [201].

Echavarren came to similar conclusions while pursuing initial mechanistic studies on the [2 + 2 + 2] cycloaddition of terminal alkyne **65** and oxoalkene **73** to 8-oxabicyclo[3.2.1]oct-3-ene **74**. Although σ-π-diaurated species was detected in the reaction mixture (Scheme 45) [202], this digold species operated outside the main catalytic cycle, and served to lower the concentration of the active species $[LAu]^+$ and to explain the rather long reaction times (this off-cycle role was also proposed in the [2 + 2] cycloaddition of alkynes with alkenes [203]). Competitive Brønsted acid catalysis for the activation of the alkyne and the oxoalkene was also observed, since the formation of σ-π-diaurated acetylides generally generated in situ an equimolar amount of strong acid $HSbF_6$.

The higher affinity of cationic gold and silver ions for σ-acetylides over non-coordinated C≡C triple bonds was further supported by Roithova [204]. Computational studies concluded that the affinity of $[Me_3PAu]^+$ to the C≡C triple bond of a gold acetylide was 0.5 eV higher than to the triple bond of a nonactivated alkyne. This energy difference was attributed to a higher electron density in the triple bond of the gold acetylide and also partially because of the aurophilic stabilization between the gold cations. Structural analysis showed that gold(I) and silver(I) cations bound in diynes in preference to the π-face of a σ-gold acetylide complex while the second triple bond was loosely coordinated to the π-coordinating metal cation (Fig. 5). Cationic gold units exchanged in gold-only complexes, but in

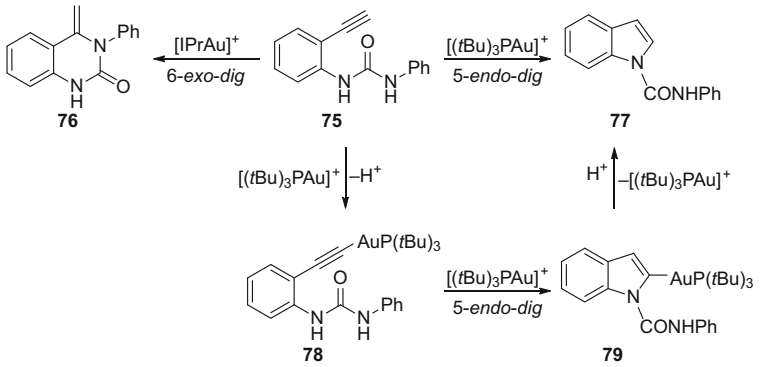

Scheme 46 Selectivity switch in the gold-catalyzed cyclization of **75** by gold activation modes of terminal alkynes

mixed Au–Ag complexes the gold cation always σ-coordinated the acetylide and the silver cation was sandwiched between the π-faces of both triple bonds.

The complexation of metal cations had consequences for electrophilic catalysis. Mulliken population analysis revealed that coordination of one gold cation to a non-activated C≡C triple bond favorably activated the given triple bond toward nucleophilic addition. On the other hand, both carbon atoms of the triple bond in diaurated and mixed silver–gold complexes bear negative charges, which deactivate the studied alkynes toward nucleophilic additions.

Hashmi's results on dual gold activation of terminal alkynes involving σ-π-diaurated acetylides are already mentioned in Sect. 1.3.1. Highly reactive carbene and vinylidene intermediates were described, which activate C–H bonds and eventually formed geminally diaurated intermediates, which were accessible by stoichiometric experiments. Most importantly, because of dual gold activation of terminal alkynes, unexpected reaction pathways were achieved which were inexplicable with traditional π-activation mechanisms.

Similar findings were also reported by Medio-Simón when studying the gold(I)-catalyzed heterocyclization of 1-(*o*-ethynylaryl)urea **75** (Scheme 46) [205]. Employment of $IPrAuSbF_6$ led to exclusive 6-*exo-dig* (Markovnikov) cyclization to **76**, but with $(t\text{Bu})_3PAuSbF_6$ 5-*endo-dig* (anti-Markovnikov) product **77** was major. This switch in selectivity is rooted in the activation mode of the terminal alkyne, either via the π-face only or σ and π-sites combined via **78**, respectively. In this reaction, no *gem*-diaurated intermediate was detected. Instead, the observation of monogold vinyl complex **79** suggested that dual activation and *gem*-diauration are not necessarily connected. It should be noted that a polyaurated trigold species was also proposed based on MALDI experiments, but the catalytic role and structure of this complex was not identified.

4 Conclusion

Multiple examples of di- and polyaurated gold complexes stabilized by attractive Au–Au interactions have now been reported in stoichiometric and catalytic reactions. Aurophilicity is clearly ubiquitous in gold chemistry, and its subsequent applications in gold catalysis. Specifically, the intermediacy of geminally and/or σ-π-diaurated complexes has been demonstrated, but several lines of data suggest that geminally diaurated species may operate off-cycle and are not directly involved in product yielding steps of the catalytic cycle, i.e., they form a catalyst reservoir. The picture looks different with the σ-π-diauration of alkynes. While some complexes were reported to operate off-cycle, other studies demonstrated an on-cycle role for dual σ-π-activation which significantly affected the reaction outcome.

The complexity that aurophilicity creates in gold catalysis is diagrammed in Scheme 47 (counteranion free). Its influence in the catalyst activation step is considerable. When silver salts are used for catalyst activation, auroargentophilic stabilization may be facilitated by the formation of a bridging $[LAu\text{-}(\mu\text{-}Cl)\text{-}Ag]^+$ complex. If this species is exceptionally stable it may impede the activation and result in the incomplete conversion to $[LAu]^+$. Gold-only activation processes can

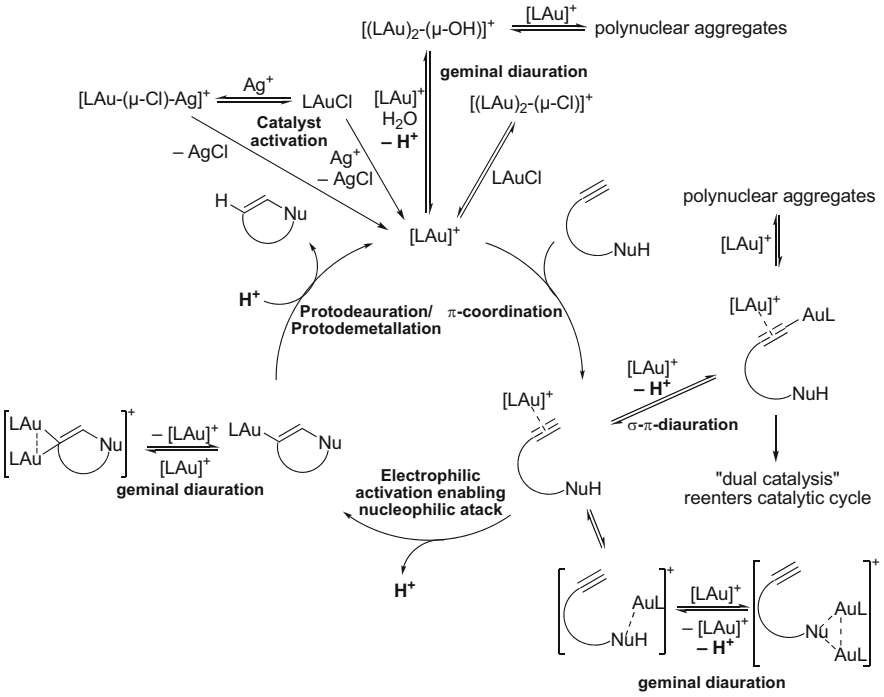

Scheme 47 Potential catalytic scenarios in gold-catalyzed reactions as a result of aurophilic interactions

also sequester the needed $[LAu]^+$. For example, in the presence of adventitious water, geminal diauration to $[(LAu)_2\text{-}(\mu\text{-}OH)]^+$ has been demonstrated, and when these species are prone to the formation of aggregates of higher order, even more active $[LAu]^+$ is consumed. Likewise, the LAuCl precatalyst may be converted with cationic gold $[LAu]^+$ to the bridged chloride species $[(LAu)_2\text{-}(\mu\text{-}Cl)]^+$ via geminal diauration of Cl. The addition of an organic substrate, especially terminal alkynes, may cause further aggregations to occur. In these cases, π-coordination enhances the acidity of the alkynic proton, which may be released by coordination of a second $[LAu]^+$ unit to σ-π-diauration. This complex may either form higher aggregates, trapping more $[LAu]^+$, or engage in beneficial dual gold activation catalysis. Alternatively, organic substrates may bind cationic gold on its nucleophilic site, which often consist of heteroatoms. Addition of a second $[LAu]^+$ unit leads to geminal diauration to an $[(LAu)_2\text{-}(\mu\text{-}Nu)]^+$ species and a proton. This further reduces the concentration of active $[LAu]^+$ and increases the overall Brønsted acidity of the reaction mixture.

Once the organic substrate has been activated by cationic gold for nucleophilic attack, a neutral gold vinyl complex is formed, accompanied by the release of a proton. This proton may reenter the cycle by protodemetalating the neutral gold vinyl, but the competing affinity of this complex towards $[LAu]^+$ may instead lead to the formation of a cationic geminally diaurated gold vinyl, again reducing the effective concentration of $[LAu]^+$ in solution.

Assuming that geminally and σ-π-diaurated complexes suffer from lower catalytic activity and operate off-cycle (unless σ-π-dual gold catalysis engages a different catalytic cycle), the effective concentration of the most active $[LAu]^+$ catalyst is generally lowered by the action of aurophilic interactions. Moreover, when the substrate is a terminal alkyne, aurophilicity additionally enhances the acidity of the reaction solution, which of course may be detrimental or beneficial depending on the situation.

At this time, it can be concluded that aurophilicity in gold catalysis has led to more negative effects than positive, and that gold-catalyzed processes could be more efficient if aurophilic interactions could be disabled. However, the emerging field of dual gold catalysis and recent reports of highly active small gold clusters as catalysts [206, 207], which are obtained from conventional gold complexes, demonstrate that under certain circumstances the advantages of aurophilicity may outweigh the disadvantages. The challenge and the opportunity for the gold catalysis community is thus to optimize catalyst design by either mitigating the negative effects of aurophilicity or channeling the positive effects to create new reactivity. The journey will be fruitful for the well informed.

References

1. Armer B, Schmidbaur H (1970) Angew Chem Int Ed 9:101
2. Schmidbaur H (1976) Angew Chem Int Ed 15:728
3. Nesmeyanov AN, Perevalova EG, Grandberg KI, Lemenovskii DA (1974) Izv Akad Nauk SSSR Ser Khim 5:1124
4. Grandberg KI (1982) Russ Chem Rev 51:249
5. Baukova TV, Dyadchenko VP, Oleinikova NA, Lemenovskii DA, Kuzmina LG (1994) Russ Chem Bull 43:1063
6. Grandberg KI, Dyadchenko VP (1994) J Organomet Chem 474:1
7. Puddephatt RJ (1978) The chemistry of gold. Elsevier, Amsterdam
8. Puddephatt RJ (1977) Gold Bull 10:108
9. Puddephatt RJ (2008) Chem Soc Rev 37:2012
10. Schmidbaur H (ed) (1999) Gold: progress in chemistry, biochemistry and technology. Wiley, Chichester
11. Schmidbaur H (2008) Chem Soc Rev 37:1931
12. Tamaki A, Kochi JK (1972) J Organomet Chem 40:C81
13. Tamaki A, Kochi JK (1973) J Chem Soc Dalton Trans 2620
14. Tamaki A, Kochi JK (1973) J Am Chem Soc 95:6487
15. Tamaki A, Kochi JK (1973) J Organomet Chem 61:441
16. Tamaki A, Magennis SA, Kochi JK (1974) J Am Chem Soc 96:6140
17. Tamaki A, Kochi JK (1974) J Organomet Chem 64:411
18. Gimeno MC (2008) In: Laguna A (ed) Modern supramolecular gold chemistry: gold-metal interactions and applications, chapter 1. Wiley, Weinheim
19. Bardají M, Laguna A (2003) Eur J Inorg Chem 17:3069
20. Melník M, Parish RV (1986) Coord Chem Rev 70:157
21. Jones PG (1986) Gold Bull 19:46
22. Abel EW, Jenkins CR (1968) J Organomet Chem 14:285
23. Osawa M, Hoshino M, Hashizume D (2008) Dalton Trans 2248
24. Schmidbaur H (1975) Acc Chem Res 8:62
25. Schmidbaur H (1995) Chem Soc Rev 24:391
26. Doerrer LH (2008) Comments Inorg Chem 29:93
27. Nesmeyanov AN, Perevalova EG, Grandberg KI, Lemenovskii DA, Baukova TV, Afanassowa OB (1974) J Organomet Chem 65:131
28. Nesmeyanov AN, Perevalova EG, Struchkov YT, Antipin MY, Grandberg KI, Dyadchenko VP (1980) J Organomet Chem 201:343
29. Scherbaum F, Grohmann A, Huber B, Krüger C, Schmidbaur H (1988) Angew Chem Int Ed 27:1544
30. Porter KA, Schier A, Schmidbaur H (2003) Organometallics 22:4922
31. Nesmeyanov AN, Perevalova EG, Krivykh VV, Kosina AN, Grandberg KI, Smyslova EI (1972) Russ Chem Bull 21:618
32. Grandberg KI, Smyslova EI, Kosina AN (1973) Izv Akad Nauk SSSR Ser Khim 12:2787
33. Negishi E-I (2010) Nobel Lectures 151
34. Suzuki A (2010) Nobel Lectures 206
35. Wegner HA, Auzias M (2011) Angew Chem Int Ed 50:8236
36. Wegner HA (2009) Chimia 63:44
37. Garcia P, Malacria M, Aubert C, Gandon V, Fensterbank L (2010) Chem Cat Chem 2:493
38. Klatt G, Xu R, Pernpointner M, Molinari L, Hung TQ, Rominger F, Hashmi ASK, Köppel H (2013) Chem Eur J 19:3954
39. Roth KE, Blum SA (2011) Organometallics 30:4811
40. Zuzek AA, Reynolds SC, Glueck DS, Golen JA, Rheingold AL (2011) Organometallics 30:1812
41. Mankad NP, Toste FD (2012) Chem Sci 3:72

42. Komiya S, Albright TA, Hoffmann R, Kochi JK (1976) J Am Chem Soc 98:7255
43. Schuster O, Liau R-Y, Schier A, Schmidbaur H (2005) Inorg Chim Acta 358:1429
44. Hashmi ASK, Ramamurthi TD, Rominger F (2009) J Organomet Chem 694:592
45. Partyka DV, Zeller M, Hunter AD, Gray TG (2006) Angew Chem Int Ed 45:8188
46. Contel M, Stol M, Casado MA, van Klink GPM, Ellis DD, Spek AL, van Koten G (2002) Organometallics 21:4556
47. Hirner JJ, Shi Y, Blum SA (2011) Acc Chem Res 44:603
48. Hashmi ASK, Lothschütz C, Döpp R, Ackermann M, de Buck Becker J, Rudolph M, Scholz C, Rominger F (2012) Adv Synth Catal 354:133
49. Peña-López M, Sarandeses LA, Sestelo JP (2013) Eur J Org Chem 2545
50. Al-Amin M, Roth KE, Blum SA (2014) ACS Catal 4:622
51. Hirner JJ, Roth KE, Shi Y, Blum SA (2012) Organometallics 31:6843
52. Shi Y, Roth KE, Ramgren SD, Blum SA (2009) J Am Chem Soc 131:18022
53. Ciu L, Zhang G, Zhang L (2009) Bioorg Med Chem Lett 19:3884
54. Zhang G, Peng Y, Ciu L, Zhang L (2009) Angew Chem Int Ed 48:3112
55. Zhang G, Ciu L, Wang Y, Zhang L (2010) J Am Chem Soc 132:144
56. Noey EL, Luo Y, Zhang L, Houk KN (2012) J Am Chem Soc 134:1078
57. Hopkinson MN, Gee AD, Gouverneur V (2011) Chem Eur J 17:8248
58. Ball LT, Lloyd-Jones GC, Russell CA (2014) J Am Chem Soc 136:254
59. Ball LT, Lloyd-Jones GC, Russell CA (2012) Science 337:1644
60. Wolf WJ, Winston MS, Toste FD (2013) Nat Chem 6:159
61. Leyva-Pérez A, Corma A (2012) Angew Chem Int Ed 51:614
62. Schmidbaur H, Schier A (2012) Chem Soc Rev 41:370
63. Zuccaccia D, Belpassi L, Macchioni A, Tarantelli F (2013) Eur J Inorg Chem 4121
64. Gorin DJ, Toste FD (2007) Nature 446:395
65. Fürstner A, Davies PW (2007) Angew Chem Int Ed 46:3410
66. Krause N, Winter C (2011) Chem Rev 111:1994
67. Corma A, Leyva-Pérez A, Sabater MJ (2011) Chem Rev 111:1657
68. Boorman TC, Larrosa I (2011) Chem Soc Rev 40:1910
69. Aubert C, Fensterbank L, Garcia P, Malacria M, Simonneau A (2011) Chem Rev 111:1954
70. Bandini M (2011) Chem Soc Rev 40:1358
71. Pradal A, Toullec PY, Michelet V (2011) Synthesis 1501
72. Rudolph M, Hashmi ASK (2011) Chem Commun 47:6536
73. Sengupta S, Shi X (2010) Chem Cat Chem 2:609
74. Fürstner A (2009) Chem Soc Rev 38:3208
75. Li Z, Brouwer C, He C (2008) Chem Rev 108:3239
76. Widenhoefer RA (2008) Chem Eur J 14:5382
77. Hashmi ASK, Rudolph M (2008) Chem Soc Rev 37:1766
78. Jiménez-Núñez E, Echavarren AM (2008) Chem Rev 108:3326
79. Arcadi A (2008) Chem Rev 108:3366
80. Hashmi ASK, Hutchings GJ (2006) Angew Chem Int Ed 45:7896
81. Obradors C, Echavarren AM (2014) Chem Commun 50:16
82. Liu L, Xu B, Mashuta MS, Hammond GB (2008) J Am Chem Soc 130:17642
83. Zhdanko A, Maier ME (2014) Angew Chem Int Ed 43:7760
84. Joost M, Estevez L, Mallet-Ladeira S, Miqueu K, Amgoune A, Bourissou D (2014) J Am Chem Soc 136:10373
85. Obradors C, Echavarren AM (2014) Acc Chem Res 47:902
86. Solorio-Alvarado CR, Echavarren AM (2010) J Am Chem Soc 132:11881
87. Solorio-Alvarado CR, Wang Y, Echavarren AM (2011) J Am Chem Soc 133:11952
88. Lebœuf D, Gaydou M, Wang Y, Echavarren AM (2014) Org Chem Front 1:759
89. Hussong MW, Rominger F, Krämer P, Straub BF (2014) Angew Chem Int Ed 53:9372
90. Seidel G, Fürstner A (2014) Angew Chem Int Ed 53:4807
91. Han X, Widenhoefer RA (2006) Angew Chem Int Ed 45:1747

92. Zhang Z, Liu C, Kinder RE, Han X, Qian H, Widenhoefer RA (2006) J Am Chem Soc 128:9066
93. Jimenez-Nunez E, Echavarren AM (2008) Chem Rev 108:3326
94. Mauleón P, Zeldin RM, González AZ, Toste FD (2009) J Am Chem Soc 131:6348
95. Shapiro N, Toste FD (2010) Synlett 5:675
96. López F, Mascareñas JL (2011) Beilstein J Org Chem 7:1075
97. Mauleón P, Krinsky JL, Toste FD (2009) J Am Chem Soc 131:4513
98. Shen HC (2008) Tetrahedron 64:3885
99. Shen HC (2008) Tetrahedron 64:7847
100. Rudolph M, Hashmi ASK (2012) Chem Soc Rev 41:2448
101. Fürstner A (2014) Acc Chem Res 47:925
102. Felix RJ, Weber D, Gutierrez O, Tantillo DJ, Gagné MR (2012) Nat Chem 4:405
103. Nolan SP (2011) Acc Chem Res 44:91
104. Marion N, Nolan SP (2008) Chem Soc Rev 37:1776
105. Wang Y-M, Lackner AD, Toste FD (2014) Acc Chem Res 47:889
106. Hamilton GL, Kang EJ, Mba M, Toste FD (2007) Science 317:496
107. Zhang Z, Widenhoefer RA (2007) Angew Chem Int Ed 46:283
108. Teller H, Flügge S, Goddard R, Fürstner A (2010) Angew Chem Int Ed 49:1949
109. Gonzalez AZ, Benitez D, Thatchouk E, Goddard WA, Toste FD (2011) J Am Chem Soc 133:5500
110. Franke R, Selent D, Börner A (2012) Chem Rev 112:5675
111. Jones JH (2000) Platinum Metals Rev 44:94
112. Zoeller JR, Agreda VH, Cook SL, Lafferty NL, Polichnowski SW, Pond DM (1992) Catal Today 13:73
113. Hashmi ASK (2007) Catal Today 122:211
114. Iqbal N, Blakstad G, Fiksdahl A (2014) Tetrahedron 70:1317
115. Raubenheimer HG, Schmidbaur H (2012) Organometallics 31:2507
116. Hashmi ASK (2007) Chem Rev 107:3180
117. Weber D, Tarselli MA, Gagné MR (2009) Angew Chem Int Ed 48:5733
118. Mézailles N, Ricard L, Gagosz F (2005) Org Lett 7:4133
119. Wen F, Englert U, Gutrath B, Simon U (2008) Eur J Inorg Chem 1:106
120. Yang Y, Ramamoorthy V, Sharp PR (1993) Inorg Chem 32:1946
121. Shi Y, Ramgren SD, Blum SA (2009) Organometallics 28:1275
122. Mohr F, Falvello LR, Laguna M (2006) Eur J Inorg Chem 833
123. Benoit RL, Fréchette M, Lefebvre D (1988) Can J Chem 66:1159
124. Hashmi ASK, Schuster AM, Rominger F (2009) Angew Chem Int Ed 48:8247
125. Hashmi ASK, Schuster AM, Gaillard S, Cavallo L, Poater A, Nolan SP (2011) Organometallics 30:6328
126. Hashmi ASK, Ramamurthi TD, Rominger F (2010) Adv Synth Catal 352:971
127. Yang W, Hashmi ASK (2014) Chem Soc Rev 43:2941
128. Liu L-P, Hammond GB (2012) Chem Soc Rev 41:3129
129. Hashmi ASK (2010) Angew Chem Int Ed 49:5232
130. Cheong PH-Y, Morganelli P, Luzung MR, Houk KN, Toste FD (2008) J Am Chem Soc 130:4517
131. Gómez-Suárez A, Nolan SP (2012) Angew Chem Int Ed 51:8156
132. Hashmi ASK (2014) Acc Chem Res 47:864
133. Weber D, Gagné MR (2009) Org Lett 11:4962
134. Wang D, Cai R, Sharma S, Jirak J, Thummanapelli SK, Akhmedov NG, Zhang H, Liu X, Petersen JL, Shi X (2012) J Am Chem Soc 134:9012
135. Schmidbaur H, Schier A (2011) Z Naturforsch 66b:329
136. Seidel G, Lehmann CW, Fürstner A (2010) Angew Chem Int Ed 49:8466
137. Roth KE, Blum SA (2010) Organometallics 29:1712
138. Weber D, Jones TD, Adduci LL, Gagné MR (2012) Angew Chem Int Ed 51:2452

139. Heckler JE, Zeller M, Hunter AD, Gray TG (2012) Angew Chem Int Ed 51:5924
140. Brown TJ, Weber D, Gagné MR, Widenhoefer RA (2012) J Am Chem Soc 134:9134
141. Cox N, Uehling MR, Haelsig KT, Lalic G (2013) Angew Chem Int Ed 52:4878
142. Hashmi ASK, Braun I, Rudolph M, Rominger F (2012) Organometallics 31:644
143. Ye L, Wang Y, Aue DH, Zhang L (2012) J Am Chem Soc 134:31
144. Graf K, Hindenberg PD, Tokimizu Y, Naoe S, Rudolph M, Rominger F, Hashmi ASK (2014) ChemCatChem 6:199
145. Hashmi ASK, Wieteck M, Braun I, Nösel P, Jongbloed L, Rudolph M, Rominger F (2012) Adv Synth Catal 354:555
146. Hashmi ASK, Braun I, Nösel P, Schädlich J, Wieteck M, Rudolph M, Rominger F (2012) Angew Chem Int Ed 51:4456
147. Nösel P, Lauterbach T, Rudolph M, Rominger F, Hashmi ASK (2013) Chem Eur J 19:8634
148. Hashmi ASK, Wieteck M, Braun I, Rudolph M, Rominger F (2012) Angew Chem Int Ed 51:10633
149. Hansmann MM, Rudolph M, Rominger F, Hashmi ASK (2013) Angew Chem Int Ed 52:2593
150. Hansmann MM, Tšupova S, Rudolph M, Rominger F, Hashmi ASK (2014) Chem Eur J 20:2215
151. Yu B, Sun J, Yang X (2012) Acc Chem Res 45:1227
152. Tang Y, Li J, Zhu Y, Li Y, Yu B (2013) J Am Chem Soc 135:18396
153. Sharma I, Bohé L, Crich D (2012) Carbohydr Res 357:126
154. Satoh H, Manabe S, Ito Y, Lüthi HP, Laino T, Hutter J (2011) J Am Chem Soc 133:5610
155. Chen Y, Chen M, Liu Y (2012) Angew Chem Int Ed 51:6181
156. Gómez-Suárez A, Dupuy S, Slawin AMZ, Nolan SP (2013) Angew Chem Int Ed 52:938
157. Ricard L, Gagosz F (2007) Organometallics 26:4704
158. Gaillard S, Bosson J, Ramón RS, Nun P, Slawin AMZ, Nolan SP (2010) Chem Eur J 16:13729
159. Ramón RS, Gaillard S, Poater A, Cavallo L, Slawin AMZ, Nolan SP (2011) Chem Eur J 17:1238
160. Weber D, Gagné MR (2013) Chem Sci 4:335
161. Oonishi Y, Gómez-Suárez A, Martin AR, Nolan SP (2013) Angew Chem Int Ed 52:9767
162. Roithová J, Janková Š, Jašíková L, Vána J, Hybelbauerová S (2012) Angew Chem Int Ed 51:8378
163. Zhdanko A, Maier M (2013) Chem Eur J 19:3932
164. Zhdanko A, Maier M (2013) Organometallics 32:2000
165. Zhdanko A, Ströbele M, Maier ME (2012) Chem Eur J 18:14732
166. Zhdanko A, Maier M (2014) Chem Eur J 20:1918
167. Zhdanko A, Maier ME (2014) ACS Catal 4:2770
168. Uson R, Laguna A, Castrillo MV (1979) Synth React Inorg Met-Org Chem 9:317
169. Tsui EY, Müller P, Sadhigi JP (2008) Angew Chem Int Ed 47:8937
170. Escalle A, Mora G, Gagosz F, Mézailles N, Le Goff XF, Jean Y, Le Floch P (2009) Inorg Chem 48:8415
171. Ito H, Saito T, Miyahara T, Zong C, Sawamura M (2009) Organometallics 28:4829
172. Harris RJ, Widenhoefer RA (2014) Angew Chem Int Ed 53:9369
173. Gómez-Suárez A, Oonishi Y, Meiries S, Nolan SP (2013) Organometallics 32:1106
174. Tang Y, Yu B (2012) RSC Adv 2:12686
175. Angermaier K, Schmidbaur H (1994) Inorg Chem 33:2069
176. Chung S-C, Krüger S, Schmidbaur H, Rösch N (1996) Inorg Chem 35:5387
177. Duan H, Sengupta S, Petersen JL, Akhmedov NG, Shi X (2009) J Am Chem Soc 131:12100
178. Yoshida T, Matsunaga S, Nomiya K (2013) Dalton Trans 42:11418
179. Young PC, Green SLJ, Rosair GM, Lee A-L (2013) Dalton Trans 42:9645
180. Mudd RJ, Young PC, Jordan-Hore JA, Rosair GM, Lee A-L (2012) J Org Chem 77:7633
181. Takino Y, Yoshinan N, Kawamoto T, Konno T (2012) Chem Lett 41:834

182. Barreiro E, Casas JS, Couce MD, Laguna A, López-de-Luzuriaga JM, Monge M, Sánchez A, Sordo J, Varela JM, Vázquez-López EM (2011) Eur J Inorg Chem 1322
183. Balzano F, Cuzzola A, Diversi P, Ghiotto F, Uccello-Barretta G (2007) Eur J Inorg Chem 5556
184. Homs A, Escofet I, Echavarren AM (2013) Org Lett 15:5782
185. Brooner REM, Brown TJ, Widenhoefer RA (2013) Chem Eur J 19:8276
186. Hamel A, Mitzel NW, Schmidbaur H (2001) J Am Chem Soc 123:5106
187. Schmidbaur H, Hamel A, Mitzel NW, Schier A, Nogai S (2002) Proc Natl Acad Sci USA 99:4916
188. Zhu Y, Day CS, Zhang L, Hauser KJ, Jones AC (2013) Chem Eur J 19:12264
189. Weber SG, Rominger F, Straub BF (2012) Eur J Inorg Chem 2863
190. Schmidbaur H, Schier A (2010) Organometallics 29:1
191. Raubenheimer HG, Schmidbaur H (2011) S Afr J Sci 107:31
192. Hooper TN, Green M, Russell CA (2010) Chem Commun 46:2313
193. Himmelspach A, Finze M, Raub S (2011) Angew Chem Int Ed 50:2628
194. Rubial B, Ballesteros A, González JM (2013) Adv Synth Catal 355:3337
195. Leyva-Pérez A, Rubio-Marqués P, Al-Deyab SS, Al-Resayes SI, Corma A (2011) ACS Catal 1:601
196. Grirrane A, Garcia H, Corma A, Álvarez E (2011) ACS Catal 1:1647
197. Grirrane A, Garcia H, Corma A, Álvarez E (2013) Chem Eur J 19:12239
198. Hashmi ASK, Lauterbach T, Nösel P, Vilhelmsen MH, Rudolph M, Rominger F (2013) Chem Eur J 19:1058
199. Brown TJ, Widenhoefer RA (2011) Organometallics 30:6003
200. Lavallo V, Frey GD, Kousar S, Donnadieu B, Bertrand G (2007) Proc Natl Acad Sci 104:13569
201. Simmoneau A, Jaroschik F, Lesage D, Karanik M, Guillot R, Malacria M, Tabet J-C, Goddard J-P, Fensterbank L, Gandon V, Gimbert Y (2011) Chem Sci 2:2417
202. Obradors C, Echavarren AM (2013) Chem Eur J 19:3547
203. Homs A, Obradors C, Lebœuf D, Echavarren AM (2014) Adv Synth Catal 356:221
204. Jašíková L, Roithová J (2013) Organometallics 32:7025
205. Gimeno A, Cuenca AB, Suárez-Pantiga S, Ramirez de Arellano C, Medio-Simón M, Asensio G (2014) Chem Eur J 20:683
206. Oliver-Meseguer J, Cabrero-Antonino JR, Domínguez I, Leyva-Pérez A, Corma A (2012) Science 338:1452
207. Oliver-Meseguer J, Leyva-Pérez A, Corma A (2013) Chem Cat Chem 5:3509
208. Gorin DJ, Sherry BD, Toste FD (2008) Chem Rev 108:3351

Top Curr Chem (2015) 357: 213–284
DOI: 10.1007/128_2014_591

Published online: 27 February 2015

Computational Approaches to Homogeneous Gold Catalysis

Olalla Nieto Faza and Carlos Silva López

Abstract Homogenous gold catalysis has been exploding for the last decade at an outstanding pace. The best described reactivity of Au(I) and Au(III) species is based on gold's properties as a soft Lewis acid, but new reactivity patterns have recently emerged which further expand the range of transformations achievable using gold catalysis, with examples of dual gold activation, hydrogenation reactions, or Au(I)/Au(III) catalytic cycles.

In this scenario, to develop fully all these new possibilities, the use of computational tools to understand at an atomistic level of detail the complete role of gold as a catalyst is unavoidable. In this work we aim to provide a comprehensive review of the available benchmark works on methodological options to study homogenous gold catalysis in the hope that this effort can help guide the choice of method in future mechanistic studies involving gold complexes. This is relevant because a representative number of current mechanistic studies still use methods which have been reported as inappropriate and dangerously inaccurate for this chemistry.

Together with this, we describe a number of recent mechanistic studies where computational chemistry has provided relevant insights into non-conventional reaction paths, unexpected selectivities or novel reactivity, which illustrate the complexity behind gold-mediated organic chemistry.

Keywords Benchmark • Computational chemistry • DFT • Gold catalysis • Reaction mechanisms

O.N. Faza (✉)
Facultade de Ciencias, Campus As Lagoas, s/n, 32004 Ourense, Spain
e-mail: faza@uvigo.es

C.S. López (✉)
Departamento de Química Orgánica, Universidade de Vigo, Lagoas/Marcosende, s/n, 36310 Vigo, Spain
e-mail: carlos.silva@uvigo.es

Contents

1 Introduction

The field of homogeneous gold catalysis has achieved maturity in the last few years. Long gone is the idea of gold as a catalytically inert metal and the conflicting remarks between the "nobleness" of this transition metal and the rich reactivity which was being discovered in the first papers exploring this chemistry. The sheer number of publications which can be retrieved by a search for "gold catalysis" in any database is proof of the vitality of the field (899 using Scopus just for the year 2013). Although there are reports dating from the 1920s and 1930s regarding the catalytic activity of gold colloids (such as nitramide decomposition [1]) or gold surfaces (formation of water starting from molecular oxygen and hydrogen [2]), a sustained interest in gold catalysis (heterogeneous at first) only started from the 1970–1980s, with work by Bond on olefin hydrogenation [3], research of Haruta et al. on the low-temperature oxidation of CO [4], and the acetylene hydrochlorination to vinyl chloride of Hutchings [5].

Homogeneous examples of the catalytic activity of gold can be considered to start with the use of gold(I) salts in the aldol reaction described by Ito et al. [6] in a strategy incorporating a chiral ligand for enantioselectivity which would not be expanded until several years later. However, it is only in the 1990s, with the work of Fukuda and Utimoto [7] and Teles et al. [8] on the activation of alkynes towards nucleophilic attack, that the "gold rush" would start. After this, a huge number of organic reactions catalyzed by gold(I) or gold(III) salts have been reported, optimized, and systematized, leading to a significant enrichment of the organic chemist's toolkit. Most of these reactions have clear advantages over alternative approaches, since they usually involve mild reaction conditions, are compatible with a wide range of functional groups, and generate high levels of complexity with high atom efficiency in a simple experimental setup. In other cases, the use of gold just opens the way for novel reactivity which wouldn't be available with other catalysts.

This interest in homogeneous gold catalysis is well reflected in the abundance of review publications, either general [9–11] or dealing with different reaction types [12–17], a specific substrate or product [17–22], the structure and fate of key intermediates in these processes [23–25], the mechanisms through which these transformations occur [11, 26–28], or the possibilities they open up in organic synthesis [29–33]. We recommend the reader refers to some of these documents to gain a wider understanding of the field.

The activity of cationic gold as a homogeneous catalyst is usually described as a result of its unusual properties in relation to its position in the periodic table. Most of these properties can be attributed to relativistic effects originating from the high velocity of electrons near the heavy nucleus. These comprise (1) the contraction of the *s* and *p* orbitals, specially the 6*s*, (2) the indirect expansion and destabilization of the *d* and *f* orbitals (caused by the increased shielding of the former), and (3) spin-orbit coupling. The contraction of the 6*s* orbital leads to stabilization of the HOMO in the metallic atom ($[Xe]4f^{14}5d^{10}6s^{1}$), resulting in a larger ionization potential and small metallic radius. The associated expansion of the 4*f* and 5*d* orbitals lowers the energy of the LUMO in cationic gold, with the result of high electron affinity and electronegativity and aurophilicity. From a reactivity point of view, contraction of the 6*s* orbital leads to stronger ligand–metal bonds, as well as making gold cations very soft carbophilic Lewis acids [34–36]. As a result of these properties, most of the reactivity of gold salts in catalysis is focused on the activation of soft nucleophiles, such as C−C unsaturation towards nucleophilic attack, leading to the formation of C−C, C−O, C−N or C−S bonds, although there are also examples of C−H and C-heteroatom activation [37–39].

The enyne and propargylic ester rearrangements manifolds are two of the best studied examples of this kind of reactivity. Gold complexation to the alkyne fragment can lead to a series of intermediates which open the way to very rich reactivity, often being the starting point of a reaction cascade which easily generates complexity in processes whose selectivity can be tuned through the nature and position of substituents on the backbone of the substrate. The deep mechanistic knowledge of these systems obtained through a combination of experimental and computational studies allows us today to use these processes in routine synthetic work and to build upon this reactivity to engineer new gold-catalyzed reactions which can expand the availability of transformations accessible to the organic chemist. Computational chemistry has played a key role in understanding these mechanisms, rationalizing the existing experimental evidence and suggesting ways to exploit this knowledge to achieve new products, improved or alternative selectivities, or better reaction conditions. Thus, although much of the mechanistic information we have nowadays on the structure and bonding in gold complexes and on their catalytic behavior originated in studies involving these systems, we are not going to delve into their description in this work, referring the reader to the abundant literature already published on the subject.

This review focuses on the most recent advances in the application of computational methods to homogeneous gold catalysis. We start with a description of the

studies on the methodology itself, followed by a description of the main results obtained through its application to different fields.

2 Computational Methods

The work dealing with the computational chemistry of gold can be roughly divided into two sections. On one hand we find a series of studies where very accurate methods, usually including the latest advances in relativistic quantum chemistry, are applied to basic questions about the properties, structure, and reactivity of very small gold compounds. Problems such as the description of aurophilicity or a comprehensive description of bonding in gold compounds are among the best represented here. On the other side, there is wide interest in obtaining mechanistic information about gold-catalyzed organic transformations, involving systems for which these very accurate methods are prohibitively expensive in terms of computer time, memory, or both, because of their size and/or the number of structures or reaction steps which need to be calculated.

2.1 Bonding and Structure in Gold Complexes

For extensive reviews on how to use computational chemistry to describe bonding in gold complexes, we recommend the works by Pykko and Schwerdtfeger [36, 40–44], where most early calculations and high quality experimental data which can be used to check their results are gathered, together with a perspective on the relativistic effects in chemistry, particularly relevant in gold catalysis. In terms of bonding, it is interesting to check the review of Frenking and Fröhlich on the nature of bonding in transition metal chemistry. Here they present both relevant chemical results and a description of the different methods which can be used to analyze bonding in such species (Natural Bond Orbitals, Charge Decomposition Analysis, Atoms in Molecules and Energy Decomposition Methods) [45]. The work of Schmidbaur on aurophilicity is also recommended for those working with bimetallic systems where these kinds of interaction may be relevant. The theoretical methods used to describe aurophilicity are also expected to perform well in the characterization of weakly-bound species or systems where dispersion is important [46].

The usually accepted description of bonding in gold complexes follows the Dewar–Chatt–Duncanson model [45]. If we take the interaction of a gold atom with an alkyne as an example, there are four main contributions to bonding, as represented in Fig. 1 in order of their usual relative strengths. The first is a σ ligand–metal donation in the plane, followed by π back-donation from the metal to the antibonding π-bond of the alkyne, also in the plane. The next interaction would be a π donation from the perpendicular π-orbital in the alkyne to the metal, and the last,

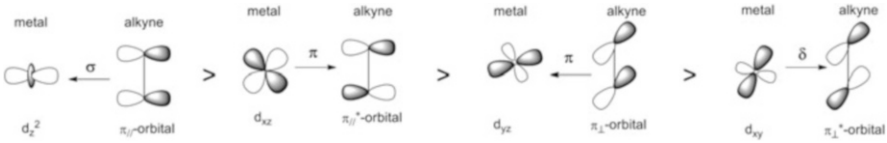

Fig. 1 Scheme of the Au(I)-alkyne bonding interactions (from strongest to weakest) within the Dewar–Chatt–Duncanson model

representing the smallest contribution, would be a δ back-donation from the metal to the out-of-plane π-orbital of the alkyne.

Calculations at high levels of theory (coupled cluster and DFT methods, also with the use of relativistic Hamiltonians) on the interaction between Au(I) and ethylene and acetylene [40, 47] used Energy Decomposition Analysis (EDA) to quantify the relevance of each of these components to bonding. They find that for the bond Au(I)–alkyne, the strongest contribution is the $\sigma(M \leftarrow L)$ (~65%), followed by $\pi_{\parallel}(M \rightarrow L)$(~27%) and $\pi_{\perp}(M \leftarrow L)$(~7%), with an almost negligible contribution (~1%) of the $\delta(M \rightarrow L)$ interaction. It is also known that about half of the total interaction between the two fragments is electrostatic in origin [48]. However, this description of bonding might not be the most accurate for the species involved in gold-catalyzed reactions, since the gold(I) center is also attached to other ligands. In a study of bonding in gold(I) carbenes/carbenoids, Toste et al. [49] found that LAu^+ species are less acidic than Au^+, since the charge is also distributed over the ligand, with the result that electrostatic interactions are reduced and the previous bond contributions are altered depending on the ligand used.

A recent study by Tarantelli et al. [50] also deals with an analysis of the bonding between some gold species of the form L-Au(I)-S (L = NHC, Cl^-) where S is a η^2-bonded substrate with a C−C multiple bond, in terms of donation and back-donation components of the Dewar–Chatt–Duncanson model. They calculate how the electron density changes between L-Au(I)-S and separated L-Au(I)+S with a partition scheme they developed with the aim of being able to compute these contributions from observables in a non-ambiguous way [51]. This scheme calculates the quantity of charge transferred from left to right through each plane perpendicular to the axis, defined by the gold atom and the center of the multiple C−C bond. The main result from this study is the rejection of the commonly accepted view that gold complexes are poor π donors (because of the large energy separation between the 5*d* orbitals in the metal center and the π* orbital in the unsaturation), since the $\pi_{\parallel}(M \rightarrow L)$ component of back-donation is in all systems studied comparable to, and often almost reaching the same value as the $\sigma(M \leftarrow L)$ component (when L = Cl^- and S = alkyne, for example). They also report that $\sigma(M \leftarrow L)$ donation is more or less constant while the $\pi_{\parallel}(M \rightarrow L)$ back-donation is highly tunable and sensitive to changes in both ligand and substrate.

Using a less common substrate, Hansmann et al. [52] experimentally characterized a series of gold–allenylidene complexes of formula $[Au{=}C{=}C{=}CR_2]^+OTf^-$, with $R = N(CH_2)_n$ or OMe ($n = 3, 4$), and performed a computational analysis of their bonding. They find that these structures are better described as gold-stabilized

propargylic cations rather than gold–vinylidene complexes. However, removing the heteroatom stabilization, the choice of ligand can then modulate the electronic structure on the system along a continuum spanning from a gold-stabilized carbocation to an Au–allenylidene. These results are in good agreement with the carbene/carbocation model put forward by Toste et al. [49] and hint towards the building of a general model.

All these studies that use computational techniques to describe apparently obscure classifications of bonding, arbitrary partitioning schemes or artificially built systems, which might be too small for being of use in catalysis or too unreal for them ever to be synthesized, provide invaluable information. For example, how electrons are distributed over the ligand–metal–substrate system in a catalysis context, which interactions are relevant for each feature of this electron distribution and how they affect the geometry and energy of the resultant structures and, more important, why this is so. When the factors contributing to each aspect of bonding, geometry or structure are dissected and identified, they provide a good point of intervention for the design of catalysts with the desired properties.

From a more practical point of view, as a result in their impact in the nature of bonding (and, as a result in energies and geometries along reaction paths), the effect of the ligands or counterions cannot be neglected in the study of gold-catalyzed reaction mechanisms, since they have been seen to affect profoundly the catalytic pathways, and they may impact on the regio- or enantioselectivity of a reaction, as we comment on in the next sections.

For example, the traditional approach of sticking a chiral ligand on the metal center to achieve enantioselectivity has not been very popular until recent years, after the seminal work by Ito et al. [6] on the aldol reaction. This is usually attributed to the linear coordination preferred by gold(I) complexes, which leaves the substrate to be activated and the chiral ligand far from each other. The availability of a single coordination site also prevents chelation, so the Au–ligand bond usually displays free rotation. These difficulties have been circumvented in different ways: using chiral biphosphine ligands which bind two gold atoms [53, 54], designing one-point binding ligands large enough to create chiral cavities for the reaction to take place [55, 56], or using the counterion to create such a chiral environment [57]. Thus, ligands directly attached to the metal center, or counterions forming ion pairs with it, can generate a chiral environment for the reaction. Another effect they can have in a reaction is to alter the mechanism, providing alternative, lower-energy paths for a given transformation. Examples of this are the ligand or counterion-assisted hydrogen transfers found in hydrogen migrations, hydrogenations, protodeaurations, and other key steps in these catalytic cycles. Instead of lowering the activation energies in a certain path, another role of the counterion can be to prevent the formation of undesired intermediates in the catalytic cycle, such as some unproductive diaurated species [58].

Computational studies can greatly help the development of new ligands or counterions to suit all of these functions, in providing information to predict and interpret the behavior of the resultant gold complexes in solution in terms of coordination geometries, lability of the ligands, barriers for ligand-exchange,

electronic properties of the generated chiral environment, etc. A good example of this can be found in the work by Fürstner et al. [55], which has achieved great success combining the results of crystallography and computational studies in designing TADDOL-based ligands for asymmetric gold catalysis, or in the combined experimental (NMR) and theoretical studies of Zuccaccia et al. [59–61] on the ion pairing in cationic gold(I) complexes with unsaturated hydrocarbons. The latter focus on describing how the choice of the ligand can affect the ion-pair structure in solution and the chemical bond between the LAu(I) fragment and the substrate in simple $[L–Au–S]^+BF_4^-$ complexes (where S is a C−C unsaturation and L a phosphine or N-heterocyclic carbene). Analyzing the charge-displacement on the Au–S bond provides a picture of the donation and back-donation components of the DCD model. A poor donor such as a phosphine enhances the acidity of the metal fragment, resulting in greater electron-withdrawing when coordinated to the substrate. In this case, the BF_4^- counterion is located on the alkyne side. Different ligands on the phosphorus atom can fine-tune these interactions and thus the charge in the alkyne, modulating the preference for this counterion approach. In fact, when tris(3,5-bis(trifluoromethyl)phenyl)phosphine is used as ligand, the counterion shifts to a position nearer the substrate because of the increased acidity of the phenyl ortho protons. Because an NHC is a stronger donor, the metal fragment $NHC\text{-}Au^+$ is less acidic and does not deplete the charge on the unsaturation as much, resulting in a more loosely bound counterion which usually prefers to be near the imidazole ring of the ligand.

2.2 Computational Methods in Homogeneous Catalysis

2.2.1 Families of DFT Functionals

Although CCSD(T) is considered the "gold standard" in computational chemistry, reliably providing "chemical accuracy" at the lowest cost possible (CASPT2 would be the equivalent for systems with multiconfigurational character), its use in everyday calculations is usually restricted to the smallest of systems, because of its $O(N^7)$ scaling with the number of basis functions. For mechanistic studies in gold homogeneous catalysis, where at a bare minimum the substrates, metal center and ligands have to be taken into account (explicit solvent molecules and counterions also often need to be simulated as well), most of the time we are restricted to using computational methods based on DFT to achieve reasonably accurate results. DFT is better than HF in that it recovers some electron correlation at a similar cost, and it greatly outperforms semi-empirical calculations out of their parametrization space.

Density functional theory has been a very active field in the last two decades, very similar to homogenous gold catalysis. And to strengthen the analogies even further, this field is currently also exploding in different directions. This situation is, on the one hand, very appealing as it implies quick development and better and

improved density functionals being released almost every month but, on the other hand, it saturates the field with an overwhelmingly increasing amount of different acronyms which are almost impossible to keep up with. Once we accept the idea of the relation between the electron density and the energy of the system as demonstrated by Hohenberg and Kohn, it is hard to justify why so many functionals are needed when we are aiming for just one. It is also surprising to see that evolution does not seem to apply to the field, since many formulations become popular and never disappear, despite the authors of new and supposedly improved formulations declaring them obsolete.

An illustrative product of the current scenario of density functional theory is the half scientific – and perhaps half comical – approach to a new functional adopted at the University of Girona. Every year M. Swart, M. Bickelhaupt, and M. Duran organize the DFT Poll including more than 40 of the probably most used density functionals (www.marcelswart.eu/dft-poll). The poll evaluates the sympathy of researchers for the different functionals, and with these results to hand, a Popularity Adapted Consensus Object (PACO) functional is released. This functional is constructed as a weighted combination of the 20 most voted functionals and it is then benchmarked against a small set of prototypical chemical structures. Despite not being developed with good performance in mind, the PACO functional does yield good results across a reasonably wide set of interactions.

In 2001, Perdew and Schmidt illustrated the development of density functionals as a ladder with different rungs, symbolizing different generations of functionals in the ascent to the exact density functional [62]. Perdew employed the biblical fragment of Jacob's dream as an analogy to this ladder: "Jacob left Beer-sheba and went toward Haran. He came to a certain place and stayed there for the night, because the sun had set. Taking one of the stones of the place, he put it under his head and lay down in that place. And he dreamed that there was a ladder set up on the earth, the top of it reaching to heaven; and the angels of God were ascending and descending on it." Since then, the symbol of the DFT ladder has helped organize not only the development but also the plethora of functionals available to users nowadays (see Table 1). Each rung represents a step forward in the development of new functionals, and it involves a more complex formula, usually increasing the dependence of the functional on an additional magnitude.

The first rung includes the local density approximation, which provides the exact (analytical) solution for a homogeneous electron gas [63]. This is the first generation of density functional theory and, for obvious reasons, not very accurate with molecular systems. This density functional only depends on the electron density where the functional is evaluated ($\rho(\mathrm{r})$). A first approximation to improve this description was making the density functional also depend on the gradient of the electron density, making it non-local ($\nabla\rho(\mathrm{r})$). This approach is still quite rough for most chemical problems but it has the clear advantage of a simple formulation and the fact that it allows the use of some algorithms which improve the way these functionals scale with the size of the systems. This approach is therefore employed in very large systems at the expense of lower accuracy. Hybrid functionals include a fraction of Hartree–Fock exchange in their formulation. The idea behind this

Table 1 The Jacob's ladder of DFT

Rung	Dependence	Generation	Examples
5	ρ, $\nabla\rho$, τ + HF	Dispersion corrected (meta-hybrid, double hybrid, Coulomb attenuated, etc.)	M06, xB97, cam-B3LYP, LC-xPBE, LC-BLYP, B2PLYP, M11, N12SX, MN12SX
4	ρ, $\nabla\rho$, τ	Meta-GGA	M06L, VSXC, TPSS, τ-HCTH, BB95, PBEKCIS, N12, MN12L
3	ρ, $\nabla\rho$ + HF	Hybrid	TPSSh, HCTHhyb, mPW1LYP, mPW1PW91, mPW3PBE, O3LYP, B1B95, B1B95, B3PW91, PBE1KCIS, PBEh1PBE, X3LYP, B3LYP
2	ρ, $\nabla\rho$	GGA	HCTH, PBEPBE, BPW91, BLYP, OLYP, mPWPW91, mPWPBE, mPWLYP
1	ρ	LDA	VWN

incorporation is that Hartree–Fock already accounts for full exchange; the problem is then how to build the rest of the density functional so that it incorporates all the electron correlation and zero exchange, hence the fractional mixture. Hybrid functionals generally perform better than GGAs, but suffer in the same areas where HF provides a deficient description of the system. Meta-GGA functionals include dependence on the kinetic energy density (τ(r)), thus retaining the convenient scaling properties of GGAs with improved accuracy, although, in general, they do not compete with the hybrid counterparts.

Given the fairly systematic evolution of density functionals ($\rho \rightarrow \nabla\rho \rightarrow \tau$ and the inclusion of HF exchange), in the last rung, one would expect to find only meta-hybrids. However, some authors have proposed unexplored approaches to improve density functionals which depart quite significantly from the beaten track. In this last rung we therefore include at least three different kinds of improvements added to hybrid functionals, most of them aimed at incorporating long-range dispersion interactions which the older DFT methods were known to fail to describe correctly. These can be: (1) since hybrid functionals incorporate a mixture of HF theory, perturbational corrections can be added to this term (this is an indirect way of including dependence on a new magnitude, the virtual orbitals, through the perturbational part); (2) including a switching function that modifies the formulation of the functional from short to long range in the exchange part (usually increasing the weight of HF exchange at long range); and (3) some functionals have been constructed in heavily parametrized forms and then a training and fitting procedure is used to obtain the final functional form. All these approaches have been shown to improve significantly the results of previous density functionals and are the method of choice in most chemical problems.

2.2.2 The Need to Benchmark

Despite the constant improvement of density functional theory over the years, there are some obscure areas in which DFT is known to fail from the earlier formulations to the most recent developments. These areas are usually related to the single determinant nature of DFT. These methods therefore fail to account correctly for diradical systems in particular, or any molecular system exhibiting a near degeneracy situation on its ground state. Excited states are also problematic for most density functionals, in particular when Rydberg states are involved. The metaphoric carpenter which Truhlar summons to explain how different tools are necessary for different tasks and therefore different functionals may be needed to solve different problems is not only applicable to DFT but also to any chemical problem to be tackled computationally. Adequate methodology is the key to accurate and meaningful results, and when the chemical system at hand defies the limits of application of DFT different methodology must be used, whether it implies expensive multi-determinant approaches such as coupled cluster or time-consuming multi-configurational wavefunction theory.

In a previous review [64] we bemoaned the lack of comprehensive studies testing the adequacy of the most popular methodologies being used for the description of gold-catalyzed organic reactions. Our argument was that most studies were using DFT [65], with B3LYP [66, 67] being the most popular functional, and 6-31G (d) with LANL2DZ [68] (or sometimes SDD [69]) as an electron core potential for gold, the most used basis set, a combination which had consistently provided surprisingly good results at a low computational cost for organic reactivity. As time advanced, larger basis sets (triple zeta with diffuse and polarization functions) started to be more common, as well as more modern functionals including dispersion contributions, such as those from the Minnesota family (specially M06), but the main problem behind this choice of methods persisted – they had not been explicitly tested against organometallic gold systems. Among the mechanistic studies which cared about justifying the choice of functional or basis set, the most extended argument in support of a given combination was the citation of some other previous mechanistic studies which had used it or an a posteriori agreement of the calculated data with the experimental observations, although in some papers some small-scale benchmarking or comparison with the result of higher level ab initio calculations (most commonly just MP2) was carried out. In this context, the finding by Benitez et al. [49] that M06 (with Hay Wadt pseudopotential and LACV3P++**(2*f*)//LACVD** for gold, and 6-311++G**// 6-31G** for main group atoms) was able to reproduce correctly the effect of the different electron-donating properties of the ligands on the experimental bond rotation barriers of gold carbenoid species, while B3LYP and BP86 failed at this task, provided a warning sign that the choice of a computational methodology for the study of gold complexes and gold-catalyzed reaction mechanisms should be approached with care, especially when applying methods which have not been developed or tested with this kind of system in mind.

Although the reaction involved is not catalyzed by gold, a recent study by Rösch et al. [70] represents a clear example of what can go wrong in a computational mechanistic study when the choice of methodology has not been considered with great care. They calculate the reaction profiles corresponding to the four mechanisms proposed for hydrosilylation of ethylene by monosilane catalyzed by a Rh (I) bis-*N*-heterocyclic carbene, a system of a certain complexity, since the four mechanisms are connected at some intermediates and the potential energy profiles of some of the alternative paths are overall flat [71]. In this study, the authors use a stepping approach where they optimize the whole four profiles with B3LYP and BP86, optimizing from two to three relevant barriers in each mechanism with an additional set of functionals (mPWPW, PBE and PBE0) to identify the rate limiting barrier in each mechanism, which would be evaluated with seven more functionals (BLYP, B3PW91, MPW1K, MPW3LYP, M06-L, M06, and TPSS). The most relevant result is that, in general, two of the four mechanisms are preferred with all functionals, while the other two have comparable highest relative barriers, with a difference of 3 kcal/mol. The height of these barriers and the step at which they occur change depending on the functional, with enthalpy barriers differing by up to 10 kcal/mol.

2.2.3 Testing Sets and DFT Benchmarks for Transition Metal Chemistry

In the last few years, several systematic benchmarking studies have appeared which tried to answer the question of which functional to use when modeling gold-catalyzed mechanisms. DFT is the method of choice for the simulation of the organometallic species involved in homogeneous catalysis, as it provides reasonably good results, recovering some electron correlation at a moderate computational cost. However, DFT also has some inherent problems, such as the self-interaction error and its failure to describe long-range correlation effects (dispersion) properly. The fact that the exact functional relating the electron density and the energy of the system is unknown has led to the development of a huge number of exchange-correlation functionals, some of them with a general purpose in mind, some of them with a very narrow focus on one type of property (such as NMR shieldings, for example) or system (such as long-range corrected functionals for systems where charge transfer is important, or even functionals explicitly parametrized to reproduce a specific reaction coordinate [72]). As a result, benchmarking is a useful tool to help the user understand a given method's performance and guide in the choice of the best functional for a concrete problem.

For this purpose, a series of general reference sets have been developed over the years, starting with those compiled by Pople et al. to test their G-n protocols for thermochemistry: G1 [73], G2 [74, 75], G3/99 [76], or G3/05 [77]. The G1 and G2 sets only included atomization energies, ionization energies, electron and proton affinities, the G3/99 incorporated enthalpies of formation for a larger set of small molecules with main group atoms from the first and second row of the periodic table

(Li-F and Na-Cl) and the G3/05 set incorporates more systems, with the main novelty being the inclusion of hydrogen-bonded systems and structures with main group third-row elements. With this set, the authors first included DFT calculations in their geometry and thermochemistry benchmarks. Other sets have been developed by Hobza et al., which can be accessed from the BEGDB database [78], such as the well-known S22 for non-covalent interactions [79], or the S66 [80], for interaction energies relevant to biomolecular structures. Two of the most comprehensive sets for main group thermochemistry, kinetics and non-covalent interactions are those compiled by Grimme et al. under the names GMTKN30 and GMTKN24, which have been used in benchmarks of density functional methods [81, 82]. However, the most relevant sets for the field of homogeneous catalysis are those compiled by Truhlar et al. [83–94] in the context of the development of the series of Minnesota functionals. They generated new reference sets for benchmarking which include reaction energies, noncovalent interactions, and, for the first time, reaction barriers, some of them of organometallic complexes of relevance to homogeneous catalysis, such as the model system for the Grubbs II metathesis catalysis [87].

In an interesting paper, Cramer and Truhlar review the up-to-date progress in the application of DFT to transition metal chemistry in general, covering a wide range of functionals (local, meta, hybrid, hybrid meta, and range-separated) and chemical problems, including catalysis [95]. They provide a detailed account of the available studies, first those addressing the general performance of different functionals for transition metal chemistry and then summarizing the published work on a metal-by-metal basis. In this review, however, there is a marked scarcity of studies on organometallic gold complexes or reactions, and the couple which are reported just use B3LYP without comparing their results with other methods. More information, however, is available in the accurate treatment of gold clusters, especially in the determination of the turning point between flat and 3D structures (between Au_{12} and Au_{13}). The reader is referred to the papers discussed in this section for more information.

The results of Truhlar's tests of different functionals against representative databases of main group and transition metal bond energies and barrier heights show that the Minnesota functionals (M05, M06, and M06-L), together with τ-HCTHhyb, ωB97X-D, and MOHLYP, perform best among the 34 functionals used for these systems [96]. It is important in homogeneous catalysis that the two kinds of reference sets are included, as both reactions directly involving the metal center and reactions in the organic part of the organometallic systems involved are usually found along the reaction paths and a good functional should reproduce well bond energies and barrier heights. B3LYP, one of the most popular funcitonals, even today, displayed in this study an AECE (averaged error for catalytic energies, an average of the MUEs of the bond energies and barrier heights) of 5.4 kcal/mol, compared with 2.9 kcal/mol for M06, for example.

2.2.4 Benchmarks for Gold Chemistry

The previous studies provide invaluable information about what kind of methods are more likely to succeed in reproducing the energetics, structures, and electronic properties of the stationary points along gold-catalyzed reaction paths, but they still force the reader to make the assumption that something which can describe well organometallic mechanisms with transition metals from the first and second rows is also going to perform when faced with third-row metals such as gold. Even if most modern functionals involve some kind of parametrization in their development, they are not considered semiempirical methods, strongly relying on the parametrization set. However, the fact that gold displays strong relativistic effects and participates in interactions which have strong dispersion components such as aurophilicity calls for some specific benchmarking which explicitly considers gold complexes and gold reactions.

The work by Neese et al. [97] on the DFT description of the geometries of a series of transition metal complexes is special in this context, because it explicitly centers its focus on the third-row metals. The reference in this case is the experimental bond distances, obtained through gas-phase electron diffraction (GED) or microwave spectroscopy (MW) with a precision better than 1 pm. The interest of this work is not only that different exchange-correlation functionals are being tested but also the approximations which can be made to account for relativistic effects. Thus, the authors evaluate the performance of ECP-based DFT calculations, compare their effectiveness with scalar-relativistic all-electron calculations, and also evaluate the performance of the SARC [98] all-electron basis set for 3*d*-, 4*d*-, and 5*d*-transition metal geometries. These are segmented all-electron relativistic basis sets which can be applied with the DKH2 and ZORA approaches to scalar-relativistic effects, i.e., those arising from terms in the relativistic kinetic energy, leading to the contraction of the *s* and, to a lesser extent, *p* orbitals. Thus, this study is relevant to the field of homogeneous gold catalysis even if only two gold structures are included in the set, namely AuClCO and $AuCH_3PMe_3$.

In this study, local (LSDA) and gradient-corrected density functionals, the latter in pure and hybrid form, have been used in combination with the SDD or LANL2DZ ECPs and the Ahlrichs-type valence basis sets SVP, TZVP, and QZVP for the metal centers, with the corresponding all-electron bases on the organic ligands. Scalar-relativistic all-electron calculations have also been carried out within the ZORA approximation with a TZVP quality SARC [98]. For some of the functionals, the effect of the empirical dispersion correction introduced by Grimme has also been studied [99, 100]. The conclusions of this study do not identify a functional clearly superior to all others, but find a slight advantage of hybrid functionals such as PBE0, B3P86, or B3PW91, recommending the first over B3LYP for general chemistry applications. The computational advantages accrued when nonhybrid (GGA or meta-GGA) functionals are used in combination with density fitting can make the PBE functional an alternative to consider. Most relevant is the finding that at least triple-ζ quality basis sets need to be used for

accurate results, and that small, unpolarized basis sets such as LANL2DZ cannot be recommended. The use of all-electron calculations with ZORA or DKH2 with the SARC basis sets provides results comparable with those obtained with well-balanced ECPs, such as the SDD at a similar computational cost. Although they are not needed for reproducing geometries, they are required if properties such as total electron densities (including the core electrons) or NMR, EPR, Mössbauer, or X-ray absorption spectra are sought.

In this context, our study on the performance of density functional theory, the first to focus specifically on homogeneous gold-catalysis mechanisms, not just structures, displays several features which set it apart from previous studies in the literature [101]. The first is the choice of reference set (see Fig. 2), the "golden carrousel" of the gold-catalyzed rearrangement of propargylic esters [102], at the same time narrow and ample. Ample, because this handful of reactions included three of the key processes found in homogeneous gold catalysis: activation of unsaturations, formation of carbocation/carbenoid species and allene chemistry. Narrow because we are restricting our study to homogeneous gold catalysis, and the choice of test system does not intend to describe all kinds of gold chemistry. Thus, we are not considering phenomena such as aurophilicity, gold clusters, or spectroscopic properties, just focusing on geometries and energies (the key elements in the study of a catalytic mechanism) of very simple organometallic gold complexes. In fact, with the latest developments in the field, and the current proliferation of exciting gold(III) catalytic reactions which go well beyond just mimicking the reactivity of gold(I) and the growing interest in Au(I)/Au(III) cycles, it would be interesting to expand this study to include Au(III) complexes, Au(I)/Au(III) redox reactions, and new types of bonding, such as those found in gold hydrides. The second is the explicit inclusion of transition structures and energies in the reference set, something which had already been done in some of the previously commented general benchmarks, but not yet for any gold system. The third is that we include in our study (in comparison with Bühl's work [97]) the last developments incorporated in functional design, such as perturbative corrections, long-range corrections, empirical dispersion terms, meta-hybrids, etc.).

Since there were no accurate experimental data available for the structures included in this study, we used as reference the CCSD/def2-TZVPP//CCSD/def2-SVP energies and geometries. Against them we compared the geometries (not only a handful of selected bond lengths – all bond lengths, angles and dihedrals have been studied, together with a full RMS fit of the DFT geometries over the references) and relative energies for the species in the catalytic cycle obtained with 32 different functionals, including classic LDA and GGA formulations, popular hybrid alternatives and the most representative candidates from the new meta-hybrid and dispersion corrected generation, HF and MP2 used with the large double-ζ quality basis set def2-SVP [103], with relativistic effects introduced through the electron core potential for gold associated with this basis set [69].

We found that, in term of geometries, the different generations of functionals in Jacob's ladder show systematic improvement. LDA offers very poor results, with GGA and meta-GGA significantly improving them, although with significant

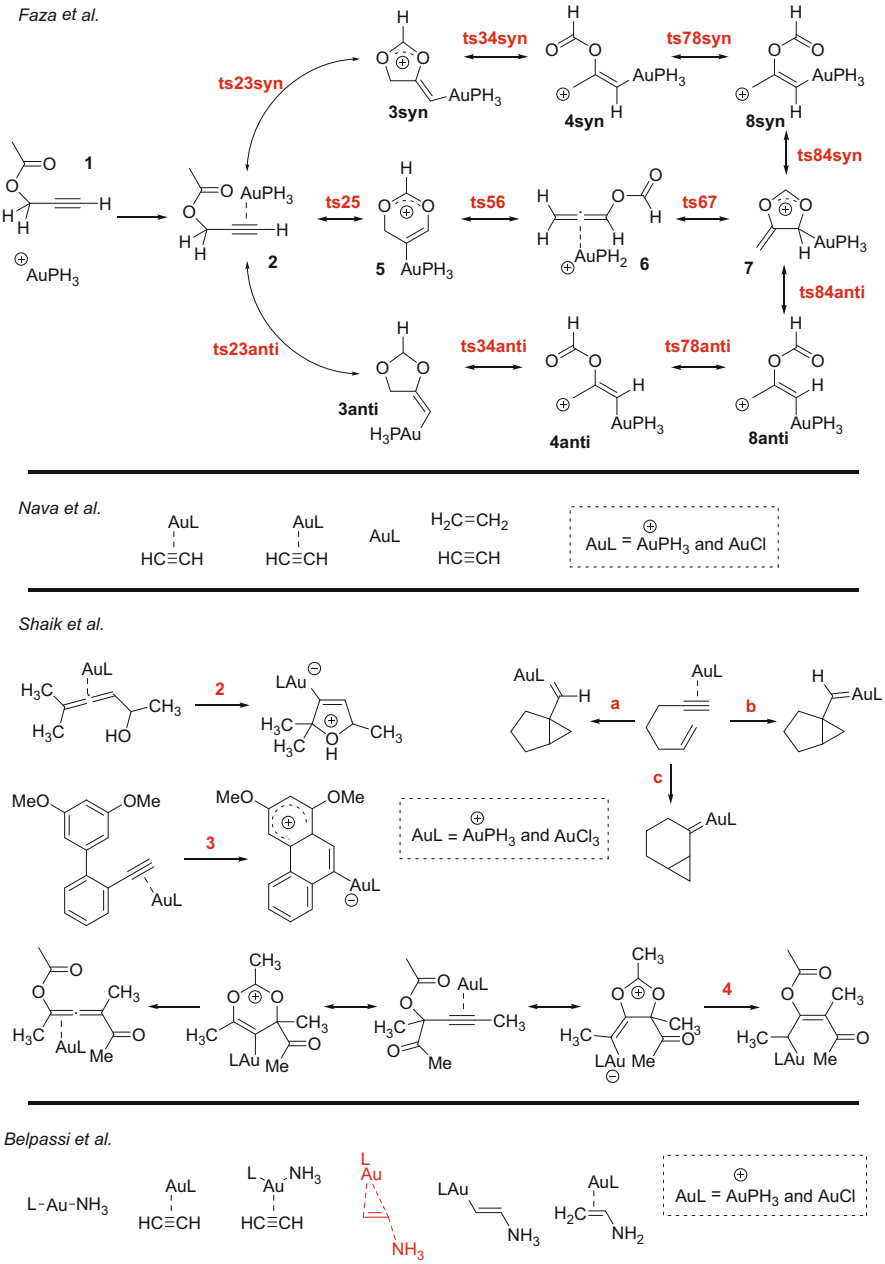

Fig. 2 Structures included in some of the benchmarks discussed in this section. Highlighted in *red* are the transition states that have been included in the test set

outliers and a large dispersion in the quality of the results (M06-L, despite belonging to the meta-GGA group, provides results comparable to those of the hybrids). HF and MP2 are better than most GGA and meta-GGA functionals, so it is not surprising that the largest improvement in the performance of DFT comes from the introduction of exact exchange found in hybrid functionals, which clearly outperform the former. The inclusion of dispersion further reduces the error in both geometries and energies. Thus, the best overall results are obtained with Grimme's perturbative double hybrid, B2PLYP, with the significantly less costly ωB97 and M06 close behind. For energies, the best performing functionals are again B2PLYP, M06, and ωB97, displaying maximum deviations smaller than 3 kcal/mol and RMSs of less than 1.7 kcal/mol with respect to the reference values. It should be noted that the deviations in geometries and energies are not homogeneous along the whole reaction path, where we can identify especially problematic species. They usually correspond to structures with a large electron delocalization and the initial η^2-coordinated alkyne gold.

Once the best methodologies for geometry optimizations were established, we used MP2, M06, and B2PLYP to assess the performance of different basis sets (Ahlrichs' def2-SVP, def2-TZVP, def2-TZVPP, def2-QZVP, and def2-QZVPP) and ECPs (SKBJ with a reduced-valence basis set, LANL2DZ, SDD, and the fully relativistic electron core potentials ecp-60-mdf and ecp-78-sdf). From these calculations, it is shown that M06 performs well, even with a relatively small split-valence basis set, with larger basis even resulting in slightly larger RMS (it could be an effect of the design of M06, built using the 6-31+G(d,p) basis set). This suggests that, after geometry optimizations carried out at the M06/def2-svp level with the ecp-60-mwb ECP, no energy refinement with a larger basis is needed. Although MP2 provides slightly lower RMS and MAD values than M06, they don't justify the extra computational cost. In terms of pseudopotentials, LANL2DZ and SDD yield larger errors than the ecp-60-mwb, with SDD providing better results. The results with the fully relativistic pseudopotentials are comparable to those obtained with DKH, although ecp-78-sdf shows significant deviations for some structures, which can be attributed to a valence shell too small to describe properly the different bonding situations found along the catalytic cycle. The results of using the second-order scalar relativistic all-electron DKH (Douglas–Kroll–Hess) model with SARC basis led to relative energies very similar to those obtained with M06 at a similar computational cost.

An aspect of this work which has garnered some criticism by Nava et al. [104] is the use of CCSD as the reference for energies, as the systematic inclusion of triple excitations in the cluster operator is deemed important to account for the long-range dispersion effects and to recruit a significant portion of missing electron correlation. The source of this evaluation of our CCSD approach as an insufficient and inaccurate reference is a benchmark on the geometries and binding energies of just the $[AuCl(C_2H_4)]$, $[AuCl(C_2H_2)]$, $[Au(PH_3)(C_2H_4)]^+$, and $[Au(PH_3)(C_2H_2)]^+$ gold complexes, two of them neutral complexes which we did not consider in our reference set, and two interaction energies which were not included either for reasons explained below.

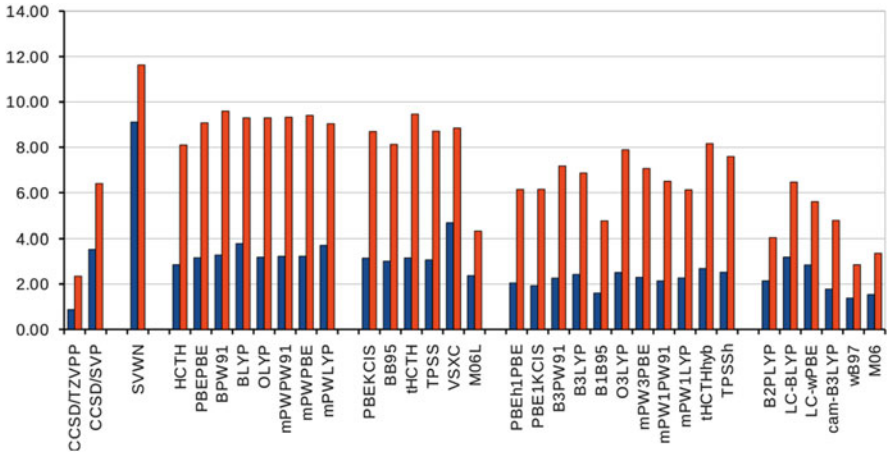

Fig. 3 Root mean square values (RMS, in *blue*) and maximum absolute deviations (MAD, in *orange*) obtained after fitting the relative energy profiles for HF, MP2, and the 32 density functionals included in reference\cite with respect to the energies computed at the CCSD(T)/def2-SVP//CCSD/def2-SVP level (values in kcal/mol)

New advances in CC theory and current computational power allow for the inclusion of further excitations combined with large basis sets at a reasonable cost. Given the controversy raised above, and taking advantage of all the momentum generated by our group in this field, we decided to recompute the energetics of the entire *gold carousel*, including triple excitations in the cluster operator and a quadruple ζ basis set. We are therefore hereby reporting domain-based local pair natural orbital coupled cluster calculations DLPNO-CCSD(T)/def2-QZVPP//CCSD/def2-SVP quality energies [105, 106]. With this new data we have updated the comparative work of the 32 density functionals which were included in our original benchmark.

It should be noted that, in our benchmark, we compared the geometries of all the structures depicted in Fig. 2. However, when we considered the energetics of the catalytic process, we found that the complexation step (**1** → **2**) has an associated energy which is very large in comparison with the actual catalytic steps. Errors in this complexation step therefore biased the statistical analysis of the overall performance of the density functionals because of the weight of this step in terms of relative energy. We therefore decided to leave this step out in the energy analysis and we included the 19 remaining structures involved in the chemical steps of homogeneous gold catalysis.

Interestingly, when we consider triple excitations in the cluster operator, the recovery of electron correlation seems so systematic that the relative energetics of the transition states and intermediates involved in this reactivity barely change. In this regard, the straightforward conclusion is that density functionals which performed well with respect to CCSD/def2-TZVPP data also do well when DLPNO-CCSD(T)/def2-QZVPP results are used as the standard. On the same line, the performance of LDA and most GGA density functionals is rather poor (see Figs. 3 and 4). To determine to what extent triples are necessary in these

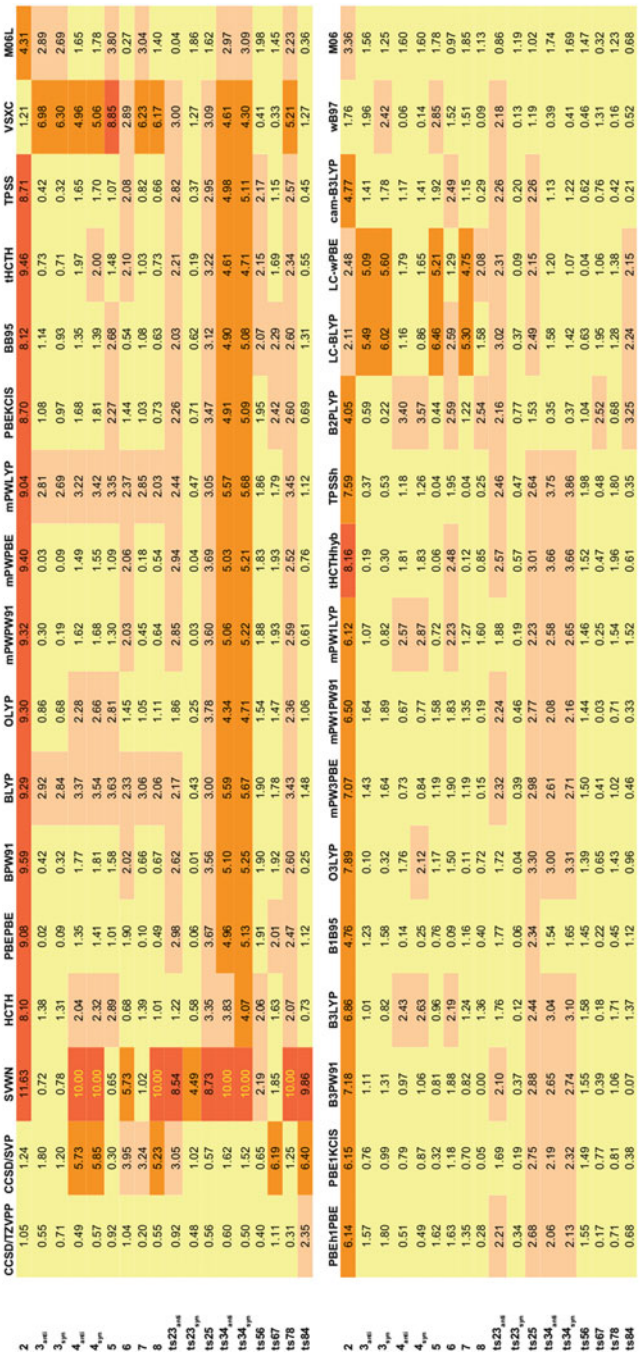

Fig. 4 Relative energy deviations per structure (in kcal/mol) for each stationary point illustrated in Fig. 2. Relative energies were RMS fitted to the CCSD(T) reference prior to this analysis. An arbitrary deviation of 10 kcal/mol has been assigned to those structures which failed to converge to the correct stationary point and have been highlighted with *yellow font color*

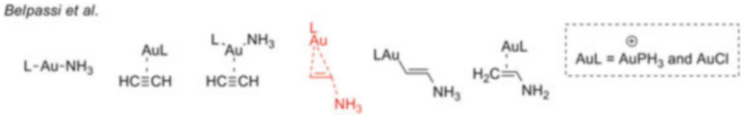

Fig. 5 Structures involved in the hydroamination of alkynes. Structures in *red* indicate transition states explicitly included in the benchmark

calculations, we included two new columns in our revised data, including results at the CCSD/def2-TZVPP and CCSD/def2-SVP. Interestingly, the CCSD energies computed with these basis sets show very different performances. CCSD energies using a double-ζ quality basis are rather poor when compared with the new reference. These energies are actually no better than those obtained with much cheaper GGA functionals. However, the use of a larger basis set, of triple-ζ quality, seems to help recover almost as much electron correlation as DLPNO-CCSD(T)/def2-QZVPP. As a result, the reference employed in our original benchmark yields very small errors when compared to the new one. Actually, CCSD/def2-TZVPP//CCSD/def2-SVP energies show the best fitting statistics of the entire benchmark, with an RMS below 1 kcal/mol and deviations generally below 1 kcal/mol from the reference, with very few exceptions (see Figs. 3 and 4).

Both the RMS and MAD obtained after the fitting procedure with the new CCSD(T)/def2-SVP energies are very similar to those reported in the original work [101]. Very small variations are also observed when considering a structure by structure analysis, as illustrated in Fig. 4. Actually, the color-coded tables obtained when fitting the energies with respect to CCSD and CCSD(T) data are almost superimposable. With this new data we can conclude that coupled clusters including single and double excitations yielded accurate energies for homogeneous gold catalysis provided that the basis set employed is large enough. However, we agree with recent studies that inclusion of triple excitations is highly recommended because there is no guarantee that the recovery of electron correlation following inclusion of the triples is as systematic as in this case.

Interestingly, similar results are reported by Belpassi et al. [107] regarding geometries. Apparently, the combination of CCSD with a triple-ζ quality basis set provides geometries for the intermediates and the transition state involved in a gold-catalyzed hydroamination reaction which are exact to the hundredth of an Angstrom when compared to a CCSD(T) reference (Fig. 5).

In 2011, Yao et al. [108] also published a study which tried to answer the same question as we did ("which density functional should we choose?") applied to gold (I) and gold(III) complexes with unsaturated aliphatic hydrocarbons. They center their work on the interaction of different gold complexes (Au^+, AuCl, $[Au(NHC)]^+$, $[Au(PH3)]^+$, and $AuCl_3$) with the simplest carbon unsaturated systems (ethene, ethyne, and propadiene). The reference data are calculated at the CCSD(T)/CBS (extrapolating to the complete basis set limit) level, so only geometries (C−C and Au−C bond lengths) of the smaller naked Au(I) complexes are used for the assessment of the performance of DFT methods in the description of geometries

(the other systems are too large for optimization with such a costly method). For bond dissociation energies, the geometries of all complexes are optimized at the CCSD/DZ [109] level and CCSD(T)/CBS is used for energy refinement.

In this study, 11 functionals covering the range from LDA to pure and hybrid GGA and meta-GGA and double hybrids have been used. For the geometries, calculations with LSDA, B3LYP, PBE0, M06, and B2-PLYP with the DZ and TZ [109, 110] basis sets were used, while the bond dissociation energies were tested for those same functionals plus PBE, M06-L, TPSS, M06-2X, TPSSh, and B2GP-PLYP with the ATZ basis set [109]. In terms of geometries, the best results are obtained by PBE0, with B2-PLYP displaying very close results. LSDA overestimates the interaction while both B3LYP and M06 underestimate it. Au−C bond lengths are also shorter with MP2 and SCSMP2 (spin-component scaled MP2), with better results for SCSMP2. For the bond dissociation energies, the order of increasing mean unsigned deviation is B2GP-PLYP < PBE0 < B2-PLYP < SCSMP2 < TPSSh < TPSS ≈ M06-L < M06 < PBE < B3LYP < M06-2X < MP2. The best overall results are for B2GP-PLYP (a reparametrized B2-PLYP) with a maximal deviation of 1.14 kcal/mol and MSE and MUE of 0.05 and 0.52 kcal/mol, respectively. The second best is PBE0, with maximal deviation of −3.79 kcal/mol and MSE/MUE of −0.36/1.60 kcal/mol. The results for the popular B3LYP have a maximal deviation of −12.49 kcal/mol and MSE/MUE values of −6.91/6.91 kcal/mol. For all systems, B3LYP and the Minnesota functionals underestimate the dissociation energies.

The inclusion of the explicit dispersion correction by Grimme et al. [81, 111–116], D3(0) or D3(BJ), considerably improves the results of B2LYP and B2-PLYP, while the Minnesota functionals barely change. TPSS, PBE, and PBE0 do not improve uniformly across the data set, and B2GP-PLYP sees its performance degraded. The recommendation for Au–carbon unsaturation complexes are B2GP-PLYP and B2-PLYP, together with the hybrid GGA PBE0. The authors suggest, however, that further studies should be carried out to ascertain whether this good performance extends to theoretical studies of homogeneous gold-catalyzed reactions.

Another study on bonding between gold(I) and unsaturated species was published in 2012 by Nava et al. [104] It studies the interaction between several small alkenes and alkynes with different substitution patterns with AuCl, $Au(PR_3)^+$ (R = H, Me, Ph), and $Au(NHC)^+$ (NHC = 1,3-dimethylimidazol-2-ylidene), using only the smallest systems AuCl and $Au(PH_3)^+$ with C_2H_4 and C_2H_2 for the benchmark calculations (Fig. 6). These involved CCSD(T)/def2-QZVPP [69, 117] geometry optimizations (using a scalar relativistic effective potential for gold) followed by ACPF [118], CASPT2 [119], and MRCI single point calculations. They show that, for the latter methods, a (6, 4) active space is needed to achieve a balanced description of the bonding and that the convergence between the results obtained with CCSD(T) and multi-configurational methods supports the use of the monodeterminantal coupled cluster approach to describe bonding in these species, at least in the fundamental state, confirming the choice of CCSD(T) as a valid reference for this study. Bond lengths and complexation energies calculated

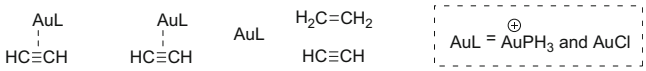

Fig. 6 Structures included in the benchmark by Nava et al.

with CCSD(T) for these four complexes are then compared with the results obtained with CCSD/def2-TZVPP//CCSD/def2-SVP, and the functionals BP86, TPSS, B3LYP, and M06 functionals with the def2-TZVP basis set. From these results they conclude that the contribution of at least perturbative triple excitations is needed to get a valid reference for benchmarking, with CCSD displaying large errors underestimating bonding for [AuCl(C_2H_2)] (6.93 kcal/mol) which make it unsuitable for benchmarking. Among the functionals, they find that BP86 and TPSS reproduce nicely the CCSD(T) results, with largest deviations of −2.63 and −3.11 kcal/mol, respectively, while M06 provides a performance considered acceptable with a maximum deviation of −3.82 kcal/mol and B3LYP displays errors up to 6.45 kcal/mol.

Although this work is not just a benchmark and also provides interesting insights into the nature of bonding in the four selected structures, in terms of the performance of DFT for gold catalysis this is study is notably incomplete. Their test set only includes four structures, and thus only four dissociation energies are considered, with no reference to the description of geometries or activation barriers of transition states (usually the most challenging). Their choice of density functionals is also very limited, with BP86, TPSS, B3LYP, and M06 being a rather sparse representation of the wealth of different approaches available to computational chemists nowadays. The absence of modern dispersion-corrected formulations is especially remarkable. In particular, the long-range corrected functional by Head-Gordon, ωB97X, which yields very good and consistent results for Au, Pt, and Ir according to a recent benchmark by Chen et al. (Fig. 7) [120]. Even more surprising is the fact that they also declined to include double-hybrid functionals, with perturbative corrections, such as B2PLYP. These functionals have been consistently the best performers in three independent and rather comprehensive benchmarks [101, 107, 120]. Both of these functionals not only have been shown to perform well for this chemistry – they have also gained substantial popularity in the last few years.

Additionally, according to this benchmark, the performance of the TPSS functional is outstanding compared to the other three functionals considered [104]. These conclusions are in contrast with the results reported by Chen et al. on the structures involved in 4 homogenous gold catalysis reactions (including transition states) with 11 density functionals and our benchmark on the 20 structures involved in the *gold carousel* and 32 density functionals. Both of these independent benchmarks conclude that TPSS performs rather poorly in homogeneous gold catalysis and that it is a bad choice when compared to other similarly expensive density functionals [101, 120].

Since the use of CCSD(T), the "gold standard" in quantum chemistry calculation, is, at this moment, restricted to relatively small systems, it is highly desirable

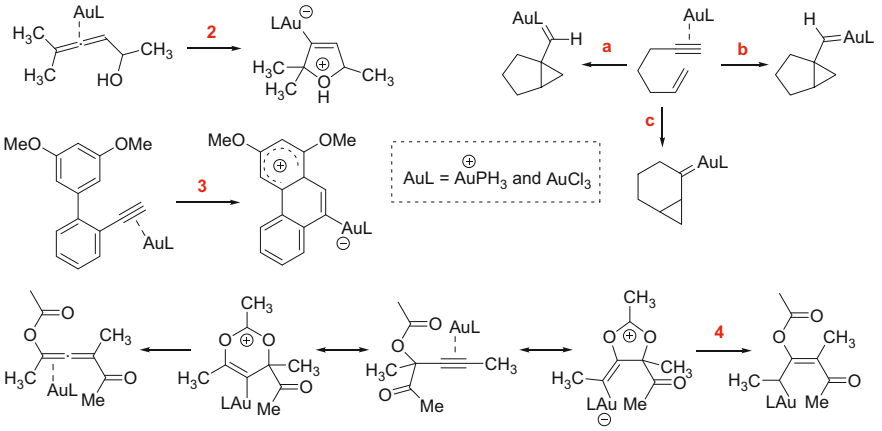

Fig. 7 Structures included in the benchmark by Chen et al. *Red* structures indicate transition states explicitly included in the benchmark

to find alternative ab initio methods with similar accuracy and a better scaling if we want really relevant reference testing sets for assessing the performance of DFT methods in the field of homogeneous gold catalysis. The Local Coupled Cluster method [119, 121–123], which uses localized molecular orbitals to exploit the local nature of electron correlation and thus reduce the scaling of coupled cluster methods through a divide-and-conquer approach, is proposed in the work by Chen et al. [120] as such an alternative. Using the barrier heights of gold-, platinum-, and iridium-catalyzed reactions, the authors propose a new computational scheme to improve the accuracy of LCC methods and find that it provides results comparable to CCSD(T)/CBS. Then they use these LCCSD(T) results to test the performance of different functionals with the triple-ζ quality cc-pVTZ/cc-pV(T + d)Z basis set on C, H, O, N/Cl, and P, and cc-pVTZ-PP on gold [109, 124]. The gold-catalyzed mechanisms included in the test set are a 1,6-enyne cycloisomerization, an allenyl carbinol cycloisomerization, and a propargyl acetate rearrangement, with $AuCl_3$ and $[AuPH_3]^+$ as catalysts, and a Friedel–Crafts alkylation with $AuCl_3$ and AuCl as catalysts. Of the 11 functionals studied, 6 showcase an MUE for the activation energies below 2 kcal/mol: B2GP-PLYP < BMK < M06-2X < wB97X < PBE0 < B2-PLYP (the other functionals tested were TPSS, TPSSh, B3LYP, BMK, and M06). One of the main conclusions of this study is that, even when restricting the range of application to reactions catalyzed by late transition metals, different types of reaction have different optimal DFT methods. In this study, for example, TPSS and TPSSh show relatively poor performance in Au-catalyzed reactions, which the authors attribute to their low percentage of HF exchange, while they are among the best for Pt/Ir. B2-PLYP is also significantly worse than B2GP-PLYP for the gold-catalyzed barriers in this study, although its performance is equivalent in the Pt/Ir C–H activation set. In this context, B2GP-PLYP, wB97X, and PBE0 are the recommended most general choice from this study. As a cautionary note, these results seem to indicate that

the type of reaction or electronic changes taking place along the reaction path might be more important in determining the performance of a functional than just the transition metal used.

Another recent study by Belpassi et al. [107] tackles the mechanism of the nucleophilic attack of ammonia on ethyne catalyzed by AuCl or $Au(PH_3)^+$, a simple model of alkyne hydroamination, one of the most exploited and studied gold(I)-catalyzed reactions (see Fig. 5). Such a mechanism is deceptively simple, since many short-lived intermediates and ramifications in the reaction paths may be involved depending on the substituents used, the type of ligands, solvent, counter-ion, etc. Often, the energies involved in determining the course of the reaction are not high, so a validation of the methodology used is very relevant to make any mechanistic study dependable.

In this last paper, as in Faza's, the authors focus on the whole mechanism, not just the gold-unsaturation complex which initiates the catalytic cycle. For this, they select six gold(I)-coordinated structures expected to participate in this mechanism (12 structures in total, since the two catalysts are used for all of them): the transition state for the nucleophilic attack, possible intermediates along the reaction path, and the energies of the individual species relative to the free reactants ($LAu + NH_3 + C_2H_2$) in the gas phase. Using CCSD(T)/def2-QZVPP//DF-LCCSD(T)/def2-TZVPP calculations as a reference, they test the performance of a variety of popular functionals (BLYP, OPBE, BP86, M06-L, B3LYP, PBE0, M06, TPSSh, and B2PLYP) with the def2-TZVP basis set when reproducing the geometries and energies of these species (the zero of energy was taken to be the sum of the energy of all the separated fragments).

Their reference geometries obtained for $[AuPH_3(C_2H_2)]^+$ and $AuCl(C_2H_2)$ at the DF-LCCSD(T)/def2-TZVPP level are directly comparable to those obtained by Nava et al. [104] using the significantly more expensive CCSD(T)/def2-QZVPP. They also show that DF-LCCSD/def2-TZVPP (without triple excitations) provides very good results on the geometries of the whole test set (MSEs around −0.005 Å), while DF-LCSSD(T)/def2-SVP leads to significantly larger deviations (MSEs between 0.009 and 0.042 Å), attesting for the importance of using a sufficiently flexible basis set within the coupled cluster approach. For the energies, it seems that the inclusion of triple excitations is needed for good accuracy, since the results obtained with the same basis set (triple-ζ) for the same geometries with CCSD(T) are significantly better than those calculated with CCSD (and also DF-LCCSD(T)); however, this improvement is completely lost when a smaller basis set is used. Despite its still wide use, MP2 is shown here to be insufficient for accurate predictions of either geometries or energies in gold chemistry.

The minimum acceptable basis set for DFT calculations is of triple-ζ quality with polarization on all atoms (def2-TZVP). Geometries are of good quality for most functionals tested, when used with a converged basis set. Energies are much more difficult to reproduce, with large nonsystematic errors between 4 and 12 kcal/mol and MSE between −7 and +5 kcal/mol. The MSEs for M06 or M06-L are very low, but they seem to be more a result of the cancellation of errors than any intrinsic

advantage of the method, since the deviations are considerable (2.4 and 2.3 kcal/mol, respectively). B2PLYP outperforms all other functionals in the study, with small absolute errors and standard deviation (~1 kcal/mol), making it a safe choice for the study of competing reaction paths. The main drawback of this double hybrid is its computational cost, since it scales as an MP2, but it can be mitigated if another functional with a sufficiently large basis set is used for the geometry optimization, reserving B2PLYP for a single point energy correction.

Among those reviewed, this is the first benchmark study offering a clear strong recommendation or "recipe" for homogeneous gold catalysis: geometry optimization with any of the tested functionals with at least a triple-ζ basis set with polarization for all atoms and a B2PLYP single point energy refinement. They also argue strongly against the use of B3LYP/6-31G* for the exploration of reaction paths in this kind of system (something very common even in the latest studies of hydroamination mechanisms), since the description of the relative energy of tricoordinated vs biscoordinated species in this mechanism is particularly unsatisfactory, probably leading to the underrepresentation of reaction paths with tricoordinated species in the literature.

Not directly focused on reaction mechanisms, but using in their reference sets structures which might be of great relevance in them, are the following studies, dealing with aspects as varied as aurophilic interactions or the structure of gold clusters.

Johnson et al. [125] studied how dispersion-corrected density functional theory performed at describing aurophilicity, an effect which is sometimes very relevant in gold chemistry. Aurophilicity, or the attraction between closed-shell Au(I) atoms has been traditionally attributed to van der Waals interactions, with a strong dispersion component. Thus, the method of choice for its study for some time was MP2, since it is the lower cost post-HF method which can account for electron correlation. However, the work by O'Grady and Kaltsoyannis [126] puts its use into question. Their study showed that the increase with atomic number of MP2 interaction energies of the $[MCl(PH_3)]_2$ dimers (M = Cu, Ag, Au, Rg) usually used to quantify this effect were in disagreement with the results obtained when electron correlation was introduced through the QCISD or coupled cluster approaches (CCSD and CCSD(T)), which displayed a maximum interaction for silver. Once MP2 use is questioned, and more accurate post-HF methods are most often unaffordable for the large structures involved in catalysis, DFT appears as an attractive alternative. Although conventional DFT is unable to capture dispersion interactions, recent advances in dispersion-corrected density functional theory (either by parametrization or by explicit incorporation of dispersion terms in the functional form) make the use of DFT very attractive for the description of systems with aurophilic interactions, since they scale better than correlated wavefunction methods (MP2, coupled cluster…). Using complete-basis-set-extrapolated CCSD (T) data as a reference, they perform PW86PBE-XDM and LC-ωPBE-XDM (XDM = exchange-hole dipole moment model of dispersion) calculations with relativistic and non-relativistic ECPs on a series of dimers. With the use of very large basis sets and extrapolation schemes, they find that the metallophilicity

increases from Cu to Ag to Au. Their main conclusion is that modern DFT is better than MP2 to account for aurophilicity, that dispersion is less important than traditionally assumed, and that the experimentally observed stronger metal–metal interaction in gold rather than in silver or copper is not caused by a "super van der Waals" interaction, but to an indirect relativistic effect, where the increased electron affinity of gold destabilizes strong ionic interactions with bridging anions, facilitating close metal-metal contacts.

Another problem usually found with DFT approaches when studying transition metal complexes is how to describe donor-acceptor interactions properly where charge transfer takes place, be it either through localization error, self interaction error, the choice of exchange functional, or the lack of dispersion (the many-electron self interaction error, together with dispersion, seems to be the main contribution to this artificial altering in the donating and accepting abilities of the fragments). The GKS (Generalized Kohn–Sham) formalism involving range-separated hybrid functionals mitigates some of these problems since (1) the HOMO and LUMO eigenvalues approach the values of IP and EA and (2) it corrects the nonlinearity of DFT energy with respect to fractional electrons. The work by Koppen et al. [127] successfully uses range-separated functionals with dispersion corrections in the Generalized Kohn–Sham framework (LRC-ωPBEα, optimizing the two parameters) to reproduce the CCSD(T)/aug-cc-pVTZ(-PP) results for the aurophilic complex $(HAuPH_3)_2$ and the binding energies between Au_4 and several ligands (SCN-, benzenethiol, benzenethiolate anion, pyridine, and trimethylphosphine). Hybrid functionals (PBE0) don't lead to good results because they don't guarantee a correct HOMO(D) and LUMO(A) gap, although this could be corrected through variation in the percent of exact exchange in the functional.

Gold clusters in the literature have usually been studied as a small model system for heterogeneous catalysis, as a proxy for surfaces or larger supported nanoparticles. However, they can also be seen as a model of the behavior of digold species or other aggregates formed in supposedly homogeneous conditions, which have been shown to catalyze many organic transformations.

In the frontier between homogeneous and heterogeneous catalysis, another benchmark study on very small gold clusters (Au_3) focuses on the H_2 activation and dissociation. This work by Brothers et al. [128] uses CCSD(T)/CBS//MP2/def2-QZVPP data as a reference for evaluating energy calculations with 30 different functionals, HF and MP2 and geometries with a smaller set of functionals (Fig. 8).

Previous computational studies of the interaction of hydrogen with small gold clusters, such as the work by Wang et al. [129] on Au_n ($n \leq 5$) use DFT methods and validate them against available experimental results. In this case, the PW91PW91 method with LANL2DZ basis set and pseudopotential, together with the 6-31++G (d,p) basis set on hydrogen seemed to provide good adiabatic ionization potentials, electron affinities and bond length and frequency for the AuH molecule.

The first benchmark of the performance of DFT against high level ab initio data also uses experimental information, but now to calibrate the accuracy of the reference first. This work by Gordon et al. [130] on the reactions between neutral and anionic Au_2 and Au_3 and hydrogen finds that CCSD(T) calculations with the

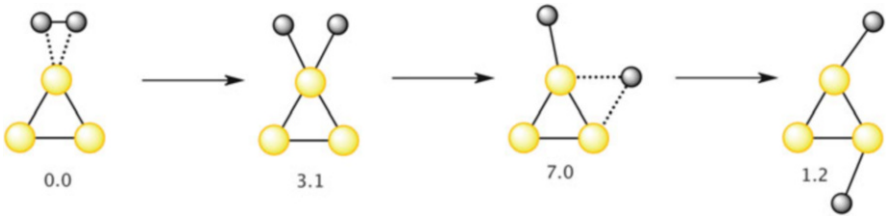

Fig. 8 Computed mechanism for the hydrogen activation by small Au_3 clusters

SKBJC ECP and basis set [131], augmented by one set of *f* polarization functions and one *s* and one set of *p* diffuse functions for gold and 6-31++G** for hydrogen [132], provide a good agreement with experimental bond lengths, dissociation energies, and vibrational frequencies, an agreement which is even better with a larger basis supplementing the SKBJC with a set of *3f/2g* polarization functions and one *s* and one set of *p* diffuse functions and using aug-cc-pVTZ for hydrogen [110]. They find that B3LYP DFT calculations with these same basis sets perform reasonably well at predicting geometries and hydrogen binding energies to small gold clusters. However, the equivalent calculations with plane wave basis with PW-PW91 and PW-rPBE tend to underestimate activation energies.

The work by Brothers et al. [128] is much more comprehensive and incorporates all the functional families in use nowadays. They find that DFT with a large basis set (they use def2-QZVPP with the associated relativistic ECP) [117] can be used to model this class of reactions accurately, with double-hybrid functionals providing the best results (specially mPW2PLYP). The range-separated hybrids HSE06 and HISSb also provide reasonable results at a significantly lower cost, something which can be determining in the study of this kind of systems, which very easily can become too large for perturbational approaches. It should be noted that the authors don't find significant differences in relative energies between the results obtained optimizing geometries with MP2 or with DFT.

Restricting the evaluation to the RMSD for the gold species (in their study they also include silver clusters), the ordering of functionals is the following:

mPW2BPLYP < B2PLYP < B2PLYPD < HSE06 ≈ mPW1PW91 ≈ PBE0 < H-ISSb < wB97XD ≈ M06L < B3LYP < wB97X < BHandHLYP < TPSSh < M06-2X ≈ M06 ≈ LC-wPBE < wB97 < M06-HF < TPSS ≈ revPBE ≈ PBE ≈ PW91 < SCS-MP2 ≈ tHCTH ≈ BMK < BLYP < SVWN < PBEsol ≈ B97D < MP2 < PBE + Πs < Π1PBE < HF

It should be noted that, among the functionals, the wavefunction methods MP2, SCS-MP2, and HF have also been included for the sake of comparison.

Although there are outliers, the general trend is double hybrids < hybrid ≈ range-separated < pure < rung 3.5 functionals, with two hybrids (mPW1PW91 and PBE0) and range-separated (HSE06) functionals (with a surprisingly good performance of the pure M06L, which could be welcome for the study of the largest systems, because of lower cost) heading the classification after the perturbatively-corrected double hybrids.

An extension of this study has been carried out incorporating a test of the hydrogen activation in gold clusters larger than Au_3 (Au_n, $n = 3, 4, 5, 7, 8, 9, 10, 13, 16$), nanoribbons (RL and RH, standing for low coverage and high coverage), nanotubes (T1L and T1H, standing for low and high coverage, and T2), and surfaces (pristine and defective Au(111)) [133]. In the study of processes in the interface between homogeneous and heterogeneous catalysis, it is necessary that the method of choice can properly describe the dependence of reactivity on the structure of gold, be it either in the form of atoms, clusters, nanowires, or surfaces (all of them have been shown to display catalytic activity). There is an abundance of computational studies on all of these systems separately, but no work until now which includes all of them in the same reference set. Although most functionals provide qualitatively good trends in reactivity (decreasing adsorption energies and increasing dissociation barriers with increasing gold coordination number), there is no clear choice of method for quantitatively accurate results, and further study of methods beyond the GGA approximation is encouraged.

Although of less direct interest for homogeneous catalysis, the study of larger gold nanoparticles or subnanometric clusters also converges with the interest of many other applied fields (optoelectronics, nanotechnology...) in a field which has become very active. Muniz-Miranda [134] tested the performance of different DFT functionals, pseudopotentials and basis sets describing the structure and optical gap of a series of gold nanoclusters. Their choice of systems relied on the availability of X-ray structures and UV–vis spectra and a balance between the small size desirable for such a comprehensive study and a variety of properties, such as stability, electronic structure, charge, or organic coating, leading to the use of $Au_{11}(SPy)_3(PPh_3)_7$, $Au_{11}Cl_3(PPh_3)_7$, and $[Au_{24}(PPh_3)_{10}(SC_2H_4Ph)_5ClBr]^+$ (in some parts of the study, bulky ligands have been simplified to phosphine or a thiol group). The reference for structures and transitions in this case are the experimental data, not high-level post-HF calculations. A wide range of functionals have been tested: simple GGA or meta-GGA (B-LYP, PBE, TPSS, PBE-LYP, B-PBE, B-PW91, B-P86, and VSXC), global hybrids (B3-LYP, B3-P86, B3PW91, B1-LYP, BHandH-LYP, O3-LYP, PBE0, M05, M06, M06HF, and mPW1-PW91), and five range-separated/long range-corrected hybrids (HSE06, CAM-B3LYP, LC-BLYP, LC-PBE, and LC-TPSS). For the full-size clusters, a modified version of the LANL2DZ ECP/basis set with an optimized outer p function (modLANL2DZ) which improves Au–Au bond length and dissociation energy of Au_2, has been used for gold (other pseudopotentials were also tested), while the main group atoms were described using 6-311G(d,p) for the smaller clusters and 6-31G* for the larger. Other basis schemes (with smaller basis sets for the atoms not directly bound to gold) have also been successfully tested, as well as ONIOM [135] calculations with DFT and PM6 [136]. They find that electronic structure (energy gaps are calculated with TDDFT) and geometry can be reasonably reproduced with many GGA and meta-GGA functionals, especially those including PBE-like correlation (BPBE, PBE, BPW91, BP86, TPSS), while some hybrid (PBE0, mPW1PW91, B3PW91, B3P86) and range-separated hybrid (HSE06) lead to good geometries despite overestimating the optical gaps by up to 0.5 eV.

CAM-B3LYP, a popular choice, leads to an inaccurate geometry for the Au_{24}^{+} cluster and range-separated hybrids overestimate the optical energy gaps. The LYP correlation functional (BLYP, PBELYP) leads to large deformation of the gold cores when used in GGA functionals, and also results in low performance of B3LYP in comparison with better hybrid combinations such as B3PW91 or B3P86. This can be attributed to a relevant metallic character in even the small gold nanoclusters which needs to be taken into account, even when the HOMO–LUMO gap is not zero. The main finding of this work is that DFT calculations can be used to simulate the structural and optoelectronic properties of gold clusters with or without organic coatings, allowing the study of their catalytic activity or other technological applications.

From the latest benchmark studies, the main conclusion, besides the good performance of some functionals (double hybrids almost always come first, and then PBE0) seems to be that there is no general functional which can be broadly applied to a wide range of transition metal-catalyzed reactions, since, despite the good overall performance, the deviations for an individual reaction can be so high so as to render the results useless. As an example, deviations up to 12 kcal/mol for the most accurate functionals PBE0 and TPSSh in the latest study by Reiher et al. [137] where they tested nine popular functionals against the WCCR10 data set of ten ligand dissociation energies of cationic transition metal complexes (only two of them included gold) deliberately set to be of a large size, so that factors which are usually overlooked in the studies with smaller complexes, such as dispersion effects, were considered. Because of the size of these systems, it is not possible at this moment to obtain ab initio computational data reliable enough for benchmarking, so experimental gas-phase ligand dissociation energies measured with mass spectrometry have been used as a reference. Only nine functionals, including GGA (GGA, BP86, PBE, BP86-D3), meta-GGA (TPSS), and hybrids (B3LYP, TPSSh, PBE0, B3LYP-D3) were included. Dispersion in this study has been included using Grimme's D3 correction (which has been shown not always to improve results for certain functionals in previous benchmarks) [112], but the inclusion of double hybrids (they almost consistently provide the best accuracy in benchmarks of gold-catalyzed homogeneous catalytic processes) would have been an interesting addition to this work.

2.2.5 Other Aspects to Consider

Although they are not often discussed in detail in computational studies related to homogeneous catalysis, there are other aspects of simulations which may need to be considered when studying a reaction mechanism, or when evaluating the competition between alternative reaction paths.

One of the clearest examples of these is the treatment of solvent. Although quantum chemistry methods are designed to provide electronic energies of the studied systems in the gas phase (i.e., in the absence of intermolecular interactions), most reactions relevant to homogeneous catalysis are carried out in solution. In

some cases, especially when working with apolar solvents, there is barely any difference between the geometries and relative energies calculated in the gas phase and those obtained using a model to account for solvation. There are also plenty of examples where the geometries of stationary points along a reaction path optimized in gas phase or in solution are effectively the same (something which is more common when there is no large charge separation in the structures), since geometries are less sensitive to the polarization induced by the medium than the energies and electronic distributions. However, in this work we present many examples of gold-catalyzed reactions where the inclusion of solvent effects not only alters some reaction barriers or a couple of polar bond lengths, but also generates new reaction paths which can completely alter the mechanism.

Most modern computational studies of gold-catalyzed homogeneous mechanisms incorporate solvent effects in some way. The most popular approaches are based on the polarizable continuum model (PCM). In these models, the solvent is treated as a continuum medium characterized by a dielectric constant. The system of interest is laying inside a cavity in this continuum which can be created, and updated along the geometry optimization, in different ways, most often involving the use of a set of parametrized atom radii or some electron density cutoff. During the SCF, the electronic density of the system polarizes the continuum and is also polarized back by it.

Because of the implementation in Gaussian09 (one of the most popular programs used in mechanistic studies) of smooth solvation potentials in the PCM routines [138, 139], geometry optimizations in solution are nowadays no more costly or difficult than gas-phase optimizations, so geometry optimizations in solution are becoming more and more common, even if there are still many examples where solvent effects are evaluated through single-point calculations on gas-phase geometries.

Because of the limitations of continuum models, intrinsic to their design, they are unable to describe explicit solvent effects such as hydrogen bonding or any other kind of interaction beyond immersion in a polar environment. Thus, when the direct involvement of a solvent molecule might play a role in the mechanism (coordinating to the metal, stabilizing reactants, products or transition structures, providing or abstracting protons, etc.), it has to be included explicitly as part of the system. This often increases the computational cost in terms of basis functions and produces a more complicated potential energy surface which is going to make the optimization process difficult. The decision whether to include just a molecule of solvent or a cluster is not always easy and, as we see later on, it can have dramatic effects on the reaction profiles. This, together with the need to deal with other phenomena, such as rapid ligand exchanges in organometallic compounds active in catalysis, or complicated potential energy surfaces which can render the application of transition state theory useless, may call for the use of molecular dynamics simulations. Despite being very common in biochemistry, where the existence of molecular mechanics force fields or well parametrized and tested semiempirical methods allow for the modeling of larger systems and/or longer timescales, these techniques are not yet widely used in the community studying homogeneous

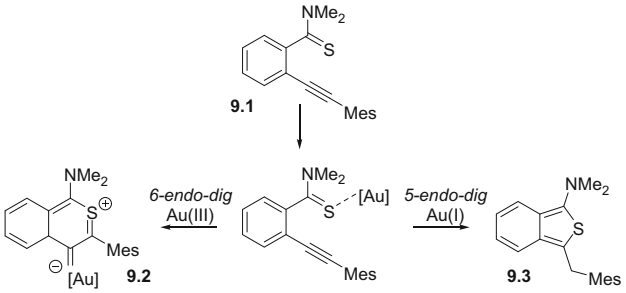

Fig. 9 Formation of two different products from alkynylbenzothioamide **9.1** through a bifurcation region

catalysis. However, examples of the successful application of ab initio molecular dynamics to some organometallic reactions, such as the water oxidation by a ruthenium catalyst [140], the Wacker process [141], or the solvent coordination of $PdPPh_3$ [142], might increase their visibility and widen their use.

An example of the consideration of dynamic effects, although through classical trajectories, instead of AIMD, in gold catalysis can be found in the work by Cavallo and coworkers [143]. They have tackled a gold-catalyzed reaction involving a bifurcation area at the rate-limiting transition state. From alkynylbenzothioamide **9.1** two different cyclization pathways can be observed experimentally. Au(I) is found to promote a 5-exo-dig cyclization to afford a benzothiophene structure, whereas Au(III) opens a different reacting route involving a 6-endo-dig cyclization to afford an interesting mesoionic complex (see Fig. 9). A relatively straightforward exploration of the potential energy surface of these rearrangements under Au(I) and Au(III) catalysis helped solve the mechanistic conundrum. Both Au(I) and (III) activate the substrate in a similar way to a π-acid acting on the triple bond. The differences arise very late in the reaction profile, right at the last cyclization event. Au(I) favors the formation of the unobserved benzothiophene kinetically, but in a reversible process. In these circumstances, the fact that the 5-exo-dig product is thermodynamically more stable becomes crucial for selectivity. On the other hand, Au(III) activates the triple bond such that only the 6-endo-dig product can be formed from the open precursor. After this, a high energy transition state communicates both products, such transition state becoming prohibitively expensive at room temperature. In other words, Au(I) catalysis enforces thermodynamic control on the reaction whereas Au(III) operates under kinetic control, hence the different product formation. Observing the latter energy profile, Cavallo and coworkers correctly suspect that the potential energy surface of this catalytic step is also outside the range of classical transition state theory. They therefore take a step further to gain more insight on the fundamentals of these changes of selectivity and run quasi-classical trajectories, the analysis of which help uncover a bifurcation situation in which the basin for the formation of the 6-endo-dig product is much

better aligned with the previous transition state, thus reinforcing the idea of the Au (III) catalytic process being governed by kinetic factors.

2.2.6 What Method to Choose?

If there is a conclusion which can be extracted from all the previously discussed papers, it is that no single functional is consistently superior to all others in the study of gold catalysis and that one has to be careful when extrapolating the results from one system to another, even if they are apparently similar. However, some general trends are found which can help guide us in the choice of method when confronted with a catalytic mechanism to be studied.

The ideal approach would be to calculate all the stationary points along the different reaction paths with a coupled-cluster method including triple excitations with a sufficiently large basis set. Using CCSD(T)/def2-QZVPP energies on DF-LCCSD(T)/def2-TZVPP geometries has been shown to be a cost-effective alternative for that [107], and newer coupled-cluster approximations, such as domain-based local pair natural orbital coupled cluster calculations DLPNO-CCSD(T) [106] could be used to reduce significantly the computational cost of conventional CCSD(T), but for most practical applications in catalysis, coupled cluster calculations are too expensive. When DFT needs to be used for the whole mechanism, but the number of atoms makes some coupled-cluster calculations feasible, it is recommended to test the performance of the chosen functional/basis against coupled cluster calculations for a reduced set of the most relevant species in the catalytic cycle or truncated or simplified versions of them. This should be optimally carried out for both geometries and energies, but single-point coupled-cluster calculations on DFT geometries can be expected to provide a reasonable approximation when coupled-cluster optimizations are not an option (and they are not an option for most systems of interest, because of their size), since geometries are usually significantly less sensitive to the choice of functional than energies.

When no high-level calculations can be performed for a given system or one wants to avoid the hassle of testing the performance of different methods against them before conducting a mechanistic study, the results of the previously discussed benchmark works can be useful.

The relativistic effects affecting catalysis can be safely described using well-designed ECPs, such as the Stuttgart–Dresden, without the need to resort to relativistic Hamiltonians. However, if for any reason full-electron scalar relativistic calculations (ZORA or DKH) need to be carried out, the recently developed Gaussian segmented basis sets (SARC) make their cost comparable. In terms of basis sets, at least a triple-ζ basis with polarization in all atoms should be used (otherwise errors produced by the reduced basis size are more significant than errors caused by the functional used).

The best choice of functional is less clear-cut. Most studies agree that double hybrids (B2GP-PLYP or B2PLYP) consistently provide the best results, both for energies and geometries, and they should be used when possible. When the computational demands associated with the time-consuming evaluation of the perturbative part of these calculations are too high to make geometry optimizations affordable, a single point energy evaluation with a double hybrid on structures optimized with other functionals are usually a good compromise. Other functionals which have provided consistently good results in the benchmarks analyzed in this chapter are PBE0, ωB97X, or M06-2X/M06, but they should be used with some caution, because their good performance is by no means universal.

Nowadays, when studying reactions in solution, the effect of the solvent should already be taken into account in the geometry optimizations (not just added as single-point energy corrections), especially when working with a polar solvent and species where charge separation is large along the reaction path. The possibility of explicit solvent effects should also be considered (proton transfer steps, association and dissociation of solvent as a ligand, etc.) and explicit solvent molecules included in the system if needed.

3 Examples of Recent Insights in Mechanisms in Gold Homogeneous Catalysis from Computational Chemistry

In this section we review recent contributions of computational chemistry to the mechanistic study of homogeneous gold-catalyzed processes. Because of the size of the field, this revision of the literature has no pretense of being comprehensive, and we just focus on a handful of systems or models of reactivity which have shown interesting developments in the last years, highlighting the role molecular modeling has played in improving our understanding of gold-catalytic chemistry and guiding new discoveries.

3.1 Nucleophilic Attacks on Activated Unsaturations

The role of gold complexes as soft, carbophilic π-acids activating unsaturations towards the inter- or intramolecular attack of a nucleophile has been one of the most exploited in diverse synthetic schemes, and also one of the best studied, experimentally and computationally. Thus, in this section, we only focus on some of the latest examples in the literature, with less conventional nucleophiles or other relevant features which set them apart. Some recent work on nucleophilic attacks on gold-activated unsaturations where there is evidence of dual activation or participation of digold species is reviewed in the corresponding section.

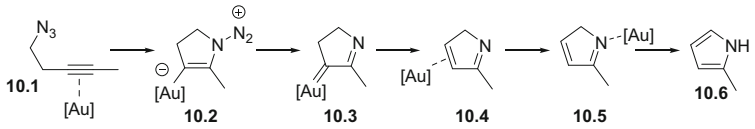

Fig. 10 Formation of pyrroles from homopropargyl azides

Xia and Huang [144] have computationally studied the mechanism of the Schmidt reaction of homopropargyl azides described by Toste et al. [145]. All calculations have been carried out at the B3LYP/6-31G*,LANL2DZ(Au) level, with PCM single point calculations using UAO radii at the gas-phase geometries used to take the effect of different solvents into account. The PPh_3 ligand was truncated to PH_3 to reduce the computational cost (Fig. 10).

After activation with the PH_3AuSbF_6 (used as a model of the PPh_3AuSbF_6 used in the laboratory), the alkyne is attacked by the proximal nitrogen of the azide group to yield **10.2** through a 10.3 kcal/mol barrier. Loss of dinitrogen leads to carbene **10.3** through a transition state with a very low activation barrier, 5.4 kcal/mol, which is, on its turn, transformed into gold-coordinated 2*H*-pyrrole **10.4** through a 1,2-H shift, in a very accessible process with an activation barrier of 8.9 kcal/mol. A migration of the gold complex from C3–C4 to the nitrogen, leading from **10.4** to **10.5**, is proposed to take place through a dissociation and a new coordination step, both of them exergonic. Tautomerization of the latter structure leads to aromatization and formation of the pyrrole product **10.6** through a 1,5-H shift. Interesting questions addressed in this work are whether the H migrations can be assisted by a protic solvent or ligands and how does the tautomerization take place (previous studies attributed to this step a high activation barrier). The 1,2-hydrogen migration seems to occur intramolecularly, as the barrier for this process is rather low. However, the direct 1,5-H shift proposed between **10.5** and gold-coordinated **10.6** is unfeasible because of the associated 42.8 kcal/mol barrier. The assistance of a 2*H*-pyrrole proton shuttle, however, considerably lowers this barrier to a much more reasonable value of 20.1 kcal/mol, still the rate limiting step of this transformation. Thus, **10.5** transfers one of the hydrogens at C5 in the form of a proton to a non-coordinated **10.5** molecule (20.1 kcal/mol activation energy), which then gives it back to the nitrogen (6.4 kcal/mol barrier).

In 2009, two groups published a DFT mechanistic study of the same reaction [146, 147], the synthesis of furans based on the gold(I)-catalyzed cycloaddition of 1-(1-alkynyl)cyclopropyl ketones with nucleophiles, the first at the BHandHLYP/PCM/6-311++G(d,p),SDD(Au)//BHandHLYP/6-31G(d,p),SDD(Au) level, the second at the B3LYP/6-31G(d),LANL2DZ(f)(Au), with PCM single point calculations to account for solvation. This is an interesting example where activation of an alkyne towards nucleophilic attack is preferred over the alternative coordination of gold to the carbonyl oxygen when two mechanisms are available. Zhao and coworkers studied the two different mechanistic pathways regarding the role of gold [146]. Carbonyl activation leads to ring expansion and subsequent furan formation whereas alkynyl activation produces the furan ring first and then the

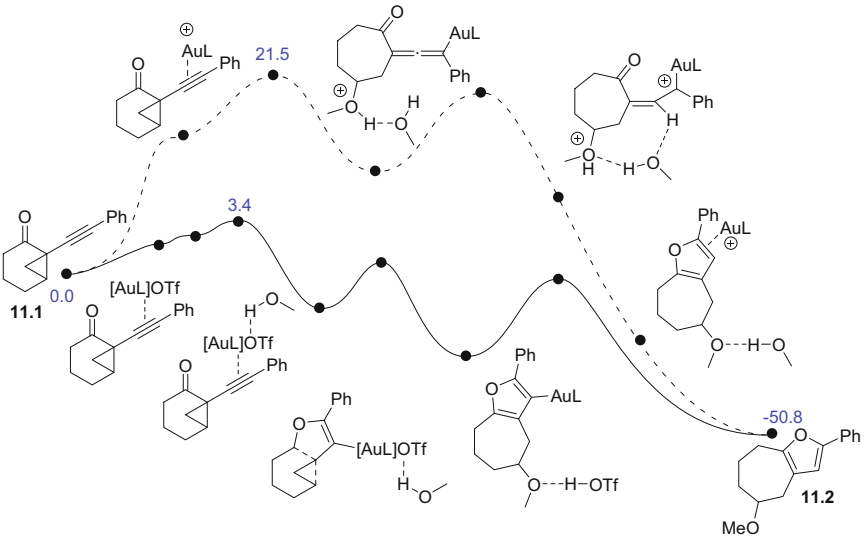

Fig. 11 Mechanistic pathway reported by Li et al.

six-member ring expansion takes place. The rate-limiting transition states have associated energies of ~20 and ~40 kcal/mol for the alkynyl and ketone activation, respectively.

In their work, Li and coworkers disregard the high energy pathway of ketone activation [147]. Instead, they focus on two different modes of activation of the operative alkynyl activation pathway. The first option is cationic gold directly activating the triple bond, obtaining a mechanism which is essentially superimposable to that reported by Zhao. In the second option they also consider the potential role of the counterion and explicit solvent molecules along the entire mechanism. They find that the counterion is not just a spectator in this chemistry and its participation has a significant impact in the mechanism (see Fig. 11). The triflate counterion considered in their work recruits a solvent molecule (methanol) into the reacting sphere which then participates intramolecularly in the proton transfer events; as a consequence, most of the transition states and intermediates are strongly stabilized. For instance, the rate-limiting transition-state energy gets reduced from 21.5 to 3.4 kcal/mol when triflate and methanol are explicitly considered in the calculations. The latter activation energy is much more consistent with a reaction which occurs in 15 min at room temperature.

Analyzing the profiles computed for this reactivity one should conclude that homogeneous gold catalysis is very prone to be strongly affected by environmental factors. Consideration of solvation (implicitly and, more importantly, explicitly), counterions, additives, etc., may have effects on the potential energy surface which are often much more drastic than those resulting from the election of one or other of the density functionals and basis available to the computational chemist.

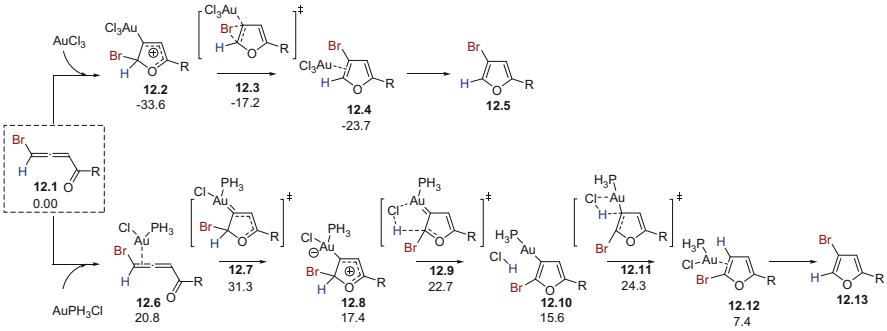

Fig. 12 Mechanism for the regioselective formation of furans on gold(I) or gold(III) activation of bromoallenyl ketones. Relative free energies in solution are given in kcal/mol

The next work is an interesting example of ligand-controlled regioselectivity in the gold-catalyzed cycloisomerization of bromoallenyl ketones, by Li et al. [148]. Depending on whether a gold(I) ($Au(PH_3)Cl$) or gold(III) ($AuCl_3$) catalyst is used, a furan product or its isomer (see Fig. 12) is obtained, in the first example of reaction where gold in different oxidation states leads to different products. B3LYP/6-31G*, LANL2DZ(Au, Br) with CPCM to account for solvation, has been used for all calculations.

When $AuCl_3$ coordinates to the distal double bond of the allene in the initial bromoallenyl ketone (**12.1**), this activated unsaturation suffers a barrierless attack of the carbonyl oxygen to yield **12.2**. This intermediate can undergo bromine or hydrogen migration, but the former is considerably more favorable, with a barrier of 16.4 kcal/mol (vs 30.7 kcal/mol). The transformation of the resultant **12.4** in the furan product **12.5** regenerating the catalyst through ligand exchange with **12.1** is highly exergonic (30.3 kcal/mol).

It was found that in the presence of water, some 1,2-H migration product is formed, a result which has been confirmed by calculations, with a water-assisted hydrogen shift with a barrier only 1.4 kcal/mol higher than that corresponding to TS **12.3**.

When the activation of the allene is done by the less electrophilic $AuPH_3Cl$, the endergonic formation of complex **12.6** is followed by a cyclization step with a 10.5-kcal/mol barrier. The resultant product can experience a direct 1,2-H or 1,2-Br migration, as in the previous mechanism, with barriers of 30.1 and 14.6 kcal/mol, respectively. However, a third possibility is a chloride-assisted 1,2-H migration, where the Cl loosely bound to gold is able to abstract a proton from C2 with a barrier of 6.3 kcal/mol and then use this same proton for the protodeauration step **12.11**, with an 8.7-kcal/mol barrier.

Thus, the regioselectivity of the reaction depends on the counterion of the catalyst used. Although in both gold(I) and gold(III) activated mechanisms the preferred migration is the 1,2-Br, when the catalyst is $Au(PR_3)L$ (L = Cl, OTf), a lower energy counterion-mediated 1,2-H shift needs to be taken into account, which reverses this preference.

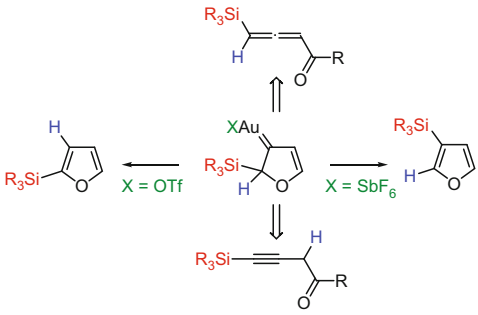

Fig. 13 Formation of furans from silyl-allenyl ketones and silyl-propargyl ketones

A very similar mechanism has also been studied with DFT calculations by Gevorgyan et al. [149] for the synthesis of silylfurans from allenyl or homopropargylic ketones (see Fig. 13). Upon gold activation and cyclization, a gold carbene with a structure analogous to **12.8** (see Fig. 12) is formed. This structure can undergo 1,2-Si or 1,2-H migrations (or even 1,2-alkyl migrations, depending on the substitution pattern on the substrate). Although silyl migration is the kinetically favored path, the effect of the counterion or solvent can reverse this preference. With cationic gold catalysts with the non-nucleophilic SbF_6^- counterion, silyl migration is always favored, independent of the solvent used. However, when the counterion is TfO^- and a non-polar solvent is used, a formal 1,2-H migration is the preferred path.

The work of Yates et al. [150] builds on the well-known chemistry of enynes under gold catalysis and DFT calculations to explain a series of experimental observations regarding the selectivity of 1,5 enynes with alcohols as a function of the substituents on the terminal alkene (H or Me), the nucleophilicity of the alcohol, and the presence or absence of a silicon center in position 3 of the enyne chain.

Calculations have been done at the M06/6-311+G(2d,p),def2-QZVP (Au)//B3LYP/6-31G(d),LANL2DZ(f)(Au) level, modeling the effect of the dichloromethane solvent with BS2 on gas-phase geometries with CPCM. PMe_3 has been used as a model for the experimentally used PPh_3 ligand.

The mechanisms for the transformation of these two substrates are summarized in Fig. 14. Enynes **14.1a** and **14.1b** behave differently upon gold complexation. While in **14.1a** the nucleophilic attack of the pendant alkene to the activated alkyne leads to bicyclic structure **14.3b** through a 15.0-kcal/mol barrier, in **14.1a** it triggers [3,3] isomerization with a 12.8-kcal/mol activation to yield product **14.3a**, never reaching a bicyclic structure analogous to **14.3b**. The difference in mechanism is attributed to the polarization of the breaking Si-C bond, not present in the equivalent all-carbon structure, which facilitates the migration.

In the presence of an alcohol, intermediate **14.3a** suffers a second nucleophilic attack which can proceed through two paths. MeOH can attack the silicon cation to yield **14.4a** (5.7 kcal/mol activation barrier), or it can barrierlessly attack the proximal carbon of the alkene in concert with the formation of a C–Si bond in **14.5a**. Methanol-assisted proton transfer processes on each of these intermediates

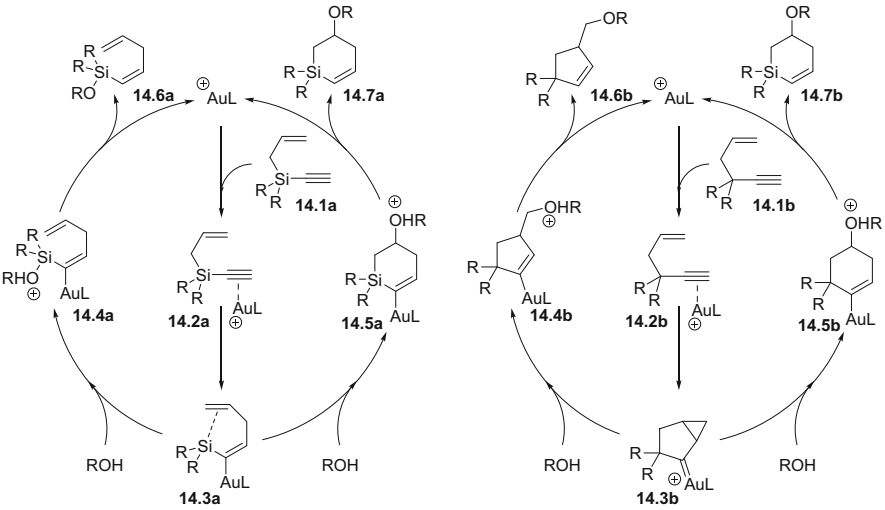

Fig. 14 Gold catalysis on 1,5 enynes with alcohols as external nucleophiles

displace the gold catalyst, leading to **14.6a** and **14.7a** with activation barriers of 4.5 and 9.3 kcal/mol, respectively. It is interesting to note that while only one solvent molecule is needed for the formation of **14.6a**, for the proton transfer to take place on **14.5a**, the participation of three molecules of solvent is required.

Under the same reaction conditions, intermediate **14.3b** can also suffer the attack of MeOH at two different positions: the secondary carbon on the cyclopropane ring (18.4 kcal/mol) or the bridging carbon further away from the gold atom (15.6 kcal/mol). In both cases the cyclopropane ring is opened at the same time, resulting in structures **14.4b** and **14.5b**, respectively. As in the previous mechanism, protodeauration takes place with the transfer of the MeOH proton in a relay mechanism assisted by a solvent molecule. The regioselectivity of the nucleophilic attack is determined by the substituents on the enyne backbone in the case of the all-carbon chain and by the concentration or nucleophilicity of the alcohol in the case of the 3-Si analogue.

Another case of regioselectivity in reactions starting from a nucleophilic attack on a gold-activated alkyne is found when the nucleophile is a sulfoxide. Fang and Yang [151] studied computationally the mechanism of the rearrangement of homopropargyl aryl sulfoxides to benzothiepinones or benzothiopines previously described by Shapiro and Toste in 2007 [152]. The mechanism proceeds through gold coordination to **15.1** followed by 5-exo-dig or 6-endo-dig nucleophilic attack of the sulfoxide oxygen to the gold-activated alkyne. This leads to an alkenyl gold species (**15.2a** or **15.2b**) which evolves through breaking of the S–O bond to an α-carbonyl gold carbenoid/carbocation (**15.3a** or **15.3b**). This intermediate then undergoes an intramolecular Friedel–Crafts alkylation of the aryl group, followed by proton migration to regenerate the catalyst and obtain the product. The rate-limiting step in the 5-exo-dig path is the Friedel–Crafts, while in the 6-endo-dig

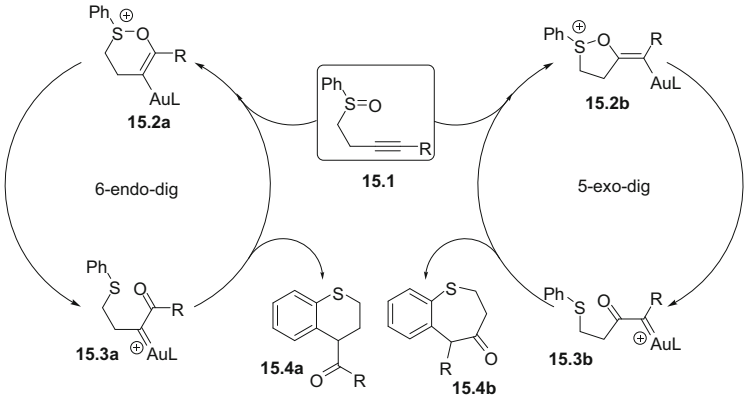

Fig. 15 Mechanism for the gold-catalyzed nucleophilic attack of an internal sulfoxide on an activated alkyne

path is the proton migration. The inclusion of an SbF_6^- counterion, which could favor this proton migration, doesn't seem to have any relevant effect. However, the consideration of an explicit molecule of water in the reaction path significantly facilitates the rearomatization through a direct proton exchange mechanism, although the protodeauration needed for the recovery of the catalyst now becomes the rate-limiting step, in accord with the isotope effect observed experimentally.

The selectivity of the reaction is affected by the substitution on the alkyne, with electron-withdrawing groups favoring the 5-exo-dig process and alkyl chains favoring the 6-endo-dig path (Fig. 15).

3.2 Cycloaddition Reactions

Recent work on gold mediated cycloadditions of allenamides and dienes has been developed by the groups of Mascareñas and Lledós from a dual experimental and computational perspective [153, 154]. Both sets of data seem very complementary and allow for a very detailed description of the factors affecting the reaction pathway. On the one hand, Mascareñas and López test the reaction experimentally considering a number of variables including: the electronic nature of the diene, the type of gold catalyzing the reaction (neutral and/or cationic), and the nature of the gold ligand and counterion (Cl- vs an N-heterocyclic carbene). In addition, they also employ several nucleophilic additives to capture key intermediates along the catalytic process. On the other hand, Lledós and Ujaque resort to computational calculations to organize all these findings and provide a full description of the reacting events which occur behind the scenes. The collaborative work concludes that the allenamide is easily activated by gold and subsequent steps on the mechanism vary and depend directly on the nature of the gold catalyst and the

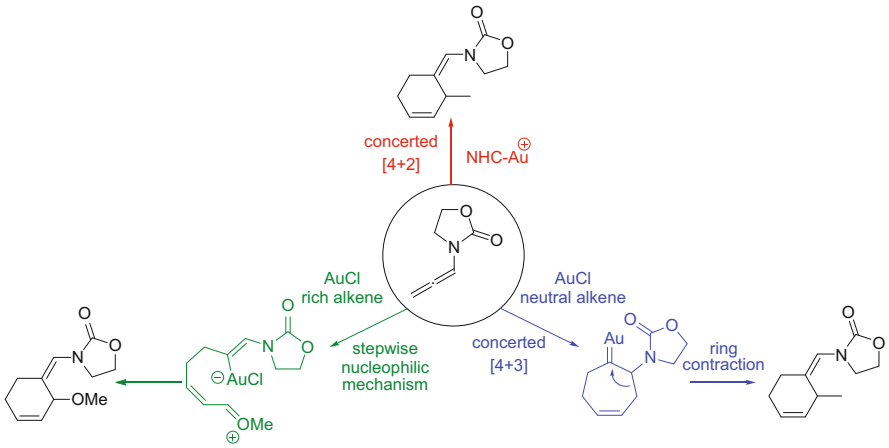

Fig. 16 The three mechanistic pathways available for the cycloaddition of allenamides and dienes. Depending on the gold catalyst and the electronic properties of the diene, the favorable pathway switches between these alternatives

diene being used. At least three different reaction channels can operate (see Fig. 16), a concerted [4+2] cyclization, a [4+3] cyclization followed by a ring contraction and also a stepwise process which also yields the formal [4+2] adduct.

Other interesting experimental examples of this type of reactivity have recently been compiled in a review article [15]. It should be noted that many of the reactions presented in this work involving gold catalysis are still awaiting mechanistic confirmation and that the vast majority of these future mechanistic studies will probably need assistance from the computational front.

3.3 Dual Gold Catalysis

The concept of dual activation by gold, only recently introduced, is a very good example of the success of the combination of experimental and computational mechanistic studies. This is a rapidly expanding field, with the discovery of new organometallic intermediates and unexpected mechanisms, and it has led to the development of new reactions with great synthetic potential. Two recent reviews by Hashmi et al. [11, 28] provide a good overview of this kind of reactivity.

In 2008, Toste et al. [155] reported a "unique" nucleophilic addition of an allene double bond to a gold(I)-complexed gold(I) acetylide, followed by a 1,5-hydrogen shift. The reaction only takes place for terminal alkynes, deuterium labeling revealing that the hydrogen transfer is stereoselective (syn to the newly formed C–C bond) and proceeds through an intramolecular hydrogen transfer and that the alkyne proton exchanges in deuterated methanol. These experimental results, together with the transient observation of a phosphinegold acetylide, suggested

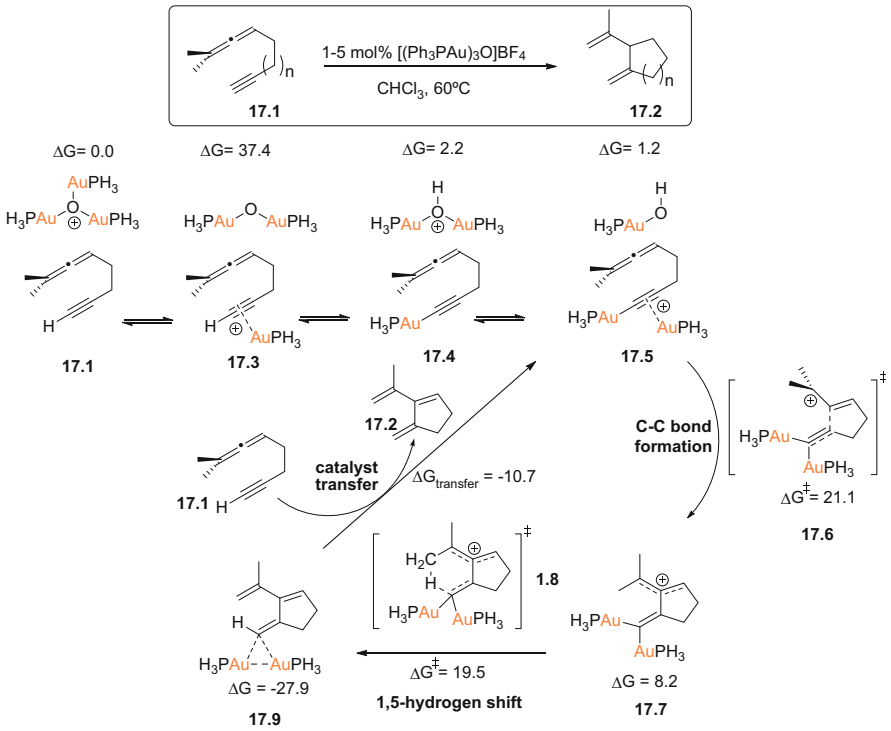

Fig. 17 Mechanism of the gold-catalyzed cycloisomerization of 1,5-allenynes via dual activation by Toste et al. [155]. Free energies are calculated at the B3LYP/6-31+G*, LANL2DZ in gas phase

that the reaction could proceed through digold species **17.5**. Computational studies at the B3LYP/6-31+G*,LANL2DZ level of different mechanistic alternatives proved the feasibility of the transfer of a phosphinegold cation to the alkyne **17.1** from the tris[phosphinegold(I)]oxonium catalyst (expected to be much more favorable than the calculated 37.4 kcal/mol for bulkier phosphines), further favorable formation of the phosphinegold acetylide **17.4** and subsequent transfer of a second phosphinegold cation leading to species **17.5**. This species would be the substrate for the C−C bond formation and subsequent 1,5-hydrogen shift proposed in Fig. 17.

This dual activation scheme or variants of it has been found for other reactions, some of them as simple as the addition of methanol to alkynes, an example of the simplest reactivity of gold(I) salts at activating alkynes towards nucleophilic attack and also a starting point of many gold(I)-initiated reaction cascades.

Roithová et al. [156] have studied in detail the reaction of methanol with 1-phenylpropyne with [AuCl(PMe$_3$)] as a catalyst using electrospray ionization mass spectrometry (ESI-MS), deuterium labeling, NMR kinetic experiments and DFT calculations, and characterizing the key reaction intermediate with IR multiphoton dissociation (IRMPD) spectroscopy.

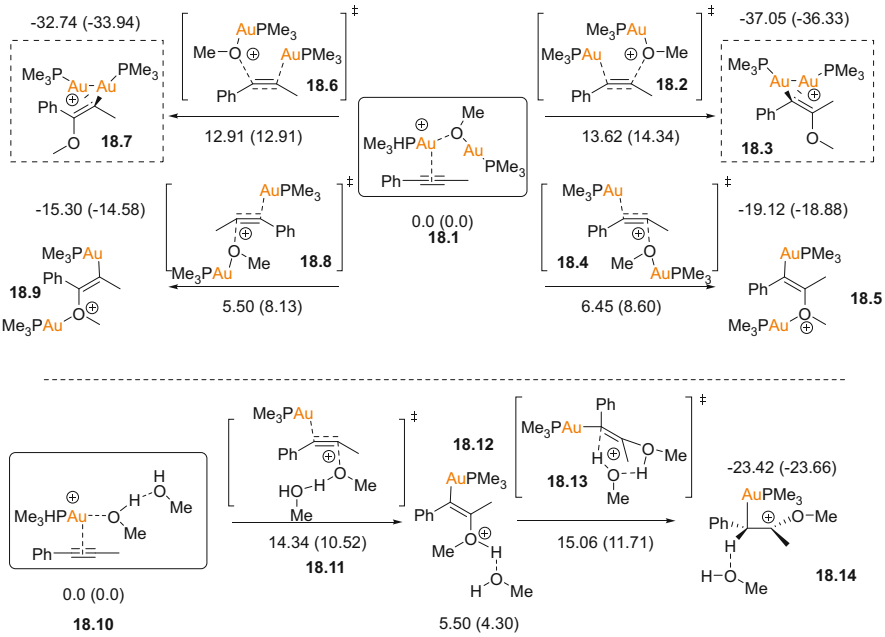

Fig. 18 Mechanisms proposed for the [AuPMe3]+-catalyzed reaction of 1-phenylpropyne with [Au(OMe)(PMe3)] or with methanol assisted by a second molecule of methanol. The free energies in kcal/mol have been calculated at the mPW1PW91/cc-pVDZ:LANL2DZ(Au) level in methanol or in gas phase[156]

The conventionally accepted mechanism (panel at the bottom of Fig. 18) involves the attack of methanol to the activated alkyne **18.10** aided by hydrogen bonding to a second free methanol molecule. Although the barrier is accessible, the reaction is endothermic by 5.5 kcal/mol. The barrier for the hydrogen migration (**18.13**), mediated by the second methanol molecule through a relay mechanism, is somewhat higher, although it could be lowered with the participation of more solvent molecules.

The mechanism involving two gold atoms starts from **18.1**, where the cationic η^2-alkyne–gold complex is bound to [Au(MeO)(PMe3)] through an Au−O bond. The nucleophilic attack of the gold-bound methoxy group to the activated alkyne can occur through the low barrier transition states **18.4** or **18.8**, generating a C−O bond anti to the C−Au in a very exothermic process. After this step, the authors propose that the trimethylphosphinogold cation, loosely bound to the oxygen, can migrate to form the more stable *gem*-diaurated complexes **18.3** and **18.7**, which have been characterized in the ESI-MS experiments. This combination of experimental and computational work shows that the mechanism involving two [Au$(PMe_3)]^+$ fragments proceeds with smaller barriers and leads to more stable intermediates than the single-gold alternative. Dual activation here takes the form of one gold complex acting as a π-acid on the alkyne while the second forms the gold

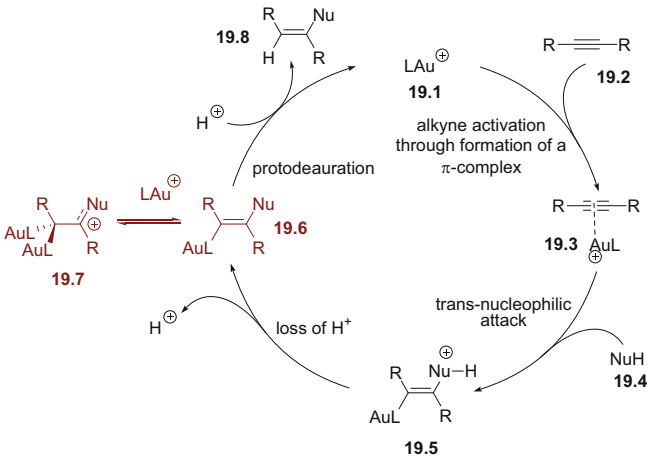

Fig. 19 Schematic representation of the mechanism for the attack of a protic nucleophile to an activated alkyne. Protodeauration competes with the formation of an inactive gem-diaurated species (in *red*) [157]

methanolate acting as a nucleophile. The result is the formation of a *gem*-diaurated gold intermediate which has been experimentally characterized; thus it is shown that dual activation by gold is not limited to systems with polyunsaturated hydrocarbons.

The formation of such *gem*-diaurated species has recently been shown to be an important factor governing the effectiveness of gold catalytic cycles in terms of reactivity and turnover numbers. The common mechanism assumed for the attack of a protic nucleophile to a π-activated alkyne is the one indicated in black in Fig. 19 [157].

Gold coordinates to the alkyne and the resulting η^2-complex **19.3** suffers the nucleophilic attack of species **19.4** trans to gold. The resultant alkenylgold **19.5** is deprotonated and then experiences a rapid protodeauration which releases the product **19.8** and regenerates the catalyst. This protodeauration is not always included in computational mechanistic studies, assumed to be fast in comparison with other steps along the reaction path. The consideration of *gem*-diaurated species **19.7** considerably changes this picture. Calculations, such as those in the previous two papers described, and experimental studies which have isolated and characterized them, have shown that these intermediates are stable and that the catalyst can successfully compete with a proton (its isolobal analogue [158]) to form these kinds of structures in a favorable equilibrium. This stops the catalytic cycle, since *gem*-diaurated products are not readily deaurated by protons. The fact that vinyl gold intermediates bind the LAu^+ catalyst preferentially over the original alkyne (by a factor of 10^6–10^9) highlights the need to take their presence into account in catalytic cycles involving these species [159]. The fact that they react with nucleophiles in an S_N2 displacement of ligands on the gold center to regenerate the vinyl gold species is also relevant for these kinds of mechanisms.

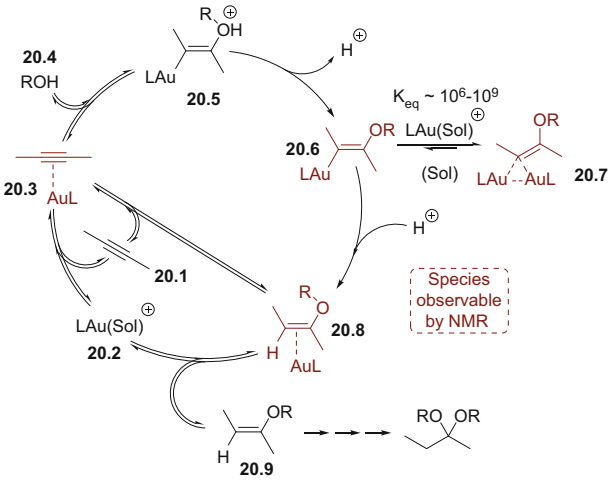

Fig. 20 Mechanism for the gold(I)-catalyzed hydroalkoxylation of alkynes built from the results of extensive kinetic studies [160]

These findings have been nicely summarized in the compilation of extensive kinetic studies on the gold(I)-catalyzed hydroalkoxylation of alkynes made by Zhdanko and Maier [160] (Fig. 20).

The alkyne **20.1** displaces a ligand on the gold-solvent catalyst **20.2** or from the η^2-coordinated intermediate **20.8** to afford the activated alkyne **20.3**, which has been characterized by NMR. All these ligand-exchange reactions on a gold (I) center are found to be equilibria. The attack of a protic external nucleophile **20.4** reversibly forms a protonated vinylgold species in an equilibrium very displaced to the left (a 1,2-elimination is very favorable on **20.5**). However, the irreversible nature of a proton transfer to a nearby molecule from this very acid structure can lead to the neutral vinylgold species **20.6** displacing this equilibrium. Once elusive species, these vinylgold intermediates with a vicinal C−X bond (where X is an electronegative atom) have been characterized by NMR in this study and even isolated as stable complexes [161, 162]. In the presence of the gold catalyst, this intermediate acquires a second gold moiety through a reversible S_N2 ligand exchange at gold in an equilibrium which is very displaced towards the formation of the *gem*-diaurated species **20.7** with an equilibrium constant between 10^6 and 10^9. An alternative to this unproductive step (**20.7** has been shown not to undergo direct protodeauration) is the irreversible addition of a proton in the first part of the protodeauration mechanism, leading to the gold-coordinated enolether **20.8**. This last product can be exchanged by either solvent or the original alkyne substrate through an S_N2 on the gold center, restoring the catalyst (**20.2**) or directly the activated species **20.3** and affording product **20.9**, which can be made to react further. Intervention on the **20.6**–**20.7** equilibrium is showcased as a key step for the improvement of catalysts (bulky ligands, branched substrates, or acid promoters could prevent it, for example) and reaction conditions.

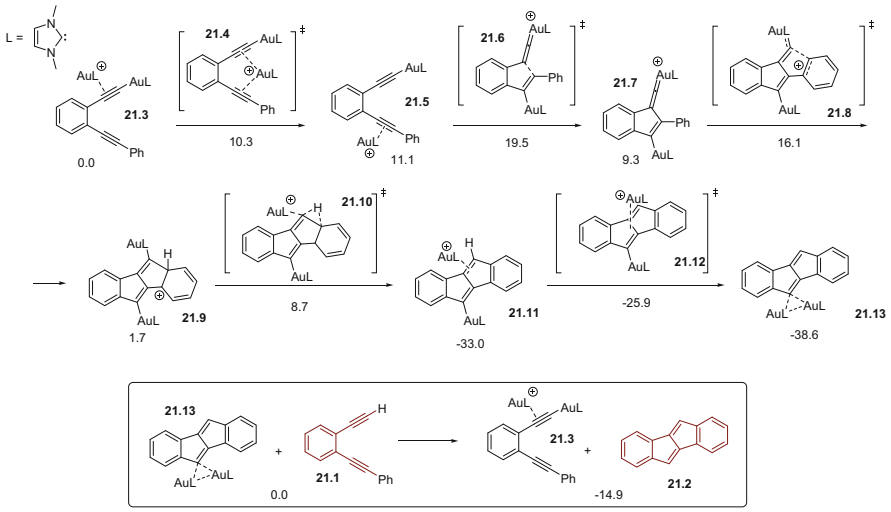

Fig. 21 Mechanism for the gold-catalyzed synthesis of dibenzopentalene. Free energies (in kcal/mol) have been calculated at the B3LYP/cc-pPDZ,SDD(Au) level with the DFT-D3 correction [163]

Another instance of dual activation in the presence of two unsaturations, as in the first example included in this section (see Fig. 21), has been reported by Vilhelmsen and Hashmi [163]. The authors use B3LYP/cc-pPDZ,SDD(Au) calculations in gas phase [110, 124], corrected for dispersion with Grimme's DFT-D3 method [112], to study the mechanism for the gold(I)-catalyzed transformation of 1-ethynyl-2-(phenylethynyl)benzene (**21.1**) into dibenzopentalene (**21.2**).

Besides explaining the experimentally observed preference for a 5-*endo* vs 6-*endo* cyclization through both a lower activation barrier and higher stability of the product, the major contribution of this work is to highlight the continuous presence of two gold fragments along the whole reaction path.

It should be noted that the more stable geminal-σ,π-acetylide (**21.3**) is not the reactive species, and has to cross a transition state (**21.4**) which transfers one gold moiety to the second alkyne, leading to the dual activated diyne **21.5**. This transition state represents the most energetically demanding step along the whole path. The 5-*endo* cyclization affording an intermediate gold vinylidene (**21.7**) is then followed by a second cyclization involving the terminal aryl group, rearomatization associated with hydrogen transfer and migration of the gold catalyst to produce the highly stable *gem*-diaurated dibenzopentalene **21.13**. An alternative mechanism could be proposed to involve protodeauration following the formation of tetracyclic **21.9**. In such a mechanism, the proton on the phenyl substituent would suffer a [1,2]-migration, which, at the same time, would restore aromaticity and remove one of the gold fragments from the system. However, the transition state found for this proton migration (**21.10**) does not completely displace gold, and is connected to **21.11**, where gold is still π-coordinated at the double bond. The latter species is then

involved in a low-barrier gold migration over the π system of the tetracycle to afford **21.13**. An intermolecular protodeauration aided by solvent or the counterion, however, cannot be ruled out with these results.

Also of great relevance for the understanding of this kind of dual activation is the proposed transfer of the catalyst to the naked diyne **21.1**. Although a detailed computational mechanism is not available so far, the fact that the preformed diaurated complex **21.13** can act as a catalyst of this transformation makes it likely that it can act as a dual catalyst donor, transferring the two gold moieties to the diyne substrate at once, instead of doing it in two separate steps. This, together with the accessibility of the **4.12** transition state and the exothermicity of the reaction of **21.13** with **21.1** to yield **21.3** and the **21.2** product (insert in Fig. 21), which is 8.4 kcal/mol more favorable than the single gold transfer to yield **21.2** and **21.1**, supports full participation of **21.13** in the catalytic cycle, instead of just being an inert intermediate as in the previously referenced studies.

A computational study of how this double transfer could take place would shed light on this key step in dual-gold catalysis, providing valuable information for many different mechanisms which have this intermediate in common.

A very similar mechanism, involving the gold-catalyzed cyclization of diethynylthiophenes, was also experimentally and computationally studied by Hashmi et al. [164]. Based on theoretical simulations, Hashmi concluded that these systems can rearrange not only via a 5-*endo* pathway equivalent to the one just discussed, but that a 6-*endo* cyclization mode should also be available depending on the structure of the cyclic ring supporting the diyne. Following these theoretical predictions, they were able to synthesize a system that undergoes the previously unobserved 6-*endo* cyclization. They also studied the factors that affect the substrate preference for one pathway or the other. They find that a rather subtle combination of electronic and structural effects are governing this reactivity. To illustrate this, they report that, for instance, 3,4-diethynylthiophene undergoes 5-*endo* cyclization whereas the 2,3-substituted thiophene prefers the 6-*endo* mode. They also report detailed analysis of the potential energy surface around the transition states and find that they are very close to each other, nearly collapsing to a single structure in certain examples. Topologically, the potential energy surface around the transition states resembles a bifurcation area. In this scenario the classical transition state theory is no longer valid to explain the observed selectivity. A study considering the full potential energy surface of the bifurcation concludes that the structure of the backbone supporting the diyne system and the aromatic stabilization of the 6-*endo* product are the key factors regarding the preference for the 5- or 6-*endo* pathways.

Mechanistically, the 6-*endo* cyclization is quite interesting (see Fig. 22). It also involves dual gold catalysis: one gold cation acts as a Lewis acid activating one triple bond whereas the other cation forms an alkynyl gold nucleophile. The cyclization step yields a benzene ring in which a gold atom is σ-bonded to a carbon atom adjacent to an sp^2 carbocation. A gold 1–2 migration saturates this carbocationic position and reveals a carbene site which triggers further reactivity.

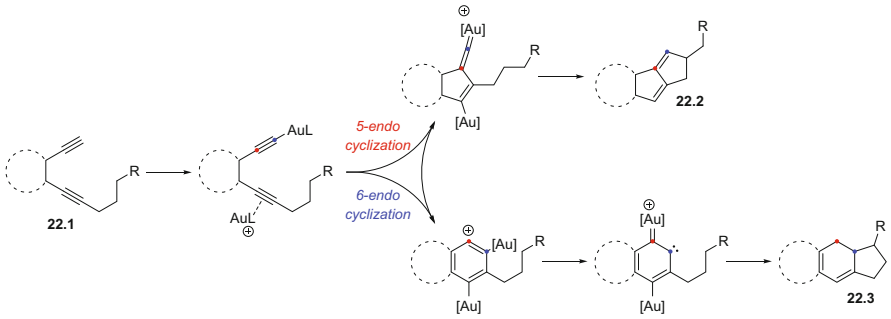

Fig. 22 5-Endo and 6-endo cyclization paths are available to **22.1** upon dual gold activation. Selectivity is regulated by backbone structure and aromatic stabilization in the cyclization product [164]

In these substrates the carbene atom inserts intramolecularly to form the tricyclic heterocycle structure of the final product.

3.4 Hydrogenation Reactions and Gold Hydrides

Hydrogenation reactions under homogeneous gold catalysis are not as popular as the different cascades originating in unsaturation activation followed by intra- or intermolecular nucleophilic attack, but the experimental and computational study of their mechanism has revealed novel behavior of gold complexes and a deeper understanding of homogeneous gold chemistry which can help greatly in the development of new transformations.

Gold complexes have been used in the hydrogenation of alkenes and imines [165]. One of the most interesting features of this reaction is the need to invoke the participation in the catalytic cycle of gold–hydride complexes, which had traditionally been considered too unstable, because of the apparent lack of β-elimination reactions on gold-catalytic cycles and their high redox potentials. Around the same time, gold hydrides were postulated as plausible intermediates in other transformations such as the dehydrogenative silylation of alcohols [166].

The early lack of experimental evidence of gold hydrides [167], where the only compounds characterized were binary gold hydride structures detected in the gas phase or in frozen gas matrices [168], however, has been replaced in the last few years by a wealth of stable gold(I)- and gold(III)–hydride complexes. These novel structures stabilized the Au–H bond by a judicious choice of ligands on the gold center, among which N-heterocyclic carbenes and pincer ligands predominate. Among these (see Fig. 23), one can count the IPrAuH (IPr = 1,3-bis(2,6-diisopropylphenyl)imidazol-2-ylidene) (**23.1**) synthesized by Tsui et al. [169], the intermediate Ito et al. had proposed for the dehydrogenative silylation of alcohols [170], (**23.2**), or the gold(III)-hydride (**23.3**) obtained by Bochmann et al. [171].

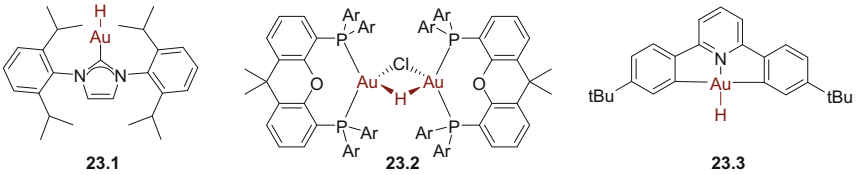

Fig. 23 Some gold(I)–hydride complexes which have been recently characterized [169–171]

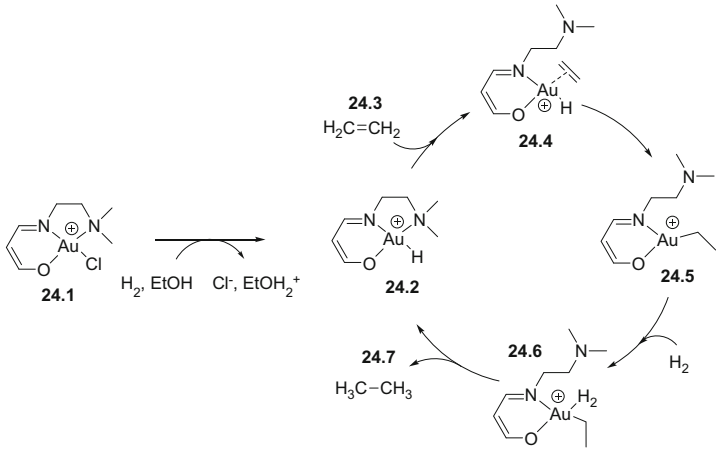

Fig. 24 Mechanism for the gold(III)-catalyzed hydrogenation of olefins. An inner-sphere mechanism with a gold–dihydrogen complex [172]

In analogy to the isoelectronic d^8 Pd(II) species, Ujaque et al. [172] presented evidence that Au(III) complexes with Schiff base ligands can hydrogenate olefins. The mechanism obtained through a combined experimental/computational approach is schematized in Fig. 24. B3LYP/6-31G(d)(O,N,C), 6-31+G(d)(Cl), 6-31G(d,p)(H), 6-31G(C,H),LANL2DZ(Au) calculations (they use larger basis sets for the H and C atoms directly participating in the reaction) calculations show that hydrogen activation takes place heterolytically with the assistance of a solvent (EtOH) molecule (the product of an oxidative addition on the Au(III) center is about 50 kcal/mol over the reactants, as expected, so the corresponding barrier would be even higher). Other possibilities, where the hydride ends attached to gold and the proton bound to chlorine, or the nitrogen or oxygen atoms in the ligand, with or without intervention of the solvent are rejected because of their higher activation energies.

The next step in the catalytic cycle is the coordination of the alkene to the gold center, which is found to displace the amine ligand (the formation of a pentacoordinated complex is more unstable), determining an inner-sphere mechanism for this hydrogenation reaction. After this, the olefin inserts in the Au–H bond through a low-barrier TS (about 4 kcal/mol). Alternatives for the transfer of the

second hydrogen atom are then analyzed (acidic proton donors in the solution, a solvent molecule, or a protonated solvent molecule), with the most favored process (a barrier of 15 kcal/mol) being the use of H_2 as the proton source through another square planar complex (other coordination modes have also been considered). The most significant energy barrier along this reaction path is the initial generation of the hydride species (28 kcal/mol), which is the rate-limiting step. This is reflected in the observation of an induction period in kinetic studies. However, hydrogen activation has a much lower activation barrier in the catalytic cycle, so after the induction period the rate-limiting step is the 19-kcal/mol barrier corresponding to the coordination of the alkene to the gold center, also consistent with the experimental kinetic curves.

The results of this mechanistic study have been used to build an efficient supported version of this catalyst, where a very polar support with surface Brönsted acid sites enhances the reactivity found in the homogeneous process instead of decreasing as usual.

A series of mechanistic studies with a strong computational component by Ujaque et al. [172, 173] culminated in a complete study of the mechanism involved in the previously mentioned enantioselective hydrogenation of alkenes with gold (I) complexes [165, 174] at the B3LYP/6-31G(d)(P,C),6-31+G(d)(O,Cl),6-31G (d,p)(H),LANL2DZ(f)(Au) level, using single-point CPCM calculations to obtain solvation energies. Figure 25 displays a summary of the computational results when applied to the hydrogenation of diethyl 2-benzylidenesuccinate catalyzed by {$(AuCl)_2$[(R,R)-Me-DuPhos]}, although many alternative paths have been explored both for simpler substrates (plain ethene and itaconic acid) and for simplified versions of the catalyst (mononuclear PMe_3AuCl and {$(AuCl)_2$[(1,2-bis(dimethylphosphino)ethene)]}) which shed light on possible ways to fine-tune the reactivity of this kind of system.

The main questions to solve are (1) whether hydrogen is activated homolytically or heterolytically, (2) whether the hydrogenation takes place through an inner-sphere or outer-sphere mechanism, (3) how the catalyst is regenerated, and (4) whether the behavior of mono- and bimetallic catalysts is different.

Calculations show that the homolytic cleavage of hydrogen has a much higher barrier than the heterolytic activation, and that hydrogen activation takes place preferentially through hydride transfer to the gold center and proton transfer to chloride assisted by a solvent molecule (EtOH), in a mechanism analogous to the one for the gold(III) complex in the previous example (step from **25.1** to **25.2** in Fig. 25).

After the formation of the gold hydride, it is found that the insertion of ethylene into the Au–H bond for the monometallic catalyst, followed by the [2+2] σ-bond metathesis of an H_2 molecule, has a barrier of 43 kcal/mol, much higher than the 27.2 kcal/mol (or 18.9 kcal/mol when cyclohexene is the substrate) found for the concerted transfer of the hydride from gold and a proton from a protonated molecule of solvent (path **A** in Fig. 25). The mechanism is thus called "ionic" since it is neither an inner-sphere mechanism, nor a conventional bifunctional outer-sphere mechanism, where both hydride and proton belong to the

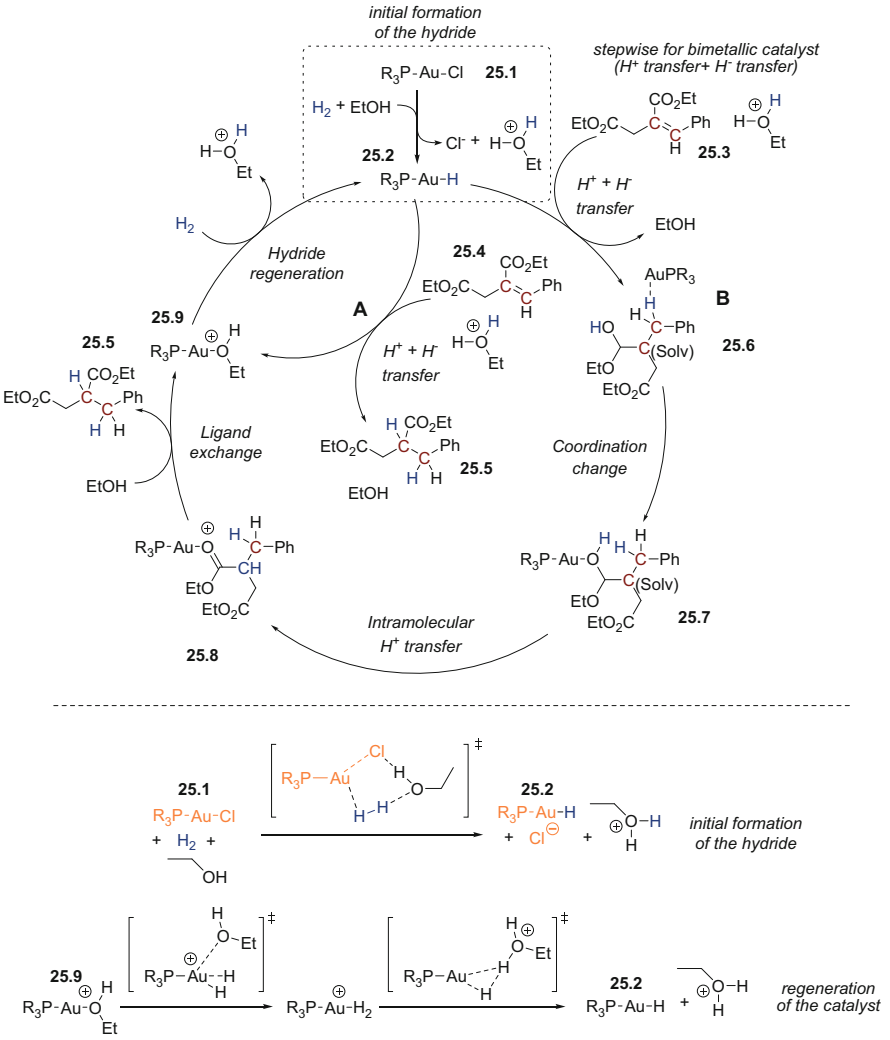

Fig. 25 Simplified mechanism for the hydrogenation of alkenes with gold(I) complexes

organometallic catalyst. It is important to note that the mechanism changes when the substrate is a more complex alkene with other functional groups, evidence that one has to be careful when simplifying or truncating relevant structures in a computational mechanistic study (a very extended practice which reduces the computational cost, sometimes allowing simulations which would be unaffordable otherwise). When itaconic acid is used, the hydrogenation involves the transfer of hydride to a carbon of the C=C bond, while the proton from the solvent is transferred to the C=O oxygen of the COOH closer to the double bond (path b in Fig. 25). This is followed by a second step where this proton is shuttled to the

second carbon in the unsaturation through a relay involving two solvent molecules, leading to **25.8**.

The use of a bimetallic system lowers the barriers for the hydrogenation process with respect to the monometallic alternative, and makes it stepwise, with proton transfer followed by hydride transfer.

After the hydrogenation, the resultant cationic gold fragment exchanges ligands (the reaction product for a EtOH molecule) and generates species **1.9**, which can, in its turn, re-initiate the catalytic cycle by displacement of the EtOH ligand with H_2 and further heterolytic dissociation of the H–H bond with the aid of a solvent molecule. From the data obtained from the modeling of the full system, the step determining the enantioselectivity when the substrate is prochiral and the catalyst uses a chiral ligand seems to be the proton transfer to the prochiral carbon.

Beyond its clear interest in providing a comprehensive study of many different mechanistic alternatives that could be involved in gold-catalyzed hydrogenation reactions, and suggesting ways of better controlling their selectivity or facilitating them (use of polar, slightly acidic, media, for example, because of the involvement of $EtOH_2^+$ species), the uncommon varieties of catalysts, substrates, and reaction paths evaluated in this study provide many examples of issues which need to be taken into account when modeling competing multistep mechanisms. One of them, the need to be careful when truncating or simplifying the structures involved in a reaction, we have already mentioned. Another is the importance of taking the solvent into account when dealing with homogeneous reactions in solution. Although the authors find that single-point CPCM calculations of solvation energies on gas phase geometries are good enough for their purposes, in some cases where they re-optimized some structures in solvent, they find variations which could be negligible or critical (the transition state for the proton transfer from the solvent to the carbonyl oxygen in itaconic acid, for example, is stabilized by 2.5 kcal/mol when optimized with CPCM vs using CPCM on gas phase geometries), depending on the energetic separation of the different paths available to the system. The same happens when they perform single-point calculations with the M06-L functional for some selected structures (or even reoptimize their geometries with it) to account for the effect of dispersion. Although the mechanistic interpretation is not altered by these results, they find, for example, that the former transition state is stabilized by about 10 kcal/mol, or that when studying the competition between the transition states for the hydrogenation of itaconic acid through proton transfer to the carbon or to the carbonyl oxygen, two barriers calculated with B3LYP to be 13.9l and 22.2 kcal/mol are stabilized by 5 and 15 kcal/mol, respectively, when using the M06-L functional, effectively reversing the preference for one mechanism or the other.

Even more relevant is the need to take into account that solvent molecules can participate in the reaction in a way that can never be described by a continuum model. This is clearly exemplified along the whole work, where hydrogen dissociation or proton transfers are assisted by one or even two molecules of solvent which need to be considered explicitly in order to get reasonable activation barriers.

The "reverse" of hydrogenation through an inner-sphere insertion mechanism on a metal hydride bond would be a β-hydride elimination. Although not frequently found processes, in contrast with the dominant reactivity of other late transition metals, computational mechanistic studies have been useful in highlighting their presence in at least one recent report.

This paper, by Alcaide et al. [175] discusses the synthesis of oxetenes from α-allenols using a gold(III) catalyst through a unusual 4-*exo-dig* cyclization. Depending on the substrate and reaction conditions, the authors obtain two different products: dihydrofurans or oxetenes, respectively the result of a 5-*endo-trig* and a 4-*endo-dig* cyclization of the parent system.

The mechanism which can be put together from the computational results is quite straightforward for the formation of the dihydrofuran **26.2**. Initial complexation of the Au(III) salt to the distal double bond of the allenol **26.1** is followed by a very favorable nucleophilic attack of the alcohol in a 5-endo-trig cyclization. Loss of HCl and protodeauration of **26.7** lead to the product. An alternative to this mechanism is the attack of the alcohol to the other carbon in the activated double bond on **26.4**, through a rarely seen 4-exo-dig cyclization. Although the reaction barrier is higher for this process than for the competing 5-endo-trig alternative, it is still quite favorable (7.6 vs 3.3 kcal/mol for R = Me). Loss of HCl leads to the neutral species **26.11**, which, after a 1,3-gold migration involving a barrier of 10–11 kcal/mol, results in the formation of gold oxetane **26.12**. Transformation of this species into the **26.2** oxetene product can proceed through two different mechanisms. Direct transfer of the hydride to the proton in HCl from **26.16** is ruled out because of the high activation barrier found for this step (34.5 kcal/mol), but a β-elimination transition state **26.13**, although very unusual in gold catalysis, can be found to lead to the product with a relatively low activation energy of 15.7 kcal/mol. A third alternative, converging with the last mechanism in structure **26.12**, can be proposed, starting from a 4-endo-dig cyclization on complex **26.15**, where gold is coordinated to the proximal double bond of the alkene. However, the high barrier found for this cyclization makes this path non-competitive with the other two.

From the data in Fig. 26, it is clear that for R = Ph the β-elimination path leading to the oxetene is favored over the protodeauration mechanism, both kinetically (21.1 vs 24 kcal/mol activation barriers) and thermodynamically. In the case of methyl-substituted allenols, the barriers are low enough to provide a mixture of products (as observed experimentally), which would resolve into the preferential formation of the dihydrofuran under thermodynamic control.

A later study by Köppel et al. [176] suggests that β-hydride elimination reactions in homogeneous gold catalysis may be restricted to gold(III) complexes, where empty *d*-orbitals may be available for bonding. They support their claim in a study of the behavior with respect to β-elimination or alkene insertion of Au(I)–alkyl or Au(I)–hydride complexes with an IPr ligand (NHCs have been shown to promote the stability of gold(I)-hydrides).

B3LYP/cc-pVDZ has been used to model these systems, with the (8*s*7*p*6*d*1*f*)/[4*s*4*p*3*d*1*f*] pseudopotential-based basis set for gold [109, 110]. The effect of solvation has been modeled using CH_2Cl_2 with PCM on the gas phase geometries,

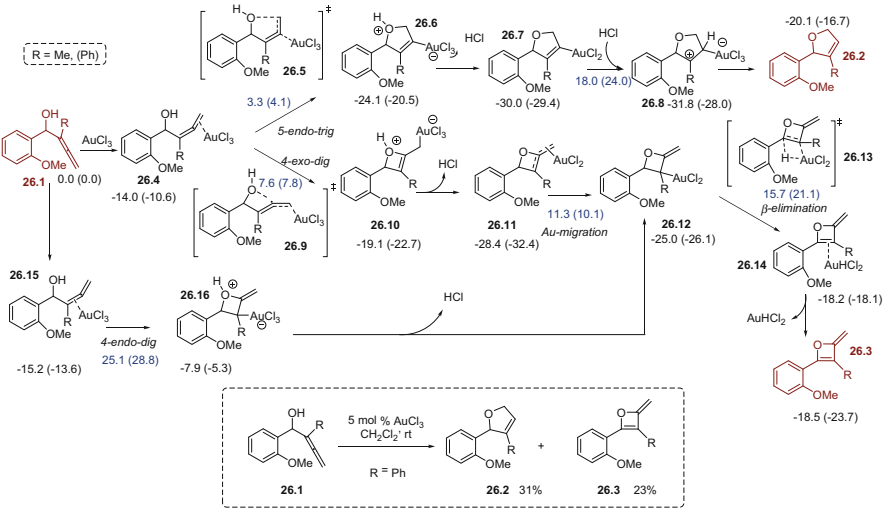

Fig. 26 Simplified reaction profile obtained at the PCM(CH2Cl2)-B3LYP/def2-SVP level for the cyclization of allenols to oxetenes and dihydrofurans. Relative free energies are in kcal/mol, the values in *blue* represent activation energies for relevant processes [175]

but it has been confirmed to be quite small. In order to account for the effect of dispersion, optimizations with BP86-D3/def2-SVP and the SDD electron core potential for gold have also been carried out, using MARI-J with the corresponding auxiliary basis sets [69, 112, 117, 177, 178].

From a purely computational point of view, it is very interesting to note that the calculated energies differ significantly between the methods used, with BP86-D3 providing results much closer to MP2 than B3LYP (something partially attributable to a better treatment of dispersion in the first two).

The focus is in the thermal decay of **27.1**–**27.4** (Fig. 27). Along this reaction path, no isomer displaying an agostic interaction between an alkyl hydrogen and the metal center was found, because of the filled *d* shell in the Au(I) complex. The high barrier for **TS1** (free energy of activation of 49.7 kcal/mol) is attributed to the same factor, as is the high energy of **27.2** relative to **27.1** and the weak bonding between gold and the alkene fragment in the latter structure, which readily converts into **27.3**. These calculations suggest that the IPr–Au–alkyl complex should be quite stable, the barrier for **TS1** would result in significant reaction rates only above 200 °C, according to transition state theory. The authors have confirmed this conclusion experimentally using ethyl, methyl and butyl groups, finding that these **27.1** analogues decompose at 180 °C, but through a different mechanism. The reverse reaction (insertion of an olefin into gold hydride **27.4**) would have a lower barrier, but still too high for the reaction to proceed below 100 °C, something that has been confirmed by the lack of insertion of an ethene at 8 bar/r.t. and at 1 bar/80 °C or insertion of more activated alkenes up to 50 °C. The main result of this

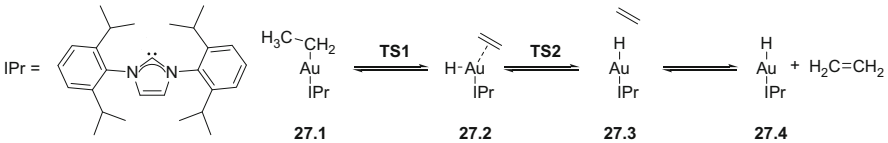

B86-D3/def2-SVP	0	53.6	33.8	36.5	22.9	27.5
B3LYP/cc-pVDZ	0	57.1	34.5	37.7	18.8	19.5
MP2/cc-pVDZ	0	-	-	-	-	28.3

Fig. 27 Reaction path for the β-elimination in (IPr)AuEt. Relative gas-phase electronic energies calculated with different methods for the stationary points optimized along the reaction path are given in kcal/mol [176]

work is establishing that β-H-eliminations or alkene insertions in a gold hydride are not feasible steps in gold(I) catalytic cycles at moderate temperatures.

3.5 Au(I)/Au(III) Catalytic Cycles

Another of the main tenets of gold chemistry is the difficulty of engaging this metal in redox reactions because of the high oxidation potential for the pair Au(I)/Au(III). The fact that most Au(I)-catalyzed reactions can proceed in the presence of air supports this idea. However, in 1974 there were already reports of oxidative additions on gold(I) centers, albeit in reactions which are not catalytic. The work by Tamaki and Kochi [179, 180] describes what is in essence an Au(I)/Au(III) alkyl–alkyl coupling mechanism, with the following steps:

$$CH_3AuPPh_3 + CH_3I \rightarrow (CH_3)_2AuIPPh_3$$
$$(CH_3)_2AuIPPh_3 + CH_3AuPPh_3 \rightarrow (CH_3)_3AuPPh_3 + IAuPPh_3$$
$$(CH_3)_3AuPPh_3 \rightarrow CH_3CH_3 + CH_3AuPPh_3$$

However, despite the interest in replacing Pd and other metals involved in "classical" cross-coupling reactions, and the possible advantages of using gold for such reactions, Au(I)/Au(III) cycles have not been used in gold catalysis until very recently [14].

One of the main strategies for involving gold in cross-coupling reactions is using it in tandem with other metals such as palladium. Thus, gold would act as a transmetalation agent, while the palladium complex has the organizing role in the catalytic cycle. This approach has many advantages in that the reactivity of these two metals is usually orthogonal, resulting in improved selectivities [181]. Examples of its application (Fig. 28) can be the palladium-catalyzed cross-coupling reactions of organogold(I) reagents with organic electrophiles of Pérez Sestelo et al. [182] or the tandem cycloisomerization/Suzuki coupling of arylethynyl MIDA boronates of Toste et al. [183].

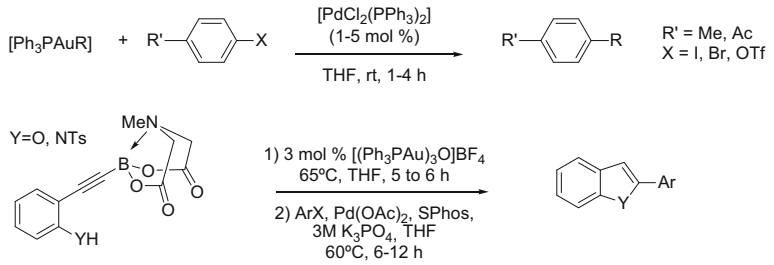

Fig. 28 Examples of the participation of gold(I) complexes in Pd-catalyzed cross-coupling reactions [182, 183]

In this context, the claim of Corma et al. [184] that the Sonogashira reaction between phenylacetylene and iodobenzene could proceed with a homogeneous PPh_3AuCl catalyst soon received much attention and questioning [185], with the argument that oxidative additions on cationic gold centers are expected to be very unfavorable and that very low concentrations of palladium impurities could be the actual catalytic species in the system. The controversy was solved using a mixture of experimental and computational techniques which proved that gold is able to catalyze the Sonogashira coupling between phenylacetylene and iodobenzene in the absence of palladium, but that the catalyst is not cationic gold complexes in solution but metallic Au(0) gold nanoparticles. This was achieved with careful application of XPS, TEM and reaction studies on deposited gold species, which showed that atomically dispersed Au(I) and Au(III) species were catalytically inert while Au (0) nanoparticles displayed high activity [186]. Further work by Corma et al. [187] on gold nanoparticles supported on cerium oxide confirmed that gold nanoparticles are catalytically active in this reaction. In this same paper, B3PW91/6-31G(d,p) calculations on the oxidative addition of PhI to PMe_3AuI ascribe to this transition state an activation barrier of 31.6 kcal/mol, too high for this reaction to be accessible at the temperatures used in the experiment. At the same time, periodic DFT calculations using PW91 within the GGA approach for the same reaction on a cuboctahedral Au_{38} cluster, display a much lower activation energy (11.3 kcal/mol). During the reaction, negative charge is being transferred from the cluster to the Ph and I fragments. The resultant positive charge in the cluster is equally spread among all the gold atoms, effectively circumventing the costly Au(I)/Au(III) oxidation of a single gold center. Thus, the computational results, together with the experimental data, help to create a clear picture of what is happening in the reactor. The explanation for the original observation that Au(I)–Schiff base complexes could catalyze this reaction in homogeneous conditions is found in the existence of an induction period, corresponding to the nucleation and growth of Au nanoparticles from the Au(I) in solution.

A third way to involve gold in cross-coupling reactions is recruiting an external oxidant to avoid the problematic oxidative addition step. An interesting review by Governeur et al. [16] summarizes the most relevant developments in oxidative coupling reactions catalyzed by gold.

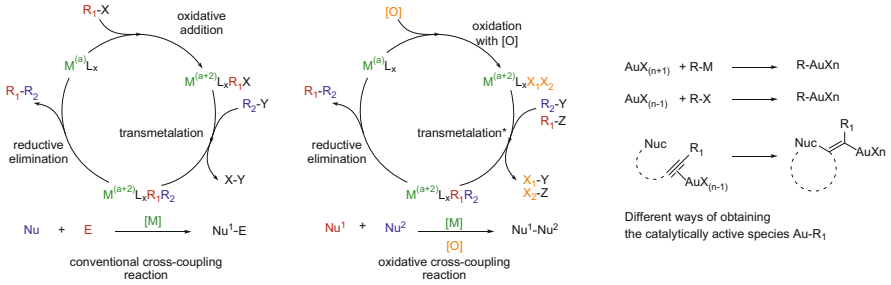

Fig. 29 Schematic representations of the mechanism of a conventional cross-coupling reaction (*left*) and an oxidative cross-coupling reaction (*right*)

Figure 29 displays a simplified scheme of the mechanism of conventional and oxidative cross-coupling reactions. In a conventional cycle, a metal center coordinated to some ligands suffers the oxidative addition of a R_1X species, where R_1 is an electrophilic fragment and X is usually a halogen, a triflate group, or similar substituent. This process increases in two units the metal oxidation state and generates two new R_1-metal and X-metal bonds. The next step is a transmetalation process where a nucleophilic R_2 fragment, attached to a metal or metalloid Y is exchanged by X on the metal coordination sphere. The resultant complex then suffers a reductive elimination where the R_1–R_2 bond is formed and the metal center recovers its initial oxidation state.

The main difference with an oxidative cross-coupling is the fact that the oxidative addition step is replaced by oxidation of the metal center with an external oxidant (usually Selectfluor, $PhI(OAc)_2$, or *t*BuOOH). This also affects the transmetalation step, which can exchange two nucleophilic R_1 and R_2 chains for two of its X ligands, or just one, when the second chain has already been incorporated in the metal center in a prior step. After this, reductive elimination again forms the new R_1–R_2 bond and regenerates the catalyst.

In 2010, Toste et al. [188] and Zhang et al. [189] independently published the same gold(I)-catalyzed intermolecular aminoarylation of alkenes using Selectfluor. The mechanisms proposed in these papers differ in the ordering of the transmetalation and gold(III) coordination to the alkene in the catalytic cycle, but only Toste's proposal is based in the results of DFT calculations. As shown in Fig. 30, Selectfluor oxidizes gold(I) complex LAuX (**30.1**) to $LAuFX^+$. This Au(III) complex coordinates them to the alkene in **30.4** resulting in its activation towards the intramolecular attack of the amine nitrogen that leads to **30.5**. The expected steps in a classical cross-coupling reaction (indicated with green arrows) would be transmetallation of phenylboronic acid **30.6** with the gold center to afford complex **30.9**, followed by a reductive elimination resulting in the coupling product (**30.8**) and regeneration of the initial Au(I) species. What their computational results show, however, is that these two steps coalesce in a single five-center transition state (**30.7**) corresponding to a bimolecular reductive elimination where the phenyl

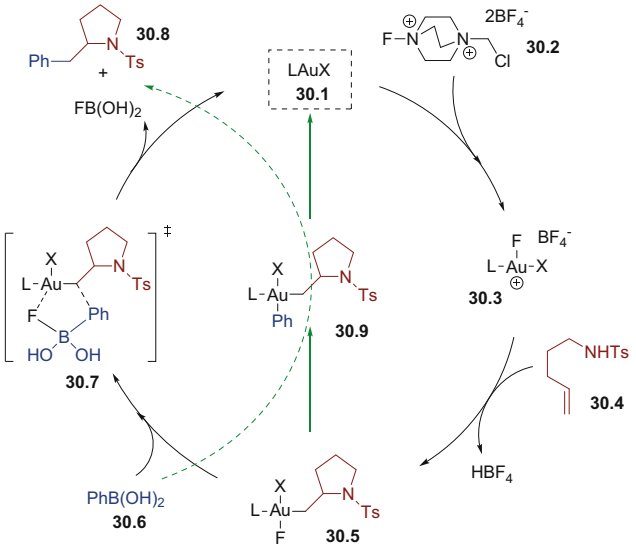

Fig. 30 Proposed mechanism for the oxidative gold-catalyzed aminoarylation reaction. The steps formally corresponding to transmetalation and reductive elimination coalesce in a single five-center transition state [188]

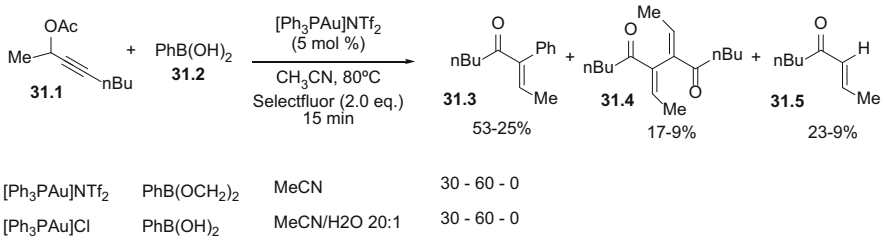

Fig. 31 Oxidative homo- and cross-coupling reaction catalyzed by gold. The ratio of products depends on the catalyst, transmetalation agent and solvent [190]

group is directly transferred from boron to carbon, while the boron center captures the fluoride ligand attached to gold.

Intrigued by this kind of Au(I)/Au(III) catalytic cycles, we decided to study in detail the mechanism of the oxidative cross coupling developed by Zhang et al. [190] In this reaction (Fig. 31), the initial propargyl acetate **31.1** experiences a "traditional" gold-catalyzed cascade reaction initiated by alkyne activation and 1,3-migration of the carboxylate group, which leads to an intermediate gold(I) complex. This complex, in its turn, is oxidized to the equivalent gold(III) species with Selectfluor and can then participate in three different processes: cross-coupling with boronic acid **31.2** (product **31.3**), homocoupling with the original gold(I) complex acting as a transmetallation agent (product **31.4**), or protodeauration (product **31.5**).

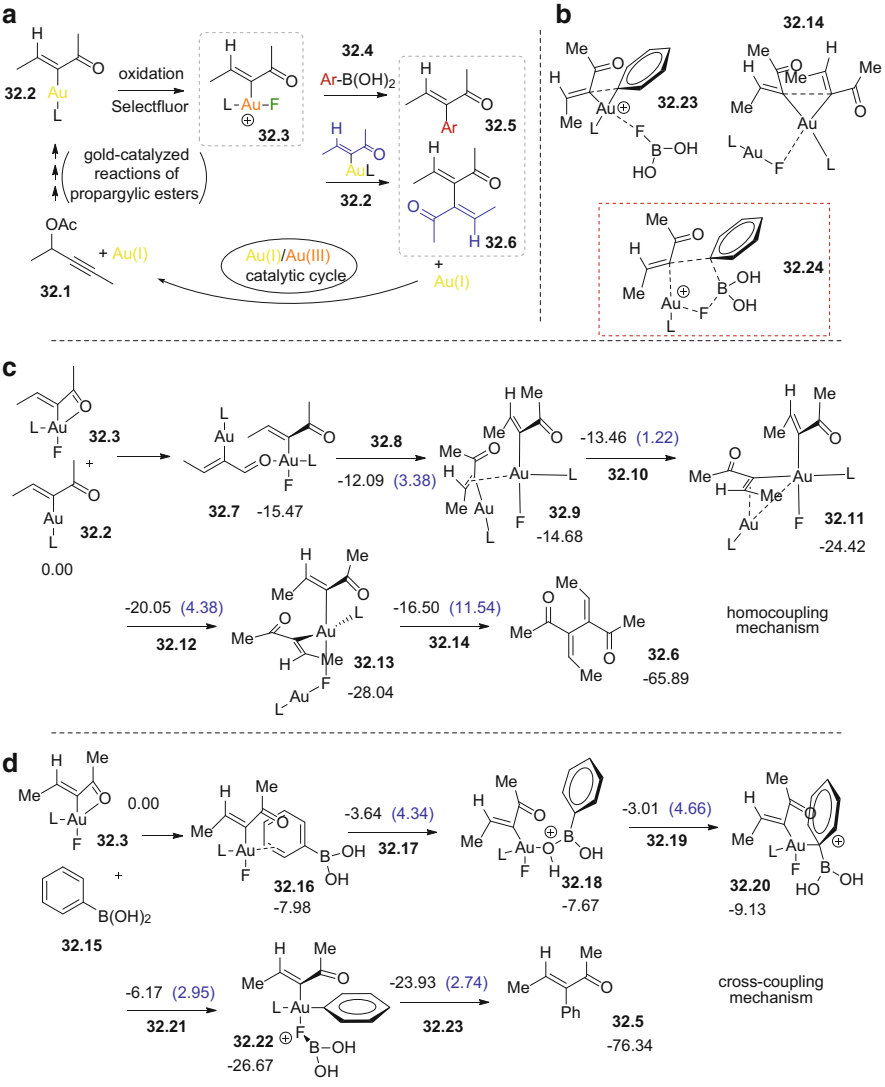

Fig. 32 (**a**) General mechanism for the oxidative cross-coupling reaction described by Zhang et al. [190]. Mechanism for the homocoupling (**c**) and cross-coupling (**d**) starting from the gold(III) intermediate **32.3** at the M06/def2-SVP (PCM) level [191]. Relative free energies are in kcal/mol. Activation energies for the transition structures are indicated in *blue* over the corresponding arrows. **(b)** Structure of the reductive elimination steps in the two mechanisms, together with Toste's proposal [188]

In our study [191], we analyzed the reaction mechanism for the homo- and cross-coupling paths at the M06/def2-SVP level, including solvation through IEFPCM with acetonitrile and UFF radii, taking into account the results about the performance of different functionals of our previous benchmark (see Fig. 32) [64]. In

order to evaluate the effects of some approximations commonly made when modeling organometallic mechanisms, we optimized complete reaction profiles both in gas-phase and in solution, with four different ligands on the gold center: PPh_3 (used in the experimental work), PMe_3 (the energies shown in Fig. 32), PH_3, and 1,3-dimethylimidazol-2-ylidene. Thus, besides providing new, basic information on the mechanisms involved in gold-catalyzed Au(I)/Au(III) cycles, this work also offers insight into the computational treatment needed for these systems.

In agreement with the experimental results, the cross-coupling mechanism (Fig. 32d) is more favorable than the homocoupling in the presence of the boronic acid. After coordination of the fragments and an aryl-oxygen ligand exchange on the Au(III) center leading to **32.18**, the system suffers a two-step transmetalation assisted by an F–B interaction. The Au–Ph bond is formed first through **32.19** (with a barrier of 4.66 kcal/mol) and then the C–B bond breaks through **32.21** (with an even lower barrier of 2.95 kcal/mol) in a very exothermic process which leaves the boron fragment attached to fluorine (**32.22**). The full transference of fluorine to the boron is only completed in the four-center reductive elimination (**32.23**, Fig. 32b), a very easy process with a low barrier (2.74 kcal/mol) which leads to the cross-coupling product **32.5**.

Analysis of the bonding along the whole reaction path and calculation of the reaction profile with other X^- ligands on gold show that the fluorine atom is key in providing a low-energy path for transmetalation, so it would be interesting to check whether this reactivity is preserved when oxidants other than Selectfluor are used.

The mechanism for the homocoupling (Fig. 32c) reaction shares some common features with that for the cross-coupling. It is not competitive with it, but the activation needed is also low. After the initial coordination and ligand exchange steps, **32.9** is obtained, where the vinylgold(I) fragment is bonded to Au(III) through an η^2 interaction. Transmetalation takes place again in two steps, the first forming a σ-bond between the Au(III) center and the enone fragment (**32.10**), the second breaking the now η^2-bond between this fragment and the Au(I) center, also with the assistance of fluorine. Reductive elimination takes place again through a four-center transition state where the C−C bond is formed in concert with the cleavage of the F–Au(I)–L fragment from the gold center (**32.14**, Fig. 32b). A five-center bimolecular transition structure for the reductive elimination (Fig. 32b), as described by Toste for the aminoarylation of alkenes [188], could be optimized only for $L = PPh_3$, but it lies about 6 kcal/mol higher than the highest stationary point in the proposed path. However, the low barriers found for the transmetalation and reductive elimination steps could result in these transition states collapsing into one depending on the electronic properties of the fragments involved in the reaction, making the two proposals converge.

In terms of the methods used, it is found that the inclusion of solvation in the optimization process is important, since it transforms some of the transition structures found in gas phase into shoulders in the potential energy surface and leads to consistently higher barriers. Thus, although the general shape of the profiles are not altered, the comparison between competitive paths could be off.

Although truncation of the ligand does not have a strong effect in the general shape of the profile, the reaction energy spans change in a window of 3 kcal/mol, and the rate-determining step can change between phosphines, something that might be acceptable or not, depending on the study.

Transmetalation (non-catalytic) between neutral gold(III) complexes (PPh_3AuCl_2Ar) and boron species ($Ar\text{-}B(OH)_2$) has been studied by Nevado et al. [192]. They find that electron-rich arylboronic acids are non-reactive at temperatures of 150 °C, in contrast with the efficient transmetalation suffered by their electron-poor equivalents.

DFT calculations on a direct transmetalation of $PPh_3AuCl_2C_6F_6$ with phenyl and (pentafluorophenyl)boronic acid, through a four-center concerted transition state where the C−Au and Cl−B bonds are formed at the same time the Au−Cl and B−C bonds are being broken, find too high activation barriers (54.1 and 57.8 kcal/mol, respectively). This can be related to the very high energies found for the transmetalation in the previous study when replacing fluorine with other halogens [191].

Although the complete mechanism has not been calculated, some intermediates have been computationally characterized which suggest that the mechanism for transmetalation in these species occurs in a stepwise fashion. Gold is first activated by abstraction of a chloride by the electrophilic boron and then the aryl fragment is transferred. The electrophilicity values (calculated from the HOMO-LUMO gap) of the initial boronic acids correlate well with the observed experimental results if this chloride transfer is considered to be the rate-limiting step.

However relevant the transmetalation steps are to the extension of cross-coupling reactivity in homogeneous gold catalysis, the main barrier to overcome is still the difficulty in accessing Au(III) from Au(I) without the intervention of an external oxidant. Echavarren et al. [193] have addressed the oxidative addition of aryl halides to Au(I) complexes in order to understand better the origin and extension of this problem.

M06/6-31+G(d),SDD(Au): PCM(water) has been used to calculate the reaction and activation energies for the oxidative additions depicted in Fig. 33. The reactions are endergonic and most exhibit barriers which are too high to make them part of a catalytic cycle. The barrier for the **33.1** → **33.2** transformation, for example, is 41.5 kcal/mol. This is in accord with the experimental observation that this reaction does not take place under the conditions studied (heating in toluene at 60 °C for several days), but disappointing, nevertheless, since the intermolecular nature of the process and the formation of a five- or six-membered ring should help the reaction. It was found that electron-withdrawing substituents on the phenyl ring lower this barrier, but even in the most favorable case it did not go below 28.0 kcal/mol.

Calculations with other, intermolecular, reactions displayed similar results (barriers between 41.5 and 48.5 kcal/mol), with the exception of those starting from a mono-coordinated Au(I) center (activation barriers of 11.7, 23.3, and 21.6 kcal/mol for **33.8**, **33.9**, and **33.10**, respectively). All these factors suggest that the main problem for obtaining oxidative additions on gold(I) complexes is a kinetic rather than a thermodynamic phenomenon and that the strong preference for linear

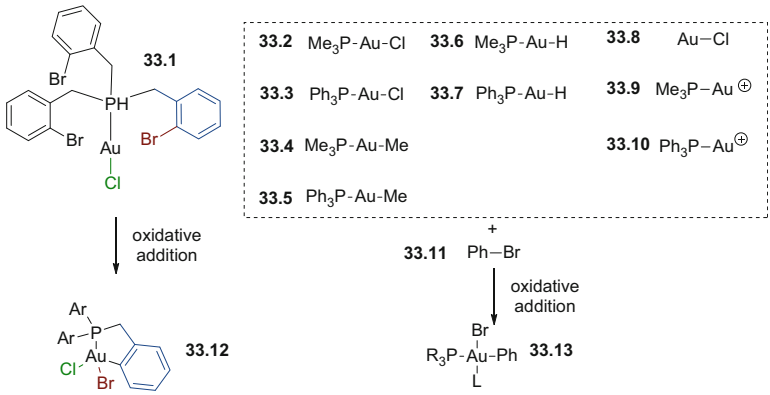

Fig. 33 Oxidative addition reactions studied at the M06/6-31+G(d),SDD(Au), PCM(water) level [193]

geometries on dicoordinate Au(I) complexes may be at the root of these high barriers.

These results point towards the possible use of monocoordinate $[LAu(I)]^+$ complexes (unknown to date) or $[LAu(I)L']A^-$ with a very weakly coordinated L' as starting points for gold(I)-catalyzed cross-coupling reactions.

3.6 Summary: Gold-Catalyzed Mechanisms from Computational Studies

Some general conclusions about gold-catalyzed mechanisms can be extracted from the previous examples of computational studies.

The first is that, for a given set of reactants and catalysts, there are usually several reaction paths with relatively low energies available. It is not uncommon that these paths involve many different steps where gold changes its coordination, and that they sometimes are interconnected.

The second, associated with it, is the fact that homogeneous gold catalysis is easily affected by environmental factors and the structure of the catalyst and the substrate, as reflected in our choice of examples of mechanisms based on nucleophilic attacks.

The effect of the environment can be most remarkable, making the explicit consideration of solvent and counterions, often neglected in this kind of studies, a necessity. Counterions and solvent are often involved in proton relays which can dramatically alter the preference for one or other reaction path, having a direct effect on the reaction barriers and the product selectivity. This preference can also be made to depend on the type of ligands or on the oxidation state of the metal center. Examples of these can be found in the 1,2-H, silyl or alkyl migrations found

along the mechanism of heterocycle formation after a intramolecular nucleophilic attack on a gold-activated alkyne. The selectivity can also be affected by the substitution pattern on the organic fragment as shown in the reactions of 1,5-enynes or sulfoxides. Cycloaddition reactions are also an example of this effect of the substrate on the preferred reaction path.

A third important feature found in the studied mechanisms is the possibility of dual gold activation, either in the formation of gold acetylides which are subsequently coordinated to another gold fragment or in the favorable generation of stable *gem*-diaurated products which are not readily deaurated by protons and which can seriously affect the reactivity and turnover number of gold catalytic cycles.

Gold hydrides, previously thought to not exist, have been postulated as intermediates in gold-catalyzed hydrogenation reactions and also experimentally characterized. The confirmation of the existence and stability of such species is a fourth example of the successful interplay between theory and experiment. The activation of dihydrogen by gold opens a new model of gold reactivity, more characteristic of other transition metals, which is clearly differentiated from its role as a π-acid. Associated with this is the report of an unexpected β-elimination step in a catalytic cycle with Au(III), although a study of Au(I) complexes concluded that alkene insertion in a gold hydride or β-hydrogen eliminations are not feasible with gold in this oxidation state.

There has at last been an important development of Au(I)/Au(III) catalytic cycles, especially those focused in cross-coupling reactions. These processes follow mechanisms similar to those found for other transition metals, but they differ in the oxidative addition step, which is problematic because of the high redox potential of the Au(I)/Au(III) pair. This can be circumvented either by the use of an external oxidant or by the involvement of gold nanoparticles in an interesting exploration of the frontiers between homogeneous and heterogeneous catalysis.

The interplay between theoretical and experimental work described in these examples has enhanced our understanding of which factors control the reactivity and selectivity in gold catalysis, thus allowing the fine-tuning of synthetic processes, and also opened new venues for the development of homogeneous gold-catalyzed reactions which go well beyond the paradigm of gold as a π-acid.

4 Conclusion

Gold chemistry is captivating the attention of chemists worldwide, not only in a product oriented fashion, because of its unprecedented reactivity. It is also stimulating studies which aim to gather deep insight into the mechanisms making these reactions possible. The fascinating processes which are being discovered only fuel further interest. Gold has been shown to maintain full potential to surprise the most experienced chemists with new intricate and complex reactions.

In this scenario, computational chemistry is an unavoidable tool for exploring the plethora of mechanistic pathways often available for any given chemical transformation. Because of the activation power of this metal, the energy barriers of most if not all the steps involved in these diverse pathways are often very low, allowing for this reactivity to occur under very mild conditions. The multistep nature of these reactions and the flat energy profile which they commonly exhibit require accurate and robust methodology when we aim for correct mechanistic answers.

It has been found that density functional theory can actually describe homogeneous gold catalysis with an acceptable performance and accuracy. However, the choice of the density functional and accompanying basis functions is not trivial, and following established good-old recipes may lead to disastrous results. In general, it seems that the newer generation of density functionals are highly recommendable. Among them, the M06, B2PLYP, and ωB97X formulations seem to be the best performers, with double hybrids clearly outperforming the rest. Anything below the triple zeta quality for basis functions implies a high risk of inaccurate results.

With the development of local variations of coupled cluster theory, it is now possible to apply this level of theory to reasonably sized systems. This alternative has proved to be very robust and provides excellent results. In this regard, when feasible, geometries obtained at the DFT level should be refined employing a coupled cluster operator including single, double and triple excitations. Because of the slow convergence of the CC methods with the basis set, a triple zeta quality is a must to ensure a reasonable recovery of electron correlation.

Computational chemistry is becoming mainstream technology which helps advance chemistry from its very roots. Its use is becoming more popular by the day, and the risk of misuse increases in parallel. In this review we have summarized current knowledge on the performance of the most used density functionals. We have also provided information on more robust and powerful methodologies. Apart from the selection of the theoretical method to describe the catalytic process, the actual chemistry being modeled also hides a number of choices which have to be made. We have provided examples of the multifaceted character of the gold chemistry – its dependence on ligands, counterions, and explicit solvent molecules, and the presence of dual activation and digold complexes. All this has to be carefully taken into account when attempting to describe a catalytic reaction in which gold is involved.

References

1. King CV (1938) Catalysis of nitramide decomposition by colloidal platinum and gold. J Am Chem Soc 60:144–154
2. Benton AF, Elgin JC (1927) The catalytic synthesis of water vapor in contact with metallic gold. J Am Chem Soc 49:2426–2438
3. Bond GC (1972) The catalytic properties of gold. Gold Bull 5:11–13

4. Haruta M, Kobayashi T, Sano H, Yamada N (1987) Novel gold catalysts for the oxidation of carbon monoxide at a temperature far below 0°C. Chem Lett 16:405
5. Hutchings GJ (1985) Vapor phase hydrochlorination of acetylene: correlation of catalytic activity of supported metal chloride catalysts. J Catal 96:292
6. Ito Y, Sawamura M, Hayashi T (1986) Catalytic asymmetric aldol reaction: reaction of aldehydes with isocyanoacetate catalyzed by a chiral ferrocenylphosphine-gold(I) complex. J Am Chem 108:6405–6406
7. Fukuda Y, Utimoto K (1991) Effective transformation of unactivated alkynes into ketones or acetals with a gold(III) catalyst. J Org Chem 56:3729–3731
8. Teles J, Brode S, Chabanas M (1998) Cationic gold (I) complexes: highly efficient catalysts for the addition of alcohols to alkynes. Chemie Int Ed 37:1415–1418
9. Hashmi ASK, Hutchings GJ (2006) Gold catalysis. Angew Chem Int Ed Engl 45:7896–7936
10. Hashmi ASK (2007) Gold-catalyzed organic reactions. Chem Rev 107:3180–3211
11. Braun I, Asiri AM, Hashmi ASK (2013) Gold catalysis 2.0. ACS Catal 3:1902–1907
12. Gorin DJ, Sherry BD, Toste FD (2008) Ligand effects in homogeneous Au catalysis. Chem Rev 108:3351–3378
13. Wang S, Zhang G, Zhang L (2010) Gold-catalyzed reaction of propargylic carboxylates via an initial 3,3-rearrangement. Synlett 2010:692–706
14. Wegner HA, Auzias M (2011) Gold for C-C coupling reactions: a Swiss-Army-knife catalyst? Angew Chem Int Ed Engl 50:8236–8247
15. López F, Mascareñas JL (2014) [4+2] and [4+3] catalytic cycloadditions of allenes. Chem Soc Rev 43:2904–2915
16. Hopkinson MN, Gee AD, Gouverneur V (2011) Au(I) /Au(III) catalysis: an alternative approach for C-C oxidative coupling. Chemistry 17:8248–8262
17. Corma A, Leyva-Pérez A, Sabater MJ (2011) Gold-catalyzed carbon-heteroatom bond-forming reactions. Chem Rev 111:1657–1712
18. Jiménez-Núñez E, Echavarren AM (2008) Gold-catalyzed cycloisomerizations of enynes: a mechanistic perspective. Chem Rev 108:3326–3350
19. Michelet V, Toullec PY, Genêt J-P (2008) Cycloisomerization of 1,n-enynes: challenging metal-catalyzed rearrangements and mechanistic insights. Angew Chem Int Ed Engl 47:4268–4315
20. Alcaide B, Almendros P (2014) Gold-catalyzed cyclization reactions of allenol and alkynol derivatives. Acc Chem Res 47:939–952
21. Zhang D-H, Tang X-Y, Shi M (2014) Gold-catalyzed tandem reactions of methylenecyclopropanes and vinylidenecyclopropanes. Acc Chem Res 47:913–924
22. Krause N, Winter C (2011) Gold-catalyzed nucleophilic cyclization of functionalized allenes: a powerful access to carbo- and heterocycles. Chem Rev 111:1994–2009
23. Zhang L (2014) A non-diazo approach to α-oxo gold carbenes via gold-catalyzed alkyne oxidation. Acc Chem Res 47:877–888
24. Hashmi ASK (2010) Homogeneous gold catalysis beyond assumptions and proposals—characterized intermediates. Angew Chem Int Ed Engl 49:5232–5241
25. Liu L-P, Hammond GB (2012) Recent advances in the isolation and reactivity of organogold complexes. Chem Soc Rev 41:3129–3139
26. Soriano E, Marco-Contelles J (2009) Mechanistic insights on the cycloisomerization of polyunsaturated precursors catalyzed by platinum and gold complexes. Acc Chem Res 42:1026–1036
27. Obradors C, Echavarren AM (2014) Gold-catalyzed rearrangements and beyond. Acc Chem Res 47:902–912
28. Hashmi ASK (2014) Dual gold catalysis. Acc Chem Res 47:864–876
29. Fürstner A (2009) Gold and platinum catalysis—a convenient tool for generating molecular complexity. Chem Soc Rev 38:3208–3221
30. Shapiro ND, Toste FD (2010) A reactivity-driven approach to the discovery and development of gold-catalyzed organic reactions. Synlett 2010:675–691

31. Fensterbank L, Malacria M (2014) Molecular complexity from polyunsaturated substrates: the gold catalysis approach. Acc Chem Res 47:953–965
32. Wang Y, Lackner AD, Toste FD (2014) Enantioselective gold catalysis. Acc Chem Res 47:889–901
33. Fürstner A (2014) From understanding to prediction : gold- and platinum-based pi-acid catalysis for target oriented synthesis. Acc Chem Res 47:925–938
34. Leyva-Pérez A, Corma A (2012) Similarities and differences between the "relativistic" triad gold, platinum, and mercury in catalysis. Angew Chem Int Ed Engl 51:614–635
35. Pitzer K (1979) Relativistic effects on chemical properties. Acc Chem Res 12:271–276
36. Pyykko P (1988) Relativistic effects in structural chemistry. Chem Rev 88:563–594
37. Zhan J-H, Lv H, Yu Y, Zhang J-L (2012) Catalytic C-F bond activation of perfluoroarenes by tricoordinated gold(I) complexes. Adv Synth Catal 354:1529–1541
38. Haibach MC, Seidel D (2014) C-H bond functionalization through intramolecular hydride transfer. Angew Chem Int Ed Engl 53:5010–5036
39. Xie J, Pan C, Abdukader A, Zhu C (2014) Gold-catalyzed C(sp(3))-H bond functionalization. Chem Soc Rev 43:5245–5256
40. Hertwig RH, Koch W, Schröder D, Schwarz H, Hrusák J, Schwerdtfeger P (1996) A comparative computational study of cationic coinage metal - ethylene complexes (C2H4)M + (M=Cu, Ag and Au). J Phys Chem 3654:12253–12260
41. Pyykkö P (2004) Theoretical chemistry of gold. Angew Chem Int Ed Engl 43:4412–4456
42. Pyykkö P (2008) Theoretical chemistry of gold III. Chem Soc Rev 37:1967–1997
43. Pyykkö P (2005) Theoretical chemistry of gold II. Inorganica Chim Acta 358:4113–4130
44. Pyykko P, Desclaux J (1979) Relativity and the periodic system of elements. Acc Chem Res 12:276–281
45. Frenking G, Fröhlich N (2000) The nature of the bonding in transition-metal compounds. Chem Rev 100:717–774
46. Schmidbaur H, Schier A (2012) Aurophilic interactions as a subject of current research: an up-date. Chem Soc Rev 41:370–412
47. Nechaev M (2004) Energy partitioning analysis of the bonding in ethylene and acetylene complexes of group 6, 8, and 11 metals: (CO) 5TM-C2H x and Cl4TM-C2H x (TM= Cr, Mo, W). J Phys Chem A 108:3134–3142
48. Fürstner A, Davies PW (2007) Catalytic carbophilic activation: catalysis by platinum and gold pi acids. Angew Chem Int Ed Engl 46:3410–3449
49. Benitez D, Shapiro ND, Tkatchouk E, Wang Y, Goddard III WA, Toste FD (2009) A bonding model for gold(I) carbene complexes. Nat Chem 1:482–486
50. Salvi N, Belpassi L, Tarantelli F (2010) On the Dewar–Chatt–Duncanson model for catalytic gold(I) complexes. Chem Eur J 16:7231–7240. doi:10.1002/chem.201000608
51. Bistoni G, Belpassi L, Tarantelli F (2013) Disentanglement of donation and back-donation effects on experimental observables: a case study of gold-ethyne complexes. Angew Chem Int Ed Engl 52:11599–11602
52. Hansmann MM, Rominger F, Hashmi ASK (2013) Gold-allenylidenes—an experimental and theoretical study. Chem Sci 4:1552–1559
53. Lalonde RL, Wang ZJ, Mba M, Lackner AD, Toste FD (2010) Gold(I)-catalyzed enantioselective synthesis of pyrazolidines, isoxazolidines, and tetrahydrooxazines. Angew Chem Int Ed Engl 49:598–601
54. Cera G, Bandini M (2013) Enantioselective gold(I) catalysis with chiral monodentate ligands. Isr J Chem 53:848–855
55. Teller H, Corbet M, Mantilli L, Gopakumar G, Goddard R, Thiel W, Fürstner A (2012) One-point binding ligands for asymmetric gold catalysis: phosphoramidites with a TADDOL-related but acyclic backbone. J Am Chem Soc 134:15331–15342
56. Francos J, Grande-Carmona F, Faustino H, Iglesias-Sigüenza J, Díez, E, Alonso I, Fernández R, Lassaletta JM, López F, Mascareñas JL (2012) Axially chiral triazoloisoquinolin-3-ylidene ligands in gold (I)-catalyzed asymmetric intermolecular (4+ 2) cycloadditions of allenamides and dienes. J Am Chem Soc 134:14322–14325

57. Hamilton GL, Kang EJ, Mba M, Toste FD (2007) A powerful chiral counterion strategy for asymmetric transition metal catalysis. Science 317:496–499
58. Homs A, Obradors C, Lebœuf D, Echavarren AM (2014) Dissecting anion effects in gold(I)-catalyzed intermolecular cycloadditions. Adv Synth Catal 356:221–228
59. Salvi N, Belpassi L, Zuccaccia D, Tarantelli F, Macchioni A (2010) Ion pairing in NHC gold (I) olefin complexes: a combined experimental/theoretical study. J Organomet Chem 695:2679–2686
60. Zuccaccia D, Belpassi L (2009) Ion pairing in cationic olefin—gold (I) complexes. J Am Chem Soc 131:3170–3171
61. Zuccaccia D, Belpassi L, Macchioni A, Tarantelli F (2013) Ligand effects on bonding and ion pairing in cationic gold(I) catalysts bearing unsaturated hydrocarbons. Eur J Inorg Chem 2013:4121–4135
62. Perdew JP, Schmidt K (2001) Jacob's ladder of density functional approximations for the exchange-correlation energy. AIP Conf Proc 577:1–20
63. Perdew JP, McMullen ER, Zunger A (1981) Density-functional theory of the correlation energy in atoms and ions: a simple analytic model and a challenge. Phys Rev A 23:2785–2789
64. Faza ON, De Lera AR (2011) DFT-based mechanistic insights into noble metal-catalyzed rearrangement of propargylic derivatives: chirality transfer processes. Top Curr Chem 302:81–130
65. Parr RG, Yang W (1989) Density functional theory of atoms and molecules. Oxford University Press, New York
66. Lee C, Yang W, Parr RG (1988) Development of the Colle-Salvetti correlation-energy formula into a functional of the electron density. Phys Rev B 37:785–789
67. Becke AD (1993) Density-functional thermochemistry. III. The role of exact exchange. J Chem Phys 98:5648–5652
68. Hay PJ, Wadt WR (1985) Ab initio effective core potentials for molecular calculations. Potentials for K to Au including the outermost core orbitals. J Chem Phys 82(299)
69. Andrae D, Häussermann U, Dolg M, Stoll H, Preuss H (1990) Energy-adjusted ab initio pseudopotentials for the second and third row transition elements. Theor Chim Acta 77:123–141
70. Wu Y, Genest A, Rösch N (2014) Does the preferred mechanism of a catalytic transformation depend on the density functional? Ethylene hydrosilylation by a metal complex as a case study. J Phys Chem A 118:3004–3013
71. Wu Y, Karttunen VA, Parker S, Genest A, Ro N (2013) Olefin hydrosilylation catalyzed by a bis-N-heterocyclic carbene rhodium complex. A density functional theory study. Organometallics 32:2363–2372
72. Albu TV, Swaminathan S (2006) Hybrid density functional theory with a specific reaction parameter: hydrogen abstraction reaction of trifluoromethane by the hydroxyl radical. Theor Chem Acc 117:383–395
73. Pople JA, Head-Gordon M, Fox DJ, Raghavachari K, Curtiss LA (1989) Gaussian-1 theory: a general procedure for prediction of molecular energies. J Chem Phys 90:5622
74. Curtiss LA, Raghavachari K, Trucks GW, Pople JA (1991) Gaussian-2 theory for molecular energies of first- and second-row compounds. J Chem Phys 94:7221
75. Curtiss LA, Raghavachari K, Pople JA (1995) Gaussian-2 theory: use of higher level correlation methods, quadratic configuration interaction geometries, and second-order Moller–Plesset zero-point energies. J Chem Phys 103:4192
76. Curtiss LA, Raghavachari K, Redfern PC, Rassolov V, Pople JA (1998) Gaussian-3 (G3) theory for molecules containing first and second-row atoms. J Chem Phys 109:7764
77. Curtiss LA, Redfern PC, Raghavachari K (2005) Assessment of Gaussian-3 and density-functional theories on the G3/05 test set of experimental energies. J Chem Phys 123:124107
78. Řezáč J et al (2008) Quantum chemical benchmark energy and geometry database for molecular clusters and complex molecular systems (www.begdb.com): a users manual and examples. Collect Czech Chem Commun 73:1261–1270

79. Jurecka P, Sponer J, Cerný J, Hobza P (2006) Benchmark database of accurate (MP2 and CCSD(T) complete basis set limit) interaction energies of small model complexes, DNA base pairs, and amino acid pairs. Phys Chem Chem Phys 8:1985–1993
80. Rezáč J, Riley KE, Hobza P (2011) S66: a well-balanced database of benchmark interaction energies relevant to biomolecular structures. J Chem Theor Comput 7:2427–2438
81. Goerigk L, Grimme S (2011) A thorough benchmark of density functional methods for general main group thermochemistry, kinetics, and noncovalent interactions. Phys Chem Chem Phys 13:6670–6688
82. Goerigk L, Grimme S (2010) A general database for main group thermochemistry, kinetics, and noncovalent interactions—assessment of common and reparameterized (meta-) GGA density. J Chem Theor Comput 6:107–126
83. Lynch BJ, Truhlar DG (2003) Small representative benchmarks for thermochemical calculations. J Phys Chem A 107:8996–8999
84. Zhao Y, Truhlar D (2011) Density functional theory for reaction energies: test of meta and hybrid meta functionals, range-separated functionals, and other high-performance functionals. J Chem Theor 7:669–676
85. Zhao Y, Truhlar DG (2005) Benchmark databases for nonbonded interactions and their use to test density functional theory. J Chem Theor Comput 1:415–432
86. Zhao Y, Truhlar DG (2006) Assessment of density functionals for pi systems: energy differences between cumulenes and poly-ynes; proton affinities, bond length alternation, and torsional potentials of conjugated polyenes; and proton affinities of conjugated Shiff bases. J Phys Chem A 110:10478–10486
87. Zhao Y, Truhlar DG (2009) Benchmark energetic data in a model system for Grubbs II metathesis catalysis and their use for the development, assessment, and validation of electronic. J Chem Theor Comput 5:324–333
88. Zhao Y, Truhlar DG (2008) Density functionals with broad applicability in chemistry. Acc Chem Res 41:157–167
89. Zhao Y, Truhlar DG (2011) Applications and validations of the Minnesota density functionals. ChEm Phys Lett 502:1–13
90. Zhao Y, Truhlar DG (2007) The M06 suite of density functionals for main group thermochemistry, thermochemical kinetics, noncovalent interactions, excited states, and transition elements: two new functionals and systematic testing of four M06-class functionals and 12 other function. Theor Chem Acc 120:215–241
91. Zhao Y, Lynch BJ, Truhlar DG (2004) Development and assessment of a new hybrid density functional model for thermochemical kinetics. J Phys Chem A 108:2715–2719
92. Zhao Y, González-García N, Truhlar DG (2005) Benchmark database of barrier heights for heavy atom transfer, nucleophilic substitution, association, and unimolecular reactions and its use to test theoretical methods. J Phys Chem A 109:2012–2018
93. Schultz NE, Zhao Y, Truhlar DG (2005) Databases for transition element bonding: metal-metal bond energies and bond lengths and their use to test hybrid, hybrid meta, and meta density functionals and generalized gradient approximations. J Phys Chem A 109:4388–4403
94. Schultz NE, Zhao Y, Truhlar DG (2005) Density functionals for inorganometallic and organometallic chemistry. J Phys Chem A 109:11127–11143
95. Cramer CJ, Truhlar DG (2009) Density functional theory for transition metals and transition metal chemistry. Phys Chem Chem Phys 11:10757–10816
96. Yang K, Zheng J, Zhao Y, Truhlar DG (2010) Tests of the RPBE, revPBE, tau-HCTHhyb, omegaB97X-D, and MOHLYP density functional approximations and 29 others against representative databases for diverse bond energies and barrier heights in catalysis. J Chem Phys 132:164117
97. Bühl M, Reimann C, Pantazis DA, Bredow T, Neese F (2008) Geometries of third-row transition-metal complexes from density-functional theory. J Chem Theor 4:1449–1459
98. Pantazis DA, Chen XY, Landis CR, Neese F (2008) All-electron scalar relativistic basis sets for third-row transition metal atoms. J Chem Theor Comput 4:908–919

99. Grimme S (2006) Semiempirical GGA-type density functional constructed with a long-range dispersion correction. J Comput Chem 27:1787–1799
100. Grimme S (2004) Accurate description of van der Waals complexes by density functional theory including empirical corrections. J Comput Chem 25:1463–1473
101. Faza ON, Rodríguez RÁ, López CS (2011) Performance of density functional theory on homogeneous gold catalysis. Theor Chem Acc 128:647–661
102. Correa A, Marion N, Fensterbank L, Malacria M, Nolan SP, Cavallo L (2008) Golden carousel in catalysis: the cationic gold/propargylic ester cycle. Angew Chem Int Ed Engl 47:718–721
103. Schäfer A, Horn H, Ahlrichs R (1992) Fully optimized contracted Gaussian basis sets for atoms Li to Kr. J Chem Phys 97:2571–2577
104. Nava P, Hagebaum-Reignier D, Humbel S (2012) Bonding of gold with unsaturated species. Chemphyschem 13:2090–2096
105. Neese F (2012) The ORCA program system. Wiley Interdiscip Rev Comput Mol Sci 2:73–78
106. Riplinger C, Sandhoefer B, Hansen A, Neese F (2013) Natural triple excitations in local coupled cluster calculations with pair natural orbitals. J Chem Phys 139:134101
107. Ciancaleoni G, Rampino S, Zuccaccia D, Tarantelli F, Belanzoni P, Belpassi L (2014) An ab initio benchmark and DFT validation study on gold(I)-catalyzed hydroamination of alkynes. J Chem Theor Comput 10:1021–1034
108. Kang R, Chen H, Shaik S, Yao J (2011) Assessment of theoretical methods for complexes of gold(I) and gold(III) with unsaturated aliphatic hydrocarbon: which density functional should we choose? J Chem Theor Comput 7:4002–4011
109. Peterson KA, Puzzarini C (2005) Systematically convergent basis sets for transition metals. II. Pseudopotential-based correlation consistent basis sets for the group 11 (Cu, Ag, Au) and 12 (Zn, Cd, Hg) elements. Theor Chem Acc 114:283–296
110. Dunning TH (1989) Gaussian basis sets for use in correlated molecular calculations. I. The atoms boron through neon and hydrogen. J Chem Phys 90(1007)
111. Becke AD, Johnson ER (2005) A density-functional model of the dispersion interaction. J Chem Phys 123:154101
112. Grimme S, Antony J, Ehrlich S, Krieg H (2010) A consistent and accurate ab initio parametrization of density functional dispersion correction (DFT-D) for the 94 elements H-Pu. J Chem Phys 132:154104
113. Grimme S, Ehrlich S, Goerigk L (2011) Effect of the damping function in dispersion corrected density functional theory. J Comput Chem 32:1456–1465
114. Johnson ER, Becke AD (2006) A post-Hartree-Fock model of intermolecular interactions: inclusion of higher-order corrections. J Chem Phys 124:174104
115. Johnson ER, Becke AD (2005) A post-Hartree-Fock model of intermolecular interactions. J Chem Phys 123:24101
116. Goerigk L, Grimme S (2010) Meta-GGA density functionals evaluation with the extended GMTKN30 database for general main group thermochemistry, kinetics, and noncovalent interactions. J Chem Theor Comput 7:291–309
117. Weigend F, Ahlrichs R (2005) Balanced basis sets of split valence, triple zeta valence and quadruple zeta valence quality for H to Rn: design and assessment of accuracy. Phys Chem Chem Phys 7:3297–3305
118. Gdanitz R, Ahlrichs R (1988) The averaged coupled-pair functional (ACPF): a size-extensive modification of MR CI (SD). Chem Phys Lett 143:413–420
119. Andersson K, Malmqvist P-A, Roos BO (1992) Second-order perturbation theory with a complete active space self-consistent field reference function. J Chem Phys 96:1218
120. Kang R, Lai W, Yao J, Shaik S, Chen H (2012) How accurate can a local coupled cluster approach be in computing the activation energies of late-transition-metal-catalyzed reactions with Au, Pt, and Ir ? J Chem Theor Comput 8:3119–3127
121. Schütz M (2002) Low-order scaling local electron correlation methods. V. Connected triples beyond (T): linear scaling local CCSDT-1b. J Chem Phys 116:8772

122. Hampel C, Werner H-J (1996) Local treatment of electron correlation in coupled cluster theory. J Chem Phys 104:6286
123. Werner H-J, Schütz M (2011) An efficient local coupled cluster method for accurate thermochemistry of large systems. J Chem Phys 135:144116
124. Figgen D, Peterson KA, Dolg M, Stoll H (2009) Energy-consistent pseudopotentials and correlation consistent basis sets for the 5d elements Hf-Pt. J Chem Phys 130:164108
125. Otero-de-la-Roza A, Mallory JD, Johnson ER (2014) Metallophilic interactions from dispersion-corrected density-functional theory. J Chem Phys 140:18A504
126. O'Grady E, Kaltsoyannis N (2004) Does metallophilicity increase or decrease down group 11? Computational investigations of 2 (M = Cu, Ag, Au). Phys Chem Chem Phys 6:680–687
127. Koppen JV, Hapka M, Modrzejewski M, Szczęśniak MM, Chałasiński G (2014) Density functional theory approach to gold-ligand interactions: Separating true effects from artifacts. J Chem Phys 140:244313
128. Moncho S, Brothers EN, Janesko BG (2013) A benchmark study of H2 activation by Au3 and Ag3 clusters. J Phys Chem C 117:7487–7496
129. Zhao S, Ren Y, Ren Y, Wang J, Yin W (2010) Density functional study of hydrogen binding on gold and silver-gold clusters. J Phys Chem A 114:4917–4923
130. Varganov SA, Olson RM, Gordon MS, Mills G, Metiu H (2004) A study of the reactions of molecular hydrogen with small gold clusters. J Chem Phys 120:5169–5175
131. Stevens W, Krauss M (1992) Relativistic compact effective potentials and efficient, shared-exponent basis sets for the third-, fourth-, and fifth-row atoms. Can J Chem 70:612–613
132. Hehre WJ (1972) Self-consistent molecular orbital methods. XII. Further extensions of Gaussian-type basis sets for use in molecular orbital studies of organic molecules. J Chem Phys 56:2257
133. Determan JJ, Moncho S, Brothers EN, Janesko BG (2014) Simulating gold's structure-dependent reactivity: nonlocal density functional theory studies of hydrogen activation by gold clusters, nanowires, and surfaces. J Phys Chem C 118:15693–15704
134. Muniz-Miranda F, Menziani MC, Pedone A (2014) Assessment of exchange-correlation functionals in reproducing the structure and optical gap of organic-protected gold nanoclusters. J Phys Chem C 118:7532–7544
135. Dapprich S, Komáromi I, Byun KS, Morokuma K, Frisch MJ (1999) A new ONIOM implementation in Gaussian 98. Part I. The calculation of energies, gradients, vibrational frequencies and electric field derivatives. J Mol Struct Theor Chem 461–462:1–21
136. Stewart JJP (2007) Optimization of parameters for semiempirical methods V: modification of NDDO approximations and application to 70 elements. J Mol Model 13:1173–1213
137. Weymuth T, Couzijn EPA, Chen P, Reiher M (2014) New benchmark set of transition-metal coordination reactions for the assessment of density functionals. J Chem Theor Comput 10(8):3092–3103 (DOI:10.1021/ct500248h)
138. Scalmani G, Frisch MJ (2010) Continuous surface charge polarizable continuum models of solvation. I. General formalism. J Chem Phys 132:114110
139. York DM, Karplus M (1999) A smooth solvation potential based on the conductor-like screening model. J Phys Chem A 103:11060–11079
140. Vallés-Pardo JL, Guijt MC, Iannuzzi M, Joya KS, de Groot HJM, Buda F (2012) Ab initio molecular dynamics study of water oxidation reaction pathways in mono-Ru catalysts. Chemphyschem 13:140–146
141. Stirling A, Nair NN, Lledós A, Ujaque G (2014) Challenges in modelling homogeneous catalysis: new answers from ab initio molecular dynamics to the controversy over the Wacker process. Chem Soc Rev 43:4940–4952
142. Vidossich P, Ujaque G, Lledós A (2014) Palladium monophosphine Pd(PPh3): is it really accessible in solution? Chem Commun (Camb) 50:661–663
143. Vummaleti SVC, Falivene L, Poater A, Cavallo L (2014) Deconstructing selectivity in the gold-promoted cyclization of alkynyl benzothioamides to six-membered mesoionic carbene or acyclic carbene complexes. ACS Catal 4:1287–1291
144. Xia Y, Huang G (2010) Mechanisms of the Au- and Pt-catalyzed intramolecular acetylenic Schmidt reactions: a DFT study. J Org Chem 75:7842–7854

145. Gorin DJ, Davis NR, Toste FD (2005) Gold(I)-catalyzed intramolecular acetylenic Schmidt reaction. J Am Chem Soc 127:11260–11261
146. Fang R, Su C, Zhao C, Phillips DL (2009) DFT study on the mechanism and regioselectivity of gold(I)-catalyzed synthesis of highly substituted furans based on 1-(1-alkynyl) cyclopropyl ketones with nucleophiles. Organometallics 28:741–748
147. Zhang J, Shen W, Li L, Li M (2009) Gold(I)-catalyzed cycloaddition of 1-(1-alkynyl) cyclopropyl ketones with nucleophiles to yield substituted furans: a DFT study. Organometallics 14:3129–3139
148. Xia Y, Dudnik AS, Gevorgyan V, Li Y (2008) Mechanistic insights into the gold-catalyzed cycloisomerization of bromoallenyl ketones: ligand-controlled regioselectivity. J Am Chem Soc 130:6940–6941
149. Dudnik AS, Xia Y, Li Y, Gevorgyan V (2010) Computation-guided development of Au-catalyzed cycloisomerizations proceeding via 1,2-Si or 1,2-H migrations: regiodivergent synthesis of silylfurans. J Am Chem Soc 132:7645–7655
150. Ariafard A, Asadollah E, Ostadebrahim M, Rajabi NA, Yates BF (2012) Theoretical investigation into the mechanism of Au(I)-catalyzed reaction of alcohols with 1,5 enynes. J Am Chem Soc 134:16882–16890
151. Fang R, Yang L (2012) Mechanism of the gold(I)-catalyzed rearrangement of alkynyl sulfoxides: a DFT study. Organometallics 31:3043–3055
152. Shapiro ND, Toste FD (2007) Rearrangement of alkynyl sulfoxides catalyzed by gold (I) complexes. J Am Chem Soc 129:4160–4161
153. López F, Mascareñas JL (2013) Gold(I)-catalyzed enantioselective cycloaddition reactions. Beilstein J Org Chem 9:2250–2264
154. Montserrat S, Faustino H, Lledós A, Mascareñas JL, López F, Ujaque G (2013) Mechanistic intricacies of gold-catalyzed intermolecular cycloadditions between allenamides and dienes. Chemistry 19:15248–15260
155. Cheong PH-Y, Morganelli P, Luzung MR, Houk KN, Toste FD (2008) Gold-catalyzed cycloisomerization of 1,5-allenynes via dual activation of an ene reaction. J Am Chem Soc 130:4517–4526
156. Roithová J, Janková Š, Jašíková L, Váňa J, Hybelbauerová S (2012) Gold-gold cooperation in the addition of methanol to alkynes. Angew Chem Int Ed Engl 51:8378–8382
157. Seidel G, Lehmann CW, Fürstner A (2010) Elementary steps in gold catalysis: the significance of gem-diauration. Angew Chem Int Ed Engl 49:8466–8470
158. Raubenheimer HG, Schmidbaur H (2012) Gold chemistry guided by the isolobality concept. Organometallics 31:2507–2522
159. Zhdanko A, Maier ME (2013) Quantitative evaluation of the stability of gem-diaurated species in reactions with nucleophiles. Organometallics 32:2000–2006
160. Zhdanko A, Maier ME (2014) The mechanism of gold(I)-catalyzed hydroalkoxylation of alkynes: an extensive experimental study. Chemistry 20:1918–1930
161. Zeng X, Kinjo R, Donnadieu B, Bertrand G (2010) Serendipitous discovery of the catalytic hydroammoniumation and methylamination of alkynes. Angew Chem Int Ed Engl 49:942–945
162. Hashmi ASK, Schuster AM, Rominger F (2009) Gold catalysis: isolation of vinylgold complexes derived from alkynes. Angew Chem Int Ed Engl 48:8247–8249
163. Vilhelmsen MH, Hashmi ASK (2014) Reaction mechanism for the dual gold-catalyzed synthesis of dibenzopentalene: a DFT study. Chemistry 20:1901–1908
164. Hansmann MM, Tšupova S, Rudolph M, Rominger F, Hashmi ASK (2014) Gold-catalyzed cyclization of diynes: controlling the mode of 5-endo versus 6-endo cyclization–an experimental and theoretical study by utilizing diethynylthiophenes. Chemistry 20:2215–2223
165. González-Arellano C, Corma A, Iglesias M, Sánchez F (2005) Enantioselective hydrogenation of alkenes and imines by a gold catalyst. Chem Commun (Camb) 9:3451–3453. doi:10.1039/b505271h
166. Ito H, Takagi K, Miyahara T, Sawamura M (2005) Gold(I)-phosphine catalyst for the highly chemoselective dehydrogenative silylation of alcohols. Org Lett 7:3001–3004

167. Crawford M-J, Klapötke TM (2002) Hydrides and iodides of gold. Angew Chem Int Ed Engl 41:2269–2271
168. Andrews L, Wang X (2003) Infrared spectra and structures of the stable CuH2-, AgH2-, AuH2-, and AuH4-anions and the AuH2 molecule. J Am Chem Soc 125:11751–11760
169. Tsui EY, Müller P, Sadighi JP (2008) Reactions of a stable monomeric gold(I) hydride complex. Angew Chem Int Ed Engl 47:8937–8940
170. Ito H, Saito T, Miyahara T, Zhong C, Sawamura M (2009) Gold(I) hydride intermediate in catalysis: dehydrogenative alcohol silylation catalyzed by gold(I) complex. Organometallics 28:4829–4840
171. Roşca D-A, Smith DA, Hughes DL, Bochmann M (2012) A thermally stable gold(III) hydride: synthesis, reactivity, and reductive condensation as a route to gold(II) complexes. Angew Chem Int Ed Engl 51:10643–10646
172. Comas-Vives A, Gonzalez-Arellano C, Corma A, Iglesias M, Sanchez F, Ujaque G (2006) Single-site homogeneous and heterogeneized gold(III) hydrogenation catalysts: mechanistic implications. J Am Chem Soc 128:4756–4765
173. Comas-Vives A, Gonzalez Arellano C, Boronat M, Corma A, Iglesias M, Sanchez F, Ujaque G (2008) Mechanistic analogies and differences between gold- and palladium-supported Schiff base complexes as hydrogenation catalysts: a combined kinetic and DFT study. J Catal 254:226–237
174. Comas-Vives A, Ujaque G (2013) Unraveling the pathway of gold(I)-catalyzed olefin hydrogenation: an ionic mechanism. J Am Chem Soc 135:1295–1305
175. Alcaide B, Almendros P, Martínez del Campo T, Fernández I (2011) Fascinating reactivity in gold catalysis: synthesis of oxetenes through rare 4-exo-dig allene cyclization and infrequent β-hydride elimination. Chem Commun (Camb) 47:9054–9056
176. Klatt G, Xu R, Pernpointner M, Molinari L, Quang Hung T, Rominger F, Hashmi ASK, Köppel H (2013) Are β-H eliminations or alkene insertions feasible elementary steps in catalytic cycles involving gold(I) alkyl species or gold(I) hydrides? Chemistry 19:3954–3961
177. Eichkorn K, Weigend F, Treutler O, Ahlrichs R (1997) Auxiliary basis sets for main row atoms and transition metals and their use to approximate Coulomb potentials. Theor Chem Acc 97:119–124
178. Sierka M, Hogekamp A, Ahlrichs R (2003) Fast evaluation of the Coulomb potential for electron densities using multipole accelerated resolution of identity approximation. J Chem Phys 118:9136
179. Tamaki A, Kochi J (1972) Catalytic mechanism involving oxidative addition in the coupling of alkylgold (I) with alkyl halides. J Organomet Chem 40:81–84
180. Tamaki A, Kochi J (1974) Oxidative addition in the coupling of alkylgold (I) with alkyl halides. J Organomet Chem 64:411–425
181. Hashmi ASK, Lothschütz C, Döpp R, Rudolph M, Ramamurthi TD, Rominger F (2009) Gold and palladium combined for cross-coupling. Angew Chem Int Ed Engl 48:8243–8246
182. Peña-López M, Ayán-Varela M, Sarandeses LA, Pérez Sestelo J (2010) Palladium-catalyzed cross-coupling reactions of organogold(I) reagents with organic electrophiles. Chemistry 16:9905–9909
183. Chan JMW, Amarante GW, Toste FD (2011) Tandem cycloisomerization/Suzuki coupling of arylethynyl MIDA boronates. Tetrahedron 67:4306–4312
184. González-Arellano C, Abad A, Corma A, García H, Iglesias M, Sánchez F (2007) Catalysis by gold(I) and gold(III): a parallelism between homo- and heterogeneous catalysts for copper-free Sonogashira cross-coupling reactions. Angew Chem Int Ed Engl 46:1536–1538
185. Lauterbach T, Livendahl M, Rosellón A (2010) Unlikeliness of Pd-free gold (I)-catalyzed Sonogashira coupling reactions. Org Lett 12:11293–11296
186. Beaumont SK, Kyriakou G, Lambert RM (2010) Identity of the active site in gold nanoparticle-catalyzed Sonogashira coupling of phenylacetylene and iodobenzene. J Am Chem Soc 132:12246–12248
187. Corma A, Juárez R, Boronat M, Sánchez F, Iglesias M, García H (2011) Gold catalyzes the Sonogashira coupling reaction without the requirement of palladium impurities. Chem Commun (Camb) 47:1446–1448

188. Brenzovich WE, Benitez D, Lackner AD, Shunatona HP, Tkatchouk E, Goddard WA, Toste FD (2010) Gold-catalyzed intramolecular aminoarylation of alkenes: C-C bond formation through bimolecular reductive elimination. Angew Chem Int Ed Engl 49:5519–5522
189. Zhang G, Cui L, Wang Y, Zhang L (2010) Homogeneous gold-catalyzed oxidative carboheterofunctionalization of alkenes. J Am Chem Soc 132:1474–1475
190. Zhang G, Peng Y, Cui L, Zhang L (2009) Gold-catalyzed homogeneous oxidative cross-coupling reactions. Angew Chem Int Ed Engl 48:3112–3115
191. Faza ON, López CS (2013) Computational study of gold-catalyzed homo- and cross-coupling reactions. J Org Chem 78:4929–4939
192. Hofer M, Gomez-Bengoa E, Nevado C (2014) A neutral gold(III)–boron transmetalation. Organometallics 33:1328–1332
193. Livendahl M, Goehry C, Maseras F, Echavarren AM (2014) Rationale for the sluggish oxidative addition of aryl halides to Au(I). Chem Commun (Camb) 50:1533–1536

Index